

**Dynamic Regulation of Oxygenic
Photosynthesis:
Study of Long term Acclimation to Photo-
oxidative Stress induced by Excess of Light**

Inaugural dissertation

for the attainment of the title of doctor
in the Faculty of Mathematics and Natural Sciences
at the Heinrich Heine University Düsseldorf

presented by

Maria Paola Puggioni
from Cagliari

East Lansing, July 2020

aus dem

IBG-2: Pflanzenwissenschaften-Forschungszentrum Juelich
der Heinrich-Heine-Universität Düsseldorf

Gedruckt mit der Genehmigung der
Mathematisch-Naturwissenschaftlichen Fakultät der
Heinrich-Heine-Universität Düsseldorf

Berichtersteller:

1. Dr. Shizue Matsubara

2. Prof. Dr. A. Weber

Tag der mündlichen Prüfung:

EIDESSTÄTTLICHE ERKLÄRUNG

Ich versichere an Eides Statt, dass diese Dissertation von mir selbständig und ohne unzulässige fremde Hilfe unter Beachtung der „Grundsätze zur Sicherung guter wissenschaftlicher Praxis an der Heinrich-Heine-Universität Düsseldorf“ erstellt worden ist.

Die Dissertation habe ich in der vorgelegten oder in ähnlicher Form noch bei keiner anderen Institution eingereicht.

Ich habe bisher keine erfolglosen Promotionsversuche unternommen.

Düsseldorf, den _____

Maria Paola Puggioni

“Oh our igloo house is bigger now
We've made each brick of ice like stone
It's a fort that can't be broken
A place no one would ever find us

We were children now we've grown
We were children now we've grown
Oh

We were children now we've grown
We were children now we've grown

Nobody knows how loud your heart gets
'Cause we're a million miles away but I still hear you
And I'm going going going going to get you

I'll tell you all my memories and you will tell me yours
The colors of my favorite trees before the winter's war
The reasons you and me should talk about the great unknown
Without the distance in between and all the obstacles we've known

The things we know we just don't know
The things we know we don't know”

How Loud Your Heart Gets
Lucius

TABLE OF CONTENT

PREFACE.....	1
SUMMARY	3
ZUSAMMENFASSUNG	5
1. INTRODUCTION	7
1.1 Oxygenic photosynthesis.....	7
1.1.1 Light reactions	8
1.1.1.1 Light harvesting.....	8
1.1.1.2 Photosynthetic electron transport.....	12
1.1.1.3 Photo-phosphorylation	14
1.1.2 Dark reactions.....	14
1.2 Photoprotection mechanisms to prevent photo-oxidative stress	15
1.2.1 Adjustment of light harvesting	16
1.2.2 Thermal dissipation of excess absorbed light energy	17
1.2.3 Photosynthetic control at level of Cyt b ₆ f	23
1.2.4 Cyclic electron transport around PSI	23
1.2.5 Chloroplast ROS production and scavenging	27
1.2.6 Photoinhibition and repair of photodamaged proteins in the photosynthetic apparatus.....	29
1.3 Long-term acclimation to EL requires Chloroplast-to-nucleus retrograde signaling	32
1.3.1 Redox state of PET components.....	34
1.3.2 Redox state of the components coupled with PET: thioredoxins	35
1.3.3 ROS signaling	36
1.4 Photoreceptors mediated light signaling	37
1.4.1 Light signaling mediated by different photoreceptors converge in regulation of the central hub COP1/SPA complex	38
1.4.2 Transcriptional regulation via photoreceptors through HY5	41
1.4.3 Phytochromes	43
1.4.4 Cryptochromes	45
1.4.4.1 Role of CRY1 in light-responsive gene expression and photo-oxidative stress ..	47
2. AIMS OF THE THESIS	51
3. RESULTS	53

3.1	Characterization <i>cry1-304</i> of under EL	53
3.1.1.	Visual and Growth phenotypes under HL and FL	53
3.1.2.	Induction of photosynthetic responses at the level of PSII in <i>cry1-304</i> in comparison with WT and other photoreceptor mutants and <i>hy5hyh</i>	54
3.1.3.	Photosynthetic response of <i>cry1-304</i> to different light intensities	60
3.1.4	Accumulation of Photosynthetic proteins	67
3.1.5	Pigment analysis	69
3.1.5	CRY1-dependent gene expression	73
3.2	Role of differential subcellular localization of CRY1 in acclimation to EL	75
3.2.1	Characterization of CRY1 overexpression lines which are already available	75
3.2.2	Generation of new CRY1 overexpression lines.....	78
3.2.3	Phenotypic characterization of the selected CRY1 overexpressor lines.....	85
3.3	Functional characterization of an unknown gene which was upregulated under FL (<i>AT3G56290</i>).....	96
3.3.1	Phylogenetic analysis	96
3.3.2	Functional protein association network of <i>AT3G56290</i>	98
3.3.3	Generation of <i>AT3G56290</i> KO mutants by Crispr/Cas9.....	102
3.3.4	Phenotypic characterization of <i>AT3G56290</i> KO lines	113
3.4	Supplementary figures	120
4.	DISCUSSION	127
4.1	Physiological role of the photoreceptor CRY1 in sustaining photosynthesis	127
4.1.1	CRY1 contributes to proper functioning photosynthesis under non-photoinhibitory condition.....	128
4.1.2	CRY1 is important in long-term acclimation to photo-oxidative stress induced by EL	131
4.1.3	The role of CRY1 in regulation of photosynthesis in mature leaves does not involve crosstalk between CRY1 and PHYB via HY5/HYH light signaling pathway	141
4.2	Role of differential subcellular localization of CRY1 in photosynthetic acclimation to EL	142
4.3	Functional characterization of an unknown gene which was upregulated under FL (<i>AT3G56290</i>).....	148
5.	CONCLUDING REMARKS AND FUTURE PERSPECTIVES	153
6.	EXPERIMENTAL PROCEDURES	157
6.1	Plant material.....	157
6.2	Growth conditions	157
6.2.1	Light conditions and treatments	157

6.3 Growth analysis.....	158
6.4 Chlorophyll fluorescence and P700 measurements.....	158
6.5 Pigment Analysis.....	159
6.6 qRT-PCR analysis.....	159
6.7 SDS-PAGE and western blotting.....	159
6.8 Statistical tests.....	160
6.9 Subcellular localization of CRY1-GFP.....	161
6.10 Generation and genotypic characterization of CRY1 complementation overexpression lines.....	161
6.11 Generation and genotypic characterization of <i>AT3G56290</i> KO mutants by CRISPR/Cas9.....	166
LIST OF FIGURES.....	169
LIST OF TABLES.....	172
LIST OF ABBREVIATIONS.....	173
REFERENCES.....	177
AKNOWLEDGMENTS.....	197

PREFACE

The PhD work presented in this thesis is summarized at the beginning of the thesis both in English and in German. The first chapter provides an introduction about photosynthesis, photosynthetic apparatus and regulation of photosynthesis under short and long term excess of light. Light signaling and retrograde signaling are also introduced in this chapter, together with photoreceptors and photoreceptors-mediated light signaling pathways. Subsequently, the aims of this work are stated in the second chapter. A third chapter contains the main experimental results produced during the PhD work. It is followed by the fourth chapter, in which the most important results are discussed in the context of the current state of the art of this research field. Finally, the fifth chapter offers concluding remarks and the future perspectives. The experimental procedures and materials are provide in the last chapter.

SUMMARY

In natural environments photosynthetic organisms experience dynamic changes of light, which are balanced by a number of short- and long-term mechanisms that have evolved to minimize damage to the photosynthetic apparatus and ensure effective photosynthetic performance in order to prosper in dynamic environments. Recent studies in *Arabidopsis thaliana* leaf transcriptome and proteome revealed that hundreds of genes and proteins are subjected to dynamic regulation under dynamic fluctuation of light (FL) compared to constant light (CL) (Schneider et al., 2019; Niedermaier et al., 2020). The results of this PhD work contribute to better understand the dynamic regulation of photosynthesis and the long-term strategies of plants to acclimate their photosynthetic apparatus to photo-oxidative stress induced by excess of light (EL).

The functional relationships between light perception, light signaling and molecular mechanisms underlying the regulation of photosynthetic acclimation to EL have been addressed through the characterization of the UV-A and blue light (BL) photoreceptor CRYPTOCHROME 1 (CRY1). Functional and physiological characterization of the knock-out (KO) mutants *cry1-304* has revealed an essential and non-redundant role of CRY1 in providing necessary components to sustain photosynthesis under both CL and FL conditions. In fact, the lack of CRY1 in *cry1-304* plants leads to a severe photosynthetic imbalance in terms of lower photoprotection and electron transport capacities at the level of both photosystem II (PSII) and photosystem I (PSI), revealing a strong limitation in the reactions downstream of PSI. The phenotype observed under no-photoinhibitory conditions was further exacerbated under FL conditions, where both PSII and PSI displayed intense photoinhibition together with strongly decreased Non Photochemical Quenching (NPQ) and PSII electron transport capacity. The severe growth phenotype observed in *cry1-304* plants under both in HL and in FL reflects the photo-oxidative stress and photosynthetic imbalance experienced under these conditions and indicates that CRY1 is required for EL tolerance. As CRY1 is a very upstream factor in the light signaling pathways, its effects certainly involve the contribution of multiple components that are mis-regulated in *cry1-304* mutant. Thus, further investigations are required to understand how the light-dependent signaling networks, controlled by CRY1 and redox signals coming from the chloroplast, are integrated during the process of long-term photosynthetic acclimation.

Since CRY1 has been detected in the nucleus and the cytoplasm, the localization-dependent functions of CRY1 were also addressed. The physiological phenotypes of the previously described transgenic lines overexpressing GFP-fused CRY1 in the nucleus, in the cytoplasm or in both (Wu and Spalding, 2007) were characterized and compared with the same set of new transgenic lines generated in this study without GFP fusion. Unfortunately, the latter lines did not show rescue of the phenotype observed in *cry1-304* mutants. Further efforts in characterize the role of these specific localized CRY1 pools might contribute in the future in dissecting the mechanisms by which cellular network components that involves multiple organelles and subcellular compartments are coordinated and mediate global light signaling responses to changing environments.

Lastly, the role of a gene with unknown function, *AT3G56290*, in photosynthetic acclimation to EL was investigated as it was found upregulated in *A. thaliana* leaf transcriptome under FL (Schneider et al., 2019) and described as a potential candidate that is involved in the integration of light and plastid signaling (Ruckle et al., 2012). Gene co-expression analysis indicated a possible functional relation with genes involved in chloroplast lipid and isoprenoid metabolism and transcriptional regulation of photosynthesis. Targeted KO plants of *AT3G56290* were successfully generated by using the CRISPR/Cas9 technology. Although these lines showed no evident changes in morphology, plant development or photosynthetic phenotypes when compared with wild type (WT) under EL, they represent a first step to further characterize these mutants and the potential role of *AT3G56290* in acclimation to oxidative stress induced from EL.

ZUSAMMENFASSUNG

In natürlichen Umgebungen erleben photosynthetische Organismen dynamische Lichtveränderungen, die durch mehrere kurz- und langfristige Mechanismen ausgeglichen werden. Diese Mechanismen haben sich entwickelt, um Schäden am photosynthetischen Apparat zu minimieren und eine effektive photosynthetische Leistung zu gewährleisten, damit die Organismen in dynamischen Umgebungen gedeihen können. Eine kürzlich durchgeführte Studie an der Blatt-Transkriptom und Proteom von *Arabidopsis thaliana* zeigte, dass hunderte von Genen und Proteinen unter dynamischer Lichtschwankung (FL) auch dynamisch reguliert werden im Vergleich zu konstantem Licht (CL) (Schneider et al., 2019; Niedermaier et al., 2020). Die Ergebnisse dieser Doktorarbeit liefern einen Beitrag zum Verständnis der dynamischen Regulation der Photosynthese und der langfristigen Strategien von Pflanzen zur Anpassung ihres photosynthetischen Apparates an den photo-oxidativen Stress, der durch einen Überschuss an Licht (EL) induziert wird.

Die funktionellen Beziehungen zwischen Lichtwahrnehmung, Lichtsignalisierung und molekularen Mechanismen, die der Regulierung der photosynthetischen Akklimatisierung an EL zugrunde liegen, wurden durch die Charakterisierung des UV-A/Blaulicht-Photorezeptors Cryptochrome 1 (CRY1) untersucht. Die funktionelle und physiologische Charakterisierung der Knock-out (KO) Mutanten *cry1-304* hat eine wesentliche und redundanzfreie Rolle des CRY1 bei der Bereitstellung der notwendigen Komponenten zur Aufrechterhaltung der Photosynthese unter CL- und FL-Bedingungen aufgezeigt.

Das Fehlen von CRY1 in *cry1-304*-Pflanzen führt tatsächlich zu einem starken photosynthetischen Ungleichgewicht in Bezug auf geringere Lichtschutz- und Elektronentransportkapazitäten, sowohl auf der Ebene von dem Photosystem II (PSII) als auch von dem Photosystem I (PSI). Dies zeigt eine strenge Einschränkung in den Downstream-Reaktionen von PSI. Der Phänotyp unter nicht-photoinhibitorischen Bedingungen wurde unter FL-Bedingungen weiter verschärft. Außerdem zeigten PSII und PSI unter FL-Bedingungen eine intensive Photoinhibition, zusammen mit einer stark verringerten „Nicht-photochemische Löschung“ (NPQ) und PSII-Elektronentransportkapazität. Der Phänotyp mit schwerer Wachstumsstörung in *cry1-304*-Pflanzen (sowohl unter HL als auch in FL) spiegelt den unter diesen Bedingungen auftretenden photo-oxidativen Stress und das photosynthetische

Ungleichgewicht wider und zeigt, dass CRY1 für die EL-Toleranz erforderlich ist. Da CRY1 ein hoher Upstream-Faktor in den Lichtsignalwegen ist, beinhalten seine Wirkungen sicherlich den Beitrag mehrfacher Komponenten, die in dem *cry1-304*-Mutant fehlreguliert sind. Aus den oben genannten Gründen sind weitere Untersuchungen erforderlich, um zu verstehen, wie die lichtabhängigen Signalnetzwerke (gesteuert durch CRY1 und Redoxsignale vom Chloroplasten) während des Prozesses der langfristigen photosynthetischen Akklimation integriert werden.

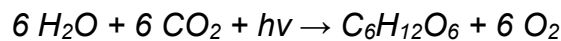
Der Photorezeptor CRY1 wurde im Zellkern und im Zytoplasma nachgewiesen, deswegen wurden auch seine Funktionen in Abhängigkeit von seiner zellulären Lokalisierung analysiert. In früheren Arbeiten charakterisierten Wu und Spalding (2007) die physiologischen Phänotypen der transgenen Linien, die GFP-fusioniertes CRY1 im Zellkern und im Zytoplasma überexprimieren. In dieser Arbeit wurde ein neuer Satz transgener Linien ohne GFP-Fusion erzeugt und mit denen von Wu und Spalding (2007) verglichen. Leider zeigten die Linien in dieser Studie keine Rettung des in *cry1-304*-Mutanten beobachteten Phänotyps. Weitere Bemühungen zur Charakterisierung der Rolle dieser spezifischen lokalisierten CRY1-Pools könnten in der Zukunft dazu beitragen, die Mechanismen zu analysieren, mit denen zelluläre Netzwerkkomponenten (die mehrere Organellen und subzelluläre Kompartimente umfassen) koordiniert werden und wie globale Lichtsignalreaktionen auf sich ändernde Umgebungen vermitteln.

Schließlich wurde in dieser Studie die Rolle von *AT3G56290* bei der photosynthetischen Akklimation an EL untersucht. *AT3G56290* ist ein spezifischer Kandidat mit unbekannter Funktion, der hochreguliert im FL-Blatt-Transkriptom gefunden wurde (Schneider et al., 2019) und als potenziell an der Integration von Licht- und Plastidensignalen beteiligt beschrieben wurde (Ruckle et al. 2012). Die Co-Expressionsanalyse ergab, dass dieses Gen funktionell mit Genen verwandt sein könnte, die am Chloroplasten-Lipid- und Isoprenoid-Stoffwechsel sowie an der Transkriptionsregulation der Photosynthese beteiligt sind. Gezielte KO-Pflanzen von *AT3G56290* wurden erfolgreich mit Hilfe der CRISPR/Cas9-Technologie erzeugt. Zuletzt zeigten diese Linien im Vergleich zur Wildtyp (WT) keine offensichtlichen Veränderungen in der Morphologie oder in der Entwicklung der photosynthetischen Phänotypen. Dennoch stellen sie einen ersten Schritt zur weiteren Charakterisierung dieser Mutanten und ihrer potentiellen Rolle bei der Akklimation an den durch EL induzierten oxidativen Stress dar.

1. INTRODUCTION

1.1 Oxygenic photosynthesis

Oxygenic photosynthesis is a biochemical process that allowed evolution of oxygen-dependent lives on earth. It consists of a series of redox reactions in which in the presence of light ($h\nu$) H_2O molecules are oxidized and inorganic carbon, in the form of carbon dioxide (CO_2), is reduced. The net product of these reactions is the formation of O_2 and carbohydrates ($C_6H_{12}O_6$)



In Eukaryotes photosynthesis takes place in chloroplasts, specialized organelles surrounded by two membranes, the outer envelope and the inner envelope, which together form the chloroplast envelope (EM). Within the chloroplast the thylakoid membrane system further defines an inner space (lumen) and an outer space (stroma). Thylakoids are organized in stacked membrane regions (grana) connected by stroma lamellae (**Figure 1.1**).

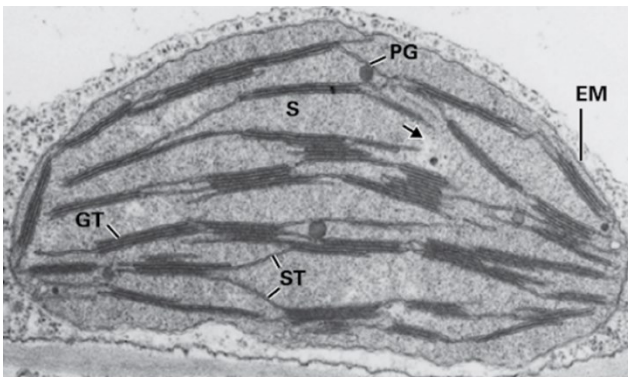


Figure 1.1 Transmission electron microscopy image of a tobacco chloroplast. Two envelope membranes (EM) together with thylakoids (stacked grana thylakoids, GT, and non-stacked stroma thylakoids, ST) define the stroma (S). PG, plastoglobuli. Figure was extracted from (Biochemistry and Molecular biology of plants 2nd edition Buchanan et al. 2000).

The photosynthetic process is composed of the light reactions (see section 1.1.1) and the dark reactions (see section 1.1.2). The first phase takes place at the level of thylakoid membranes and needs light energy to produce adenosine triphosphate (ATP) and reduced nicotinamide adenine dinucleotide phosphate (NADPH). Four multi-subunits complexes localized in thylakoid membranes are essential to drive the light reactions: PSII mediates water splitting by oxygen-evolving complex (OEC) and reduction of plastoquinones (PQ).

Cytochrome b_6f complex (Cyt b_6f) mediates electron transfer between the two photosystems, oxidizing the reduced PQ and reducing plastocyanins (Pc). PSI reduces the final electron acceptor NADP^+ via ferredoxin (Fd) and Fd-NADP-oxidoreductase (FNR). This linear electron transport (LET) from PSII to PSI is coupled with generation of proton motive force (pmf) that is used to form ATP by ATP-synthase complex (ATPase). During the dark reactions, which happen in the stroma, both ATP and NADPH are used to fix CO_2 in organic compounds in the Calvin-Benson-Bassham cycle (CBB cycle). The photosynthetic complexes are not distributed uniformly over the thylakoid membranes. Indeed PSI and ATPase are mainly localized in the stroma-exposed thylakoids, margins, and grana extremities, while most of PSII are located in the stacked thylakoids of grana.

1.1.1 Light reactions

The four multi-subunits complexes localized in thylakoid membranes are responsible of three processes that lead to the ATP and NADPH production: light harvesting, electron transport and photo-phosphorylation.

1.1.1.1 Light harvesting

Light is absorbed through peripheral and internal antennae associated with both PSII and PSI. In eukaryotes the peripheral antennae are composed of pigment-protein complexes called Light Harvesting Complexes (LHC), containing chlorophylls (Chl) *a* and *b* and carotenoids (Car). After light absorption, excited electrons in these pigments can decay through rapid transfer of energy from a pigment to another until it reaches the photosystem reaction center (RC) where charge separation takes place. A special pair of Chl associated to each RC. PSII and PSI RCs have their maximum absorption peaks at 680 nm (red light) and 700 nm (far red light), respectively, and thus are called P680 and P700.

1.1.1.1.1 PSII reaction center and light harvesting complexes

PSII is a large multisubunit protein complex containing a dimeric core and several peripheral antenna complexes embedded in the membrane (**Figure 1.2**). The core complex is composed of 20-23 protein subunits, depending on the organism (**Figure 1.2 A and B**). The RC is the catalytic heart of the core and it consists of four subunits, PsbA (D1), PsbB (CP47), PsbC (CP43) and PsbD (D2), which are also the largest membrane-intrinsic subunits. Charge separation and electron transfer start in the photochemical RC, composing of PsbA and PsbD, which bind in total six Chl. PsbA binds also two pheophytins. The internal antenna proteins of the RC are formed by PsbB and PsbC, which bind 14 and 16 Chl respectively. These two subunits are involved in light harvesting and transporting excitation energy from peripheral antenna subunits towards the photochemical RC (Dekker and Van Grondelle, 2000; Nelson and Yocum, 2006; Mitchell, 2011; Bobik et al., 2015; Roose et al., 2016; Wei et al., 2016; van Bezouwen et al., 2017). Other small intrinsic subunits (PsbE, PsbF, PsbH, PsbI-M, PsbTc, PsbX, PsbY and PsbZ) are present in all oxygenic photosynthetic organisms (Roose et al., 2016; Wei et al., 2016; van Bezouwen et al., 2017). In plant-type PSII the OEC includes the subunits PsbO, PsbP, PsbQ and PsbR. (Roose et al., 2016; Wei et al., 2016; van Bezouwen et al., 2017). LHCII are heterotrimers composed of a different combination of Lhcb1, Lhcb2 and Lhcb3. The dimeric plant core complex forms supercomplexes with up to six LHCII trimers. These trimers are linked to the core complex by the minor monomeric antenna proteins Lhcb4 (CP29), Lhcb5 (CP26) and Lhcb6 (CP24) (Caffarri et al., 2004; van Bezouwen et al., 2017). Lhcb4 binds three Car (one lutein, Lut, one violaxanthin, V, and one neoxanthin, N) and 13 Chl (eight Chl *a* and four Chl *b* plus an additional Chl *a/b* site). Lhcb5 and Lhcb6 contain 13 and 10-11 Chl. Each LHCII monomer in the trimer contains 14 Chl (eight Chl *a* and six Chl *b*) and four xanthophyll binding sites have been identified (see section 1.1.1.1.3) (Liu et al., 2004a; Standfuss et al., 2005; Pan et al., 2011; van Bezouwen et al., 2017).

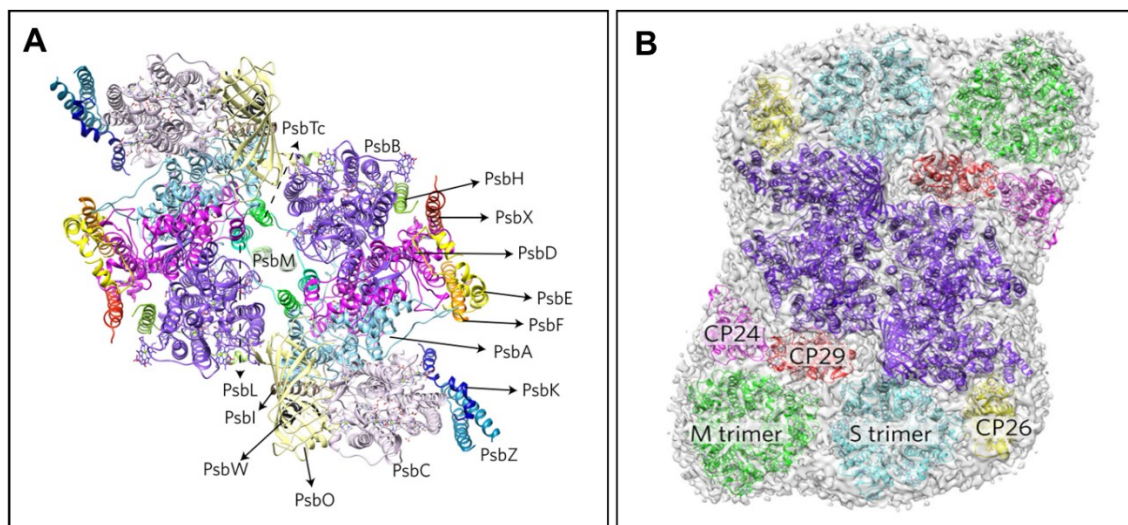


Figure 1.2 Overviews of the dimeric PSII core associated with LHCII. **A)** PSII core complex with the assigned subunits; **B)** structure of the PSII-LHCII supercomplex from the luminal side. The core region (purple), the S-LHCII trimer (cyan), the M-LHCII trimer (green), CP29 (red), CP26 (yellow) and CP24 (pink) are shown. Figure modified from van Bezouwen et al., 2017.

1.1.1.1.2 PSI reaction center and light harvesting complexes

Contrarily to PSII, in higher plants PSI is a monomer and its peripheral antenna, LHCI, is stably associated with the core complex (Croce et al., 2002; Ballottari et al., 2004) (**Figure 1.3**). In plant the PSI core complex consists of 12 subunits (PsaA, PsaB, PsaC, PsaD, PsaE, PsaF, PsaG, PsaH, PsaI, PsaJ, PsaK, and PsaL). The two largest subunits, PsaA and PsaB, form a symmetric dimer, which binds the majority of the pigments. LHCI is composed of four subunits (Lhca1, Lhca2, Lhca3 and Lhca4) that are assembled into two heterodimers (Lhca1-Lhca4, Lhca2-Lhca3) and linked at one side of the PSI core complex. A recent high resolution structure from *Pisum sativum* (Mazor et al., 2015; Mazor et al., 2017) showed the PSI core subunits arranged together with the four proteins of the LHCI complex to form a super-complex (**Figure 1.3**). PSI contains 214 prosthetic groups, including 156 Chl, 32 Car, and 14 lipids (Amunts et al., 2010; Mazor et al., 2015). Two minor LHCI proteins, Lhca 5 and Lhca6, contribute to the interaction of each PSI-LHCI with the chloroplast NADH dehydrogenase-1 like complex (NDH-1 complex), by substitution of Lhca4 and Lhca2 (Otani et al., 2018). In addition to LHCI, also LHCII can associate with PSI during state transition to modulate the distribution of excitation energy between PSII and PSI (see section 1.2.1). This LHCII-PSI association happens at the opposite site of the LHCI-PSI association and it involves PsaH, PsaL, PsaK (Kouřil et al., 2005).

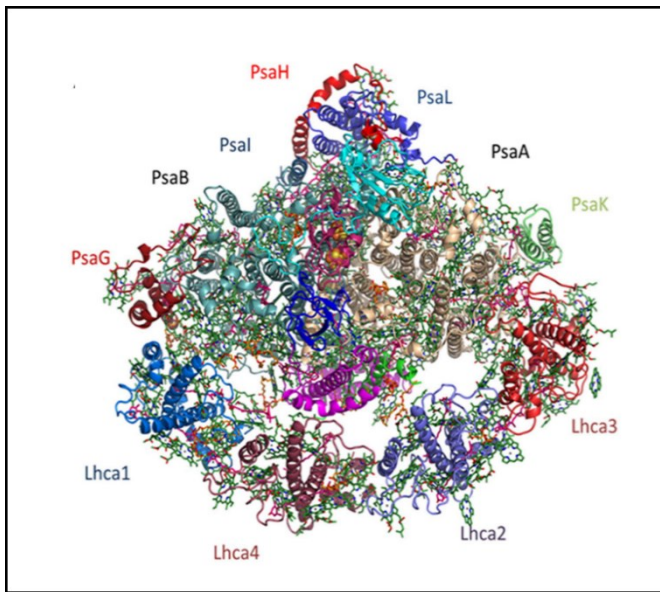


Figure 1.3. Structure and organization of the *Pisum Sativum* PSI-LHCI supercomplex. **A)** PSI-LHCI from the stromal side of the membrane. **B)** Pigment organization in PSI-LHCI supercomplex. The central pigments of the internal electron transport chain are shown in red, Chl of the core antenna in green, Chl *a* in cyan and Chl *b* in magenta, Car in blue and lipids in orange. Figure modified from Mazor et al., 2015

1.1.1.1.3 Xanthophyll binding sites in antenna proteins

In the trimeric LHCII complex four xanthophylls binding sites have been identified, which are termed based on their binding specificity (**Figure 1.4**). The L1 and L2 sites bind two Lut and are associated with the two central transmembrane helices A and B. The site N1 is located in the more peripheral helix B and binds N. The site V is located at the monomer interface and binds V. Different antenna proteins share high sequence and structural similarity. Thus, a similar protein structure has been predicted for the LHCII minor antennae Lhcb4, Lhcb5 and Lhcb6, as well as for LHCI (Lhca1 to Lhca4). However, they differ for the oligomeric state and pigment composition. Indeed, Lhcb1–3 are organized in trimers, Lhcb4–6 are monomers and Lhca1/4 and Lhca 2/3 form dimers. Each monomer of the trimeric LHCII and dimeric LHCI binds 14 Chl, while monomeric Lhcb proteins (Lhcb4, Lhcb5 and Lhcb6) bind less Chl (13, 10-11 molecules). All the LHC proteins bind Lut in the L1 site, while the xanthophyll binding of the other sites is variable and differs in each of the LHC subcomplexes (Morosinotto et al., 2003; Standfuss et al., 2005; Wehner et al., 2006; Jahns et al., 2009; Di Valentin et al., 2009; Jahns and Holzwarth, 2012). In LHCII the V molecules bound to antenna proteins have an important role in photoprotection (see section 1.2.2.1), while the role of the LHCI-bound-V has not been clarified yet. It is mostly accepted that the V molecules bound to LHCI proteins are involved in antioxidant activities rather than energy dissipation (Wehner et al., 2004; Tian et al., 2017).

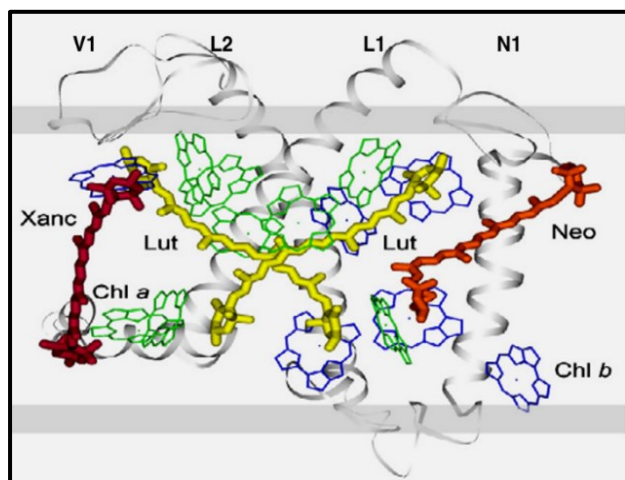


Figure 1.4. Xanthophyll binding sites in spinach LHCII structure (derived from Liu et al., 2004). L1 and L2 sites bind two Lut (in yellow) and are associated with the two central transmembrane helices A and B, N (orange) is bound to the N1 site located in the more peripheral helix B. V (red) is bound in the V1 site at the monomer interface. Chl *a* and Chl *b* are indicated in green and blue, respectively. Figure from Jahns and Holzwarth, 2012.

1.1.1.2 Photosynthetic electron transport

In the grana-localized PSII, D1, D2 and Cyt b_{559} coordinate the molecules involved in the charge separation: the special Chl *a* pair (P680), another Chl *a* molecule (Chl_{D1}), pheophytin (Phe) and the quinone acceptors, PQ_A and PQ_B. The photons excite P680 to P680*, which donates the electron to Chl_{D1}. Once P680 undergoes charge separation, it becomes oxidized (P680⁺) and recovers neutrality by accepting an electron from the H₂O splitted by OEC. OEC splits water molecules, releasing O₂ and H⁺ in the lumen (H⁺_{in}). Chl_{D1} reduces Phe, which in turn donates one electron to PQ_A tightly bound to the RC (**Figure 1.5**). Following the transport of two electrons to the mobile acceptor PQ_B, it becomes protonated to plastoquinol (PQH₂) by taking two H⁺ from the stroma (H⁺_{out}) and it diffuses in the membrane. Reduction of PQH₂ contributes to the formation of an electrochemical gradient across the thylakoid membrane by transferring H⁺ from the stroma (H⁺_{out}) to the lumen (H⁺_{in}). (Tikhonov, 2017). The Cyt b_{6f} complex interconnects PSII and PSI, transferring electrons from PQH₂ to Pc, a water-soluble protein that serves as the primary electron donor of PSI. Cyt b_{6f} is organized in a functional dimer in which each monomer consists of four subunits: the iron-sulfur Rieske protein, Cyt b_6 , Cyt *f* and the subunit IV. Four redox centers provide the catalytic function of this complex: an iron-sulfur cluster, two hemes of Cyt b_6 and one heme *f*. Two PQ binding sites, Q_o (quinol oxidase) and the Q_i (quinone reductase) are located in the Rieske protein and in the stromal side of the complex, respectively (Yamashita et al., 2007). The Q_o has high affinity for PQH₂ which releases two H⁺ in the lumen (H⁺_{in}). Two electrons proceed in two different chains according to the Q-cycle mechanisms (Mitchell, 1975) (**Figure 1.5**).

One electron is transferred to Pc through the high potential chain, while the other electron is directed to PQ at the Q_i site in the low potential chain. Through two sequential steps of PQ reduction at Q_i , two protons are taken from the stroma to regenerate PQH_2 . The net products of the Q-cycle are thus two reduced Pc, four H^+ pumped into the lumen ($4 H^+_{in}$), two H^+ consumed in the stroma ($2 H^+_{out}$) and one PQH_2 regenerated when two molecules of PQH_2 are oxidized. The reduced Pc diffuses through the lumen to PSI ($P700^+$) which transfers the electron to Fd in the stroma (Tikhonov, 2017). PsaA and PsaB proteins coordinate a special pair of Chl *a* which represent the primary electron donor ($P700$). When the light induces charge separation of $P700$, it donates an electron to the following electron acceptors and becomes oxidized. $P700$ is re-reduced by the electron coming from PSII and Cyt b_6f via Pc. In PSI the electron chain proceeds in two branches (A and B) to other two pairs of Chl (Chl₂ and Chl₃) and one phylloquinone (A_1). The two branches converge at F_x , the first of the three $[FeS]_4$ clusters, followed by F_A and F_B . The PSI electron transport ends with the reduction of Fd. Electrons are then transferred from reduced Fd to $NADP^+$ via FNR. To synthesize one molecule of NADPH, two reduced Fd need to be oxidized (**Figure 1.5**). The LET overall results in oxidation of two H_2O molecules, synthesis of one NADPH and pumping of six H^+ into the lumen (Tikhonov, 2017).

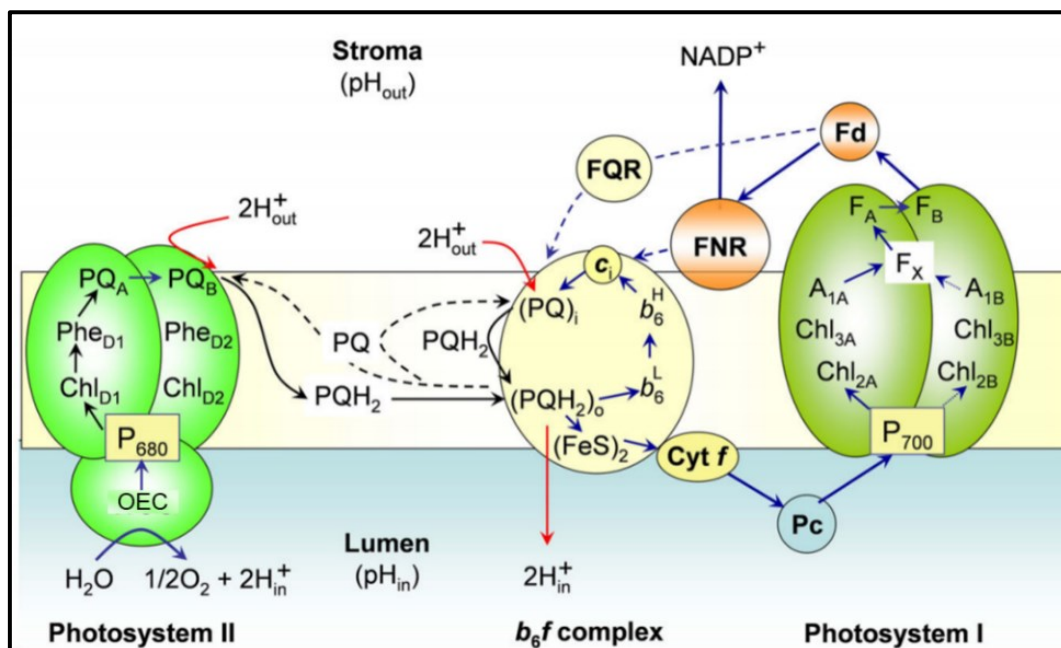


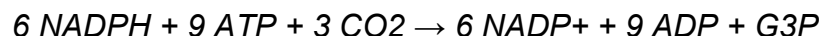
Figure 1.5 Schematic representation of LET in the thylakoid membrane of chloroplasts. Figure was modified from Tikhonov, 2017.

1.1.1.3 Photo-phosphorylation

During LET the H⁺ released in the lumen by OEC and at Cyt b₆f generates pmf, a trans-thylakoid potential that includes an electric ($\Delta\Psi$) and a chemical (ΔpH) component and it is exploited by the ATPase to generate ATP from ADP and inorganic phosphate (Boyer et al., 1977; Cukier and Nocera, 1998; Mitchell, 2011; Junge and Nelson, 2015). Like PSI, the ATPase is exclusively located in stroma lamellae. Chloroplast ATPase consists of 26 protein subunits, 17 of which are completely or partially embedded in the membrane. ATP synthesis is catalyzed by the hydrophilic head (cF₁) which face the stroma and it is powered by a rotary motor (cF₀), located in the membrane. cF₁ contains 11 subunits ($\alpha_3\beta_3\gamma_1\delta_1\epsilon_1$), while the rotary motor cF₀ contains 14 subunits (a₁b₂c₁₀) each of which possess a conserved protonatable glutamate. cF₀ confers a hydrophilic channel spanning the membrane to allow dissipation of pmf which drives the catalytic activity. ATPase catalyze the synthesis of three ATP per revolution (Hisabori et al., 2013; Hahn et al., 2018a). The chloroplast γ subunit has a region of ca. 40 amino acid conserved in green algae and higher plants which is thought to work as a redox-controlled inhibitor of ATP hydrolysis. In this region two cysteine residues work as redox sensor and are target of redox regulation via thioredoxins (Trx) and NADPH-dependent thioredoxin reductase (NTRC) (Carrillo et al., 2016; Hahn et al., 2018a; Nikkanen and Rintamäki, 2019). (see section 1.3.2).

1.1.2 Dark reactions

Inorganic carbon in the form of CO₂ is fixed into carbohydrate via the CBB cycle (Bassham et al., 1954), which consumes the ATP and NADPH produced during the light reactions and regenerate ADP, P_i and NADP⁺. Overall, the synthesis of one molecule of glyceraldehyde 3-phosphate (G3P) requires nine molecules of ATP and six molecules of NADPH, with a ratio of ATP/NADPH about 1.5.



The activity of the light and dark reactions is coordinated. Since the light reactions strongly impact the stroma environment in which the dark reactions occur, the CBB activity is modulated based on the activity of the light reactions. Many regulatory enzymes of the CBB cycle have their optimal activity at pH values of ca. pH 8. When the electron transport is active in the light, alkalization of the chloroplast stroma concomitant with lumen acidification leads to a light dependent shift in pH from pH 7 in the dark to pH 8 in the light.

The increased stromal pH is accompanied by an increased concentration of Mg^{2+} in the stroma. Furthermore, also the redox state of the stroma is subjected to changes as a consequence of the reduction of Fd and $NADP^+$. Reduction of disulfide groups of some key enzymes of the CBB such as fructose-1,6-bisphosphatase (FBPase), seduheptulose-1,7-bisphosphatase (SBPase), glyceraldehyde-3-phosphate dehydrogenase (GAPDH), and phosphoribulokinase (PRK), is essential for their activation and can be achieved via the ferredoxin/thioredoxin system (Yoshida et al., 2015; Buchanan, 2016; Nikkanen et al., 2016; Nikkanen and Rintamäki, 2019; Sharkey, 2019).

1.2 Photoprotection mechanisms to prevent photo-oxidative stress

In natural environments photosynthetic organisms are exposed to highly dynamic environmental factors and they experience constantly changing conditions that affect their physiology and photosynthetic performance. Variable environmental conditions (irradiance, temperature, water and gas availability) can easily lead to overreduction of electron transport chain, limiting photosynthetic efficiency. In particular sunlight intensity can change quickly and dramatically, and the changes can last for a short or long time. In order to respond to dynamic fluctuations of irradiance, the photosynthetic apparatus requires dynamic regulation of light harvesting and electron transport at different levels (Aro et al., 1993; Niyogi, 1999b; Krieger-Liszkay, 2005; Allahverdiyeva and Aro, 2012; Kono and Terashima, 2014; Chaux et al., 2015; Gururani et al., 2015; Li et al., 2018; Schneider et al., 2019). Indeed, when absorbed light energy exceeds the photosynthetic utilization capacity of plants, overreduction of electron transport chain can lead to the production of reactive oxygen species (ROS) at level of both PSII and PSI and consequently photo-oxidative stress (Aro et al., 1993; Niyogi, 1999b; Krieger-Liszkay, 2005; Allahverdiyeva and Aro, 2012; Chaux et al., 2015; Gururani et al., 2015; Li et al., 2018). The balance between the absorption and the utilization of light energy requires continuous regulation of light harvesting and electron transport. Multiple mechanisms act in concert to prevent excessive damage and to avoid oxidative stress induced by EL. These mechanisms are commonly referred as “photoprotection” and include avoiding the absorption of EL, dissipation or re-directioning of the absorbed EL and excess electrons, ROS scavenging and repair mechanisms (**Figure 1.6**). Some of them are constitutively present, such as the carotenoids bound to photosystems, which also exert an antioxidant function. Other protection mechanisms are activated by EL at different timescales.

Despite these numerous photoprotective defense mechanisms, damage to the photosynthetic machinery still occurs and requires turnover and replacement of damaged proteins. Prolonged EL triggers sustained quenching mechanisms to ensure dissipation of EL. If photodamage is not avoided, limited or repaired, it leads to a decreased efficiency of photosynthesis, termed “photoinhibition”. Also, long term acclimation to EL requires a global reprogramming in gene expression to regulate light harvesting and increase the synthesis of several antioxidant molecules (Havaux and Kloppstech, 2001; Xu et al., 2017). These gene expression changes are induced by the EL perceived in the chloroplast and signaling between chloroplast and nucleus gene expression are mediated by chloroplast-to-nucleus retrograde signaling (see paragraph 1.3). Photoreceptors contribution in these processes is described in paragraph 1.4.

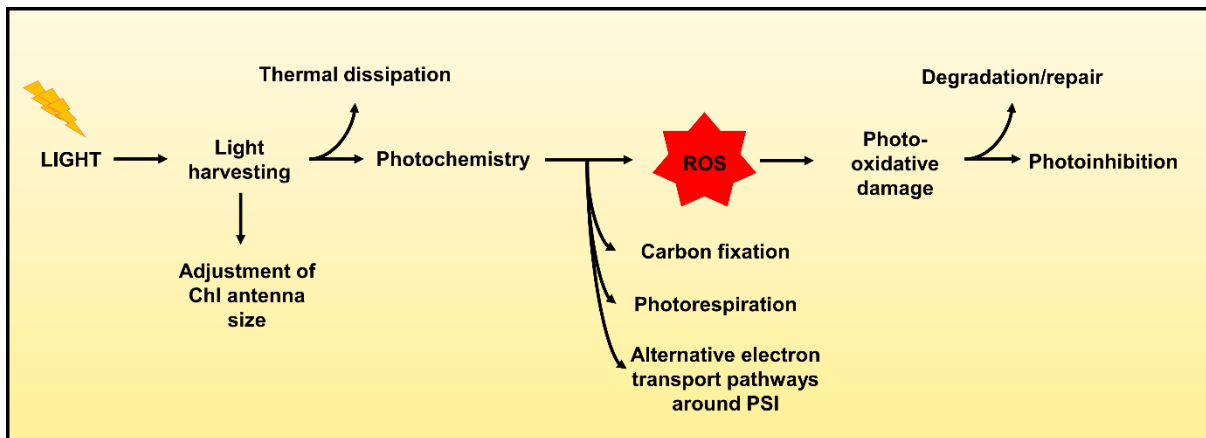


Figure 1.6. Schematic diagram of photoprotective processes occurring within chloroplasts. Figure re-adapted from (Niyogi, 1999a)

1.2.1 Adjustment of light harvesting

Short-term alteration of the relative antenna sizes of PSII and PSI can occur during the so-called “state transitions”, in which LHCII can dissociate from PSII and associate to PSI to balance the distribution of excitation energy transfer between the two photosystems. This mechanism is triggered by electron transfer at the level of Cyt b_6/f , where the binding of PQH₂ to Q_o subunits serves as a signal for the activation of the STN7 kinase (Bellafiore et al., 2005), which phosphorylates LHCII. Phosphorylated LHCII moves from PSII to PSI in a conformation called “State II”. LHCII is then dephosphorylated by the phosphatase TAP38/PPH1 and returns to the initial conformation “State I” (Pribil et al., 2010).

During long-term acclimation to EL changes in the size of the antennae associated with PSII and PSI, through changes in LHC gene expression and/or LHC protein degradation, are required to balance light absorption and utilization (Park' et al., 1997; Niyogi, 1999b; Jackowski et al., 2003; Ballottari et al., 2007; Timperio et al., 2012). *A.thaliana* plants exposed to HL showed 52% less Chl associated with PSII antenna proteins compared to the CL plants; on the contrary, low light (LL) acclimated plants underwent a 46% increase in PSII Chl content (Ballottari et al., 2007). In particular, the levels of Lhcb1, Lhcb2 and Lhcb3 (LHCII) are strongly increased in LL, whereas it is decreased in HL (Ballottari et al., 2007). At the level of PSI, Lhca proteins do not display major changes during acclimation to different light conditions (Ballottari et al., 2007), except Lhca5 and Lhca6 which were found increased in HL and FL conditions (Rolland et al., 2017; Schneider et al., 2019).

1.2.2 Thermal dissipation of excess absorbed light energy

When Chl absorbs light, it is excited from its ground state to $^1\text{Chl}^*$. It can relax to the ground state by emitting light (fluorescence), by fueling photochemical reaction, or by being de-excited by thermal dissipation (**Figure 1.7**), in the so called NPQ. Under EL conditions, when photochemical reactions and NPQ processes are not able to deal with the absorbed excess photons, the excitation energy is accumulated in the antennae and increases the lifetime of $^1\text{Chl}^*$, resulting in increased production of Chl triplets ($^3\text{Chl}^*$) by intersystem crossing (Müller et al., 2001). Even though $^3\text{Chl}^*$ are not harmful per se, they are stable enough to react with O_2 , generating singlet oxygen and other ROS (Krieger-Liszkay, 2005). NPQ thermally dissipates the fraction of absorbed EL through the de-excitation of $^1\text{Chl}^*$. NPQ has multiple components which are differently activated and deactivated depending on the duration and the intensity of EL (Jahns and Holzwarth, 2012).

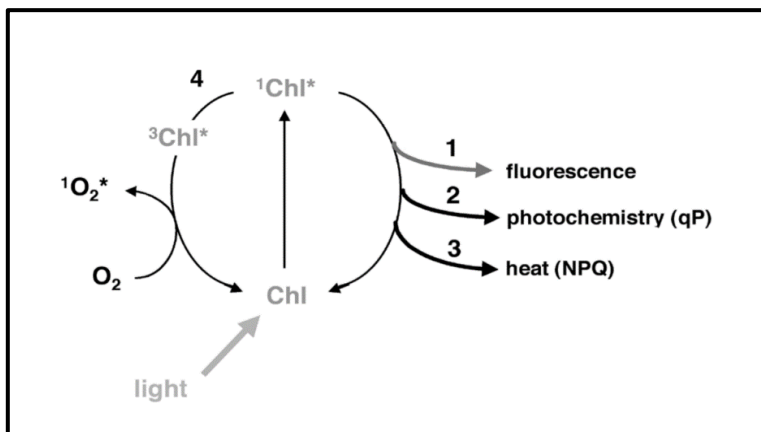


Figure 1.7. Possible destiny of excited Chl. When Chl is excited from its ground state to its singlet excited state, $^1\text{Chl}^*$ can be brought back to the ground state by 1) emitting fluorescence, 2) providing energy for photochemistry, or 3) dissipating the energy in form of heat. Alternatively, $^1\text{Chl}^*$ can be converted to 4) $^3\text{Chl}^*$ which can react with O_2 and produce $^1\text{O}_2^*$. Figure from (Müller et al., 2001).

The energy-dependent quenching (qE) is the fastest component and it is activated and relaxed in a few seconds. qE is triggered by pH-dependent activation of PSII subunit S (PSBS) protein (Niyogi et al., 2000; Li et al., 2002; Holt et al., 2004; Li et al., 2004) and Zeaxanthin (Z) accumulation (Nilkens et al., 2010) (**Figure 1.8**, see section 1.2.2.2). Prolonged steady-state EL leads to activation of the Z-dependent quenching component (qZ), which is activated more slowly than qE and it relaxes in the time scale of minutes (Nilkens et al., 2010) (see section 1.2.2.3). Persistent EL triggers sustained photoinhibitory quenching processes, qH and qI, which are slowly activated and slowly reversed (see section 1.2.2.4) (Demmig-Adams, 1990; Adams and Demmig-Adams, 1992; Demmig-Adams and Adams, 1993; Niyogi et al., 1998; Jahns and Holzwarth, 2012; Malnoë et al., 2018; Malnoë, 2018; Amstutz et al., 2020).

1.2.2.1 Violaxanthin cycle

Z has a central role in photoprotection in chloroplasts, as it is involved in both ROS scavenging and quenching of $^1\text{Chl}^*$, contributing directly or indirectly to all the components of NPQ, except qH. Violaxanthin de-epoxidase (VDE) catalyzes the two-step de-epoxidation of V to A and to Z. The VDE activity requires ascorbate as cofactor and it is located in the lumen, where lumen acidification (pH values <5.8) triggers VDE activation (**Figure 1.8**). The de-epoxidation of V to Z occurs in the lipid phase of the thylakoid membrane. Activation of VDE is pH dependent: at pH values higher than 6.5 VDE is mobile in the lumen, while when the pH decreases below 6.5 it is able to attach to the thylakoid membranes (Fufezan et al., 2012). The reverse epoxidation reaction from Z to V ($Z \rightarrow A \rightarrow V$) is catalyzed by the stroma localized zeaxanthin epoxidase (ZEP). This reaction is observed under LL or darkness, because under moderate HL VDE reaction is much faster than ZEP. The ZEP activity occurs at pH values about 7.5 and it needs NADPH and O_2 as cofactors (**Figure 1.8**).

The re-conversion of Z to V via epoxidation reactions catalyzed by ZEP are slower compared to the de-epoxidation reaction (Niyogi et al., 1997; Jahns et al., 2009; Nilkens et al., 2010; Jahns and Holzwarth, 2012; Kress and Jahns, 2017).

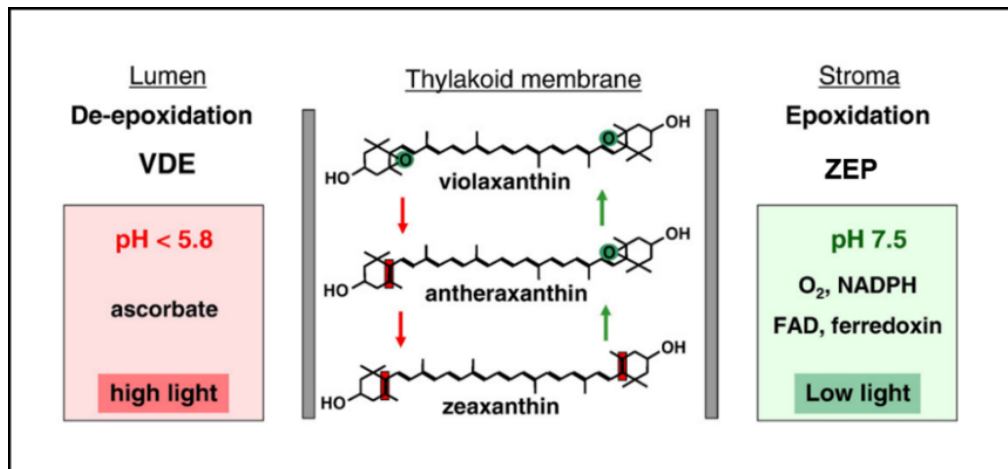


Figure 1.8 Violaxanthin cycle. Lumen acidification (ca 5.8) activates V de-epoxidase (VDE) which catalyzes the sequential de-epoxidation of V to A and then to Z. Δ pH breakdown deactivates VDE and causes the slow reversion of Z to V catalyzed by Z epoxidase (ZEP). Figure modified from (Jahns et al., 2009)

Release of V from its binding sites in the antenna proteins and diffusion of V to the lipid phase are essential for de-epoxidation. Furthermore, it represents the rate-limiting steps for de-epoxidation, which explains the slower de-epoxidation from V to A compared to the de-epoxidation of A to Z (Latowski et al., 2000; Latowski et al., 2002; Jahns et al., 2009). The conversion of V to Z in the thylakoid membrane is highly dependent on the binding affinity (and thus the ability to be released) of V to its binding sites, which differs in each antenna protein (Jahns et al., 2009; Kress and Jahns, 2017). Xanthophyll binding sites in antenna proteins LHCII and LHCI are described in section 1.1.1.1.3 (see **Figure 1.4**). In general, V is loosely bound to the V1 sites (in LHCII and Lhca3) and thus it is easily releasable and rapidly convertible to Z (within about 10 min), contributing to the fast activated qE component of NPQ. V bound to the L2 sites is less releasable and thus slowly convertible to Z (within about 60 min in Lhcb6 and Lhca4) or not convertible at all (in Lhcb4, Lhca1, Lhca2), suggesting that the first might contribute to the slowly activated qZ component and eventually to qI. V bound to L1 is not convertible to Z (Bassi and Caffarri, 2000; Jahns et al., 2001; Morosinotto et al., 2003; Liu et al., 2004b; Wehner et al., 2004; Standfuss et al., 2005; Wehner et al., 2006; Jahns et al., 2009; Di Valentin et al., 2009; Nilkens et al., 2010; Jahns and Holzwarth, 2012; Kress and Jahns, 2017).

Different views about the quenching function of Z in the antenna system or in the membrane has been proposed: (i) a direct quenching function of Z in qZ requires xanthophyll exchange in the V1 site of LHCII trimers and in the inner L2 site of the minor antennae (Dall'Osto et al.,

2012). This would imply first the release and the diffusion to the lipid phase of the thylakoid membranes of the V bound to the V1 and L2 site and re-binding of the Z to those specific binding sites (Dall'Osto et al., 2012); (ii) because the release of L2-bound V and the re-binding of Z after de-epoxidation would require a huge structural reorganization another view proposes that Z might act indirectly in the membrane or at the periphery of antenna complexes and that it has a more indirect role, especially in qZ and qI, for which is possible to observe a close correlation of their relaxation with Z epoxidation (Kress and Jahns, 2017).

1.2.2.2 The rapidly activated NPQ: energy-dependent quenching (qE)

The fast activation of qE allows a fine control of the absorbed EL. Indeed, qE is quickly activated under EL (10-200 s) but it also rapidly relaxes when light intensity decreases (10-60 s) and ΔpH decreases, allowing fast adjustment of LET to CO_2 fixation. The qE component of NPQ depends on ΔpH that is responsible for activation of both PSBS protein (PSBS-dependent qE) and VDE for Z accumulation (Z-dependent qE), ensuring that qE occurs only when absorbed EL needs to be dissipated. PSBS protein is a 22-kDa integral membrane protein composed of four helices and located in the thylakoid membrane of plants. Its function in qE was discovered 20 years ago (Niyogi et al., 2000) and a number of structural and functional information has been collected. However, its mechanism of action has not been completely dissected yet. PSBS has been found as dimer both in the inactive and active form (Fan et al., 2015) but several evidences proposed that PSBS is a dimer in the inactive form and acts as monomer in the active NPQ state (Correa-Galvis et al., 2016; Sacharz et al., 2017). Under EL the increased ΔpH leads to protonation of multiple glutamate residues exposed to the thylakoid lumen, which have been shown to be essential to induce a conformational change leading to PSBS activation (Li et al., 2004; Liguori et al., 2019). However, what happens after PSBS activation and how it can trigger the quenching of the absorbed EL is highly debated. Even though PSBS is a member of the LHC multigenic family and two putative Chl-binding sites are conserved in its sequence (Jansson et al., 2000), the recent PSBS crystal structure, obtained at pH 5, clearly shows that these sites are necessary to stabilize the structure but they do not bind pigment (Fan et al., 2015), suggesting that PSBS is not a quencher itself (Croce, 2015; Fan et al., 2015).

Protonation drives a systematic unfolding of a PSBS region which induce conformational changes and it seems to be important for protein-protein interactions, possibly docking to LHCII (Liguori et al., 2019) (**Figure 1.9**). While *in vivo* evidences are needed to better clarify the PSBS mechanism of action, PSBS activation has been proposed to induce conformational changes

in the LHCII through direct interaction with LHCII proteins. Indeed, in the dark-adapted state PSBS has been found to interact both with PSII core and LHCII proteins, while in the qE-active light-adapted state the interaction with LHCII trimers, and particularly with Lhcb1, has been documented (Correa-Galvis et al., 2016; Sacharz et al., 2017).

In the dark-adapted state, synthesis of qE-active Z represents the limiting-step for the qE induction. The generation of the Z-dependent qE happens within about 1–3 min upon illumination. Within this short time, a limited amount of Z can be synthesized through deprotonation of a specific pool of V bound to the V1 site of LHCII trimers (see paragraphs 1.1.1.1.3 and 1.2.2.1) (Nilkens et al., 2010). Furthermore, it seems that the presence of Z promotes the further interaction between PSBS and LHCII, involving not only the LHCII trimers (Correa-Galvis et al., 2016) but also the binding to the minor LHCII antenna Lhcb4, Lhcb5 and Lhcb6 (Sacharz et al., 2017).

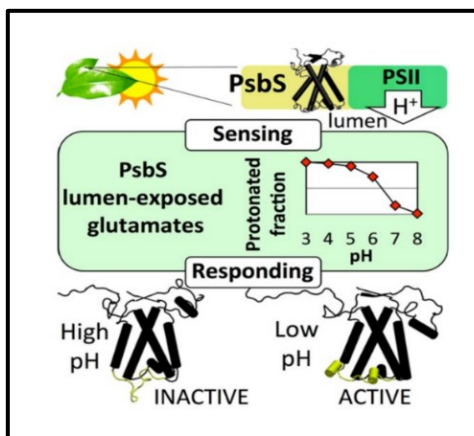


Figure 1.9. Model of PSBS activation and conformational change upon protonation of glutamate residues exposed to the luminal side of thylakoid membrane. Under EL PSBS is activated and deactivated by increased or decreased H^+ concentration in the thylakoid lumen. Multiple glutamates act as pH sensors and their protonation trigger a conformational change, exposing regions possibly involved in protein–protein interactions. Figure from Liguori et al., 2019.

1.2.2.3 The slow Z-dependent NPQ component (qZ)

qZ is a separate phase, distinct from qE and it is uniquely dependent on Z, which, except for its synthesis, does not require lumen acidification. This PsbS- and pH-independent qZ quenching process is generated within 10-20 min and involves probably the V pool bound to the more slowly releasable L2 binding sites in the LHCII (see sections 1.1.1.1.3 and 1.2.2.1). Relaxation of this phase requires 10-60 minutes (Nilkens et al., 2010).

1.2.2.4 qH and Inhibitory quenching (qI)

The antenna quenching component qH is a sustained slowly reversible form of energy dissipation that has been recently included within the several NPQ components (Malnoë et al., 2018; Malnoë, 2018). It includes mechanisms that previously has been attributed to the component qI, but it is independent of known components required for other types of NPQ, such as PSBS, Z, Δ pH formation, (Brooks et al., 2013). This component was thus termed qH to differentiate it from qI (Malnoë et al., 2018; Malnoë, 2018). qH component requires the plastid lipocalin (LCNP) (Malnoë et al., 2018; Malnoë, 2018) and its activation is prevented by SUPPRESSOR OF QUENCHING-1 (SOQ1) under non-stress conditions (Brooks et al., 2013). LCNP is a soluble protein of 29 kDa localized in the thylakoid lumen, whose expression is increased during abiotic stress (Malnoë et al., 2018; Malnoë, 2018). Determining the interactors of LCNP will provide insights in this newly described NPQ component. Speculations suggest that LCNP might act in the proximity or within the antenna proteins, triggering a conformational change that promote a dissipative state (Malnoë, 2018). SOQ1 is a chloroplast-localized membrane protein of 104 kD containing a thioredoxin-like and a β -propeller domain located in the lumen and a haloacid-dehalogenase domain exposed to the chloroplast stroma. SOQ1 was proposed to prevent formation of qH maintaining the efficiency of light harvesting (Brooks et al., 2013; Malnoë et al., 2018; Malnoë, 2018). Redox regulation of its activity was proposed based on the presence of the thioredoxin-like domain (Brooks et al., 2013; Malnoë et al., 2018; Malnoë, 2018).

The last component of NPQ, qI, reflects the processes that are associated with inactivation, degradation and replacement of photodamaged PSII components, especially the D1. qI has been associated with PSII photoinhibition rather than regulation of light harvesting. This very slow component develops slowly in the case of persistent EL (more than 30 min) and it is almost irreversible, taking several hours for relaxation which requires PSII repair processes and D1 turnover. qI also includes mechanisms for sustained quenching, as demonstrated by retention of high level of Z, which is very slowly reconverted to V (Nilkens et al., 2010; Jahns and Holzwarth, 2012; Townsend et al., 2018). It is not clear whether Z contribution to qI involves a direct interaction between Z and the PSII RC, if its function is limited to the protection of the PSII antenna proteins or if it is restricted to antioxidative function (Jahns and Holzwarth, 2012).

The sustained Z retention together with sustained downregulation and photoinhibition of PSII correlate with the slow Z epoxidation in this phase due to the gradual downregulation of ZEP after exposure to strong EL for a few hours or longer (Reinhold et al., 2008). In several higher plant species, degradation of ZEP protein was observed under photoinhibitory conditions in parallel with the D1 protein of PSII (Bethmann et al., 2019). Retention of high levels of Z accompanied by sustained Δ pH-independent energy dissipation and down-regulation of PSII activity has been observed under severe stress, as documented in overwintering evergreen plants (Verhoeven et al., 1998; Adams III et al., 2002; Öquist and Huner, 2003; Adams et al., 2004; Yamazaki et al., 2011), and it has been associated with PSII photoinhibition and the q1 component of NPQ (Bethmann et al., 2019).

1.2.3 Photosynthetic control at level of Cyt b₆f

In order to avoid PSI over-reduction, Cyt b₆f activity is thought to be finely regulated. Indeed, when PSI is limited by the availability of stromal acceptors (acceptor side limitation), electrons in excess can directly react with O₂ or with the PSI FeS clusters leading to photodamage of PSI RC and PSI photoinhibition (Tiwari et al., 2016). In response to the EL-induced luminal acidification, the affinity of Q_o sites for PQH₂ seems decrease, allowing a lower rate of electron transfer from PQH₂ to Pc and limiting in this way the amount of PSI electron donors and protecting PSI from photodamage induced by EL (Nishio and Whitmarsh, 1993; Joliot and Johnson, 2011; Colombo et al., 2016; Tikhonov, 2018). Photosynthetic control is strictly depending on Δ pH for its function and a correlation with cyclic electron transport (CET) has been reported (Colombo et al., 2016; Yamamoto and Shikanai, 2019) (see paragraph 1.2.4).

1.2.4 Cyclic electron transport around PSI

During the light reactions ca. three H⁺ are theoretically released in the lumen per each transported electron. The synthesis of a single molecule of ATP requires 4.7 H⁺ (Petersen et al., 2012). Thus, for every four electrons transported in the LET, two molecules of NADPH and 2.6 molecules of ATP are produced, leading to an ATP/NADPH ratio approximatively of 1.3. In C₃ photosynthesis under non-photorespiratory conditions, the fixation of one molecule of CO₂ in the CBB cycle requires three ATP and two NADPH, with a ratio of 1.5 (Arnon and Chain, 1975). The short ATP supply would slowdown photosynthesis at the final acceptors of LET, causing overreduction of LET components. In order to increase ATP/NADPH ratio, alternative pathways operate around PSI.

Among them, CET is able to re-address the electrons from PSI acceptors (Fd) to PQH₂ at Cyt b₆f, preventing the formation of further NADPH while increasing ATP production. Indeed, the electron recycling by CET provides an additional contribution to the generation of pmf needed for ATP synthesis and it balances the ATP/NADPH ratio according to the CBB cycle demand, consequently alleviating overreduction of PSI acceptors. Two major CET pathways have been described so far and they are unevenly distributed among photosynthetic organisms (Peltier et al.; Munekage et al., 2004; Yamori and Shikanai, 2016; Alboresi et al., 2019; Storti et al., 2020b) (**Figure 1.10**). The first depends on Proton Gradient Regulator 5 (PGR5) and PGR5-Like 1 (PGRL1) proteins (Munekage et al., 2002; DalCorso et al., 2008) and the second is mediated by NDH-1 complex, a multimeric complex which shares structural and evolutionary aspects with the mitochondrial respiratory complex I (Peltier et al.; Shikanai, 2015). The pmf formation is mostly due to LET, but CET also contributes to pmf generation: in isolated chloroplasts of *A. thaliana* the CET contribution to pmf has been estimated to be about 35% independently of NADPH production, balancing the ATP/NADPH; a contribution of ca. 30% and 5% has been estimated for PGR5- and NDH-1-dependent CET pathways, respectively (Kawashima et al., 2017).

The first CET pathway mediated by PGR5 and PGRL1 proteins is important in photoprotection under several environmental conditions and at different developmental stages, including under HL and FL (Munekage et al., 2002; DalCorso et al., 2008; Munekage et al., 2008; Suorsa et al., 2012; Suorsa et al., 2013; Suorsa, 2015; Colombo et al., 2016; Suorsa et al., 2016). Recycling electrons from Fd to PQ, the PGR5-PGRL1-dependent pathway should contribute to pmf formation with the release of four H⁺ in the lumen for every two electrons during the Q cycle. In *A. thaliana pgr5* mutants, the reduced pmf causes impairment of NPQ induction (Munekage et al., 2002; Kalituho et al., 2007), besides it does show much lower NPQ than what expected from the contribution of this pathway to pmf (Kawashima et al., 2017). Also, *pgr5* shows saturation of PSII electron transport at lower light intensity than in the WT. The resulting LET over-reduction accompanied by lower levels of ATP synthesis limits the CBB cycle and leads to a strong acceptor side limitation, and consequently PSI photodamage (Munekage et al., 2002; Kalituho et al., 2007). This also explains the lethal phenotype of *pgr5* mutant under certain regimes of FL (Tikkanen et al., 2010; Suorsa et al., 2012; Tikkanen et al., 2012; Allahverdiyeva et al., 2015; Suorsa et al., 2016).

NDH -1 complex has been proposed to pump four H⁺ into the lumen in addition to the 4 H⁺ translocated by the Q cycle at Cyt b₆f, thus translocating eight H⁺ for every two electrons transported (Shikanai and Yamamoto, 2017). However, in contrast to what has been shown for *pgr5* mutants, mutants lacking NDH-1 activity analyzed in several species such as *M. polymorpha*, *P.patens*, *N.tabacum*, *A.thaliana* and *O. sativa* and under several conditions showed very mild photosynthetic and growth phenotypes (Endo et al., 1999; Ishikawa et al., 2008; Yamori et al., 2011; Ueda et al., 2012; Martín et al., 2015; Yamori et al., 2015; Yamori et al., 2016; Storti et al., 2020a). Recently it has been shown that NDH-1 supports the lumen acidification in PSI-photoinhibited chloroplasts (Rantala et al., 2020). A physiological role of NDH in FL and in dark to light transitions has been recently proposed based on studies in *O. sativa* (Yamori et al., 2016), *A. thaliana* (Strand et al., 2017) and *P.patens* (Storti et al., 2020a). In *P.patens* mutants lacking the subunit NDH-M an increased PSI acceptor side limitation during limiting light condition and in the dark was observed, suggesting that NDH could be active in maintaining PSI acceptor side oxidized also in the darkness or under limiting light intensities, when the light-driven electron transport is reduced and thus the NDH activity could become physiologically more relevant (Storti et al., 2020a).

In *A.thaliana* and *P.patens* the lack of both the PGR5/PGRL1-dependent and NDH-dependent pathways causes much larger defect in electron transport capacity and growth compared to the two single mutants depleted either in PGR5 or NHD-1 activity (Munekage et al., 2004; Storti et al., 2020b), suggesting that the two pathways might have a redundant function in pmf formation. Genes encoding components of both NDH-1 and PGR5-PGRL1 pathways were found upregulated under FL compared to CL conditions (Schneider et al., 2019). Also, both PGR5 and NDH-1 systems were reported to be upregulated by PSI photoinhibition to protect the remaining functional PSI RC by enhancing the pH-dependent regulation of electron transfer from PSII to PSI (Rantala et al., 2020). Because of the slow turnover and less efficient repair mechanisms compared to PSII (see paragraph 1.2.6), PSI is efficiently protected by the presence of multiple, redundant mechanisms to ensure its stability under several environmental conditions. The redundancy of CET pathways underlines that not only they serve as regulatory mechanisms to respond to dynamic environmental changes, but they are also indispensable for photosynthesis, as demonstrated by the drastic impairment of photosynthesis and plant growth observed when they are completely absent (Munekage et al., 2004; Storti et al., 2020b).

The CET-dependent pmf, especially related to the PRGR5-PGRL1 pathway, it is also important to trigger those mechanisms that are dependent on luminal pH for their activation, such as NPQ (see paragraph 1.2.2) at the level of PSII and photosynthetic control at Q_o sites in the Cyt b_6/f (see paragraph 1.2.3) (Colombo et al., 2016; Suorsa et al., 2016; Yamamoto and Shikanai, 2019) (**Figure 1.10**). The estimated contribution of CET pathways to the total electron transport (Kawashima et al., 2017) does not correlate with the severe phenotype observed in mutants lacking both CET pathways (Munekage et al., 2004; Storti et al., 2020b). Rather than generate a sustained electron transport, the main biological role of CET is to protect PSI from over-reduction and damage by modulating photosynthetic control and slowing down the ETR to PSI and eventually allowing for re-oxidation of stromal acceptors (Kanazawa et al., 2017; Yamamoto and Shikanai, 2019; Rantala et al., 2020; Storti et al., 2020a; Storti et al., 2020b). Thus, CET protects photosystem I at both donor and acceptor sides, by increasing PSI donor side limitation and relaxing the acceptor side limitation (Yamamoto and Shikanai, 2019; Storti et al., 2020b). The strength of photosynthetic control and CET needs to be finely regulated to optimize electron distribution between PSII and PSI and to avoid the photoinhibition of both photosystems (Yamamoto and Shikanai, 2019).

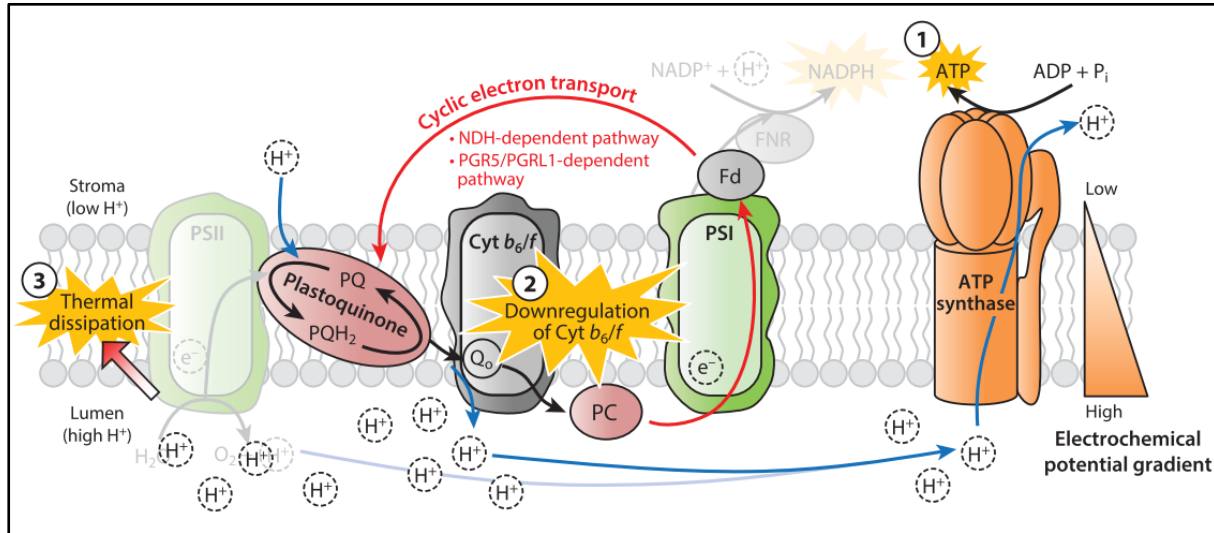


Figure 1.10. Physiological functions of PSI CET. In angiosperms, the two partially redundant pathways, PGR5/PGRL1-dependent pathway and the NDH-dependent pathway, contribute to generate pmf of across the thylakoid membrane. The ΔpH is used primarily to drive ATP synthesis without net production of NADPH in order to increase the ATP/NADPH ratio; The consequent acidification of the thylakoid lumen contributes to other regulatory mechanisms, such as the downregulation of electron transport through the Cyt b_6/f complex (photosynthetic control) and the induction of thermal dissipation (qE component) in PSII. These functions are essential to protect photosystems from irreversible photodamage. The solid black arrows indicate LET, the solid red arrows indicate CET around PSI, and the solid blue arrows indicate the movement of H⁺. Figure from Yamori and Shikanai, 2016.

1.2.5 Chloroplast ROS production and scavenging

The photoprotective mechanisms described in the previous sections are essential to limit the ROS production in the thylakoid membrane and thereby protect the photosynthetic apparatus from severe photodamage. However, ROS production is part of normal consequence of photosynthetic electron transport (PET) and it occurs at the levels of LHC (especially LHCII) and RCs of both PSII and PSI. Higher rates of ROS are generated when plants are exposed to environmental conditions that lead to saturation of PET (e.g EL or decreased CO₂ availability), requiring an increased antioxidant capacity which is acquired during long-term acclimation to those conditions. In the following sections, ROS production sources and scavenging systems in chloroplasts will be introduced.

1.2.6.1 ROS production in photosynthetic electron transport

PET reactions in the thylakoids lead to the production of several ROS, including the hydroxyl radical (OH \cdot), the superoxide anion radical (O₂ \cdot^-), singlet oxygen (¹O₂) and hydrogen peroxide (H₂O₂) (Leister, 2017; Czarnocka and Karpiński, 2018). As the majority of Chl is located in LHCs, generation of ³Chl* within the LHCs occurs commonly. However, it is also more easily scavenged by the antenna Car. ¹O₂ is the most common ROS generated during the PET processes, especially at level of PSII. As unsaturated fatty acid side chains are abundant in thylakoid membrane, reaction between ¹O₂ and these lipids can occur and produces hydroperoxides, initiating peroxy radical chain reactions in the thylakoid membrane. On the PSII electron donor side, perturbation of the enzymatic activity of the OEC can be coupled with incomplete oxidation of water to H₂O₂, which can react with the PSII-bound metals in a subsequent reaction, forming OH \cdot . Even though the production of ¹O₂ by charge recombination in the RCs has been described to mostly occur at level of PSII under photoinhibitory conditions, has also been described in PSI. Under EL the transient state of the excited P600 and P700 chlorophyll in PSII and PSI is de-excited to the triplet state (³P680 and ³P700) which can react with O₂ to produce ¹O₂ (Takagi et al., 2016). ¹O₂ production in RCs can be quenched by Car, tocopherol, PQ, and ascorbate (Miret and Munné-Bosch, 2015; Leister, 2017; Czarnocka and Karpiński, 2018). Since ¹O₂ is highly reactive, its generation in RCs can damage lipids, critical pigment cofactors, and protein subunits. In PSII the D1 damage has been largely described (see section 1.2.6.1) especially the D1 protein, resulting in photo-oxidative inactivation of the entire RC and consequently PSII photoinhibition (Aro et al., 1993; Niyogi, 1999a;

Allahverdiyeva and Aro, 2012; Li et al., 2018). $^1\text{O}_2$ seems to be one of the major cause of light-induced loss of PSII activity (Havaux, 2014; Pospíšil, 2016; Czarnocka and Karpiński, 2018). Also at Cyt b_6/f , plastosemiquinone ($\text{PQ}^{\cdot-}$) can react with molecular oxygen and produce $\text{O}_2^{\cdot-}$. PSI is the major site of ROS production in the PET (Takagi et al., 2016). Compared to PSII, PSI is more tolerant to EL but it is very sensitive to excess of electrons coming from PSI electron donors on the lumenal side, or/and insufficient capacity of electron acceptors at the stromal side (Tiwari et al., 2016). In these conditions electrons can reduce O_2 during the Mehler reaction and produce $\text{O}_2^{\cdot-}$, which is known to inactivate PSI iron-sulfur (FeS) clusters and cause PSI inhibition (Kono and Terashima, 2016; Takagi et al., 2016; Tiwari et al., 2016; Tikkanen and Grebe, 2018; Lima-Melo et al., 2019a; Yamamoto and Shikanai, 2019) (see section 1.2.6.2). At level of PSI ROS are generated by both excess electrons and EL: excess of electrons from PSII to PSI can be reduced by downregulating PSII activity and therefore LET. However, EL affects both photosystems and can induce formation of triplet P700, which trigger the production of $^1\text{O}_2$ to cause PSI photoinhibition (Takagi et al., 2016). Even though triplet P700 it is usually rapidly quenched by carotenoids, a contribution from $^1\text{O}_2$ generated from triplet P700 to photoinhibition under EL cannot be excluded (Takagi et al., 2016; Shimakawa and Miyake, 2018).

1.2.6.2 ROS scavenging

In order to balance redox activities and ROS production and prevent severe photodamage, chloroplasts possess both enzymatic and non-enzymatic antioxidants (Noctor et al., 2000; Bela et al., 2015). Enzymatic antioxidants include a broad range of enzymes such as superoxide dismutases, catalases, ascorbate peroxidases, glutathione reductases, monodehydroascorbate reductases, dehydroascorbate reductases, glutathione peroxidases (GPXs) and glutathione-S-transferases (Czarnocka and Karpiński, 2018). Generally, under oxidative stress conditions the activity of these enzymes (or some isoforms of these enzymes) increases as with enhanced tolerance of plants to such kind of stress (Kornas et al., 2010; Dietz and Pfannschmidt, 2011). In *A. thaliana* two GPXs, GPX1 and GPX7, are localized in the chloroplast and their expression is induced under both HL and FL (Bela et al., 2015; Schneider et al., 2019). Photoinhibition of PSII has been observed in plants with depletion in chloroplast GPX activity compared with WT, which were more sensitive to long-term photo-oxidative stress (Chang et al., 2009).

Besides enzymatic ROS scavengers, also non-enzymatic antioxidants such as ascorbic acid, glutathione, α -tocopherol and Car are important to mitigate ROS produced during photo/oxidative stress. Ascorbic acid is the most abundant antioxidant compound in plants and it serves as electron donor to a broad range of enzymatic and non-enzymatic reactions. It also participates in the regeneration of tocopherols and, in its reduced state acts as the cofactor of VDE in the xanthophyll cycle (Czarnocka and Karpiński, 2018; Noctor et al., 2018) (Hasanuzzaman et al., 2017; Czarnocka and Karpiński, 2018; Noctor et al., 2018). Tocopherols are lipophilic antioxidants, efficient in scavenging $^1\text{O}_2$ (protecting PSII) and, as they prevent the propagation of lipid peroxidation by lipid radicals, are essential in protecting biological membranes. α -tocopherol (vitamin E) has the highest antioxidant power and its levels change significantly in response to environmental stress conditions, conferring tolerance to adverse conditions such as EL (Havaux et al., 2005; Traber and Stevens, 2011; Czarnocka and Karpiński, 2018). Car are lipophilic antioxidants, involved not only in light absorption and NPQ but also in ROS scavenging, as demonstrated by their increased levels under abiotic stress conditions (Nisar et al., 2015; Czarnocka and Karpiński, 2018).

1.2.6 Photoinhibition and repair of photodamaged proteins in the photosynthetic apparatus

When the ROS production exceeds the capacity of ROS scavenging, cellular compounds and macromolecules are oxidized, leading to photodamage of proteins in the RCs and/or photo-inactivation of RC with consequent decrement in the maximum photosynthetic efficiency named photoinhibition. The net loss of photosynthetic activity occurs only when the rate of photodamage exceeds the rate of repair (Allahverdiyeva and Aro, 2012).

1.2.6.1 PSII repair

Photoinhibition is caused by dynamic imbalance between PSII photodamage and the turnover (inactivation, degradation, repair and replacement) of its components. When the photodamage of proteins in the PSII RC is not compensated by efficient repair mechanisms, PSII becomes downregulated and/or inactivated, with a consequence of decrease in photosynthetic efficiency. The D1 and D2 proteins contain binding sites for all the redox-active cofactors involved in the primary and secondary electron transfer in PSII. However, D1 protein more frequently undergoes irreversible oxidative photodamage by ROS generated in PSII.

Repair processes of PSII D1 protein have been described in detail (Baena-González and Aro, 2002) and its turnover has been shown to be an essential requisite for PSII recovery from photoinhibition. Under moderate EL, photoinhibition is reversible and the damaged D1 is removed, degraded and replaced with a neo-synthesized D1. However, under severe EL photoinhibition can be irreversible due to aggregation of D1 which prevent its removal and therefore the turnover (Aro et al., 1993; Allahverdiyeva and Aro, 2012; Yamamoto, 2016). After photodamage occurred, the LHCII antenna complex and OEC are separated from the PSII dimer to allow a partial disassembly of the core proteins. After monomerization of the PSII, monomers that need to be repaired migrate from the grana to the stroma-exposed membranes, where the degradation of the damaged D1 protein by specific proteases and the synthesis of the new D1 protein take place. Only the damaged PSII monomers are moved and repaired and the rest of the PSII proteins remains intact. Following the degradation of photodamaged D1, the de novo synthesized D1 protein is co-translationally inserted into the thylakoid membrane into the PSII monomers, and after re-assembly of the other subunits they can migrates back to the grana thylakoids (rewied by Allahverdiyeva and Aro, 2012). Interestingly, a close correlation of ZEP regulation and degradation with PSII photoinhibition and D1 repair has been recently reported in *A. thaliana*, *P. sativum*, *N. benthamiana* and *S. oleracea* during prolonged exposure to strong HL stress (Bethmann et al., 2019).

1.2.6.2 PSI repair

PSI is generally tolerant to HL but it is very sensitive to excess of electrons, conditions that occur either by delivery of excess electrons from the donor side (PSII) or by over-reduction of the electron acceptors at the acceptors side when CET and $\text{cyt}_{b_6/f}$ photosynthetic control are not efficient and/or stromal metabolism is slowed down. Under EL all the photoprotective mechanisms acting at the level of PSII, including NPQ, state transition and PSII photodamage itself, indirectly protect PSI against excess of electrons. However, when PSI photodamage occurs a long and costly process of repair is necessary to recover photosynthetic efficiency. Contrarily to PSII repair processes, in which PSII repair and photodamage happen concomitantly and photoinhibition is manifested as a sign of imbalance between these two events, repair of PSI starts only after plants are shifted to non-stressful conditions (Zhang and Scheller, 2004). PSI repair is a very slow process and still incomplete even after one week (Zhang and Scheller, 2004; Sonoike, 2011; Allahverdiyeva and Aro, 2012).

PSI photoinhibition studied in *A.thaliana* exposed to 8 h of chilling stress revealed that the damaged PSI was not degraded during the 8 h of light-chilling treatment, but after 12 h of recovery at 20°C (Zhang and Scheller, 2004). Unlike photodamaged PSII, the PSI core complex is not repaired but completely degraded. Also, while PSII fully recovered after 8 h at 20°C, the amount of PSI per leaf area remained low even after 1 week at 20°C (Zhang and Scheller, 2004). Thus, while in PSII repair the D1 protein undergoes a very fast turnover and the rest of the subunits are mostly recycled, all the PSI core subunits seem to be completely degraded while LHCl proteins are degraded much more slowly and to a smaller extent than the core subunits (Reviewed by Sonoike, 2011; Allahverdiyeva and Aro, 2012). PSI photoinhibition cause permanent loss of PSI activity and photoinhibited PSI RCs complexes are not repaired and/or replaced during the photoinhibitory conditions (Kudoh and Sonoike; Sonoike, 2011). Since the presence of light- absorbing pigment in the photoinhibited complexes that have lost the capacity to transfer electron can cause the further production of ROS and secondary damages, removal of P700 Chl without protein degradation has been postulated (Kudoh and Sonoike; Sonoike, 2011; Pinnola and Bassi, 2018) and loss of Chl absorption associated with photobleaching during the light treatment has been shown in photoinhibited LHCl-PSI (Ballottari et al., 2014). When plants are shifted back to recovery conditions destruction of P700 together with degradation of the PSI core proteins can occur (Zhang and Scheller, 2004; Allahverdiyeva and Aro, 2012; Chaux et al., 2015; Tiwari et al., 2016; Kono et al., 2017; Shimakawa and Miyake, 2018; Tikkanen and Grebe, 2018; Kadota et al., 2019; Lima-Melo et al., 2019a; Shimakawa and Miyake, 2019; Rantala et al., 2020).

1.2.6.3 Turnover of other proteins during photodamage

PSII repair has been studied for a long time and described in details (Adir et al., 2003) while PSI recovery from photoinhibition has been difficult to study and some of the mechanisms have been reported only in the last few years (Zhang and Scheller, 2004; Sonoike, 2011; Tiwari et al., 2016). A rapid turnover comparable to D1 protein has been recently reported for protein within the cytb₆f and the chloroplast NDH-1 complex, indicating a role of cytb₆f and the NDH-1 in photodamage and photoinhibition (Chotewutmontri and Barkan, 2016; Li et al., 2017; Li et al., 2018).

1.3 Long-term acclimation to EL requires Chloroplast-to-nucleus retrograde signaling

Long-term responses are globally called acclimation and involve reprogramming and regulation of nuclear and chloroplast gene expression. Persistent changes in the surrounding environment lead to the activation of long-term mechanisms which are slowly activated and slowly reversed. Responses such as reduction in LHC antennae size, PSI/PSII ratio, and the total number of RCs and LHC antennae are the result of transcriptional, translational and proteolytic regulation to adjust PET and metabolic sinks to better exploit the available excitation energy. Also the synthesis and accumulation of antioxidant molecules are induced or more pronounced during acclimation to EL (Havaux and Kloppstech, 2001; Xu et al., 2017). All these changes provide high flexibility to adjust photosynthetic performance to the changing environment. The acclimatory changes are ultimately reflected in chloroplast ultrastructure as well as plant growth and morphology. Molecular mechanisms of long-term acclimation involve communications between multiple cell compartments, cell types and organs (Davis et al., 2013; Wientjes et al., 2013; Dietz, 2015; Schumann et al., 2017). Chloroplast multi-subunits complexes in the photosynthetic apparatus, the transcription and the translation machineries, as well as the ancillary proteins needed for their folding and assembling, contain proteins encoded in both the nuclear and the plastid genomes (Timmis et al., 2004; Woodson and Chory, 2008; Leister et al., 2017). Thus, accurate coordination and regulation of the gene expression in these two compartments is essential for the proper functioning of the chloroplast metabolism. The plastid-encoded-plastid RNA polymerase (PEP) is a multi-subunit enzyme complex composed of plastid-encoded core subunits associated with a nuclear-encoded sigma factor (SIG), which directs and specifies the transcription initiation of plastid-encoded genes (PEG). SIGs are involved in acclimation processes as demonstrated by changes in their expression under different environmental conditions (Fujiwara et al., 2000; Tsunoyama et al., 2002; Nagashima et al., 2004; Onda et al., 2008). Numerous nuclear-encoded proteins (NEP) of plastids affect chloroplast activity and its gene expression through the so-called anterograde signaling. Chloroplast is also able to perceive its functional state and transmit this information to the nucleus through retrograde signaling in order to modulate and coordinate the nuclear gene expression (NGE) of NEP accordingly (Timmis et al., 2004; Woodson and Chory, 2008; Leister et al., 2017).

Chloroplast retrograde signals can be related to chloroplast biogenesis (biogenic control) or its operation in response to environmental changes (operational control) (Pogson et al., 2008; Estavillo et al., 2011; Woodson et al., 2011; Ramel et al., 2012; Xiao et al., 2012; Avendaño-Vázquez et al., 2014; Kleine and Leister, 2016; Phua et al., 2018).

The Car biosynthetic inhibitor norflurazon (NF) causes severe photooxidative damage which is accompanied by photobleaching, defects in chloroplast biogenesis and differentiation, and repression of gene expression of NEP such as *LHCB1.2*. NF has been used in the past to identify a collection of *A. thaliana* mutants which can accumulate LHCB1 mRNA despite the plastid development and chloroplast biogenesis had been blocked by the NF treatment (Pogson et al., 2008; Kleine and Leister, 2016). As these mutants seem to lack important component of retrograde signaling and communication between the nuclear and chloroplast genomes, they were named “genomes uncoupled” (GUN). Five GUN mutants (GUN1-GUN5) were identified in the first screening (Susek et al., 1993). Except GUN1, the other four were all found to be involved in tetrapyrrole biosynthesis (Susek et al., 1993; Mochizuki et al., 2001; Larkin et al., 2003), while GUN1 seems to integrate multiple retrograde signals derived from defects in the chloroplast redox state, plastid gene expression, proteostasis and tetrapyrrole biosynthesis both in seedlings and adult plants by interacting with proteins involved in these processes (Gray et al., 2003; Kleine and Leister, 2016; Tadini et al., 2016; Llamas et al., 2017; Pesaresi et al., 2019). Interestingly, a second screening identified other GUN mutants with more subtle phenotypes compared to the previous ones. This second screening identified some mutants that were allelic to the UV-A and blue light (BL) photoreceptor CRYPTOCHROME-1 (CRY1) and LONG HYPOCOTYL-5 (HY5), a transcription factor (TF) that is responsible for activation of many light-responsive genes. These findings suggest an interaction between plastid-to-nucleus retrograde signaling and nucleus-to-plastid light signaling. It has been proposed that plastid signals may modify light signaling, which plays an important role both in biogenic and operational control (Ruckle et al., 2007). The operational control of chloroplast retrograde signaling is linked to the function of the photosynthetic light reactions and guides the acclimation of the photosynthetic machinery to environmental changes to optimize photosynthetic performance, influencing also development, growth and physiological responses. Since changes in the chloroplast redox state reflect functional perturbation in photosynthesis caused by environmental fluctuations, redox signals from photosynthesis serve as the initial plastid signals that are mediated to the nucleus.

Environmental changes affect PET and result in changes in the redox state of the PET components (see section 1.3.1), such as the PQ pool, or those coupled to the PET, such as the thioredoxin pool (see section 1.3.2). Another important component of retrograde signaling directly connected to the PET functioning and redox state is the production of ROS (Pogson et al., 2008; Pfalz et al., 2012) (see section 1.3.3).

1.3.1 Redox state of PET components

The energetic state of PET reflects the functional balance between PSII and PSI as well as the balance between the PET and the energy consumed by metabolism. Excitation energy distribution and PET are dynamically regulated at the level of both photosystems and Cyt b_6/f to rapidly rebalance the redox state of PET upon environmental changes. The failure to effectively maintain PET generates signals by which the chloroplast can transmit information about environmental stress conditions and induce long-term acclimation responses through regulation of NGE. The redox state of PQ is very sensitive to any imbalance in the relative activities of PSII and PSI, as it is the intermediate electron carrier that connects PSII and Cyt b_6/f in PET (Gray et al., 2003; Pfalz et al., 2012; Gollan et al., 2015; Tikhonov, 2018). Under conditions favoring PSII, PSI becomes rate-limiting and the PQ pool receives more electrons from PSII than it can deliver to PSI, resulting in reduction of PQ. Under conditions favoring PSI the opposite situation is established and the pool becomes oxidized. In photosynthesis the PQ redox state controls phosphorylation of LHCII and the relative allocation of the mobile antenna between the two PS (termed state transitions; described in the section 1.2.1). (Gollan et al., 2015). State transition is important for maintaining the redox balance of PET and minimizes the formation of PSII-derived reactive molecules (Tikkanen et al., 2014a; Mekala et al., 2015). The failure in regulating state transition induces a prominent imbalance in PET and over-reduction of the PQ pool, which initiates light-responsive retrograde signaling mechanisms. The rate of PQH₂ oxidation is controlled by the ΔpH : the perturbed NGE profile observed in plants lacking PGR5 (see section 1.2.4) highlights the major role of ΔpH -mediated control of PET in chloroplast signaling (Gollan et al., 2015; Gollan et al., 2017).

1.3.2 Redox state of the components coupled with PET: thioredoxins

The Chloroplast TRX system provides protection against oxidative damage in fluctuating environments as it coordinates the activity and the rate of photosynthetic light reactions with carbon flow and metabolic processes downstream to PET, as well as the metabolism of ROS produced within the chloroplast during photosynthetic reactions, accordingly with the environmental conditions. TRXs regulate directly and indirectly several chloroplast processes by inducing reductive cleavage of a disulfide bond in the target proteins, increasing or decreasing their activity (Pogson et al., 2008; Leister, 2017; Nikkanen et al., 2018; Nikkanen and Rintamäki, 2019). TRXs targets participate in several metabolic pathways and stress-response: many enzymes in the CBB cycle, starch biosynthesis, chlorophyll biosynthesis and proteins involved in CET and state transition are target of TRXs. (Nikkanen and Rintamäki, 2014; Leister, 2017; Nikkanen and Rintamäki, 2019).

Two classes of TRX can be distinguished depending on the sources of reducing power: (i) NADPH-dependent chloroplast thioredoxin reductase (NTRC) is reduced by NADPH, which is generated both in the light by PET and in the darkness in the Oxidative Pentose Phosphate Pathway; (ii) Ferredoxin-thioredoxin reductases (FTR) are reduced by fd produced during PET in the light (Pérez-Ruiz et al., 2006; Schürmann and Buchanan, 2008; Nikkanen et al., 2016; Nikkanen et al., 2018; Nikkanen and Rintamäki, 2019). In the darkness a small fraction of NTRC is already partially active due to NADPH produced in the Oxidative Pentose Phosphate Pathway. During the dark to light transitions this NTRC pool transiently activates CET (see section 1.2.4) that helps to alleviate the pressure at the PSI acceptor side before the full activation of the CBB cycle (Thormählen et al., 2017; Nikkanen et al., 2018; Nikkanen and Rintamäki, 2019). Also, under light intensities limiting photosynthesis, NTRC activates the ATP synthase (see section 1.1.1.3) and redox-regulated enzymes of the CBB cycle (see section 1.1.2), increasing the electron sink capacity of the stroma and alleviating the PSI acceptor side limitation (Carrillo et al., 2016; Nikkanen and Rintamäki, 2019). In conjunction with NTRC activity (Nikkanen et al., 2016; Nikkanen and Rintamäki, 2019), FTR types TRXs are activated under growth light and higher irradiance, by the photosynthetically reduced fd and further activate CET, to avoid over-reduction of the photosynthetic electron transport chain and allow efficient oxidation of PSI, protecting it from photodamage (Nikkanen et al., 2018; Nikkanen and Rintamäki, 2019).

1.3.3 ROS signaling

The maintenance of a balance between ROS production and ROS scavenging ensures energy and metabolic fluxes, adjusting different cell functions and triggering acclimation responses against oxidative stress through retrograde signaling (Pfalz et al., 2012; Suzuki et al., 2012; Czarnocka and Karpiński, 2018; Foyer, 2018). Among the ROS produced during PET, OH^\cdot , $\text{O}_2^{\cdot-}$ and $^1\text{O}_2$ have a short lifetime and it is unlikely that they can leave the chloroplast and acts as signal in the nucleus. However, OH^\cdot might be formed in the nucleus from H_2O_2 (Leister, 2017) and both $\text{O}_2^{\cdot-}$ and $^1\text{O}_2$ have been associated with regulation of NGE, with specific transcriptome signatures (Scarpeci et al., 2008; Leister, 2017). It has been proposed that $^1\text{O}_2$ -dependent retrograde signaling pathway uses second messenger metabolites, initiated in the thylakoid membrane (Havaux, 2014; Wang et al., 2016; Leister, 2017). For example, during the $^1\text{O}_2$ -mediated lipid peroxidation, quenching of $^1\text{O}_2$ by chloroplast antioxidants (especially β -carotene) gives rise to reactive electrophile species (RES), that can act as second messengers to relay the $^1\text{O}_2$ signal beyond the chloroplast (Farmer and Mueller, 2013; Leister, 2017). H_2O_2 signaling is known to occur under both biotic and abiotic stress. It is produced by SOD-mediated dismutation of $\text{O}_2^{\cdot-}$ or via oxidases activity. Compared to the other ROS, it is more stable and able to cross membranes. Besides the chloroplast, H_2O_2 production takes place also in the apoplasts, mitochondria, and peroxisomes, which makes it difficult to distinguish chloroplast-signaling from signaling triggered in other cellular compartments. It has been proposed that H_2O_2 produced in chloroplasts might reach the nucleus avoiding the transit in the cytosol through the chloroplast stromules, which provide physical connections with the nucleus (Farmer and Mueller, 2013; Leister, 2017; Mullineaux et al., 2020).

1.4 Photoreceptors mediated light signaling

Light information is perceived both at the level of chloroplast and via photoreceptors. Photoreceptors are sensors that transmit light information, allowing plants to adjust physiology and development according to the light environment (**Figure 1.11**). As described in the previous section, the plastid signals generated under EL are able to influence the nuclear and chloroplast gene expression through retrograde signaling (**Figure 1.11 A**). However, this transcriptional adjustment, which is part of acclimation processes to photo-oxidative stress, seems to involve several signaling pathways, in which photoreceptors also play direct and indirect roles (**Figure 1.11 B**) (Kleine et al., 2007; Alboresi et al., 2011; Fankhauser and Ulm, 2011b; Engelhard et al., 2014; Consentino et al., 2015; Fortunato et al., 2015; Rusaczek et al., 2015; Pearce et al., 2016; Petroutsos et al., 2016; Demarsy et al., 2018). Variations in light environment are sensed by photoreceptors, which are photo-reversible proteins with a prosthetic group/cofactor or an intrinsic amino acid (tryptophan) as a chromophore (D'Amico-Damião and Carvalho, 2018). Plants possess multiple and specialized classes of photoreceptors that are able to perceive the light environment in terms of quality and quantity (**Figure 1.12**). In *A. thaliana* five classes of photoreceptors have been identified (**Figure 1.12 A**) (Kami et al., 2010), which are conserved in most higher plants.

UV-B (280–315 nm) is sensed by ULTRAVIOLET-B RECEPTOR-8 (UVR8) (Kliebenstein et al., 2002; Rizzini et al., 2011a; Cloix et al., 2012), UV-A and BL perception (315–500 nm) involves three classes of photoreceptors: I) cryptochromes (CRYs; CRY1, CRY2 and CRY3), II) phototropins (PHOT; PHOT1 and PHOT2) and III) zeitunglupe family (ZTL; FKF1 and LKP2) (Fankhauser and Staiger, 2002). Although CRY3 (or cry-DASH) belongs to the CRY family, it is thought to be involved in DNA repair and its role in light perception is not clear (Pokorny et al., 2008; Zirak et al., 2009; Gärtner, 2017). Lastly, five phytochromes (PHY; PHYA-PHYE) mainly absorb red (RL, 600–700 nm) and far-red light (FRL 600–700 nm) (Rockwell et al., 2006; Jiao et al., 2007; Franklin and Quail, 2010; Kami et al., 2010; Rockwell and Lagarias, 2010). Photoreceptors are essential to perceive light and trigger light-dependent processes controlling the developmental transitions and physiological responses to sustain plant growth and development. For example, PHYs, CRYs, and UVR8 photoreceptors are involved in regulation of de-etiolation, during which plants switch from the growth in darkness (skotomorphogenesis) to the growth in the light (photomorphogenesis) (**Figure 1.13 B**).

Photomorphogenesis includes many changes in seedling morphology, such as a short hypocotyl and open green cotyledons, which require a broad reprogramming of gene expression for the photosynthetic lifestyle (Jiao et al., 2007; Kami et al., 2010; Podolec and Ulm, 2018). Other photomorphogenic processes mediated by photoreceptors include germination, phototropism, shade avoidance, leaf and rosette morphogenesis, chloroplast movement and flowering transition (Jiao et al., 2007; Kami et al., 2010; Podolec and Ulm, 2018). Several of these photomorphogenic responses are largely governed by the photosynthetically active, visible light spectrum (400–700 nm).

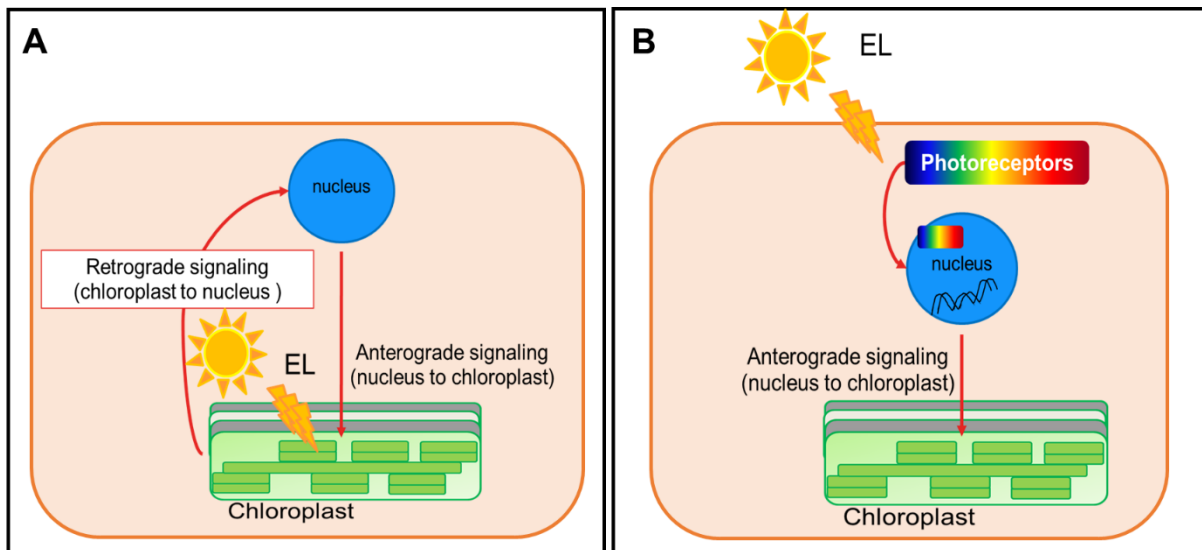


Figure 1.11. EL perception and gene expression regulation through plastid and photoreceptor signaling. **A)** Light stress perception by chloroplast triggers retrograde signaling to the nucleus to regulate the nuclear gene expression in response to photo-oxidative stress. **B)** Light signaling via photoreceptors leads to transcriptional regulation of light-responsive genes, many of which encode proteins in plastids (anterograde signaling).

1.4.1 Light signaling mediated by different photoreceptors converge in regulation of the central hub COP1/SPA complex

Upon light activation UVR8, CRY1, CRY2 and PHYs physically interact with TFs as well as with the E3 ubiquitin ligase system. This central light signaling hub is composed of CONSTITUTIVELY PHOTOMORPHOGENIC 1 (COP1) and SUPPRESSOR OF PHYA-105 (SPA) proteins (**Figure 1.12 C**) and represents a major repressor of photoreceptor-mediated photomorphogenic responses (Podolec and Ulm, 2018). The COP1 E3 ubiquitin ligase activity depends on SPA accessory proteins.

In *A. thaliana* genome contains four genes encoding SPA proteins (*SPA1-4*), which share functional redundancy (Hoecker, 2005; Fittinghoff et al., 2006). It has been shown that after COP1 homodimerization, it directly interacts with two of the four possible SPA proteins, forming COP1/SPA tetrameric complexes with nuclear E3 ubiquitin ligase activity (Zhu et al., 2008; Podolec and Ulm, 2018). COP1/SPA regulates the stability of photomorphogenesis-promoting TFs that regulate the expression of many light responsive genes (**Figure 1.12 C**) Thus, the photoreceptor-mediated inhibition of COP1/SPA repressive activity results in activation of light-responsive genes and photomorphogenic responses (**Figure 1.12 C**).

The activity of the COP1/SPA complex is required during seedling etiolation in the dark, which is inhibited by light signaling mediated by the action of PHYs, CRYs and UVR8 (Reviewed by Podolec and Ulm, 2018; Lau et al., 2019). The convergence of the photoreceptor signaling pathways at COP1/SPA enables plants to integrate different light signals to trigger appropriate photomorphogenic responses in response to the light environment (reviewed by Podolec and Ulm, 2018; Lau et al., 2019). However, the interactions of light-activated photoreceptors with the COP1/SPA complex are distinct for each photoreceptor. Both CRY1 and CRY2 interact directly with COP1 (Wang et al., 2001; Yang et al., 2001). However, whereas the CRY1-COP1 interaction is dependent on SPA proteins, the CRY2- COP1 interaction does not involve them (Holtkotte et al., 2017; Podolec and Ulm, 2018). RL-activated PHYA and PHYB interact with SPA proteins and inhibit COP1/SPA complex activity by disrupting the interaction between COP1 and SPA proteins, releasing TFs such as HY5, LONG HYPOCOTYL IN FAR-RED 1 (HFR1), LONG HYPOCOTYL AFTER FAR-RED 1 (LAF1) and CONSTANS (CO) from the COP1/SPA1 repression (Lu et al., 2015b; Sheerin et al., 2015; Podolec and Ulm, 2018). UV-B-activated UVR8 interacts directly with COP1, but in contrast to PHYs and CRYs it does not interact with SPA and the COP1–SPA interaction remains intact upon interaction with UVR8 (Favory et al., 2009; Rizzini et al., 2011b; Heijde et al., 2013; Huang et al., 2013; Podolec and Ulm, 2018) (**Figure 1.12 C**).

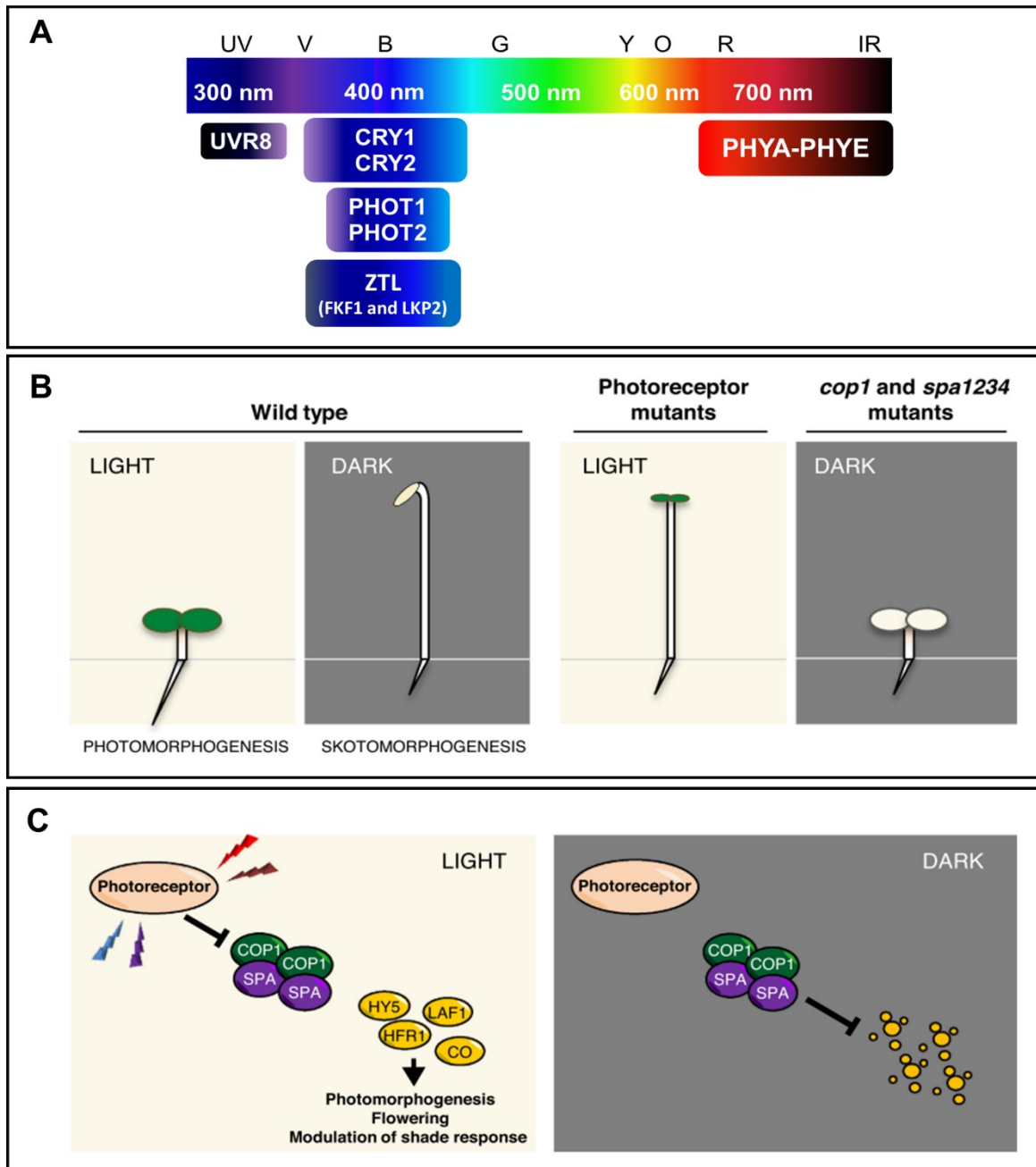


Figure 1.12. Photoreceptors and their roles in photomorphogenesis. **A)** Different photoreceptors identified in *A. thaliana*. **B)** Light-grown WT seedlings undergo photomorphogenesis (open green cotyledons, short hypocotyl) as opposed to dark-grown seedlings that undergo skotomorphogenesis (closed cotyledons, apical hook, elongated hypocotyl). Photoreceptor mutants grown in light resemble dark-grown WT seedlings, whereas dark-grown *cop1* and *spa1234* mutants exhibit constitutive photomorphogenesis. **C)** Regulation of photomorphogenesis by photoreceptors and the COP1/SPA complex: Light-activated photoreceptors inactivate the COP1/SPA complex through various mechanisms, repressing its E3 ubiquitin ligase activity and stabilizing photomorphogenesis-promoting TFs. In darkness, photoreceptors are inactive and photomorphogenesis-promoting TFs are ubiquitinated by the COP1/SPA complex and degraded by the 26S proteasome. Figures B) and C) were modified from Podolec and Ulm, 2018

1.4.2 Transcriptional regulation via photoreceptors through HY5

Light triggers transcriptional reprogramming of ca 35% of the whole *A. thaliana*'s genome (Tepperman et al., 2004). The perception of light by photoreceptors activates several intermediary TFs that belong to diverse families and specifically act downstream of either single or multiple photoreceptors (Gangappa et al., 2013b; Gangappa and Botto, 2016). Among the TFs that integrate signals from photoreceptors, HY5 emerges as a central regulator of fundamental developmental processes such as seedling development in terms of cell elongation, cell proliferation, chloroplast development, pigment accumulation, and nutrient assimilation (Gangappa et al., 2013b). HY5 acts downstream to PHYs, CRYs, and UVR8 and plays a key role in promoting photomorphogenesis in all light conditions. Indeed, *hy5* mutant seedlings exhibit very long hypocotyl under RL, BL, FRL and UV-B light (Gangappa and Botto, 2016). Also, HY5 stability seems to be directly proportional to the increasing light intensity, indicating a key role of HY5 in dynamic response to environmental cues such as EL (Osterlund et al., 2000; Gangappa and Botto, 2016). HY5 is a basic domain/leucine zipper (bZIP) TF which is able to bind to several consensus sequences in promoters of many genes (Gangappa and Botto, 2016) to regulate their transcription. Besides its role in photomorphogenesis, HY5 has also been shown to induce transcriptional regulation of genes involved in anthocyanin biosynthesis, chlorophyll biosynthesis, sucrose metabolism, and ROS signaling (**Table 1.1**) (Gangappa and Botto, 2016). Interestingly HY5 induces its own expression in all light conditions by directly binding to its own promoter, suggesting a mechanism of autoregulation (Abbas et al., 2014; Binkert et al., 2014; Gangappa and Botto, 2016). HY5 regulates both early and late anthocyanin biosynthetic genes (Shin et al., 2007; Shin et al., 2013; Gangappa and Botto, 2016), and it is also required for chlorophyll and carotenoids biosynthesis (Toledo-Ortiz et al., 2014) and components of LHCBs (Lee et al., 2007; Toledo-Ortiz et al., 2014). The most important genes involved in some of these HY5-regulated pathways are reported in **Table 1.1** (re-adapted from Gangappa and Botto, 2016). HY5 acts also in synergy with other TFs such as HYH (*ELONGATED HYPOCOTYL 5-HOMOLOG*) and members of the B-box (BBX) family (Gangappa et al., 2013b). HY5 and HYH act both as heterodimers and homodimers, mediating light-regulated expression of overlapping as well as distinct target genes (Holm et al., 2002a; Jing et al., 2013). HYH is predominantly involved in BL signaling and its function partially overlaps with that of HY5. Indeed, the accumulation of HYH protein is dependent on the presence of HY5 and its expression is induced by HY5 itself (Holm et al., 2002a).

Pathway	Target gene
Light signaling	<i>HY5 (ELONGATED HYPOCOTYL-5)</i>
	<i>BBX-22 (B-BOX DOMAIN PROTEIN- 22)</i>
	<i>COP1 (CONSTITUTIVE PHOTOMORPHOGENIC-1)</i>
	<i>FHL (FHY1-LIKE)</i>
	<i>HYH (ELONGATED HYPOCOTYL 5-HOMOLOG)</i>
	<i>HFR1 (LONG HYPOCOTYL IN FAR-RED 1)</i>
Photosynthesis-related genes	<i>CAB1/LHCB1.3 (LIGHT-HARVESTING CHLOROPHYLL A/B 1.3)</i>
	<i>PSY (PHYTOENE SYNTHASE)</i>
	<i>LHCA4 (PHOTOSYSTEM I LIGHT HARVESTING COMPLEX)</i>
	<i>PORC (PROTOCHLORPHYLLIDE OXIDOREDUCTASE C)</i>
	<i>GUN5 (GENOME UNCOUPLED 5)</i>
	<i>ELIP-2 (EARLY LIGHT INDUCED PROTEIN 2)</i>
	<i>RBCS-1A (RIBULOSE BISP HOSPHATE CARBOXYLASE SMALL CHAIN 1A)</i>
ROS-related genes	<i>APX2 (ASCORBATE PEROXIDASE 2 SIGNALING)</i>
	<i>SIB1 (SIGMA FACTOR BINDING PROTEIN 1)</i>
	<i>ERF4 (ETHYLENE RESPONSIVE ELEMENT BINDING FACTOR 4)</i>
	<i>SIB4 (SIGMA FACTOR BINDING PROTEIN 4)</i>
	<i>NDB2 (NAD(P)H DEHYDROGENASE B2)</i>
Anthocyanin biosynthesis	<i>CHS (CHALCONE SYNTHASE)</i>
	<i>CHI (CHALCONE ISOMERASE)</i>
	<i>FLS (FLAVONOL SYNTHASE)</i>
	<i>MYB12 (MYB DOMAIN PROTEIN 12)</i>
	<i>MYB111 (MYB DOMAIN PROTEIN 111)</i>
	<i>PAP1 (PRODUCTION OF ANTHOCYANIN PIGMENT1)</i>
	<i>MYBD (MYB-LIKE DOMAIN)</i>

Table 1.1 Key genes that are regulated by HY5 (modified from Gangappa and Botto, 2016).

1.4.3 Phytochromes

The PHYs are a multigenic family that in *A. thaliana* is composed of five PHYs (PHYA-PHYE) (Quail, 1994; Wang and Wang Deng, 2004; Krahmer et al., 2018). PHYA is most abundant in dark-grown seedlings and undergoes rapid degradation upon exposure to RL or white light, while PHYB-PHYE are light-stable (Somers and Quail, 1995; Clough and Vierstra, 1997; Clough et al., 1999; Wang and Wang Deng, 2004; Rattanapisit et al., 2016). In light-grown plants PHYB is the most abundant isoform, while PHYC-PHYE are less abundant (Hirschfeld et al., 1998; Wang and Wang Deng, 2004).

PHYs are dimeric apoproteins with covalently linked to phytochromobilin, a linear tetrapyrrole that functions as chromophore (Chen and Chory, 2011; D'Amico-Damião and Carvalho, 2018). PHYs sense primarily RL and FRL (600-750 nm). RL is absorbed by the inactive form of PHY (Pr), which absorbs maximally at 660nm. Upon RL illumination, the Pr form undergoes conformational changes and thereby become converted to the biologically active form (Pfr) which absorbs maximally at 730 nm. Concomitantly, PHY moves from the cytosol to the nucleus, where, besides the interaction with COP1/SPA1 system, it regulates transcription through direct binding to PHYTOCHROME INTERACTING FACTORS (PIFs) (Ngoc Pham et al., 2018).

PIFs negatively regulate photomorphogenesis by interacting with PHYs and thereby hindering the promoter binding of the latter (Ngoc Pham et al., 2018; Al-Sady et al., 2006; Castillon et al., 2007; Leivar and Quail, 2011; Leivar and Monte, 2014). Also, PIFs facilitate phosphorylation and proteolysis of PHYs. In the darkness PIF1 interacts with COP1 to enhance the repressive activity of the COP1/SPA complex. Upon exposure to light, PIF1 is destabilized in a PHY-dependent process, which contributes to inactivation of the COP1/SPA complex (Xu et al., 2014; Zhu et al., 2015). Upon absorption of FRL or via slow dark reversion in the absence of light, the Pfr form is converted back to the Pr form and moves back to the cytosol (Kendrick and Kronenberg, 1994; Quail, 1994; Wang and Wang Deng, 2004; Franklin and Quail, 2010; Krahmer et al., 2018).

Phytochromes are involved in shade avoidance response (SAR), which allows plants to sense the presence of neighbor plants and involves several reprogramming at the level of growth and metabolism to better cope with potential shading and competition for light. While several PHYs contribute to SAR, PHYB plays a particularly prominent role. Indeed, *phyB* KO mutants display classical SAR traits such as perturbed seedling deetiolation, altered leaf morphology with elongated petiole, small leaf blades and reduced biomass (Yang et al., 2016; Kraehler et al., 2018). A complex regulatory network involving all PHYs and especially PHYB has been shown to participate in a wide range of processes which indirectly affect photosynthesis.

RL induces the formation of Chl in *A. thaliana* WT seedlings within hours (Ghassemian et al., 2006; Kraehler et al., 2018), while sequential PHY depletion in RL-grown *phyB*, *phyABDE*, and *phyABCDE* mutant seedlings leads to concomitant reduction in chlorophyll levels (Hu et al., 2013; Kraehler et al., 2018). Short-term irradiation of plants with low-intensity RL, which increases the content of Pfr, has been associated with an increased accumulation of Car and flavonoids and a shift in the balance between oxidants and antioxidants towards the latter (Kraehler et al., 2018; Kreslavski et al., 2018). Indeed, PHYs regulate positively HY5 and negatively PIFs, which alters the transcription and the abundance of various photosynthetic components such as CAB genes (encoding for LHCs), Rubisco small subunit (Thompson and White, 1991; Kraehler et al., 2018; Kreslavski et al., 2018), as well as Chl and Car biosynthetic genes, such as PHYTOENE SYNTHASE (PSY), PROTOCHLOROPHYLLIDE REDUCTASE C (PORC) VDE and GUN5 (Leivar et al., 2009; Kraehler et al., 2018).

Together with CRYs, PHYs also contribute to transcriptional regulation of proteins involved in chloroplast metabolism and the CBB cycle (e.g Rubisco and Rubisco activase) and play a role especially at medium to high fluence light (Fox et al., 2017; Kraehler et al., 2018). Indeed, under these conditions the quadruple *phyA;phyB;cry1;cry2* mutant displayed reduced levels of Chl, LHCs, and the CBB-cycle proteins together with reduced CO₂ fixation (Fox et al., 2017). Interestingly, PHYB also influences stomatal density and leaf thickness, two other important factors for leaf photosynthetic performance (Boccalandro et al., 2009; Kraehler et al., 2018).

1.4.4 Cryptochromes

CRYs are the only photoreceptors present across the most lineages and are widely distributed in bacteria and eukaryotes (Lin and Todo, 2005; Chaves et al., 2011), indicating a vital role during the evolution of organisms on earth. Their function has evolved differently in different organisms, undergoing diverse specialization. In plants CRYs govern several developmental processes in response to UV-A and BL, such as light-mediated suppression of hypocotyl elongation, control of flowering time, promotion of leaf and cotyledon expansion and root growth, resetting of circadian clock, regulation of chlorophyll and anthocyanin biosynthesis and other physiological and developmental processes (Yu et al., 2010).

CRYs are flavoproteins consisting of an apoprotein with two prosthetic groups (**Figure 1.13 A**), the N-terminal photolyase homology-related domain (PHR) and a CRY C-terminal extension domain (CCE). The PHR domain has high homology to DNA photolyases but without photolyase activity and it contains the non-covalent binding site for two chromophores, 5, 10-methenyl tetrahydrofolate (MTHF) and flavin adenine dinucleotide (FAD). FAD is a chromophore for BL while MTHF chromophore is a derivative of pterine that acts in the UV-A region, transferring excitation energy to FAD, which is a catalytic cofactor (D'Amico-Damião and Carvalho, 2018). On BL /UV-A light exposure, the pterin chromophore acts as a “light-harvesting antenna pigment”, which transfers the excitation energy to the catalytic cofactor, FAD. The FAD chromophore can exist in multiple redox states (**Figure 1.13 B**): oxidized (FAD_{ox}), semiquinone (FADH^{\bullet}), and fully reduced (FADH_2). Each of these states has different absorption characteristics: the maximum absorption for FAD_{ox} is 450 nm, while that for pterin is 380 nm (Saxena et al., 2005; Hoang et al., 2008; Mishra and Khurana, 2017). Notably, FAD is oxidized in the dark-adapted state of the receptor and it becomes reduced in the presence of light, forming the neutral radical (FADH^{\bullet}) which is correlated with the signaling function. Subsequent to FAD reduction, flavin re-oxidation occurs in a light-independent reaction, leading to the production of ROS (Consentino et al., 2015; El-Esawi et al., 2017). In addition to perceiving the light, the PHR domain is also responsible for the dimerization of CRY. Moreover, photoactivation of CRYs requires BL-dependent phosphorylation events which take place at multiple sites along the CCE domain. BL-dependent phosphorylation correlates with the physiological activities of CRYs and the level of phosphorylation increases with increasing BL fluence rate and irradiation periods (Shalitin et al., 2002; Shalitin et al., 2003; Tan et al., 2013; Liu et al., 2016).

In *A. thaliana* three CRYs were identified (CRY1, CRY2, and CRY3). The amino acid sequence of CRY2 contains a nuclear localization signal (NLS) which targets CRY2 to the nucleus (Kleiner et al., 1999), while CRY1 lacks NLS and has been detected both in the nucleus and cytoplasm in both dark and light conditions without a drastic change of relative subcellular concentrations (Cashmore et al., 1999; Wu and Spalding, 2007; Yu et al., 2010). Considering the dual localization of CRY1, a mechanism of nucleus-to-cytoplasm translocation has been proposed, which supposedly occurs upon transition from dark to BL (Ahmad et al., 1998; Yang et al., 2000; Lin and Shalitin, 2003). Such relocation of CRY1 was observed in wheat (Xu et al., 2009) but not in rice (Matsumoto et al., 2003). The functions of these two pools of CRY1 with different subcellular localizations are still unclear. Since regulation of gene expression is generally associated with nuclear localization and CRY1 is known to regulate gene expression of a large number of light-regulated genes, it is usually assumed that CRY1 exerts its function (i.e. active) when it is in the nucleus. However, a study carried out by Wu and Spalding (2007) has demonstrated separate functions for nuclear and cytoplasmic CRY1 in controlling distinct processes related to photomorphogenesis in *A. thaliana* seedlings. The nuclear CRY1 protein seems to be responsible for BL-dependent inhibition of hypocotyl elongation, whereas the cytosolically localized CRY1 may mediate BL stimulation of cotyledon expansion and root elongation (Wu and Spalding, 2007; Yu et al., 2010). In contrast, CRY2 appears to complete its post-translational life cycle in the nucleus and mediates floral induction and inhibition of hypocotyl elongation (Yu et al., 2007).

The light-stable CRY1 acts under relatively high-intensity BL, while the light-labile CRY2 acts mainly under low-intensity BL during early seedling development (Ahmad et al., 1998a; Lin et al., 1998; Lin, 2002; Shalitin et al., 2002). For example, during de-etiolation of *A. thaliana* at low light fluence rates both CRY1 and CRY2 contribute to the BL-induced inhibition of hypocotyl elongation and promotion of cotyledon expansion; at higher light fluence rates, CRY2 is degraded and the light-stable CRY1 is thought to mediate the BL responses (Liu et al., 2017). Among CRYs, only CRY1 and CRY2 are thought to function as photoreceptors in light signaling pathways, while CRY3, which is localized in chloroplast and mitochondria (Kleine et al., 2003), seems to be a DASH protein that serves for repairment of UV-damaged organelle DNA in a light-dependent manner (Mishra and Khurana, 2017; D'Amico-Damião and Carvalho, 2018). Both CRY1 and CRY2 interact with COP1 and SPA1 protein (reviewed by Liu et al., 2016; Podolec and Ulm, 2018).

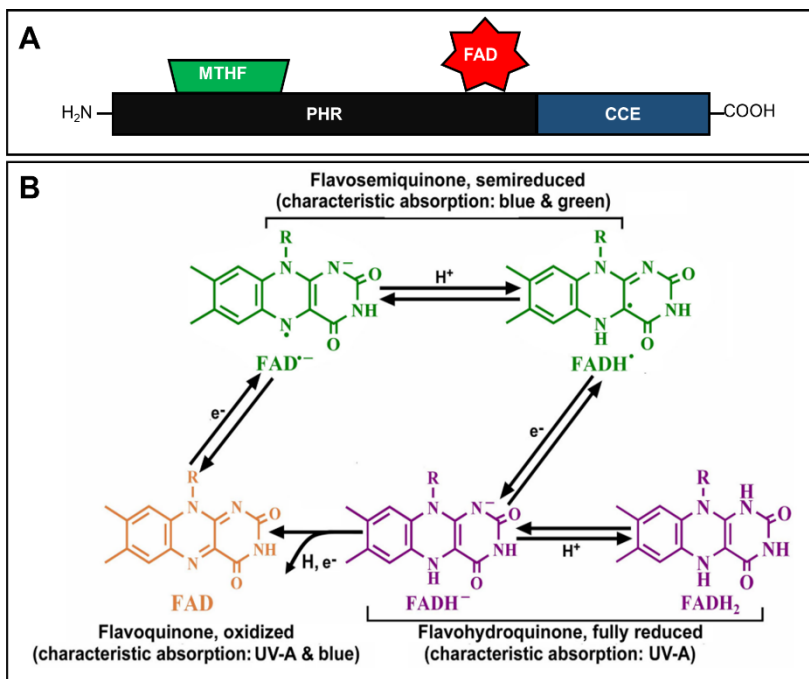


Figure 1.13. Domain structure of CRYs and associated chromophores. **A)** CRY's apoproteins consist of the N-terminal photolyase-homologous region (PHR) domain and the CRY C-terminal extension (CCE) domain. The CRY chromophores MTHF and FAD are bound to PHR. **B)** Five possible redox forms of flavin chromophore (R indicates different side groups in different flavins) are shown. The two different forms of semiquinone radicals: anion radical (FAD^{•-}) and neutral blue radical (FADH[•]), and two forms of reduced flavins: protonated hydroquinone (FADH₂) and anionic hydroquinone (FADH^{•-}). Figure B from (Yu et al., 2010).

1.4.4.1 Role of CRY1 in light-responsive gene expression and photo-oxidative stress

In *A. thaliana* CRY1 and CRY2 regulate ca. 45 BL-induced genes encoding proteins which tend to be localized in chloroplasts (Ohgishi et al., 2014). BL and CRYs are responsible for the induction of proteins involved in both photosynthetic light reactions (e.g D2), and the CBB cycle (e.g phosphoribulokinase, sedoheptulose bisphosphatase, and fructose bisphosphate aldolase) (Ohgishi et al., 2004). Some of these genes were also found upregulated in leaf transcriptome of FL-treated *A. thaliana* plants compared to CL plants (Schneider et al., 2019).

As described in paragraph 1.3, it is known that specific nuclear-encoded SIGs of PEP RNA polymerase activate subsets of plastid gene promoters, inducing the transcription of important components of the photosynthetic machinery such as PSII RC proteins D1 and D2, encoded by *psbA* and *psbD*, respectively (Onda et al., 2008). Transcription of SIGs in *A. thaliana* is regulated by photoreceptors and photosynthesis (Onda et al., 2008; Mellenthin et al., 2014; Belbin et al., 2017). In particular, *SIG1* was strongly increased under RL, while BL illumination of dark-adapted plants rapidly and strongly increased the level of both *SIG5* and *SIG1*, and slowly induced a low/medium transcription of *SIG2*, *SIG3*, *SIG4* and *SIG6* (Onda et al., 2008).

Interestingly, BL induction of *SIG5* showed a two-phase fluence response: a lower-fluence induction followed by an enhancement in response to increasing fluence rates. Both CRY1 and CRY2 are involved in the lower-fluence induction of *SIG5*, while only CRY1 is responsible for the greater induction observed under higher fluences (Onda et al., 2008). *SIG5* was also found to be upregulated in WT leaf transcriptomes of *A. thaliana* in EL conditions, such as HL and FL (Kleine et al., 2007; Schneider et al., 2019). Notably, the CRY-dependent rapid induction of *SIG1* is mostly mediated by CRY1 at both lower and higher BL fluences (Onda et al., 2008). It has been proposed that *SIG5* may promote light-responsive transcription in plastids through the activation of its expression by photoreceptors. In particular, the circadian regulation of plastid transcription mainly depends on BL and CRYs whereas the response to RL to FRL ratio was found to involve PHYs and photosynthetic signals (Belbin et al., 2017). Numerous studies have demonstrated the contribution of CRYs in acclimation responses to HL stress by looking at the regulation of redox equilibrium of PET, Chl *a* to Chl *b* ratio (Chl *a/b*) and LHCB contents under HL (Walters et al., 1999; Weston et al., 2000; D'Amico-Damião and Carvalho, 2018).

In *A. thaliana* the BL- and CRY1-dependent transcriptional induction of HL-responsive genes has been investigated by comparing *cry1* and *hy5* knock-out (KO) mutants with WT under BL, CL and HL (Kleine et al., 2007). PSII photoinhibition and photobleaching was observed in *cry1* KO plants (*cry1-304*) under HL. Furthermore, analysis of seedling leaf transcriptome revealed 48 genes that were differentially expressed in *cry1-304* compared to WT under the CL and 77 genes under the HL condition. Interestingly, the expression of *HY5* was induced by HL exposure in WT and the response was dependent on CRY1, as *HY5* was downregulated in *cry1* compared to WT both under CL and HL. Among the 77 HL-induced genes, 26 were commonly misregulated also in *hy5* KO mutant, indicating that those genes are under the control of CRY1 through light signaling pathways mediated by *HY5* (Kleine et al., 2007).

Consistent with the involvement of both CRY1 and *HY5* in the induction of anthocyanin biosynthetic genes, genes encoding the TFs PAP1 (PRODUCTION OF ANTHOCYANIN PIGMENT1; MYB75) and PAP2 (PRODUCTION OF ANTHOCYANIN PIGMENT2, MYB90), both involved in the regulation of anthocyanin biosynthesis components, were found downregulated in *cry1* and *hy5* KO mutants under HL (Kleine et al., 2007). Some of these strongly HL-induced genes code for stress-related proteins, such as GPX7 and EARLY LIGHT INDUCED PROTEINs (ELIP) 1 and 2, which were found misregulated in both *cry1-304* and *hy5* mutants (Kleine et al., 2007). GPX7 is a chloroplast GPX with a crucial role in regulation of photo-oxidative tolerance during acclimation to photo-oxidative stress (Chang et al., 2009).

ELIPs are thylakoidal proteins typically expressed under environmental conditions inhibiting photosynthesis such as HL, UV and cold stress (Hayami et al., 2015, Adamska et al., 1999). It is thought that ELIPs are involved in protective mechanisms (Adamska et al., 1999) and their expression increases in condition of PSII photodamage (Heddad et al., 2006). Interestingly the expression *SIG5*, *GPX7* and *ELIPs* was also upregulated (3-4 fold change or more) in leaves of WT during acclimation to photo-oxidative stress induced by FL (Schneider et al., 2019). Under these conditions also BLUE-LIGHT INHIBITOR OF CRYPTOCHROMES-1 (*BIC1*), which encodes a protein that inhibits light-induced dimerization and activation of CRYs, was upregulated together with *HYH*, but not *HY5* (Schneider et al., 2019). These observations further support a role of BL and especially CRY1 in acclimation to EL. However, the mechanisms by which CRY1 controls acclimation to EL and photooxidative stress are not yet understood.

In a screening to identify the genes involved in the integration of light and plastid signaling, mutants that were allelic to CRY1 and HY5 were identified as GUN mutants suggesting an interaction between retrograde signaling and light mediated anterograde signaling (Ruckle et al., 2007) (see paragraph 1.3). In *cry1* mutants treated with inhibitors of chloroplast biogenesis the *LHCB* mRNA accumulation was less impaired compared to treated WT, indicating that CRY1 represses *LHCB* expression when chloroplast biogenesis is blocked. (Ruckle et al., 2007; Larkin and Ruckle, 2008). In *cry1gun1* double mutants *LHCB* was synergistically derepressed, suggesting that CRY1 and GUN1 are responsible almost of the entire repression of *LHCB* in BL. These data indicate that a plastid signal can convert CRY1 into a negative regulator of *LHCB* (Larkin and Ruckle, 2008). Plastid signals that affect photomorphogenesis in *A. thaliana* are dependent on GUN1 and CRY1 (Ruckle and Larkin, 2009). These evidences suggest that GUN1 and CRY1 contribute to integrate chloroplast function with photomorphogenesis (Ruckle et al., 2007; Larkin and Ruckle, 2008; Ruckle and Larkin, 2009; Ruckle et al., 2012).

In this context, the role of CRY1 in ROS signaling and ROS production during CRYs inactivation deserve some considerations (Consentino et al., 2015; El-Esawi et al., 2017). Recently, it has been reported that plant CRYs release ROS including H_2O_2 and $O_2^{\cdot-}$ during reoxidation of the flavin cofactor from the light-activated radical ($FADH^{\cdot}$) or reduced ($FADH^-$) state back to the oxidized ($FADox$) dark-adapted state. ROS production by CRYs has also been proposed to play a signaling role in response to BL exposure, which acts additively and complementary to the known signaling mechanisms (Consentino et al., 2015; El-Esawi et al., 2017).

Despite their capacity to produce ROS, it would not be predicted to have a great impact on overall ROS production in the cell, as the CRY photocycle is relatively slow (several minutes) and therefore only a few molecules of ROS would be generated in this timescale. However, as they are localized in the nucleus it has been proposed that the amount of ROS produced in this compartment might be powerful enough to directly contribute to ROS signaling by increasing the local concentration of ROS near TFs to which CRYs have not been reported to bind directly, but which are assembled into the same complexes (Consentino et al., 2015; El-Esawi et al., 2017). For example, G-Box binding TFs are known to bind promoter elements related to HL stress signaling and are localized in close proximity to CRYs in the nucleus, as both are bound either directly or indirectly to COP1 (Gangappa et al., 2010; Gangappa et al., 2013d; Gangappa et al., 2013c). Thus, light activation and inactivation of CRYs could provide a localized burst of ROS that may be sufficient to induce a transcriptional response around light- and stress-responsive G-box promoters (Consentino et al., 2015; El-Esawi et al., 2017).

Is not clear yet whether these elements are subjected to redox regulation and how ROS interact with these TFs to alter their transcriptional regulation. ROS-responsive elements in the promoters of the responsive genes, have been described (He et al., 2018) and Intra-or intermolecular disulfide bond formation serves as a direct regulatory switch for several TFs (Antelmann and Helmann, 2011; He et al., 2018). For example, The *A. thaliana* bZIP16 binds to the HL-responsive G-box-containing LHCB2.4 and a conserved cysteine residue was shown to be necessary for redox regulation and enhancement of DNA binding activity (He et al., 2018).

2. AIMS OF THE THESIS

Extensive studies in the past have advanced our knowledge on regulatory mechanisms of photosynthesis and photoprotection. However, most of these studies were conducted in plants that were grown under CL, which is very different from dynamically changing light environments found in nature. In this work I studied dynamic regulation of photosynthesis and long-term strategies of plants to acclimate their photosynthetic apparatus to photo-oxidative stress induced by EL in the model organism *A. thaliana*. A previous study carried out in our research group (Schneider et al., 2019) have identified many differentially expressed genes in leaves of *A. thaliana* under photo-oxidative FL conditions compared to CL conditions. Long-term acclimatory responses involve reprogramming, regulation and coordination of nuclear and chloroplast gene expression and therefore communications between multiple cell compartments, cell types and organs is an essential requisite (Davis et al., 2013; Wientjes et al., 2013; Dietz, 2015; Schumann et al., 2017). A role of circadian clock and light signal, in particular the CRY-dependent BL signaling, in orchestrating the global adjustments of gene expression during acclimation to dynamic EL (i.e. FL) conditions has been proposed (Schneider et al., 2019), which may operate in parallel with, or interact with the chloroplast-to-nucleus retrograde signaling (Kleine et al., 2007; Ruckle et al., 2007; Larkin and Ruckle, 2008; Ruckle and Larkin, 2009; Ruckle et al., 2012)

Thus, this study first addresses the question about the functional relationship between CRY1-dependent BL signaling and plant photosynthetic acclimation to different light conditions (*i*). Since CRY1 has been found in the nucleus as well as in the cytoplasm (Cashmore et al., 1999; Wu and Spalding, 2007; Yu et al., 2010), an attempt was also made to inspect the physiological functions of nuclear and cytoplasmic localization of CRY1 in photosynthetic acclimation to EL (*ii*). Additionally, possible functions of an interesting candidate gene, which was upregulated in *A. thaliana* leaves under FL (Schneider et al., 2019) and has been suggested as one of the genes involved in the integration of light and plastid signaling (Ruckle et al., 2012), were also investigated (*iii*).

In concrete, the aims, questions and approaches of each section are as follows:

- (i) To characterize the role of CRY1 in photosynthetic acclimation by comparing the *cry1* KO mutant, *cry1-304*, with the corresponding WT plants under different light conditions. To further examine the previously described HL sensitive phenotype of *cry1-304* (Kleine et al., 2007) and to evaluate the photosynthetic and growth responses under FL regimes. To find out the cause of the EL sensitivity of this mutant.
- (ii) To study the photosynthetic phenotypes of the previously described transgenic *A. thaliana* lines overexpressing CRY1 exclusively in the nucleus, in the cytoplasm, or in both (Wu and Spalding, 2007). To generate the same set of new CRY1 transgenic lines but without the fusion to green fluorescent protein (GFP) to rule out possible side effects of GFP on CRY1 activity. To validate the photosynthetic phenotypes related to specific CRY1 localization in these new lines.
- (iii) To infer possible functions of the candidate gene (*AT3G56290*) via *in silico* analyses, such as protein sequence and phylogenetic analysis as well as gene co-expression analysis. To generate targeted KO lines of *AT3G56290* by means of the CRISPR/Cas9 method (Hahn et al., 2017a; Hahn et al., 2017b) and characterize their photosynthetic phenotypes under different light conditions (CL, FL and HL) to assess physiological consequence of the gene mutation.

3. RESULTS

3.1 Characterization *cry1-304* of under EL

In order to clarify the role of CRY1 in photosynthetic acclimation, the photosynthetic and growth phenotypes were analyzed in plants of wildtype (WT Col-0) and *CRY1* KO mutant (*cry1-304*) under EL. Plants grown under constant low light (CL, 100 $\mu\text{mol photons m}^{-2} \text{s}^{-1}$) were exposed to a dynamic EL (fluctuating light, FL, abrupt HL pulses of 1000 $\mu\text{mol photons m}^{-2} \text{s}^{-1}$ for 30 s every 10 min in the background of CL) or to constant EL (high light, HL, 1000 $\mu\text{mol photons m}^{-2} \text{s}^{-1}$) and compared with the plants that stayed under CL. Leaf growth and photosynthetic parameters were monitored during long-term EL exposure, along with the analyses of protein levels, pigment composition, and gene expression.

3.1.1. Visual and Growth phenotypes under HL and FL

Under CL little differences were observed between WT Col-0 and *cry1-304* (**Figure 3.1**). As expected, *cry1-304* plants showed elongated petiole compared to WT Col-0 (Ahmad and Cashmore, 1996; Ahmad and Cashmore, 1997; Ahmad et al., 2002; Millenaar et al., 2009; Keller et al., 2011). However, they were very sensitive to HL, as reported previously (Kleine et al., 2007), showing photobleaching of leaves already on the second day of the treatment. This severe phenotype was not observed in the WT Col-0 under the same conditions, even though it showed some typical HL responses, such as anthocyanin accumulation (Chalker-Scott, 1999; Gould, 2004; PAGE et al., 2012; Maier and Hoecker, 2015) and leaf curling (Mishra et al., 2012), which were not observed in HL-treated plants of *cry1-304*. The FL treatment did not cause bleaching or cell death in *cry1-304* and WT Col-0 (**Figure 3.1 A**). Leaf growth was monitored for six days by measuring the projected leaf area every two days by using the GROWSCREEN-FLUORO (Jansen et al., 2009). Under CL the projected leaf area of *cry1-304* increased exponentially as it did in WT Col-0. Leaf expansion was slowed down both in WT Col-0 and *cry1-304* in the HL and FL conditions compared to the CL condition. The projected leaf area of *cry1-304* decreased in HL because the cotyledons and first true leaves bleached and thus were not detected as leaf area (**Figure 3.1 B**). Growth impairment was observed in *cry1-304* under both FL and HL treatments compared to the CL and WT Col-0 in the same conditions.

Since the FL treatment did not cause leaf bleaching in *cry1-304*, but it still had a clear effect on the growth phenotype, the following analyses were performed focusing on the FL-treated plants in comparison with the CL-treated plants.

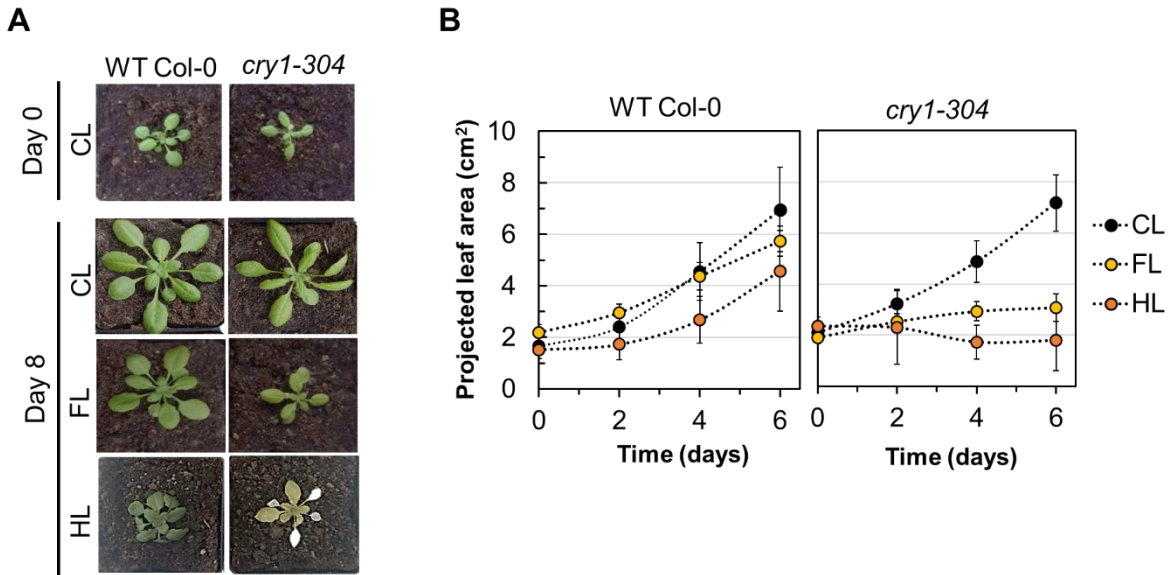


Figure 3.1. Visual and growth phenotypes of WT Col-0 and *cry1-304* growing under different light regimes (constant low light, CL, fluctuating light, FL and constant high light, HL). **A**) Visual phenotypes of representative plants before the onset of the light treatments (day 0) and at the end of the treatments (day 8). **B**) Leaf expansion growth monitored as changes in the total projected leaf area (cm²) for six days. Data are mean values \pm SD (n = 10-26 plants).

3.1.2. Induction of photosynthetic responses at the level of PSII in *cry1-304* in comparison with WT and other photoreceptor mutants and *hy5hyh*

While some light signaling pathways are mediated by specific photoreceptors, other signaling components can interact with multiple photoreceptors. Indeed, many photoreceptors signaling pathways converge in the transcriptional activation of genes controlled by HY5 by inactivating the COP1/SPA1 complex in the nucleus (Osterlund et al., 2000; Gangappa and Botto, 2016; Podolec and Ulm, 2018; Lau et al., 2019b). This has been shown for CRY1, CRY2 (Wang et al., 2001; Yang et al., 2001; Mao et al., 2005; Fankhauser and Ulm, 2011), PHYA (Saijo et al., 2003) and PHYB (Lu et al., 2015a), as well as for UVR8 (Cloix et al., 2012). In order to check whether the CRY1-mediated photosynthetic acclimation to EL is influenced by other major photoreceptors (CRY2 and PHYB) or involves light-responsive transcription factors (HY5 and/or HYH), plants of *CRY1CRY2* double KO (*cry1cry2*), *PHYB* KO (*phyB*) and *HY5HYH*

double KO (*hy5hyh*) mutants were studied under the FL condition along with WT Col-0 and *cry1-304*. Since the *hy5hyh* mutant is in Wassilewskija (Ws) background, Wt Ws was also included as the control for this line.

The Chl fluorescence parameters related to PSII activity were evaluated by measuring light induction curves in mature leaves after three days of CL and FL exposure (**Figures 3.2 – 3.4**). The maximum quantum yield of PSII in the overnight dark-adapted state (F_v/F_m) in mature leaves is shown in **Figure 3.2 A**, together with the color-coded images (**Figure 3.2 B**) illustrating the heterogeneity among different leaves within the rosette. CL-treated plants of *cry1-304* displayed comparable values of F_v/F_m with WT Col-0 and the other genotypes analyzed (**Figure 3.2 A**). However, after three days of exposure to FL *cry1-304* exhibited significantly lower F_v/F_m values compared to CL-plants and to the other genotypes under the same conditions, indicating PSII photoinhibition, especially in the mature leaves. In contrast, F_v/F_m did not change much in the other genotypes. Although FL-treated plants of *phyB* also showed significantly lower F_v/F_m compared to WT Col-0 under the same condition, their values did not significantly differ between FL and CL. In both conditions *phyB* tended to have lower F_v/F_m values than WT Col-0 (**Figure 3.2 A**), especially in young leaves (**Figure 3.2 B**) which were not used for the light induction measurements.

The induction measurements (**Figure 3.3**) showed reduced quantum yield of PSII in the light ($Y(II)$) in both CL and FL-treated plants of *cry1-304* compared to all other genotypes. Consequently, the CL-treated plants of *cry1-304* had lower relative electron transport rate of PSII ($ETR(II)$) than the other genotypes at the end of the light induction measurements, with a decrease of ca. 33% compared to WT Col-0. Notably, the FL-treated plants of *cry1-304* showed full reduction of PSII (zero $Y(II)$) upon illumination and no sign of photosynthetic induction (leading to re-oxidation of PSII or increase in $Y(II)$) until the end of the 260-s exposure to the blue actinic light (AL) intensity of $550 \mu\text{mol photons m}^{-2} \text{s}^{-1}$. In contrast, the other genotypes as well as the CL plants of *cry1-304* were capable of increasing $Y(II)$ during the 260-s light induction and thus also $ETR(II)$ values derived thereof. A slightly lower $ETR(II)$ was also observed in the CL plants of *cry1cry2* compared to WT Col-0 (ca. 16% less) but the FL plants of this mutant were able to perform photosynthetic induction to achieve $ETR(II)$ values comparable with WT Col-0.

The light-induced development of NPQ (**Figure 3.3** and **3.4**) was comparable in all the genotypes analyzed, except for *cry1-304*. NPQ tended to be lower in the CL plants of *cry1-304* compared to the corresponding plants of WT Col-0 and the other genotypes. The FL-treated plants of WT Col-0, *phyB*, WT Ws and *hy5hyh* tended to increase the NPQ capacity after 3-d exposure to FL (**Figure 3.3**), especially in young leaves (**Figure 3.4 B**). In contrast, NPQ developed quickly in the CL plants of *cry1-304* upon illumination but it did not increase further (**Figure 3.3**). The FL-treated plants of *cry1-304* had even lower NPQ levels and there was almost no relaxation of NPQ during the 60-s dark recovery, indicating that their NPQ was not rapidly reversible qE. When the NPQ values measured after 160 s of AL illumination were compared (**Figure 3.4 A**), the CL and FL plants of *cry1-304* had ca. 42% and 81% lower NPQ respectively, compared to the corresponding plants of WT Col-0, especially in the mature leaves (**Figure 3.4 B**). Somewhat reduced levels of NPQ were also found in mature leaves of the FL plants of *cry1cry2* and *phyB* compared to WT Col-0 after 160 s of AL illumination, but these mutants did not display severe NPQ impairment as found in *cry1-304* plants (**Figure 3.4 A**). Indeed, CL- and FL-treated *cry1cry2* had ca. 14% and 26% lower NPQ values, respectively, compared to WT Col-0 in the same conditions, while in CL- and FL-treated *phyB* plants NPQ was 13% and 15% lower than WT Col-0 under the same conditions (**Figure 3.4 A**).

It should be noted that the NPQ levels shown in **Figures 3.3.** and **3.4** do not include photoinhibitory quenching (qi) that was already present in some of the plants prior to the AL illumination, as can be noted by the low values of F_v/F_m reported in **Figure 3.2 A**. Thus, the NPQ data in **Figures 3.3** and **3.4** represent only the fraction of NPQ that developed during the AL illumination.

Overall, the results in **Figures 3.1 – 3.4** confirm the high sensitivity of *cry1-304* to EL, and in addition, suggest its limited ability to rapidly activate photosynthesis and develop NPQ (specifically qE) upon illumination. These limitations were already detected in the CL plants of *cry1-304* but were strongly exacerbated following a few days of FL exposure. The phenotype observed in *cry1cry2* plants was milder compared to *cry1-304*. The depletion of CRY2 in *cry1cry2* double mutant does not seem to intensify the negative effects on photosynthetic responses observed in the *cry1* single mutants, but it rather alleviates a part of these effects, suggesting that CRY1 and CRY2 do not have redundant roles in acclimation to EL. Thus, the roles of CRY2, PHYB, HY5 and HYH in photosynthetic acclimation to EL examined in the CL and FL conditions seemed to be minor compared to CRY1.

At the level of PSII, *cry1-304* was the only genotype that displayed strikingly lower photosynthetic and photoprotective capacity both under CL and EL conditions and were not able to acclimate to EL (neither to FL nor to HL).

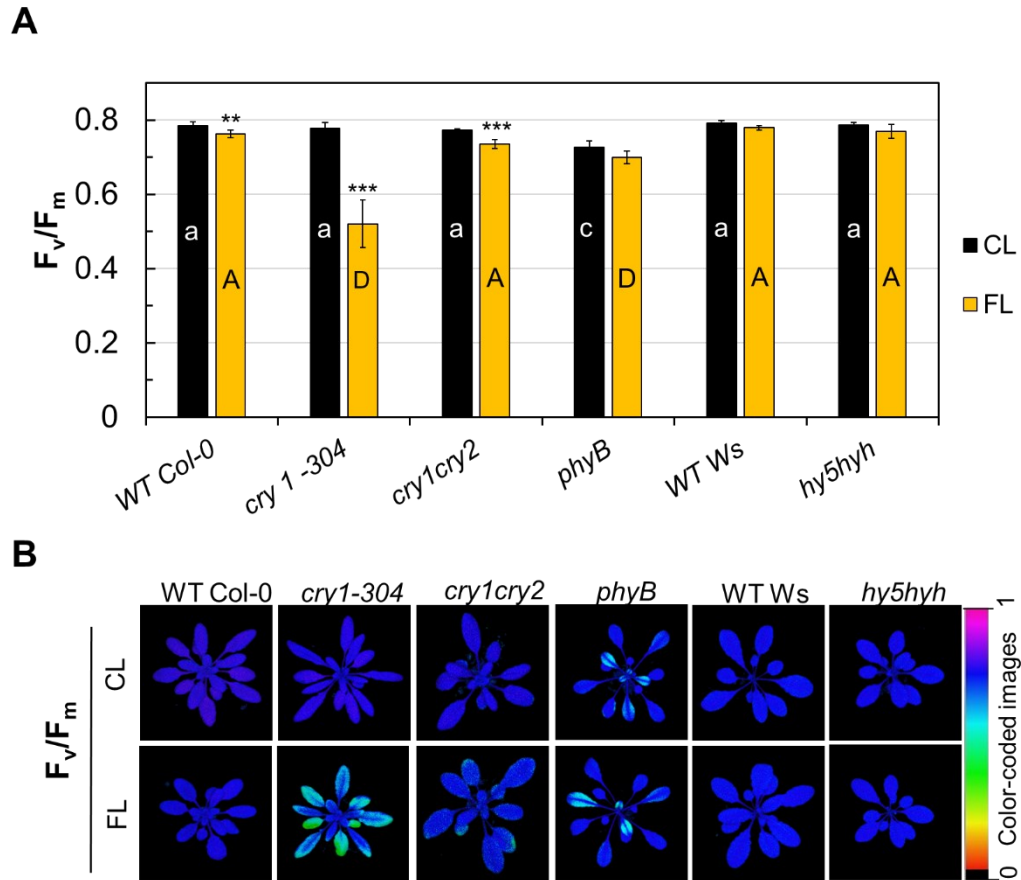


Figure 3.2: Maximum quantum yield of PSII in the overnight dark-adapted state (F_v/F_m) after three days under CL and FL. **A)** F_v/F_m values of the mature leaves used for the photosynthetic induction measurements shown in Figure 3.3. Significant differences between the genotypes as well as between the light conditions (CL and FL), and the interaction (genotype X light condition) were assessed by two-way ANOVA followed by Tukey's multiple comparison test. Different letters in the panel indicate significant differences in comparison to the corresponding WT: *cry1-304*, *cry1cry2* and *phyB* were compared to WT Col-0 and *hy5hyh* to WT Ws. Letter shared in common between the genotypes indicate not significant difference between their mean (c, $P \leq 0.01$; D, $P \leq 0.001$). Lowercase and uppercase letters are for the comparison between the genotypes under CL and FL, respectively. The differences between the light treatments within the same genotype (FL vs CL) were assessed by unpaired independent Student t-test and significant differences are indicated by asterisks (** $P \leq 0.01$, *** ≤ 0.001). Mean values \pm SD are shown ($n = 3-11$ plants). **B)** Spatial heterogeneity of F_v/F_m in whole rosettes. The color bars on the right show the scale of the color code.

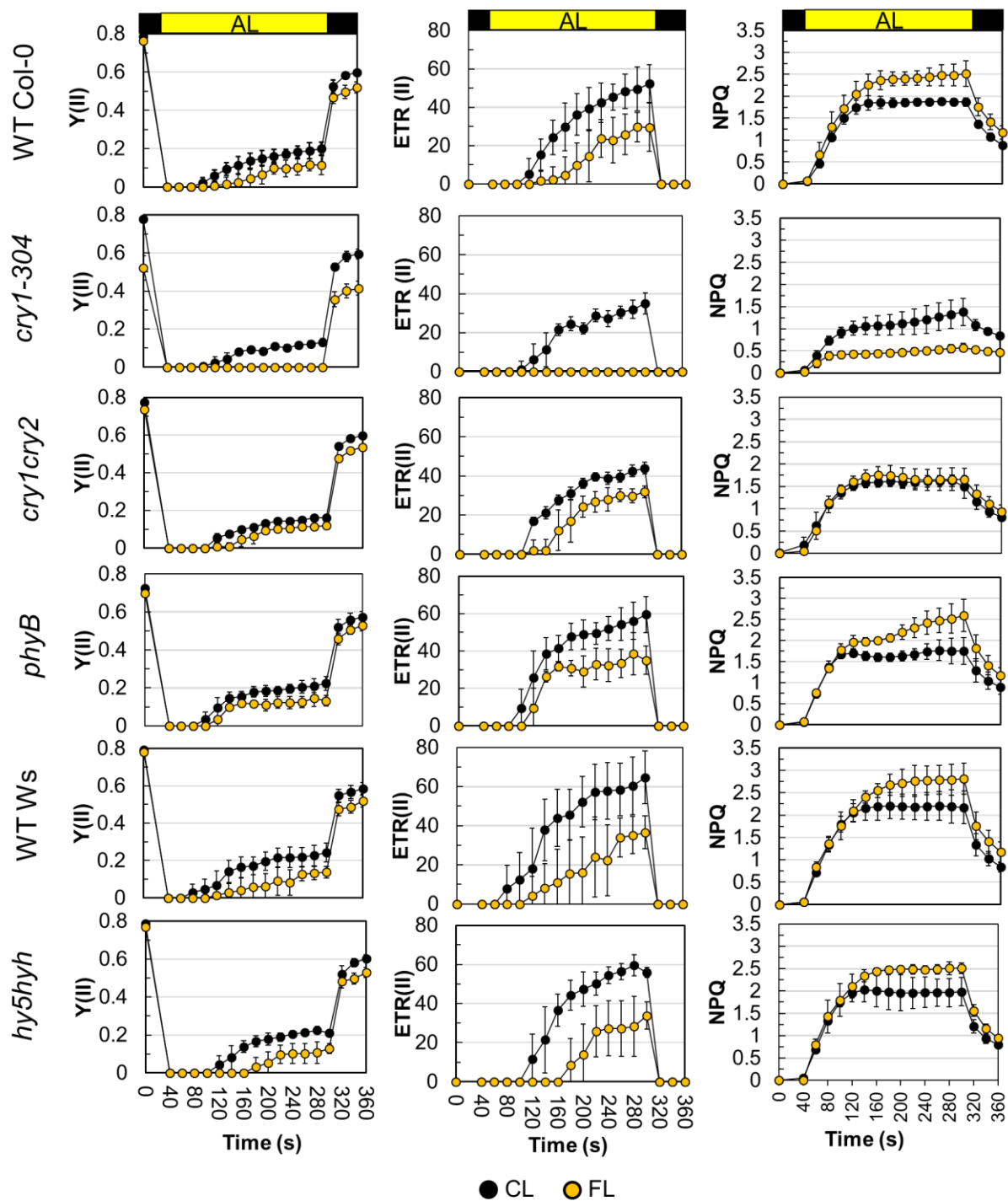


Figure 3.3: Characterization of PSII activity after three days under CL and FL in leaves of overnight dark-adapted plants of WT Col-0, *cry1-304*, *cry1cry2*, *phyB*, WT Ws and *hy5hyh*. Photosynthetic induction was evaluated for 260 s under actinic light (AL) illumination of ca. $550 \mu\text{mol photons m}^{-2} \text{s}^{-1}$, during which saturation pulses (SPs) were triggered every 20 s. The AL period was followed by 60 s of dark relaxation. Y(II), quantum yield of PSII; ETR(II), relative electron transport rate of PSII; NPQ, non-photochemical quenching. Mean values \pm SD are shown ($n = 3-11$ plants).

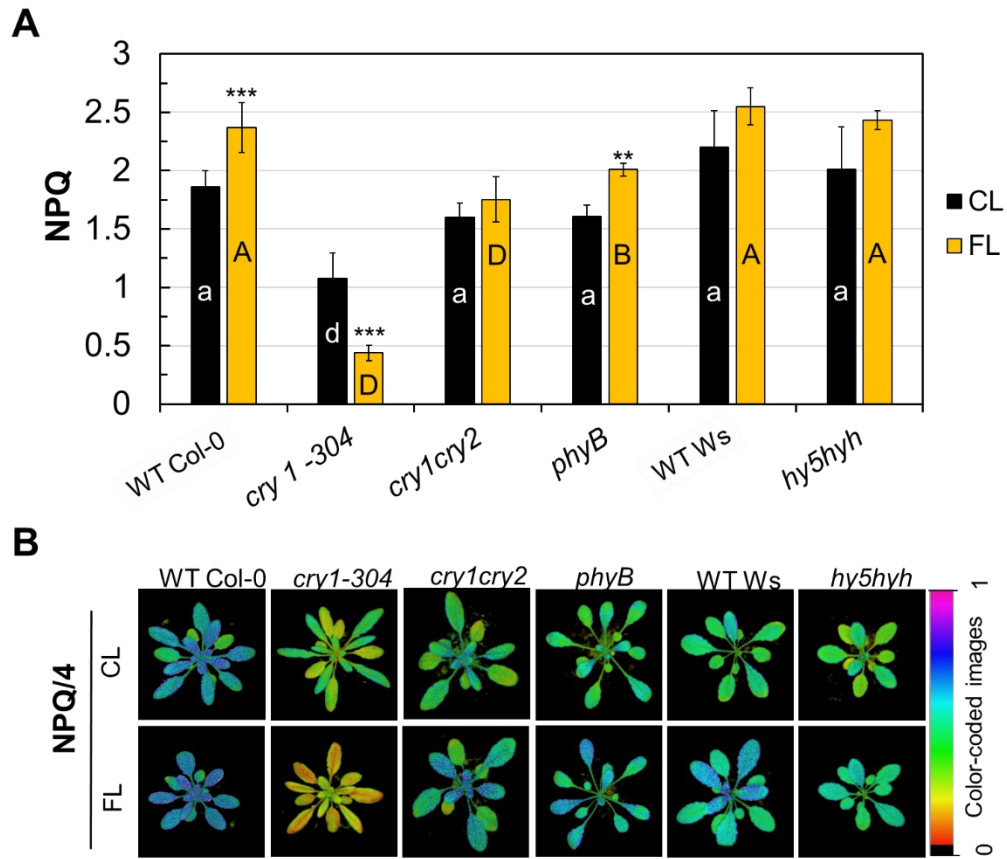


Figure 3.4. NPQ measured after 160-s of AL illumination in WT Col-0, *cry1-304*, *cry1cry2*, *phyB*, WT Ws and *hy5hyh* after three days under CL and FL. **A)** NPQ values of the mature leaves used for the photosynthetic induction measurements shown in Figure 3.3. Significant differences between the genotypes as well as between the light conditions (CL and FL), and the interaction (genotype X light condition) were assessed by two-way ANOVA followed by Tukey's multiple comparison test. Different letters in the panel indicate significant differences in comparison to the corresponding WT: *cry1-304*, *cry1cry2* and *phyB* were compared to WT Col-0 and *hy5hyh* to WT Ws (B, $P \leq 0.05$; D and d, $P \leq 0.001$). Lowercase and uppercase letters are for the comparison between the genotypes under CL and FL, respectively. The differences between the light treatments within the same genotype (FL vs CL) were assessed by unpaired independent Student t-test and significant differences are indicated by asterisks (** $P \leq 0.01$, *** ≤ 0.001). Mean values \pm SD are shown ($n = 3-11$ plants). **B)** Spatial heterogeneity of NPQ after 160-s AL illumination. The color bars on the right show the scale of the color code. Note that NPQ values were divided by four (NPQ/4) to use the scale between 0 and 1.

3.1.3. Photosynthetic response of *cry1-304* to different light intensities

The response of PSII (**Figure 3.5**) and PSI (**Figures 3.6** and **3.7**) to increasing light intensities was evaluated by measuring rapid light response curves in mature leaves of *cry1-304* and WT Col-0 after three days of exposure to CL and FL. Unlike the induction measurements, in which dark-adapted whole plants were suddenly exposed to blue AL of 550 $\mu\text{mol photons m}^{-2} \text{s}^{-1}$ and the PSII parameters were calculated for selected areas of mature leaves (**Figure 3.3**), rapid light response curves were measured in mature leaves detached immediately before the measurements from dark-adapted plants and exposed to stepwise increase in the intensity of red AL.

As already shown in **Figure 3.2 A**, at the level of PSII (**Figure 3.5**) FL-treated *cry1-304* plants showed higher photoinhibition (i.e. lower F_v/F_m) compared to CL condition and WT Col-0 under the same conditions (**Figure 3.5 A**). Also, *cry1-304* plants displayed lower values of $Y(\text{II})$, $\text{ETR}(\text{II})$ and NPQ compared to WT Col-0 regardless of whether they were treated with CL or FL (**Figure 3.5 B**). However, FL-treated plants of *cry1-304* displayed strongly decreased $\text{ETR}(\text{II})$ compared to WT Col-0 under the same conditions and to CL *cry1-304* plants. NPQ levels were also lower in FL plants of *cry1-304* compared to WT Col-0, but they were not significantly different from CL plants of *cry1-304* at light intensities lower than 480 $\mu\text{mol photons m}^{-2} \text{s}^{-1}$. At higher light intensities they were not able to upregulate NPQ capacity further, showing lower values compared to CL plants. At the highest light intensity (830 $\mu\text{mol photons m}^{-2} \text{s}^{-1}$) NPQ in *cry1-304* was ca 44% (CL) or ca. 65% (FL) lower than the corresponding values measured in the WT Col-0.

To check whether the EL-induced inhibition of PSII activity in *cry1-304* depends on the severity of FL treatment, an additional experiment was conducted by exposing plants to a milder FL treatment (FL2) in which the light intensity was changing sigmoidally between HL (ca. 20 s) and CL every 5 min during the light period in the growth chamber (**Figure S.1**). In both genotypes the FL2 treatment led to $Y(\text{II})$ and $\text{ETR}(\text{II})$ values which were between the CL and FL plants (**Figure S.1**). As for NPQ, the FL and FL2 plants of WT Col-0 had similar values except at very low light intensities ($< 80 \mu\text{mol photons m}^{-2} \text{s}^{-1}$) in which the FL plants showed stronger NPQ than the FL2 plants (**Figures 3.5 B** and **S.1 B**). Interestingly, when the FL2 treatment caused mild reduction of F_v/F_m (**Figure S.1 A**), $Y(\text{II})$ and $\text{ETR}(\text{II})$ in *cry1-304* (**Figure S.1 B**), this mutant did not show suppression of NPQ but was able to enhance the NPQ capacity compared to the CL plants (**Figure S.1 B**).

These results indicate that the inhibitory effects of FL observed in *cry1-304* depend on the severity of the treatment. In addition, while mature leaves of *cry1-304* had reduced capacities for ETR(II) and NPQ (especially qE) compared to the corresponding leaves of WT Col-0 under all light conditions examined, a part of the severe NPQ inhibition found in this mutant under the FL condition seems to be a consequence of impaired electron transport to build up a pH gradient (ΔpH) across the thylakoid membrane.

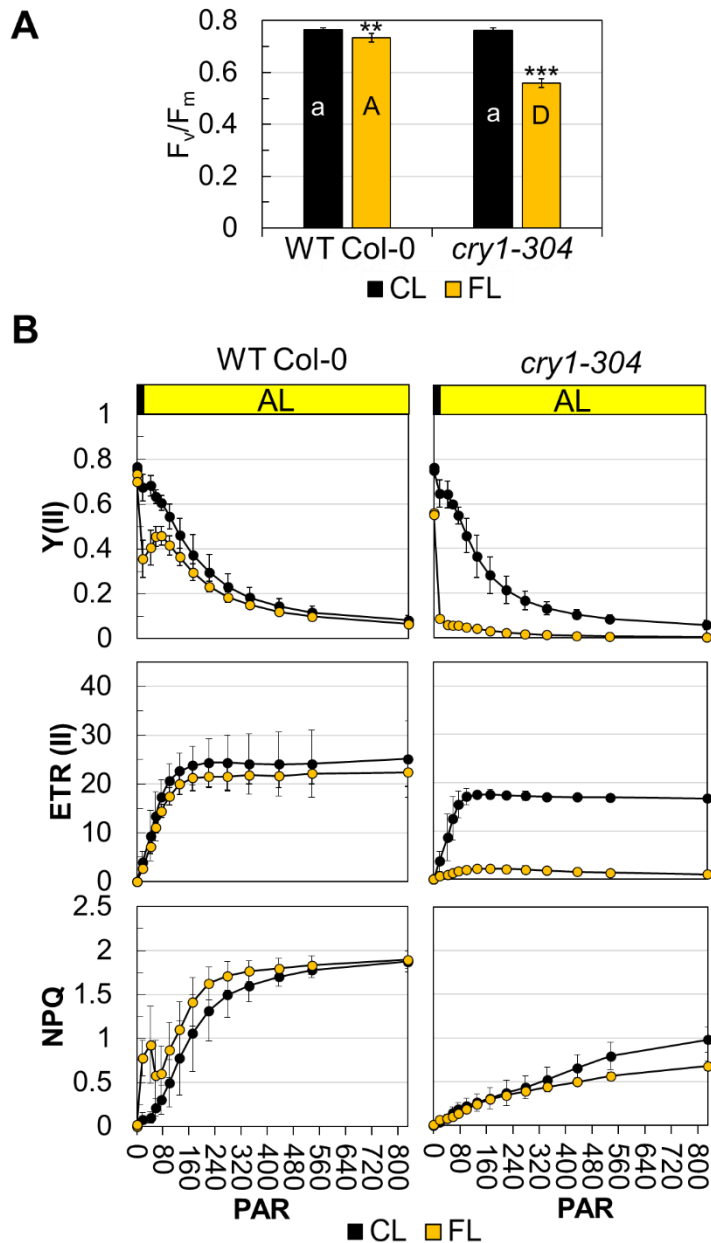


Figure 3.5. Characterization of PSII after three days under CL and FL in plants of WT Col-0 and *cry1-304*. **A**) F_v/F_m . Significant differences between the genotypes as well as between the light conditions (CL and FL), and the interaction (genotype X light condition) were assessed by two-way ANOVA followed by Tukey's multiple comparison test. Different letters in the panel indicate significant differences in comparison to WT Col-0. Letter shared in common between the genotypes indicate not significant difference between their mean ($D P \leq 0.001$). Lowercase and uppercase letters are for the comparison between the genotypes under CL and FL, respectively. The differences between the light treatments within the same genotype (FL vs CL) were assessed by Tukey multiple comparison and indicated by asterisks (** $P \leq 0.01$, *** ≤ 0.001). Mean values \pm SD ($n = 3-6$). **B**) Rapid light response curves measured in leaves of overnight dark-adapted plants of WT Col-0 and *cry1-304*. The intensity of AL was gradually increased in 14 steps from 0 to 830 $\mu\text{mol photons m}^{-2} \text{s}^{-1}$ with 90 s of dwell time at each step. Y(II), quantum yield of PSII; ETR (II), relative electron transport rate of PSII; NPQ, non-photochemical quenching.

In parallel to Chl fluorescence, also P700 redox changes were monitored during the measurements of rapid light response curves (**Figure 3.6**). The maximum photo-oxidizable P700 (Pm), which reflects the functional PSI, was slightly but not significantly lower in CL-treated plants of *cry1-304* compared to WT Col-0 (**Figure 3.6 A**). Lower values of Pm were observed in both WT Col-0 and *cry1-304* plants after three days of FL exposure, indicating PSI photoinhibition. However, FL-treated plants of *cry1-304* displayed more severe PSI photoinhibition, as indicated by Pm which was decreased to ca. 23% of the WT values under the same condition and to ca. 21% of the CL *cry1-304* plants. FL2 treatment caused intermediate Pm values, which were reduced to 44% and 39% of the values observed in FL2-treated plants of WT Col-0 and CL *cry1-304* plants, respectively (**Figure S.2 A**).

The Pm' values determined in the light after each SP in both CL- and FL-treated plants of WT Col-0 remained stable at ca 1.2 and 1, respectively, during the exposure to different light intensities from 0 to 830 $\mu\text{mol photons m}^{-2} \text{s}^{-1}$. In contrast, in CL-treated *cry1-304* plants, Pm' strongly decreased from ca 1.0 to 0.1, inversely proportional to the increase of light intensity, indicating a decreased ability of PSI to re-oxidize and thus a decreased capacity to release electrons to the downstream acceptors (**Figure 3.6 B**). In FL and FL2-treated *cry1-304* plants Pm' values were already low at low light intensities and they did not decrease further, remaining stable at ca. 0.2 (**Figure 3.6 B and S.2 B**).

Accordingly, as PSI parameters are calculated from Pm values, the quantum yield of PSI (Y(I)) was found to be limited by a strong increase in PSI acceptor side limitation (Y(NA)), indicating that the PSI capacity was largely limited (90-95%) by saturation of its electron acceptors (**Figures 3.6 C and S.2 C**). Except at the lowest light intensities, Y(I) decreased as with the increasing intensity of the AL in both WT Col-0 and *cry1-304* (**Figures 3.6 C and S.2 C**). In the CL and FL2 plants of WT Col-0, this was accompanied by a large increase in PSI donor side limitation (Y(ND)) and little changes in Y(NA), suggesting growing limitation on the PSI donor side with minor limitation on the acceptor side at higher light intensities (**Figures 3.6 C and S.2 C**). On the contrary, the decrease in Y(I) coincided with a marked increase in Y(NA) with nearly no increase in Y(ND) in the CL and FL2 plants of *cry1-304*, meaning that PSI efficiency was limited by the acceptor side (**Figures 3.6 C S.2 A**). Only when PSII activity was severely impaired in *cry1-304* plants by the FL treatment (**Figure 3.5 B**), Y(ND) increased and Y(NA) decreased (**Figure 3.6 C**). Still, the FL plants of *cry1-304* had higher Y(NA) than the FL plants of WT Col-0.

The ETR(I)/ETR(II) ratio, which is supposed to be related CET around PSI (Yamori et al., 2011; Kono et al., 2014), was between 1 and 1.5 in the CL and FL2 plants of WT Col-0 (**Figures 3.6 D S.2 B**) while it increased up to >2 in the FL plants, especially at very low light intensities (**Figure 3.6 D**) in which they exhibited strong NPQ induction (**Figure 3.5 B**). In comparison, ETR(I)/ETR(II) was very low in the CL plants of *cry1-304* (**Figure 3.6 D**), due mainly to their low ETR(I) saturating at low light intensities (**Figure 3.6 C**). However, at 100 $\mu\text{mol photons m}^{-2} \text{s}^{-1}$ (corresponding to the growth light condition in CL) the CL plants of the two genotypes had similar ETR(I)/ETR(II) values (**Figure 3.6 D**). The PSII photoinhibition (**Figure 3.5 A**) and thus the increase in Y(ND) (**Figure 3.6 C**) observed in the FL plants of *cry1-304* resulted in a strong increase in ETR(I)/ETR(II) (**Figure 3.6 D and E**). The ETR(I)/ETR(II) ratio also increased in the *cry1-304* FL2 plants and in both FL2 and FL plants of WT Col-0 compared to the CL plants (**Figures 3.6 D and E; S.2 D and E**), suggesting upregulation of CET in both genotypes under dynamic EL conditions.

To inspect the acceptor and donor side limitations of PSI more closely, traces of P700 signal were extracted from the experiment shown in **Figures 3.5 B and 3.6 C** before, during and after the saturation pulse (SP) at six different AL intensities (**Figure 3.7**). Between 0 and 75 $\mu\text{mol photons m}^{-2} \text{s}^{-1}$ the CL plants of *cry1-304* and WT Col-0 showed similar patterns of P700 oxidation (upon SP) and reduction (during and/or after the SP). However, at light intensities higher than the growth light in CL (100 $\mu\text{mol photons m}^{-2} \text{s}^{-1}$) P700 oxidation became slower in the *cry1-304* CL plants, reaching the maximum only at the end of the 400-ms SP. Also, *cry1-304* FL plants always displayed relatively low P700 signal, which became especially low at higher light intensities. Tiny peaks of P700 oxidation were induced by the SP in these plants at all AL intensities, followed by also tiny and slow decline by re-reduction. Also, the re-reduction of P700 after the SP was slower and less marked compared to CL plants and WT Col-0 under the same conditions. At the same time, the data of *cry1-304* FL plants, showing substantial decrease in P700 signal (including the peak level) with increasing AL intensities, imply strong reduction of P700 due to acceptor-side limitation. This is consistent with the progressive decrease in Pm' values observed in CL-treated plants of *cry1-304* starting from light intensity higher than the growth light conditions and the very low but stable values observed in FL-treated plants (**Figure 3.6 B**). It should be noted that if the SP, applied to determine the maximal P700 signal (Pm) and Pm'), was not fully oxidizing P700 in these plants, the PSI parameters calculated by using Pm and Pm' values, such as Y(I), Y(NA), Y(ND) and ETR(I), must be used with caution, as these parameters assume full oxidation of P700 during the Pm determination.

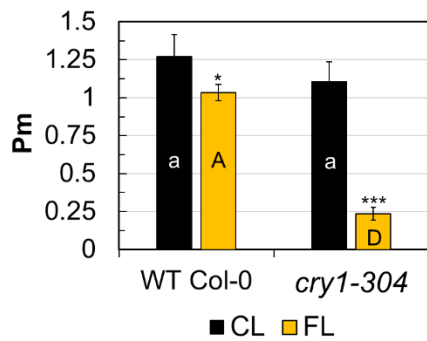
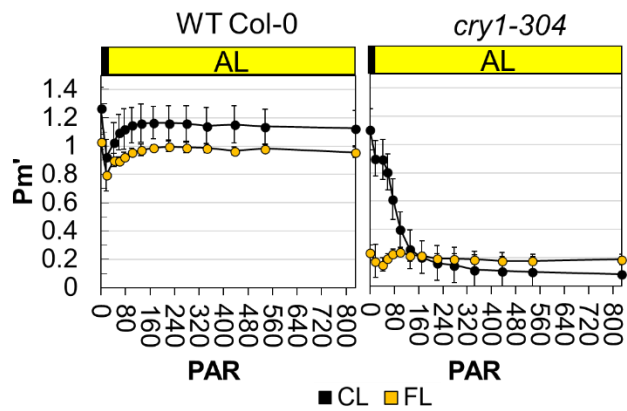
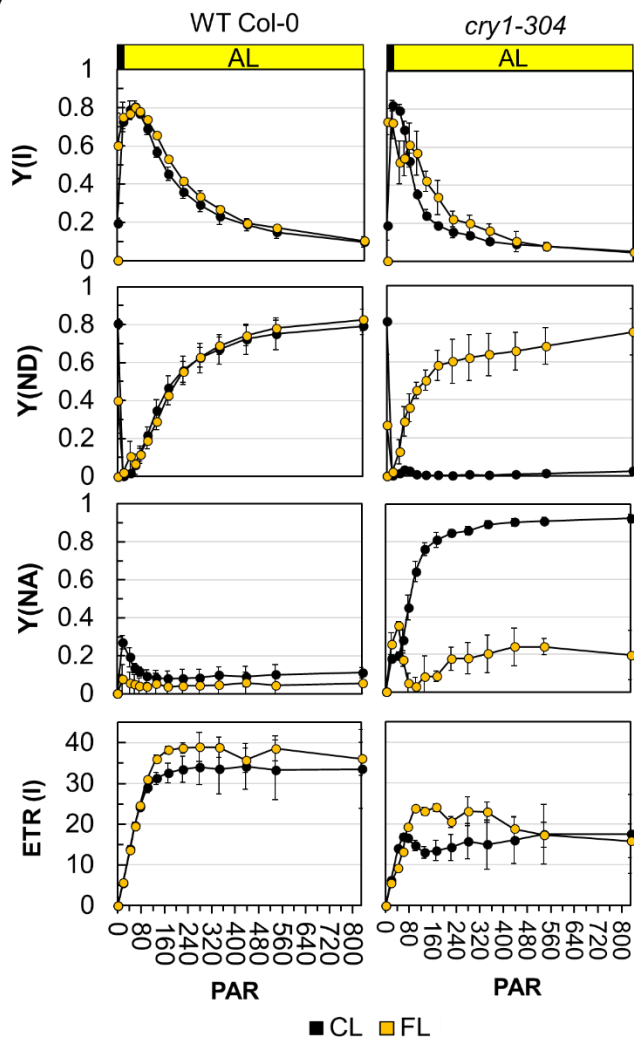
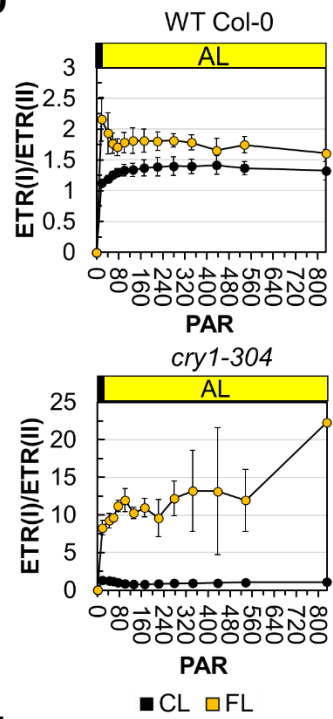
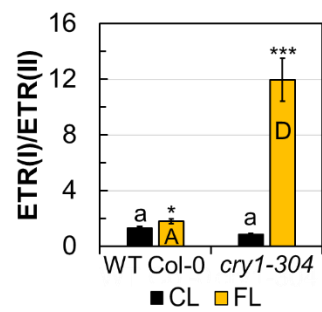
A**B****C****D****E**

Figure 3.6. Characterization of PSI after three days under CL and FL. Rapid light response curves were measured in leaves of overnight dark-adapted plants of WT Col-0 and *cry1-304*. The intensity of AL was gradually increased in 14 steps from 0 to 830 $\mu\text{mol photons m}^{-2} \text{s}^{-1}$ with 90 s of dwell time at each step. **A)** Pm, maximal change of the P700 signal upon transformation from the fully reduced to the fully oxidized state, determined by far-red pre-illumination and application of a SP. **B)** Pm', maximal change of the P700 signal in a given light state upon application of a SP without far-red illumination. **C)** Y(I), quantum yield of PSI; Y(ND), quantum yield of PSI donor-side limitation; Y(NA), quantum yield of PSI acceptor-side limitation; ETR(I), relative electron transport rate of PSI. **D)** Ratio between ETR (II) and ETR (I), ETR (I) /ETR (II) **E)** ETR (I) /ETR (II) at the light intensity ($100 \mu\text{mol photons m}^{-2} \text{s}^{-1}$) corresponding to the growth light in CL and the intensity of low-light periods in FL. Significant differences between the genotypes as well as between the light conditions (CL and FL), and the interaction (genotype X light condition) were assessed by two-way ANOVA followed by Tukey's multiple comparison test. Different letters in the panel show significant difference between *cry1-304* and WT Col-0 ($P \leq 0.001$). Lowercase and uppercase letters indicate the comparison between the genotypes under CL and FL, respectively. The differences between the light treatments within the same genotype (FL vs CL) were assessed by unpaired independent Student t-test and significant differences are indicated by asterisks ($* \leq 0.05$, $*** \leq 0.001$). Mean values \pm SD ($n = 3-6$) are shown

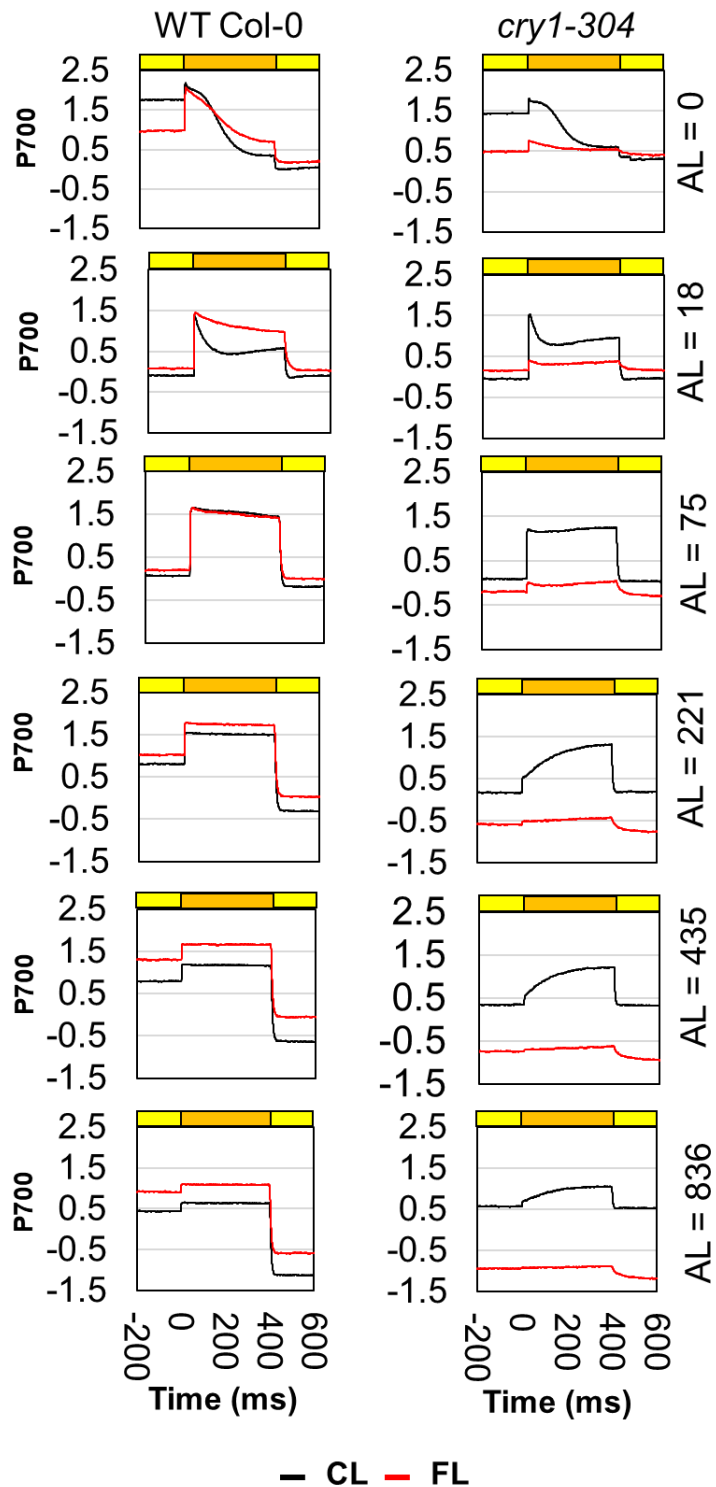


Figure 3.7: Changes in P700 redox state during light response measurements in WT Col-0 and *cry1-304* after three days under CL (black lines) and FL (red lines). Traces of P700 signal were extracted from the experiment shown in Fig. 3.6 before, during and after the SP at six different AL intensities. Dark-yellow bar indicates the SP. Light-yellow bars denote the periods immediately before and after the SP. Mean values of three replicate plants are presented for each genotype in both CL and FL conditions. Error bars are not shown for clarity. The P700 signal was measured as difference of the transmittance signals at 875 nm and 830 nm. A positive change of the P700 signal indicate P700 oxidation, a negative change indicates P700 reduction. A calibration was carried out, so that the changes of the P700 signal are scaled in $\Delta I/I \times 10^{-3}$ units.

3.1.4 Accumulation of Photosynthetic proteins

The alterations of photosynthetic performance observed in *cry1-304* plants at the levels of PSII (**Figures 3.2 – 3.5**) and PSI (**Figures 3.6, 3.7, S.1 and S.2**) can be a consequence of changes in composition and/or accumulation of protein of the photosynthetic machinery. In order to test this hypothesis, the accumulation of major components of PSII (D1, LHCBI) and PSI (PSA-A) as well as thylakoid ATP synthase (ATP-C) were analyzed. Also, the accumulation of PSBS and PGR5 was examined to investigate the possible cause of the low NPQ capacity and the high ETRI/ETRII observed in this mutant. Moreover, the level of RBCL was considered as the major component of the Calvin-Benson cycle (**Figure 3.8**). Representative Western blots are shown in **Figure 3.8 A**. The samples of total leaf protein extracts were loaded based on their total Chl contents. For comparison between genotypes and conditions, the protein levels were expressed relative to WT Col-0 under CL (**Figure 3.8 B**).

Despite the contrasting pictures found in *cry1-304* and WT Col-0 at the level of PSII and PSI activities, these plants had similar levels of all seven proteins examined both under CL and FL conditions, with the single exception of D1 in FL (**Figure 3.8 B**). The D1 content increased in WT Col-0 from CL to FL while it remained unchanged in *cry1-304*. The PSBS protein levels tended to increase in both genotypes from CL to FL, even though the increase was significant only in WT Col-0 and not in *cry1-304*. The reduced NPQ capacity and the strong qE deficiency observed in *cry1-304* plants under CL and FL, respectively, cannot be explained by corresponding changes in PSBS protein abundance. Similarly, the PGR5 protein levels did not significantly differ between *cry1-304* and WT Col-0 under both conditions, although WT Col-0 showed a small increase in PGR5 under FL compared to CL, which was not evident in *cry1-304*. The marked differences in ETR(I)/ETR(II) found between these two genotypes do not seem to involve changes in the PGR5 protein level.

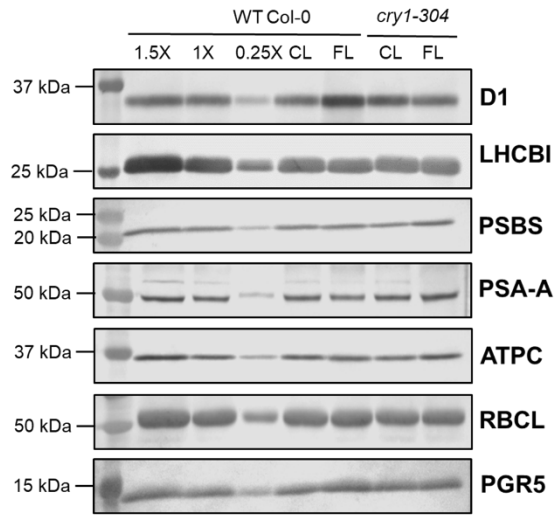
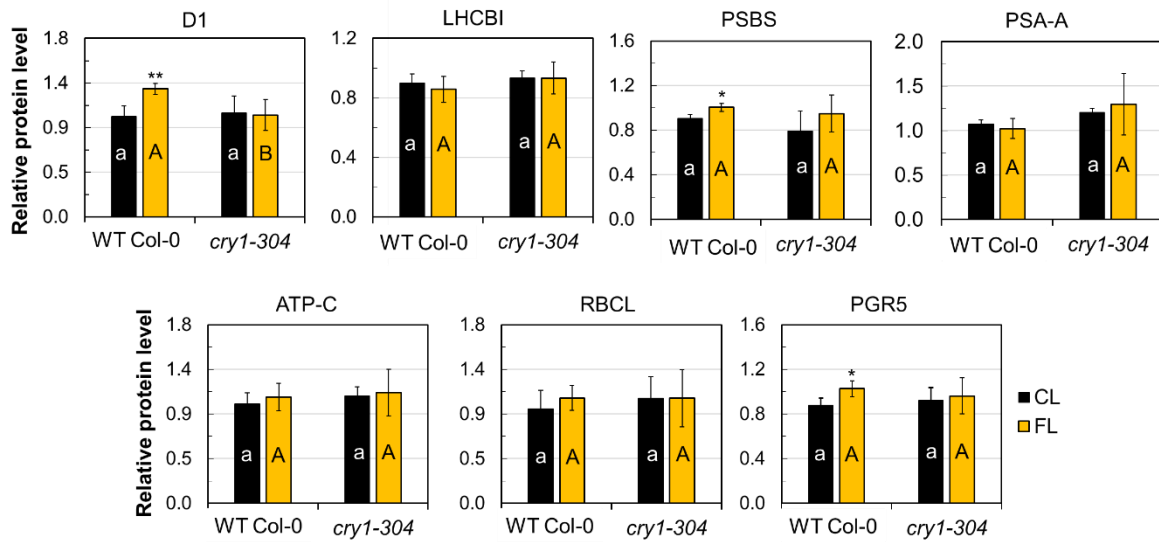
A**B**

Figure 3.8. Levels of key proteins of photosynthesis and its regulation (D1, LHCBI, PSBS, PSA-A, ATPC, RBCL and PGR5) in leaves of WT Col-0 and *cry1-304* after three days under CL and FL. **A)** Representative Western blots. **B)** Relative protein levels compared to WT Col-0 in CL. The loading amounts of the samples were based on Chl contents as follows: 2.0 µg Chl for D1, LHCBI, PSA-A, ATP-C and RBCL; 5.0 µg Chl for PSBS and PGR5. 0.25X and 1.5X were also loaded for WT CL. Significant differences between the genotypes as well as between the light conditions (CL and FL), and the interaction (genotype X light condition) were assessed by two-way ANOVA followed by Tukey's multiple comparison test. Different letters in the panel indicate significant difference between *cry1-304* and WT Col-0 ($P \leq 0.05$). Lowercase and uppercase letters indicate the comparison between the genotypes under CL and FL, respectively. Significant differences between the light treatments within the same genotype (FL vs CL) are indicated by asterisks ($* \leq 0.05$, $** P \leq 0.01$). Mean values \pm SD are shown ($n = 3-4$ from 6 independent experiments).

3.1.5 Pigment analysis

Pigment composition was analyzed in leaves of WT Col-0 and *cry1-304* at the end of overnight dark adaptation (dark-adapted) and after exposure to 260-s AL (ca. 550 $\mu\text{mol photons m}^{-2} \text{s}^{-1}$) followed by 60 s of dark recovery (**Figure 3.9**). Under the conditions used in these experiments the levels of Chl *a* and *b* did not differ between WT Col-0 and *cry1-304* in both CL- and FL-treated plants in dark-adapted and AL-exposed samples (**Figure 3.9 A**).

Besides PSBS, Z is another important component of NPQ and qE (Niyogi et al., 1997a; Niyogi et al., 1997b; Niyogi et al., 1998). The strong AL illumination should activate VDE which converts V to A and Z. The dark-adapted samples, on the other hand, should contain no or little Z unless plants were already stressed while growing in the FL or CL condition.

Levels of individual pigments in the xanthophyll cycle were analyzed in both WT Col-0 and *cry1-304* plants (**Figure 3.9 B**). After AL exposure and 1-min dark recovery, the CL and FL plants of WT Col-0 showed a decrease in V with a concomitant increase in both A and Z, suggesting light-induced activation of VDE (**Figure 3.9 B, Table 3.3**). Accordingly, the de-epoxidation state (DES) of the xanthophyll-cycle pigments increased in these plants from 0.2 in the dark to 0.6 or 0.7 after the AL illumination (**Table 3.1**). For *cry1-304*, in contrast, only the CL-treated plants showed similar AL-induced V de-epoxidation; the plants in FL had higher levels of A and Z even in the dark-adapted state (DES = 0.4) and AL neither induced further increase in A and Z nor reduced the V content (**Figure 3.9, Tables 3.1 and 3.3**). However, the size of the total xanthophyll-cycle pool (VAZ) was comparable between the two genotypes. The growth light conditions (FL and CL) had a dominant influence on the accumulation of these pigments and DES, with some interactions with genotype and/or AL exposure (**Table 3.2**). The effects of AL (regardless of the growth light and genotype) were significant for A, VAZ and DES, while A was the only component that showed a significant difference between *cry1-304* and WT Col-0 independently of the growth light and AL (**Table 3.2**). Except for A, genotypic differences were found only in interaction with growth light condition.

Taken together, these results suggest that the NPQ deficient phenotype observed in *cry1-304* (**Figures 3.3 – 3.5**) is not due to limited Z (or A) accumulation. The CL plants of this mutant are able to operate the xanthophyll cycle normally. The dark retention of Z and A found in *cry1-304* under FL (**Figure 3.9 and Table 3.1**) is consistent with their low F_v/F_m (**Figure 3.2 A**).

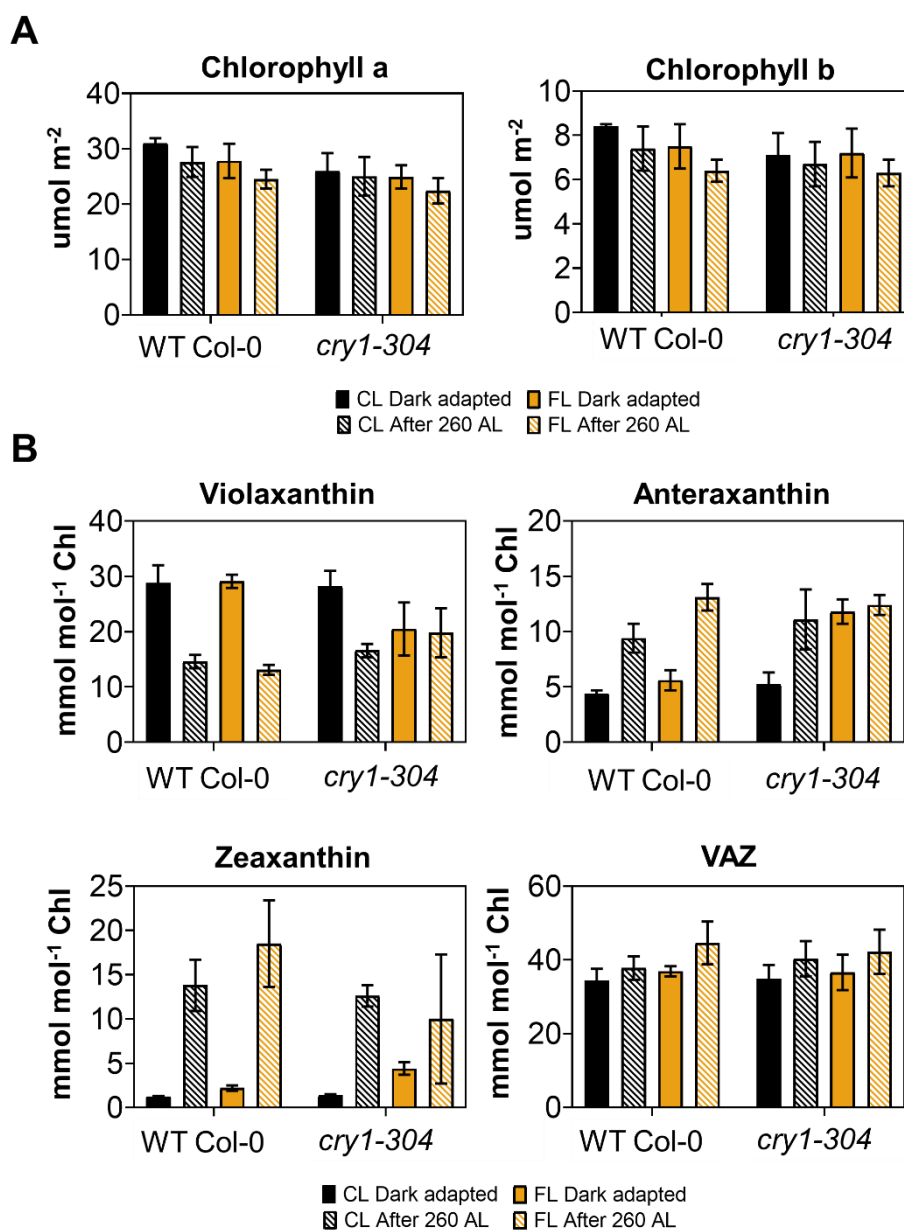


Figure 3.9. Leaf pigment composition in dark- and light-adapted leaves of WT Col-0 and *cry1-304* after three days under CL and FL. Leaf samples were taken before (dark-adapted) and after the 260-s AL illumination ($550 \mu\text{mol m}^{-2} \text{s}^{-1}$) followed by 1-min dark recovery of the photosynthetic induction measurements shown in Figs. 3.2 – 3.4. **A)** Chlorophyll a and chlorophyll b contents per leaf area **B)** The levels of the xanthophyll-cycle pigments violaxanthin, anteraxanthin, zeaxanthin and the sum of the three (VAZ) relative to the total Chl content. The number of replicate plants were four for each genotype in both CL and FL conditions. Mean values \pm SD are shown. Results of statistical test are reported in Tables 3.2 and 3.3. Pigment extraction and HPLC analysis were performed by Anh Banh (IBG-2, FZJ).

	CL		FL	
Genotype	WT Col-0	<i>cry1-304</i>	WT Col-0	<i>cry1-304</i>
Dark-adapted	0.2 ± 0.0	0.2 ± 0.0	0.2 ± 0.0	0.4 ± 0.1
After 260 s AL	0.6 ± 0.1	0.6 ± 0.0	0.7 ± 0.0	0.5 ± 0.1

Table 3.1. De-epoxidation state (DES) of VAZ calculated as (A + Z)/ (V + A + Z). Samples for pigment analysis were taken from overnight dark-adapted plants and after 260-s exposure to AL (550 $\mu\text{mol m}^{-2} \text{s}^{-1}$) followed by 1-min dark recovery. Mean values \pm SD (n = 4) are shown. Results of statistical are reported in Tables 3.2 and 3.3. Pigment extraction and HPLC analysis were performed by Anh Binh (IBG-2, FZJ).

Factors	Chl a	Chl b	V	A	Z	VAZ	DES
Genotype	21.7 **	9.0 ns	0.0 ns	7.7 ***	1.9 ns	0.0 ns	0.0 ns
Short Light induction (Dark, AL)	13.2 *	7.6 ns	1.1 ns	19.6 ***	1.3 ns	11.3 *	1.6 *
Light condition (CL, FL)	13.8 *	18.1 *	63.2 ***	43.2 ***	74.4 ***	32.6 ***	76.6 ***
Genotype x Short light induction (Dark, AL)	1.0 ns	4.0 ns	0.4 ns	1.1 ns	1.0 ns	2.1 ns	0.0 ns
Genotype x Light condition (CL, FL)	1.5 ns	1.0 ns	11.2 ***	4.3 **	5.2 *	0.0 ns	6.3 ***
Short light induction (Dark, AL) x Light condition (CL, FL)	0.3 ns	0.6 ns	2.9 *	0.9 ns	0.1 ns	1.2 ns	1.6 *
Genotype x Short light induction (Dark, AL) x Light condition (CL, FL)	0.4 ns	0.3 ns	5.6 **	7.3 ***	3.1 *	1.1 ns	6.3 ***

Table 3.2. Differences between the genotypes (WT Col-0 and *cry1-304*), the light conditions (CL and FL) and the pigments levels in the dark or after 260 s of exposure to AL as well as the interactions between these factors were tested by three-way ANOVA. Percentage of the contribution of these factor to the total variation and significant levels (ns P > 0.05, * \leq 0.05, ** P \leq 0.01, *** P \leq 0.001) are reported.

Tukey's multiple comparisons test	Chl a	Chl b	V	A	Z	VAZ	DES
WT Col-0:CL Dark adapted vs. WT Col-0:CL After 260 AL	0.62 ns	0.74 ns	<0.001 ***	<0.001 ***	<0.001 ***	0.93 ns	<0.001 ***
WT Col-0:FL Dark adapted vs. WT Col-0:FL After 260 AL	0.65 ns	0.64 ns	<0.001 ***	<0.001 ***	<0.001 ***	0.19 ns	<0.001***
WT Col-0:CL Dark adapted vs. WT Col-0:FL Dark adapted	0.59 ns	0.75 ns	>0.99 ns	0.83 ns	>0.99 ns	0.97 ns	>0.99 ns
WT Col-0:CL After 260 AL vs. WT Col-0:FL After 260 AL	0.79 ns	0.8 ns	>0.99 ns	0.002 **	0.51 ns	0.41 ns	0.39 ns
cry1-304:CL Dark adapted vs. cry1-304:CL After 260 AL	>0.99 ns	>0.99 ns	<0.001 ***	<0.001 ***	<0.001 ***	0.58 ns	<0.001 ***
cry1-304:FL Dark adapted vs. cry1-304:FL After 260 AL	0.88 ns	0.82 ns	>0.99 ns	>0.99 ns	0.22 ns	0.56 ns	0.3 ns
cry1-304:CL Dark adapted vs. cry1-304:FL Dark adapted	>0.99 ns	>0.99 ns	0.01 *	<0.001 ***	0.86 ns	>0.99 ns	0.002 **
cry1-304:CL After 260 AL vs. cry1-304:FL After 260 AL	0.86 ns	>0.99 ns	0.8 ns	0.77 ns	0.93 ns	>0.99	0.3 ns
WT Col-0:CL Dark adapted vs. cry1-304:CL Dark adapted	0.16 ns	0.44 ns	>0.99 ns	0.99 ns	>0.99 ns	>0.99 ns	>0.99 ns
WT Col-0:CL After 260 AL vs. cry1-304:CL After 260 AL	0.86 ns	0.94 ns	0.98 ns	0.58 ns	>0.99 ns	0.99 ns	>0.99 ns
WT Col-0:FL Dark adapted vs. cry1-304:FL Dark adapted	0.69 ns	>0.99 ns	<0.001 ***	<0.001 ***	0.95 ns	>0.99 ns	<0.001 ***
WT Col-0:FL After 260 AL vs. cry1-304:FL After 260 AL	0.96 ns	>0.99 ns	0.11 ns	0.98 ns	0.03 *	>0.99 ns	0.004 **

Table 3.3. Significant differences in pigment levels reported in **Figure 3.8** and **Table 3.1** were tested by multiple comparison tests (Tukey). P values and significant symbols are reported (ns P > 0.05, * ≤ 0.05, ** P ≤ 0.01, *** P ≤ 0.001). P values shown in bold indicate the major points of difference between *cry1-304* and WT Col-0.

3.1.5 CRY1-dependent gene expression

Under EL conditions the LHCII undergoes reorganization and its gene expression is downregulated (Timperio et al., 2012). At the same time, genes involved in protective mechanisms against photo-oxidative stress, such as the ROS scavengers, are upregulated together with light-responsive genes (Karpinski et al., 1997; Tikkanen et al., 2014a). Previous studies in FL (Schneider et al., 2019) and HL (Kleine et al., 2007) showed upregulation of *ELIP2* and *GPX7* in WT Col-0, both of which were shown to be misregulated in *cry1-304* mutants (Kleine et al., 2007). *HY5* and *HYH* are light-responsive transcription factors known to act in the downstream of light signaling pathways mediated by CRY1 and other photoreceptors. The lack of CRY1 in *cry1-304* seems to misregulate also HL-induced upregulation of *HY5* gene expression (Kleine et al., 2007).

In order to test if the photosynthetic phenotypes observed in *cry1-304* mutants are related to misregulation of these CRY1-regulated light- and stress-related genes, their expression was analyzed in *cry1-304* and WT Col-0 under CL and FL by qRT-PCR (**Figure 3.10**). *LHCB1.2* was strongly and similarly downregulated in both WT and *cry1-304* under FL. *ELIP2* and *GPX7* were significantly upregulated in the FL condition in both genotypes. Although *cry1-304* under CL showed downregulation of *GPX7* compared to WT Col-0, FL-induced upregulation was more pronounced in *cry1-304*. No significant changes were found for *HY5* and *HYH* between the two genotypes except that *cry1-304* had lower expression of *HYH* in CL. Unlike the upregulation found in the previous studies in HL (*HY5*, Kleine et al., 2007) and FL (*HYH*, Schneider et al., 2019), the expression of these genes decreased in WT Col-0 after three days of exposure to FL. This downregulation was not observed in *cry1-304*.

Overall, these results cannot explain the EL sensitive phenotype observed in *cry1-304* plants under FL. The *GPX7* downregulation in CL-treated plants of *cry1-304* confirm that CRY1 signaling takes part in regulating *GPX7* gene expression. At the same time, the strong upregulation of *GPX7* in FL-treated *cry1-304* suggests that these plants were experiencing high levels of oxidative stress and in such conditions *GPX7* expression is controlled by other factors besides CRY1. Together, the substantial levels of gene expression and similar FL responses of these CRY1-related genes in *cry1-304* and WT Col-0 are indicative of additional factors involved in regulating the expression of these genes.

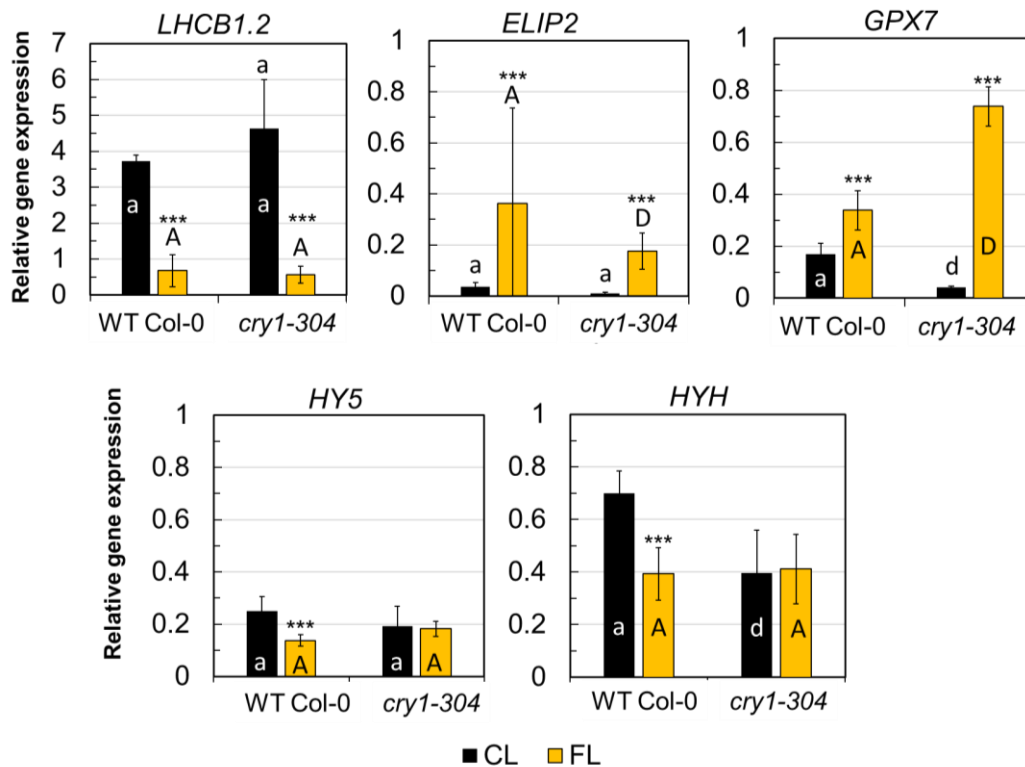


Figure 3.10. Expression of *LHCb1.2*, *ELIP2*, *GPX7*, *HY5* and *HYH* genes in WT Col-0 and *cry1-304* after three days of exposure to CL (black bars) and FL (yellow bars). Gene expression analysis was performed in leaves harvested 2 h after switching on the light of CL or FL in the climate chamber. The values reported are normalized to the expression level of RCE1 (RUB1 CONJUGATING ENZYME 1) in CL and FL in both genotypes. Primers sequences are reported in table 5.1. Significant differences between the genotypes as well as between the light conditions (CL and FL), and the interaction (genotype X light condition) were assessed by two-way ANOVA followed by Tukey's multiple comparison test. Different letters in the panels show significant differences between *cry1-304* and WT Col-0 (d or D, $P \leq 0.001$). Lowercase and uppercase letters are for the comparison between the genotypes under CL and FL, respectively. Significant differences between the light treatments within the same genotype (FL vs CL) are indicated by symbols (***) $P \leq 0.001$. Mean values \pm SD are shown ($n = 6$, replicates coming from three independent experiments)

3.2 Role of differential subcellular localization of CRY1 in acclimation to EL

3.2.1 Characterization of CRY1 overexpression lines which are already available

The differential roles of nuclear and cytoplasmic CRY1 have been described only partially for growth and developmental processes (Wu and Spalding, 2007), while questions regarding the roles in photosynthetic acclimation remain unanswered. Thus, photosynthetic phenotypes were analyzed in the transgenic lines reported in the study by Wu and Spalding (2007) in order to compare acclimation processes in these lines. These authors generated the transgenic lines by overexpressing *CRY1* gene, which was fused to *GFP* (*cry1_{control}*), in the KO mutant *cry1-304*. In order to identify specific functions of CRY1 in the nucleus and in the cytoplasm, they also generated *cry1_{NLS}* and *cry1_{NES}*, in which NLS or nuclear export signal (NES) was added to the *CRY1* gene to target CRY1 protein to the nucleus (*cry1_{NLS}*) or the cytoplasm (*cry1_{NES}*), respectively (Wu and Spalding, 2007).

In the *cry1_{control}* line the GFP signal (fused to CRY1) was detected mostly in the nucleus but also in the cytoplasm, whereas in *cry1_{NES}* it was only in the cytoplasm (**Figure 3.11 A**). These observations confirmed the original report of GFP localization in these plants by Wu and Spalding (2007). In contrast, the exclusive nuclear localization of GFP signal could not be confirmed in the plants of *cry1_{NLS}* in this study. This genotype was therefore excluded from the experiments. The *CRY1* gene expression was hardly detectable in the background mutant *cry1-304*, while it was partially recovered in *cry1_{control}* and strongly increased in *cry1_{NES}* compared to WT Col-0 (**Figure 3.11 B**).

Seedlings grown in the dark show enhanced hypocotyl elongation and cannot de-etiolate to develop green cotyledons. When seedlings perceive the light through photoreceptors, hypocotyl elongation is suppressed and cotyledons develop (Kami et al., 2010). According to Wu and Spalding (2007), the inhibition of hypocotyl elongation is regulated by BL signaling via the nuclear CRY1. In order to exclude the possible presence and activity of the cytoplasmic CRY1 in *cry1_{NES}*, seeds of *cry1_{NES}* were germinated in the dark (**Figure 3.12 A**) or under low BL (**Figure 3.12 B**) together with *cry1-304* and WT Col-0. In the dark all the genotype displayed similar skotomorphogenic phenotypes characterized by hypocotyl elongation and inhibition of cotyledon development.

In BL the plants of *cry1-304* showed elongated hypocotyl, as expected, while the hypocotyl length of *cry1_{NES}* was intermediate between WT Col-0 and *cry1-304*. These observations suggest, unlike in the original study by Wu and Spalding (2007), that BL- and CRY1-dependent suppression of hypocotyl elongation is partly active in the *cry1_{NES}* plants. Greening of cotyledon, on the other hand, was not completely inhibited in any of the genotypes under BL (**Figure 3.12 B**), suggesting a minor role, if any, of CRY1 in greening.

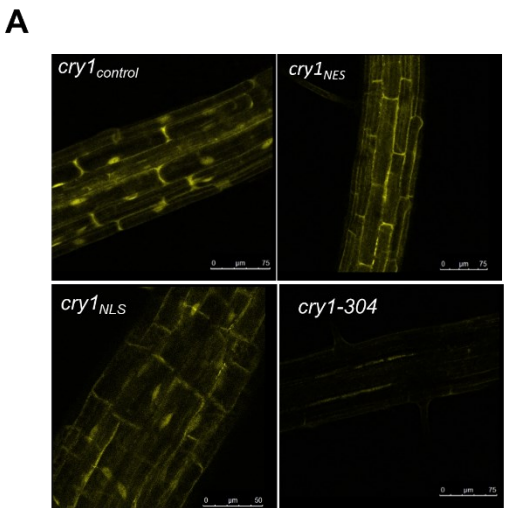


Figure 3.11. A) Subcellular localization of chimeric CRY1-GFP proteins in root. Root tips of 4-day old seedlings of *cry1_{control}*, *cry1_{NES}*, *cry1_{NLS}* and *cry1-304* (as negative control) were observed by confocal microscopy to detect the GFP signal. **B)** CRY1 gene expression in leaves of *cry1_{control}* and *cry1_{NES}* compared to WT Col-0 and *cry1-304*. Seeds of all genotypes were kindly provided by Edgar Spalding (Wu and Spalding, 2008).

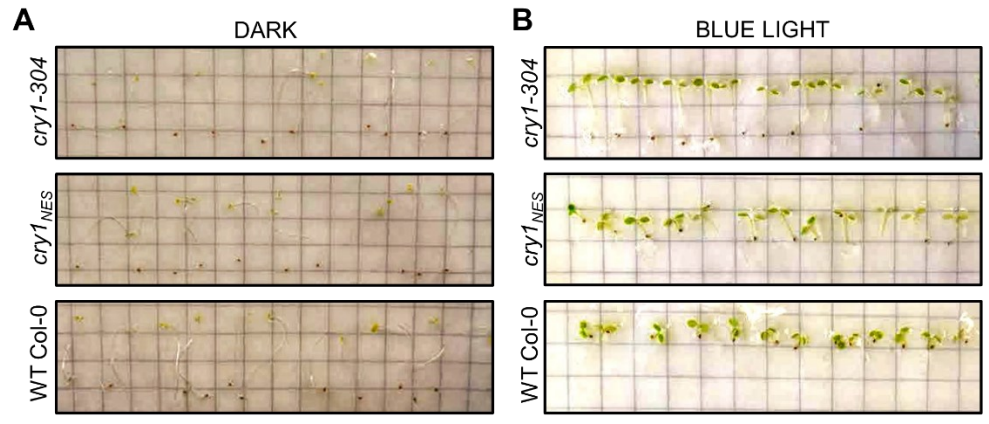
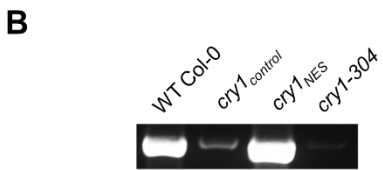


Figure 3.12 Visual phenotype of seedlings grown in the dark (left panel) or under low-fluence blue light (right panel; ca.30 $\mu\text{mol photons m}^{-2} \text{s}^{-1}$). 4-day old seedlings of WT Col-0, *cry1_{NES}* and *cry1-304* are shown.

With the aim to clarify the functions of nuclear- and cytoplasm-localized CRY1 in photosynthetic acclimation, photosynthetic and growth phenotypes of *cry1_{control}* and *cry1_{NES}* were analyzed under CL and EL and compared with *cry1-304* and WT Col-0. Under CL there weren't any visually detectable differences between the genotypes except *cry1_{control}* (**Figure 3.13 A**) which showed constitutive inhibition of growth probably because of the strong accumulation of CRY1 in the nucleus, as reported previously (Wu and Spalding, 2007). Under FL and HL leaf expansion was slowed down in all genotypes but especially *cry1-304* and *cry1_{control}*. While older leaves of *cry1-304* bleached under HL, neither *cry1_{control}* nor *cry1_{NES}* showed a sign of bleaching. In general, *cry1_{NES}* was more comparable with WT Col-0 than with *cry1-304* under CL, FL and HL conditions. While *cry1_{control}* exhibited photoinhibition and NPQ deficiency under FL as *cry1-304* did, *cry1_{NES}* showed F_v/F_m and NPQ phenotypes which were comparable with WT Col-0 under CL and FL (**Figure 3.13 B**). These observations suggest that the nucleus-localized CRY1 in the *cry1_{control}* is not able to rescue the photosynthetic phenotypes of CRY1-KO plants observed at the level of PSII under EL conditions. On the other hand, the cytoplasmic CRY1 in *cry1_{NES}* seemed to completely rescue the phenotypes of the fluorescence parameters (**Figure 3.13 B**) with minimal changes in visual growth phenotype compared to WT Col-0. The unspecific localization of CRY1 in *cry1_{NLS}*, the very low *CRY1* gene expression in *cry1_{control}* (**Figure 3.11 B**) and the rather ambiguous hypocotyl growth phenotypes found in *cry1_{NES}* under BL (**Figure 3.12 B**) made it difficult to attribute the photosynthetic and photoacclimatory phenotypes observed in these plants to specific CRY1 protein localization. Furthermore, while the GFP fusion allows *in vivo* tracking of CRY1 protein localization, it may affect the CRY1 activity. To overcome these limitations, new CRY1-overexpressing lines were generated by using a similar approach but without GFP.

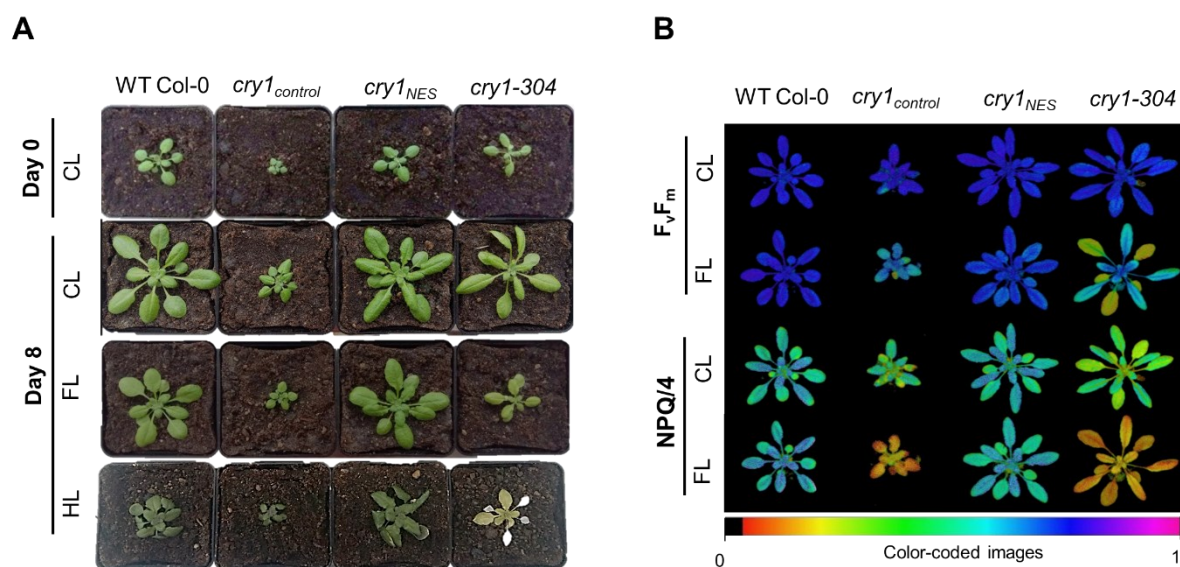


Figure 3.13. Visual phenotypes and photosynthetic characterization of WT Col-0, *cry1_{control}*, *cry1_{NES}* and *cry1-304* growing under CL, FL and HL. **A)** Visual phenotypes of representative plants before the onset of the light treatments (day 0) and at the end of the treatments (day 8). **B)** Spatial heterogeneity of F_v/F_m and NPQ in whole rosettes of representative plants after 3-d exposure to CL and FL. The color bar at the bottom shows the scale of the color code.

3.2.2 Generation of new CRY1 overexpression lines

New transgenic lines overexpressing *CRY1* gene under the control of the cauliflower mosaic virus promoter (35S) were generated to analyze the *CRY1* functions in the nucleus and the cytoplasm. Three constructs were made to transform *cry1-304*: *35S_CRY1* without any localization signal (**Figure 3.14 A**), *35S_NLS_CRY1* with the NLS (**Figure 3.15 A**) and *35S_NES_CRY1* with the NES (**Figure 3.16 A**). As in the study by Wu and Spalding (2007), NLS and NES were introduced at the N-terminus of *CRY1* gene. In addition, to identify possible interaction partners of *CRY1* in the nucleus and the cytoplasm, another type of constructs were made by including the Gs tandem affinity purification tag (GsTAP) (Van Leene et al., 2008) in the aforementioned constructs. Unfortunately, vector construction was not successful for *35S_GsTAP_NLS_CRY1* and no positive transformant could be isolated for *35S_GsTAP_CRY1*. Only the transformation with *35S_GsTAP_NES_CRY1* (**Figures 3.17 A**) produced several independent transgenic lines.

Plants in T0, T1 and T2 generation were first grown on selective medium containing Kanamycin and surviving plants were transferred to soil to cultivate further for leaf and seed harvesting. Using these leaf samples, the plants were then screened by PCR for the presence of 35S fused to *CRY1* in the genomic DNA. The results of PCR screening in T2 lines of *35S_CRY1*, *35S-NLS_CRY1*, *35S_NES_CRY1* and *35S_GsTAP_NES_CRY1* are shown in **Figures 3.14 B, 3.15 B, 3.16 B and 3.17 B**, respectively. The *CRY1* gene expression was also assessed in the leaf samples of T2 plants to compare with WT Col-0 and *cry1-304* (**Figures 3.14 C, 3.15 C, 3.16 C and 3.17 C**).

Since there is no functional anti-*CRY1* antibody that is commercially available for plants, *CRY1* protein levels could not be checked in the lines without GsTAP (*35S_CRY1*, *35S-NLS_CRY1* and *35S_NES_CRY1*). In the case of *35S_GsTAP_NES_CRY1*, accumulation of protein G could be confirmed in several lines, in which *CRY1* gene was highly expressed (**Figure 3.17 C**). The Gs tag contains protein G (with two IgG-binding domains) and a small (38 amino acids) streptavidin-binding peptide which are separated by two cleavage sites of tobacco etch virus (Van Leene et al., 2008). The size of protein G is ca. 32 kDa and *CRY1* is ca. 76 kDa, yielding an expected total molecular weight of ca. 110 kDa. Protein bands were detected in the region slightly higher than 100 kDa in a western blot of the selected *35S_GsTAP_NES_CRY1* lines (**Figure 3.17 C**). The corresponding signal was absent in the negative control *cry1-304*. These results suggest that *CRY1* proteins linked to protein G were expressed and accumulating in these transgenic lines. Since the vector construct of *35S_GsTAP_NES_CRY1* was the same as that of *35S_NES_CRY1* except the presence of GsTAP tag in front, it can be assumed that *CRY1* protein could accumulate also in the *35S_NES_CRY1* lines overexpressing *CRY1* gene. Likewise, as the vectors of *35S_CRY1* and *35S-NLS_CRY1* were identical with that of *35S_NES_CRY1* except the presence or absence of localization signal (NLS or NES), the overexpression of *CRY1* gene most likely led to *CRY1* protein accumulation also in *35S_CRY1* and *35S-NLS_CRY1* lines. The efficacy of *CRY1* protein targeting by the localization signals was assumed to be the same as was shown by the GFP-fusion lines described in Wu and Spalding (2007). **Table 3.4** summarizes the outcome of genotypic characterization in the T2 plants of *35S_CRY1*, *35S-NLS_CRY1*, *35S_NES_CRY1* and *35S_GsTAP_NES_CRY1* lines. A qualitative estimation of the levels of *CRY1* gene expression in the transgenic lines in comparison with WT Col-0 is also indicated. The introduction of *CRY1* gene in genomic DNA of *cry1-304* mutant led to various levels of *CRY1* gene expression in leaves.

Two independent lines, which were strongly overexpressing *CRY1* gene compared to the level in WT Col-0, were selected from each of *35S_CRY1*, *35S-NLS_CRY1* and *35S_NES_CRY1* to continue with phenotyping. The overexpression of *CRY1* gene was also confirmed in the T3 plants of some of the selected overexpressor (OE) lines (**Figure 3.18**).

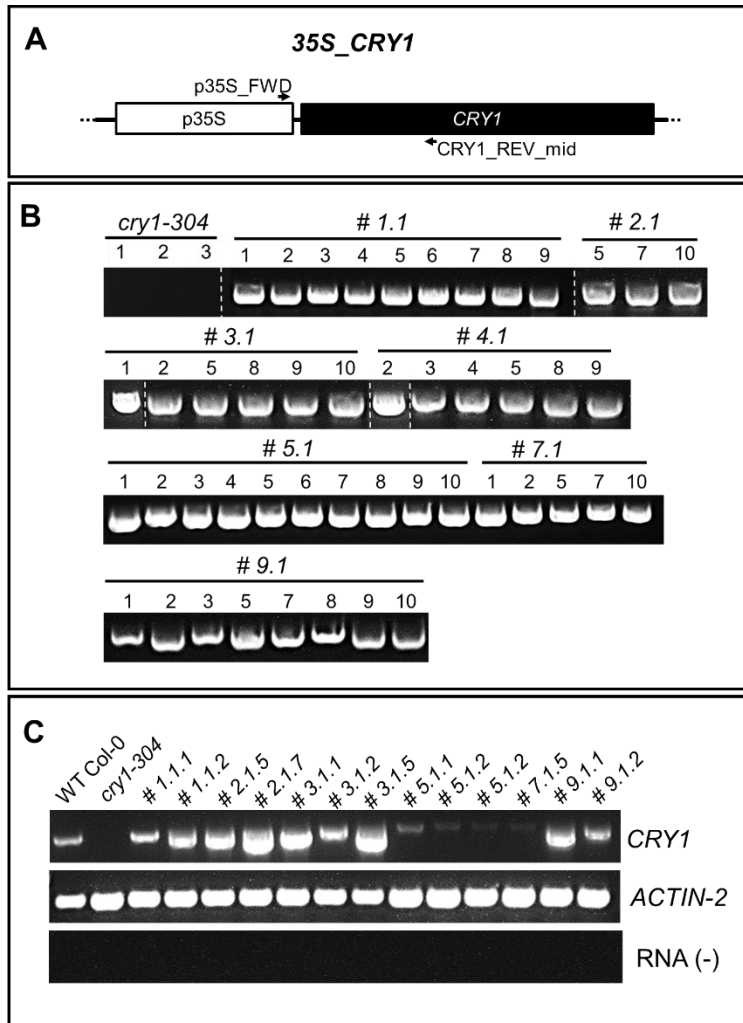


Figure 3.14. Construct and genotypic characterization of *CRY1* OE lines under the control of 35S promoter (*35S_CRY1*) **A**) Construct design showing the primers used for genetic screening of the plants in T1 and T2 generation. **B**) Screening PCR on g DNA of the positively selected transgenic plants (based on kanamycin resistance) in T2 generation. A region including both 35S and *CRY1* gene coding sequence was amplified by PCR. *cry1-304* was used as negative control. *cry1-304* was the background of the transgenic lines. **C**) *CRY1* gene expression was analyzed by reverse transcription-PCR (RT-PCR) in leaves of plants positively screened in T2 generation. WT Col-0 and *cry1-304* were included as positive and negative control, respectively. For all the plants *ACTIN-2* PCR product was also amplified as internal reference and RNA was used as negative control. Plant transformation was done with the help of Ahn Bahn (IBG-2, FZJ) and the selection of the positive lines with the help of the trainees Sven Gerlach and Nadine da Silva.

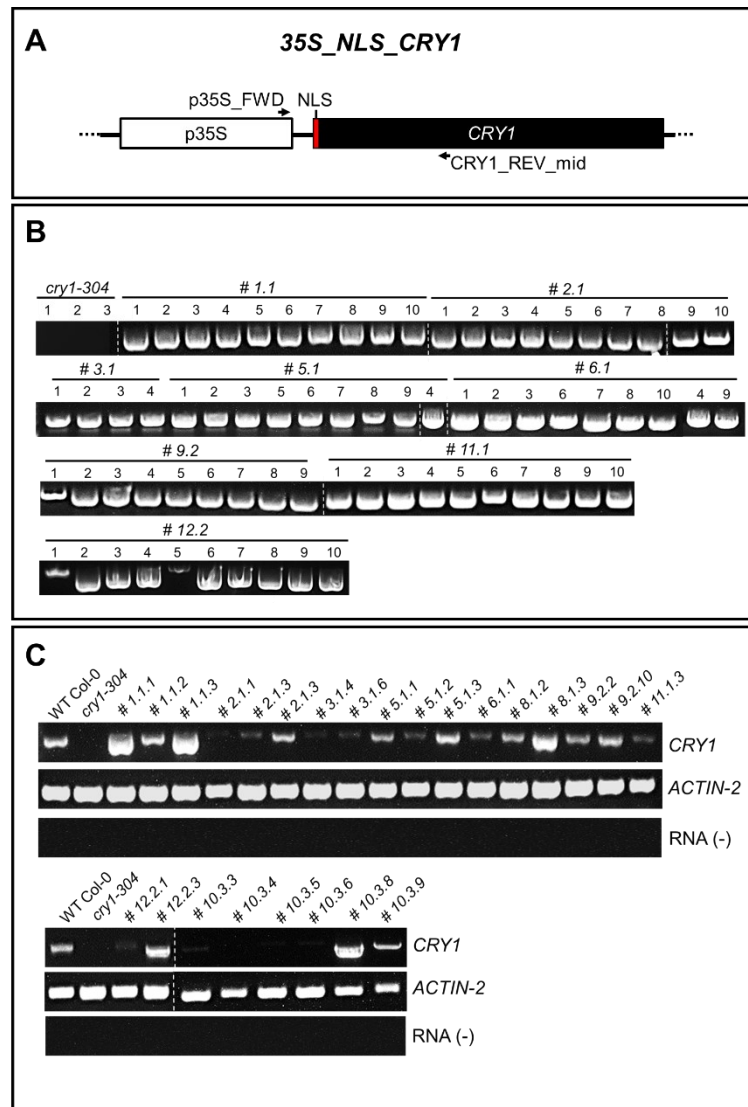


Figure 3.15 Construct and genotypic characterization of *CRY1* OE lines with nuclear localization signal under the control of the 35S promoter (**35S-NLS-CRY1**) **A**) Construct design showing the primers used for screening of the plants in T1 and T2 generation. **B**) Screening PCR on genomic DNA of the positively selected plants in T2 generation. A region including both 35S and *CRY1* gene coding sequence was amplified in the positive plants. *cry1-304* was used as negative control. *cry1-304* was the background of the transgenic lines. **C**) *CRY1* gene expression was analyzed by reverse transcription-PCR (RT-PCR) in leaves of plants positively screened in T2 generation. WT Col-0 and *cry1-304* were included as positive and negative control, respectively. For all the plants *ACTIN-2* PCR product was also amplified as internal reference and RNA was used as negative control. Plant transformation was done with the help of Ahn Bahn (IBG-2, FZJ) and the selection of the positive lines with the help of the trainees Sven Gerlach and Nadine da Silva.

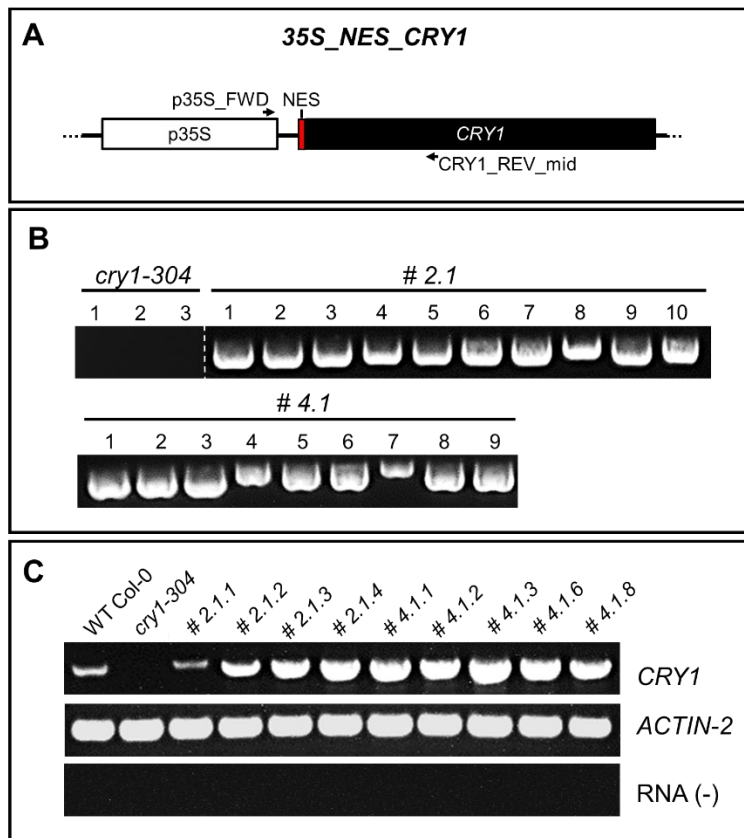


Figure 3.16. Construct and genotypic characterization of *CRY1* OE lines with nuclear export signal under the control of the 35S promoter (35S_NES_CRY1) **A**) Construct design showing the primers used for screening of the plants in T1 and T2 generation. **B**) Screening PCR on genomic DNA of the positively selected plants in T2 generation. A region including both 35S and *CRY1* gene coding sequence was amplified in the positive plants. *cry1-304* was used as negative control. *cry1-304* was the background of the transgenic lines. **C**) *CRY1* gene expression was analyzed by reverse transcription-PCR (RT-PCR) in leaves of plants positively screened in T2 generation. WT Col-0 and *cry1-304* were included as positive and negative control, respectively. For all the plants *ACTIN-2* PCR product was also amplified as internal reference and RNA was used as negative control. Plant transformation was done with the help of Ahn Bahn (IBG-2, FZJ) and the selection of the positive lines with the help of the trainees Sven Gerlach and Nadine da Silva.

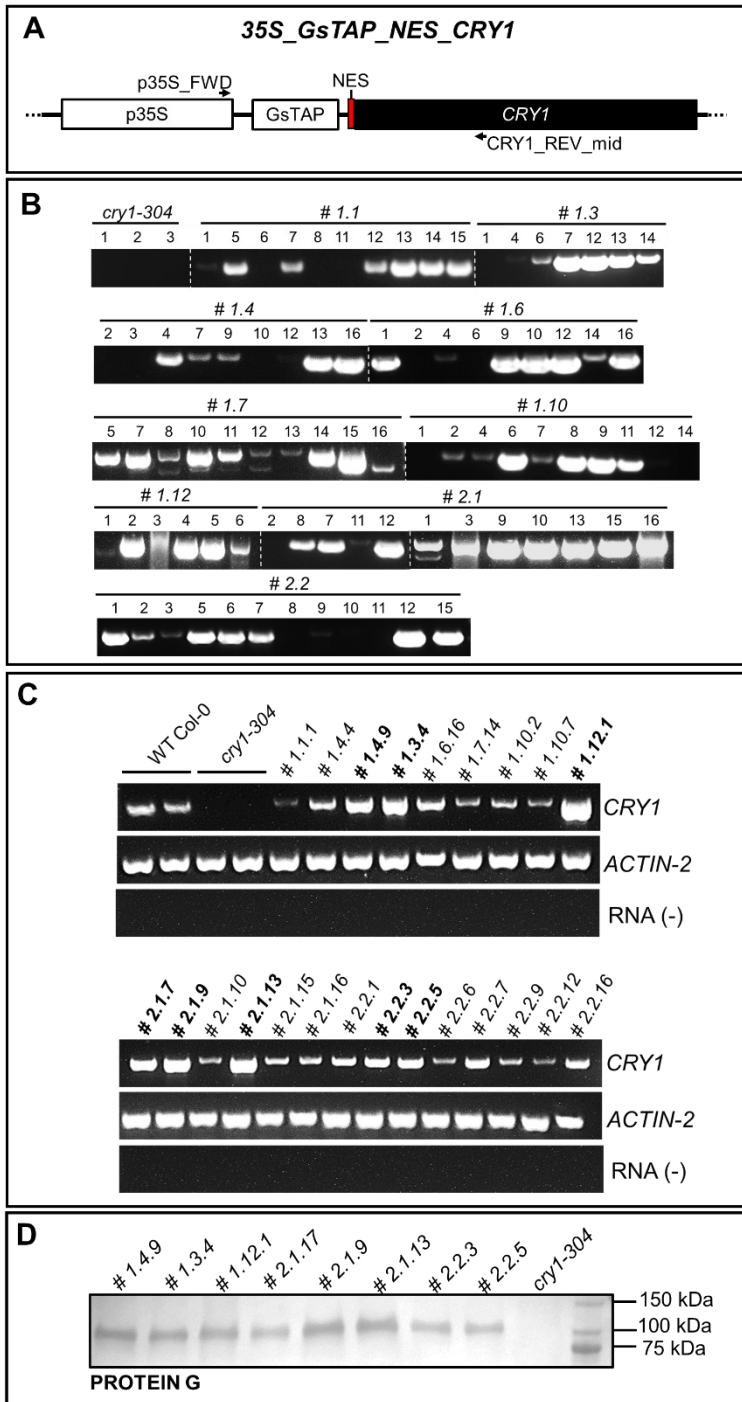


Figure 3.17. Construct and genotypic characterization of *CRY1* OE lines with the nuclear export signal and GsTAP under the control of the 35S promoter (35S_GsTAP_NES_CRY1) **A)** Construct design showing the primers used for screening of the plants in T1 and T2 generation. **B)** Screening PCR on genomic DNA of the positively selected plants in T2 generation. A region including both 35S and *CRY1* gene coding sequence was amplified in the positive plants. *cry1-304* were used as negative controls. *cry1-304* was the background of the transgenic lines. **C)** *CRY1* gene expression was analyzed by reverse transcription-PCR (RT-PCR) in leaves of plants positively screened in T2 generation. WT Col-0 and *cry1-304* were included as positive and negative control, respectively. For all the plants *ACTIN-2* PCR product was also amplified as internal reference and RNA was used as negative control. **D)** Western blot analysis to confirm the presence of the protein G in positive plants expressing the GsTAP. The expected molecular size of protein G is 32 kDa, that of *CRY1* protein is 76 kDa. Plant transformation was done with the help of Ahn Bahn (IBG-2, FZJ) and the selection of the positive lines with the help of the trainees Sven Gerlach and Nadine da Silva.

35S_CRY1		35S-NLS_CRY1		35S_NES_CRY1		35S_GsTAP_NES_CRY1	
Line	CRY1 gene expression	Line	CRY1 gene expression	Line	CRY1 gene expression	Line	CRY1 gene expression
#1.1.1	WT like	#1.1.1	OE (+++)	#2.1.1	KD	#1.1.1	KD
#1.1.2	OE (+)	#1.1.2	WT like	#2.1.2	OE (++)	#1.4.4	WT like
#2.1.5	OE (++)	#1.1.3	OE (+++)	#2.1.3	OE (+++)	#1.4.9	OE (++)
#2.1.7	OE (+++)	#2.1.1	KD	#2.1.4	OE (+++)	#1.3.4	OE (++)
#3.1.1	OE (+++)	#2.1.2	KD	#4.1.1	OE (+++)	#1.6.16	OE (+)
#3.1.2	OE (+)	#2.1.3	WT like	#4.1.2	OE (+++)	# 1.7.14	KD
#3.1.5	OE (+++)	#3.1.4	KD	#4.1.3	OE (+++)	#1.10.2	KD
#5.1.1	KD	#3.1.6	KD	#4.1.6	OE (+++)	#1.10.7	KD
#5.1.2	KD	#5.1.1	KD	#4.1.8	OE (+++)	# 1.12.1	OE (+++)
#7.1.2	KD	#5.1.2	KD			#2.1.7	OE (++)
#7.1.5	KD	#5.1.3	WT like			#2.1.9	OE (++)
#9.1.1	OE (+)	#6.1.1	KD			#2.1.10	KD
#9.1.2	WT like	#8.1.2	KD			#2.1.13	OE (++)
		#8.1.3	OE (+++)			#2.1.15	WT like
		#9.2.2	KD			#2.1.16	WT like
		#9.2.10	KD			#2.2.1	OE (+)
		#11.1.3	KD			#2.2.3	OE (+)
		#12.2.1	KD			#2.2.5	OE (+)
		#12.2.3	OE (+)			#2.2.6	KD
		#10.3.3	KD			#2.2.7	OE (+)
		#10.3.5	KD			#2.2.9	KD
		#10.3.6	KD			#2.2.12	KD
		#10.3.8	OE (++)			#2.2.16	WT like
		#10.3.9	OE (+)				

Table 3.4. Summary of genotypic characterization of transgenic lines 35S_CRY1, 35S-NLS_CRY1, 35S_NES_CRY1 and 35S_GsTAP_NES_CRY1 in T2 generation. Transgenic plants expressing CRY1 are categorized as knock down-like (KD), WT-like or overexpressor (OE) based on the intensity of the CRY1 PCR product compared to WT Col-0 and *cry1-304*. Different levels of CRY1 gene overexpression are indicated with +, ++ and +++ symbols. The lines from 35S_CRY1, 35S-NLS_CRY1 and 35S_NES_CRY1, which were selected for phenotypic characterization, are highlighted by light-grey shading. The lines from 35S_GsTAP_NES_CRY1, which were positive for the presence of protein G, are written in bold. Selection of the positive lines was performed with the help of the trainees Sven Gerlach and Nadine da Silva

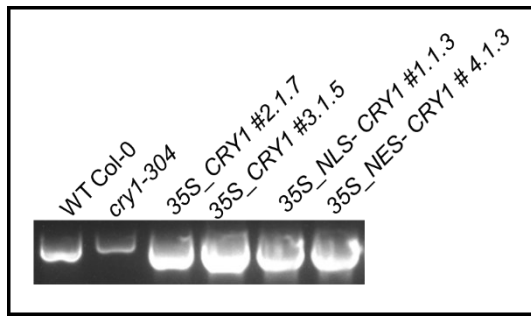


Figure 3.18 *CRY1* gene expression analyzed by reverse transcription-PCR (RT-PCR) in leaves of plants positively screened in T3 generation. WT Col-0 and *cry1-304* were included as positive and negative control, respectively.

3.2.3 Phenotypic characterization of the selected *CRY1* overexpressor lines

With the aim to clarify whether the overexpression of *CRY1* in *cry1-304* mutant can rescue the *CRY1* KO phenotype and whether the nuclear or the cytoplasmic fraction of *CRY1* has a predominant role in photosynthetic acclimation, two independent lines of the newly generated *35S_CRY1*, *35S_NLS_CRY1* and *35S_NES_CRY1* were examined for their phenotypes under different light conditions and compared with WT Col-0 and *cry1-304*. Phenotypic traits related to hypocotyl growth, shoot morphology, leaf growth and PSII parameters were analyzed in T3 generation plants of these lines. The phenotyping experiments described below (sections 3.2.3.1, 3.2.3.2 and 3.2.3.3) were performed by Nina Natascha Boots for her bachelor thesis (Heinrich Heine University, 2019).

3.2.3.1 Visual phenotype of seedlings grown under LL and in the darkness

In order to evaluate the photomorphogenic phenotype, seeds of *35S_CRY1* (#3.1.1 and #2.1.7), *35S_NLS_CRY1* (#1.1.3 and #8.1.3) and *35S_NES_CRY1* (#4.1.3 and #2.1.4) were germinated in the dark or under LL and compared to WT Col-0 and *cry1-304* (**Figure 3.19**). Similar to the experiment described in **Figure 3.12**, all the genotypes showed hypocotyl elongation and absence of de-etiolation in the dark, while under LL WT Col-0 and *cry1-304* showed strong and little inhibition of hypocotyl elongation, respectively. All the *CRY1* OE lines displayed elongated hypocotyls under LL, as seen in *cry1-304*.

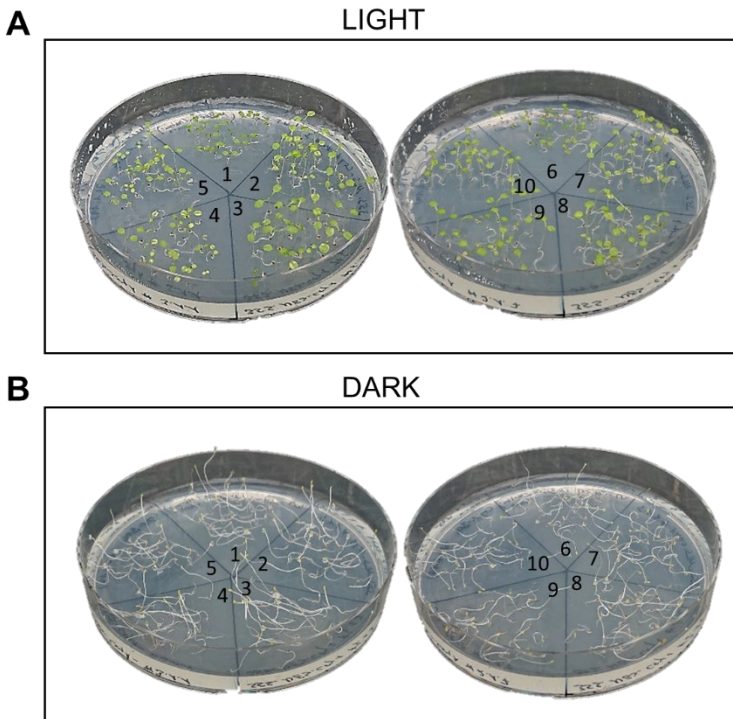


Figure 3.19 Visual phenotype of seedlings of *CRY1* OE lines grown for 4 days **A**) in the dark **B**) or under low light ($100 \mu\text{mol photons m}^{-2} \text{s}^{-1}$) 1) WT-Col-0; 2) *cry1-304*; 3) *35S_CRY1* #3.1.1; 4) *35S_NES_CRY1* #4.1.3; 5) *35S-NLS_CRY1* #1.1.3; 6) WT-Col-0; 7) *cry1-304*; 8) *35S_CRY1* #2.1.7; 9) *35S_NES_CRY1* #2.1.4; 10) *35S-NLS_CRY1* #8.1.3. Picture modified from Nina Natascha Boots' bachelor thesis (HHU, 2019).

3.2.3.2 Visual and Growth phenotype under EL

Plants of *35S_CRY1* (#3.1.5 and #2.1.7), *35S-NLS_CRY1* (#1.1.3 and #8.1.3) and *35S_NES_CRY1* (#4.1.3 and #2.1.4) were exposed to EL along with WT Col-0 and *cry1-304*. Because it was not possible to apply exactly the same HL and FL treatment as described in section 3.1, slightly different regimes were used in this experiment, and they are called HL2 and FL2 for clarity. Compared to HL conditions in section 3.1, in which plants were exposed exactly to $1000 \mu\text{mol photons m}^{-2} \text{s}^{-1}$, in HL2 the light intensity ranged from ca. $600\text{--}800$ to $1000 \mu\text{mol photons m}^{-2} \text{s}^{-1}$ in the treatment area. To avoid positional effects and obtain results comparable with the previous one, plants belonging to different genotypes were randomized and rotated daily. In FL2 the light intensity was changing sigmoidally between HL ($1000 \mu\text{mol photons m}^{-2} \text{s}^{-1}$, every ca. 20 s) and CL every 5 min during the light period in the growth chamber, as described in 3.1.3.

Under CL leaf morphological differences between the transgenic lines, WT Col-0 and *cry1-304* were relatively small and all the *CRY1 OE* lines were more similar to *cry1-304*, having somewhat elongated petioles and leaves compared to WT Col-0 (**Figure 3.20 A**). After seven days in FL2 all the genotypes had flat leaves compared to the CL condition. The seven-days exposure to HL2 caused photobleaching of *cry1-304*, as already described in section 3.1.1 for HL-treated plants (**Figure 3.1**) and previously shown by Kleine et al. (2007). None of the selected transgenic lines indicated rescue of the HL2 sensitivity of *cry1-304*. Pigmentation in the abaxial leaf surface was also compared in the genotypes under the three light conditions. Reddish coloration due to anthocyanin accumulation was seen in the lamina and petiole of HL2-treated WT Col-0, whereas in *cry1-304* and the *CRY1 OE* lines it was restricted to the petiole (**Figure 3.20 B**). The role of *CRY1* in anthocyanin biosynthesis and accumulation has been established in different plant species including *A. thaliana* (Ahmad et al., 1995), tomato (Ninu et al., 1999), *Brassica napus* (Chatterjee et al., 2006) and eggplant (Jiang et al., 2016).

Leaf growth was monitored by measuring the projected leaf area using the GROWSCREEN-FLUORO method (Jansen et al., 2009) (**Figure 3.21 B**). Under CL the projected leaf area of WT Col-0, *cry1-304* and the selected transgenic lines all increased exponentially. Leaf expansion was slowed down in all the transgenic lines under both FL2 and HL2, in the same way as in *cry1-304*. The inhibition of leaf expansion was especially evident under HL2 since the effects of FL2 were milder. Compared to the experiment in **Figure 3.1 B**, HL2-treated plants of *cry1-304* showed negative or no leaf expansion (due to bleaching of older leaves) only in the first few days of the HL2 treatment (**Figure 3.21**). Thereafter leaf expansion recovered in *cry1-304* as well as in the transgenic lines although these plants remained smaller than the corresponding plants in CL until the end of the 7-d experiment.

These results indicate that the *CRY1* gene overexpression in *cry1-304* did not rescue the well-known *CRY1*-dependent phenotypes related to hypocotyl and petiole elongation or anthocyanin accumulation. No sign of rescue was found also for EL-sensitive phenotype assessed by photobleaching and growth impairment in HL. The findings do not agree with the phenotypes found in *cry1_{control}* and *cry1_{NES}* plants in the previous section (3.2.1).

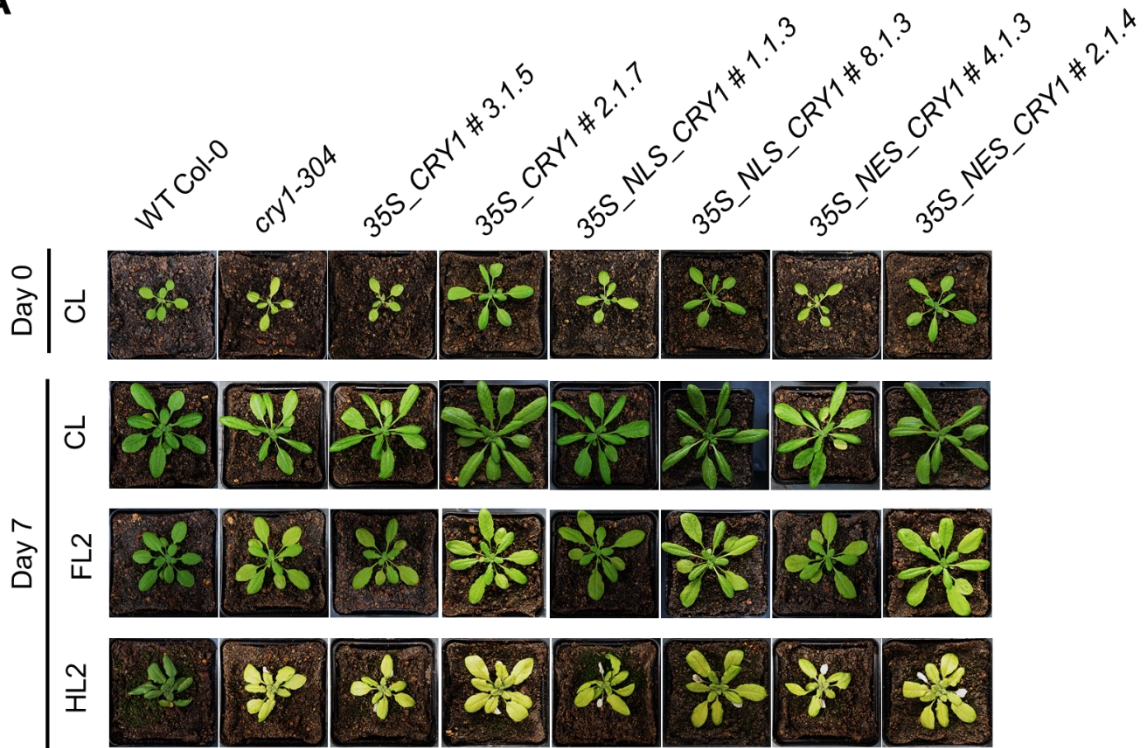
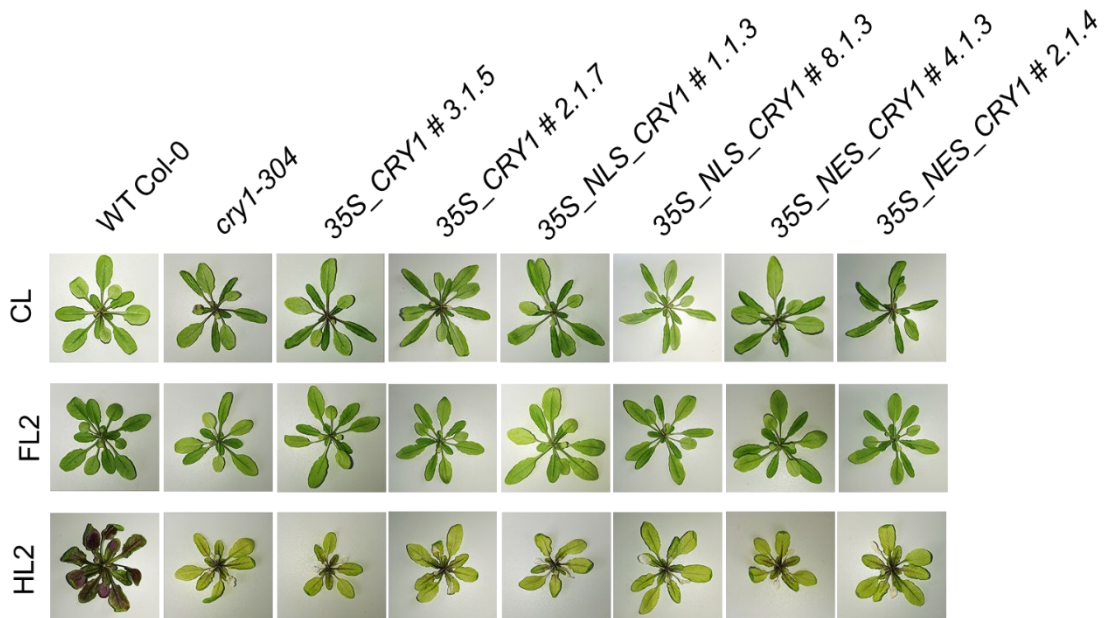
A**B**

Figure 3.20. Visual phenotypes of WT Col-0, *cry1-304*, 35S_CRY1, 35S-NLS_CRY1 and 35S_NES_CRY1 before the onset of the CL, FL2 and HL2 treatments (day 0) and at the end of the treatments (day 7). **A)** Representative plants shown from adaxial side. **B)** Abaxial leaf surface of representative plants at the end of the treatments (day 7). Picture modified from Nina Natascha Boots' bachelor thesis (HHU, 2019)

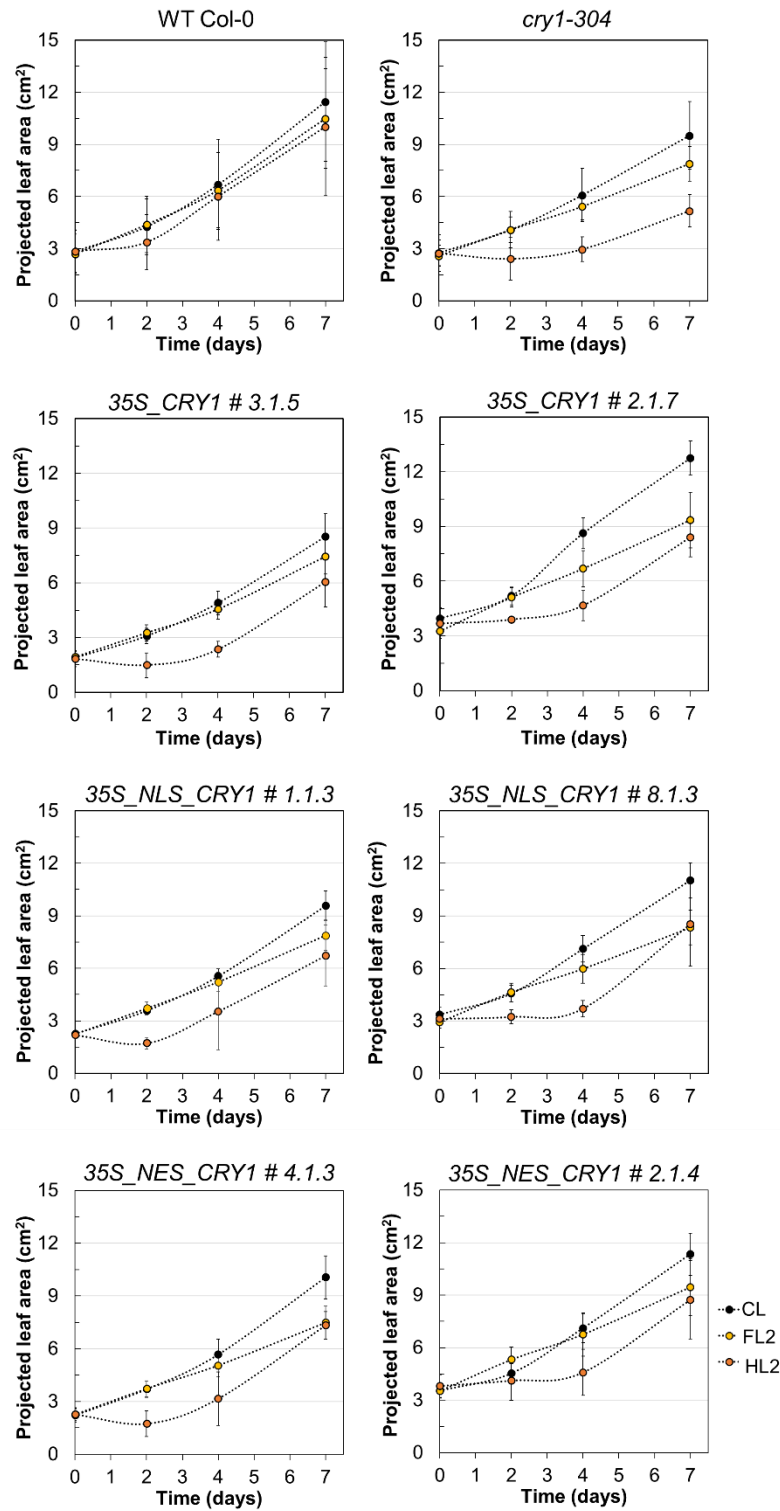


Figure 3.21. Leaf expansion growth of WT Col-0, *cry1-304*, 35S_CRY1, 35S-NLS_CRY1 and 35S_NES_CRY1 monitored as changes in the total projected leaf area (cm²) for seven days of exposure to CL, FL2 and HL2. Data are mean values \pm SD (n = 16-4 plants). The measurements were conducted by Nina Boots for her bachelor thesis (HHU, 2019).

3.2.3.3 Photosynthetic phenotype under EL

The Chl fluorescence parameters related to PSII activity were evaluated in mature leaves after one or three days of exposure to HL2 and FL2, respectively. Measurements of light response curves were followed by a dark recovery period of 90 s to assess the rapidly reversible component (qE) of NPQ.

After three days of exposure to FL2 F_v/F_m slightly decreased in *cry1-304* and the transgenic lines compared to WT Col-0 (**Figures 3.22**). Y(II) decreased slightly in the FL2-treated plants of WT Col-0 compared to their counterparts which stayed in the CL condition, while the FL2 plants of *cry1-304* and the transgenic lines exhibited drastic decrease in Y(II), which was detectable already at relatively low AL intensity (**Figure 3.22**). Y(II) remained low in these plants during the dark recovery period compared to the same plants of the CL treatment or WT Col-0 of the FL2 treatment (**Figure 3.22**). Accordingly, *cry1-304* and the transgenic lines had also lower capacity for ETR(II), which is calculated from Y(II), compared to WT Col-0 following the treatment with both CL and FL2 (**Figure S3**).

As expected from the results shown in **Figure S1**, *cry1-304* had lower NPQ compared to WT Col-0 after the CL and FL2 treatment (**Figure 3.23**). Only the CL plants of 35S_NES_CRY1 # 4.1.3, in which extremely low Y(II) and ETR were measured (**Figures 3.24 and S3**), had NPQ values which were more similar to WT Col-0 than *cry1-304* (**Figure 3.23**). All the other transgenic lines showed *cry1-304*-like NPQ phenotype (**Figure 3.23**). Albeit at lower levels than in WT Col-0, the FL2 plants of *cry1-304* and the transgenic lines were able to upregulate NPQ after three days of exposure to FL2 (**Figure 3.23**). Extracted data from the same experiment are shown in **Figure 3.24**. None of the transgenic lines 35S_CRY1, 35S_NLS_CRY1, 35S_NES_CRY1 seemed to rescue the photosynthetic phenotype observed in *cry1-304* under CL and FL2. All the FL2 treated transgenic lines showed comparable F_v/F_m with *cry1-304* (**Figure 3.24 A**). Their ETR(II) (**Figure 3.24 B**) and NPQ (**Figure 3.24 C**) values during the induction measurements were also comparable with *cry1-304* both in CL and FL2.

The corresponding data set of the HL2-treated plants are shown in **Figures S4 – S6** together with the CL plants. Similar to the FL2 treatment, one day of exposure to HL2 caused PSII photoinhibition in *cry1-304* and all the transgenic lines, as indicated by their lower values of F_v/F_m compared to WT Col-0 (**Figure 3.26 A**).

This strong impairment of PSII capacity in the HL2 plants of *cry1-304* and the transgenic lines was reflected in the light response curves and the very limited dark recovery of Y(II) (**Figure S4**). Consequently, ETR(II) was almost abolished in *cry1-304* and the transgenic lines after one day of HL2 exposure (**Figures 3.26 B and S5**). Only at the very low intensities of AL these HL2 plants had positive values of ETR(II), which probably contributed to the development of NPQ (**Figures 3.26 C and S6**). While NPQ increased to up to 3 at the highest AL intensity in the HL2 plants of WT Col-0, it did not exceed 1.5 or 2 in the corresponding plants of *cry1-304* and the transgenic lines (**Figure S6**). Only the HL2 plants of *35S_CRY1 #3.1.5* showed a significant increase in NPQ at $\sim 460 \mu\text{mol m}^{-2} \text{s}^{-1}$ compared to the HL2 plants of *cry1-304* (**Figure 3.26 C**) although such an increase was not found at all AL intensities (**Figure S6**) and also not in the FL2 treatment (**Figure 3.24 C**).

Overall, as was found in the analyses of visual and growth phenotypes, the overexpression of *CRY1* gene in *cry1-304* did not rescue the EL-sensitive phenotype of photosynthetic acclimation in any of the transgenic lines under dynamic (FL2) and static (HL) EL conditions. These findings again differ from the observations made in the *cry1_{control}* and *cry1_{NES}* plants in 3.2.1.

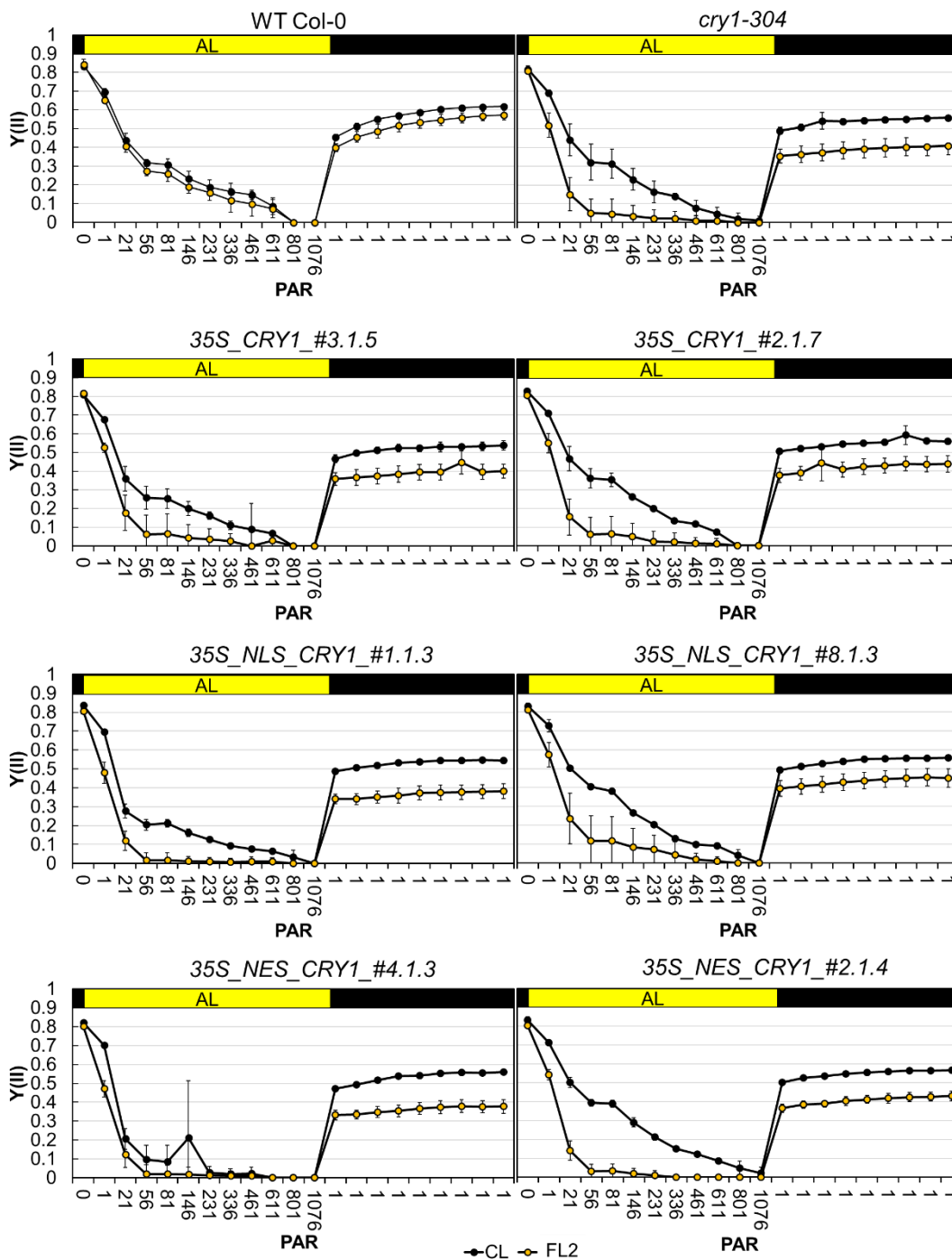


Figure 3.22. Characterization of PSII quantum yield, $Y(II)$, before the onset of the experiment under CL (black symbols) and after three-day exposure to FL2 (yellow symbols) in WT Col-0, *cry1-304*, *35S_CRY1*, *35S-NLS_CRY1* and *35S_NES_CRY1*. Rapid light response curves were measured in leaves of overnight dark-adapted plants. The intensity of AL was gradually increased in 12 steps from 0 to 1076 $\mu\text{mol photons m}^{-2} \text{s}^{-1}$ with 30 s of dwell time at each step. The light response curves were followed by a dark recovery of 90 s with SP every 10 s. Mean values \pm SD ($n = 3-6$) are shown. The measurements were conducted by Nina Boots for her bachelor thesis (HHU, 2019).

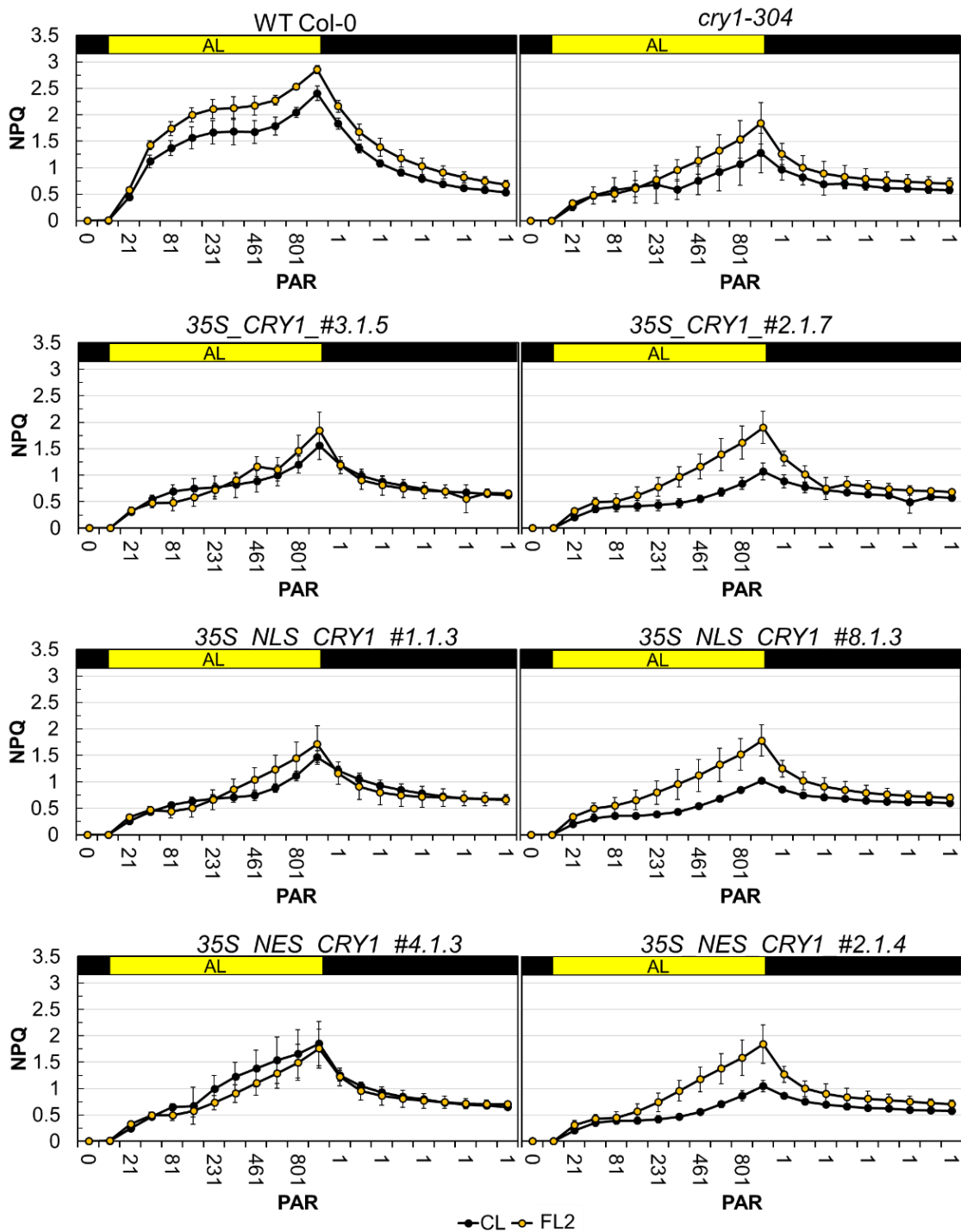


Figure 3.23. Characterization of non-photochemical quenching (NPQ) before the onset of the experiment under CL (black symbols) and after three-day exposure to FL2 (yellow symbols) in WT Col-0, *cry1-304*, *35S_CRY1*, *35S_NLS_CRY1* and *35S_NES_CRY1*. Data are from the same measurements as shown in the rapid light response curves of Fig. 3.22. Mean values \pm SD ($n = 3-6$) are shown. The measurements were conducted by Nina Boots for her bachelor thesis (HHU, 2019).

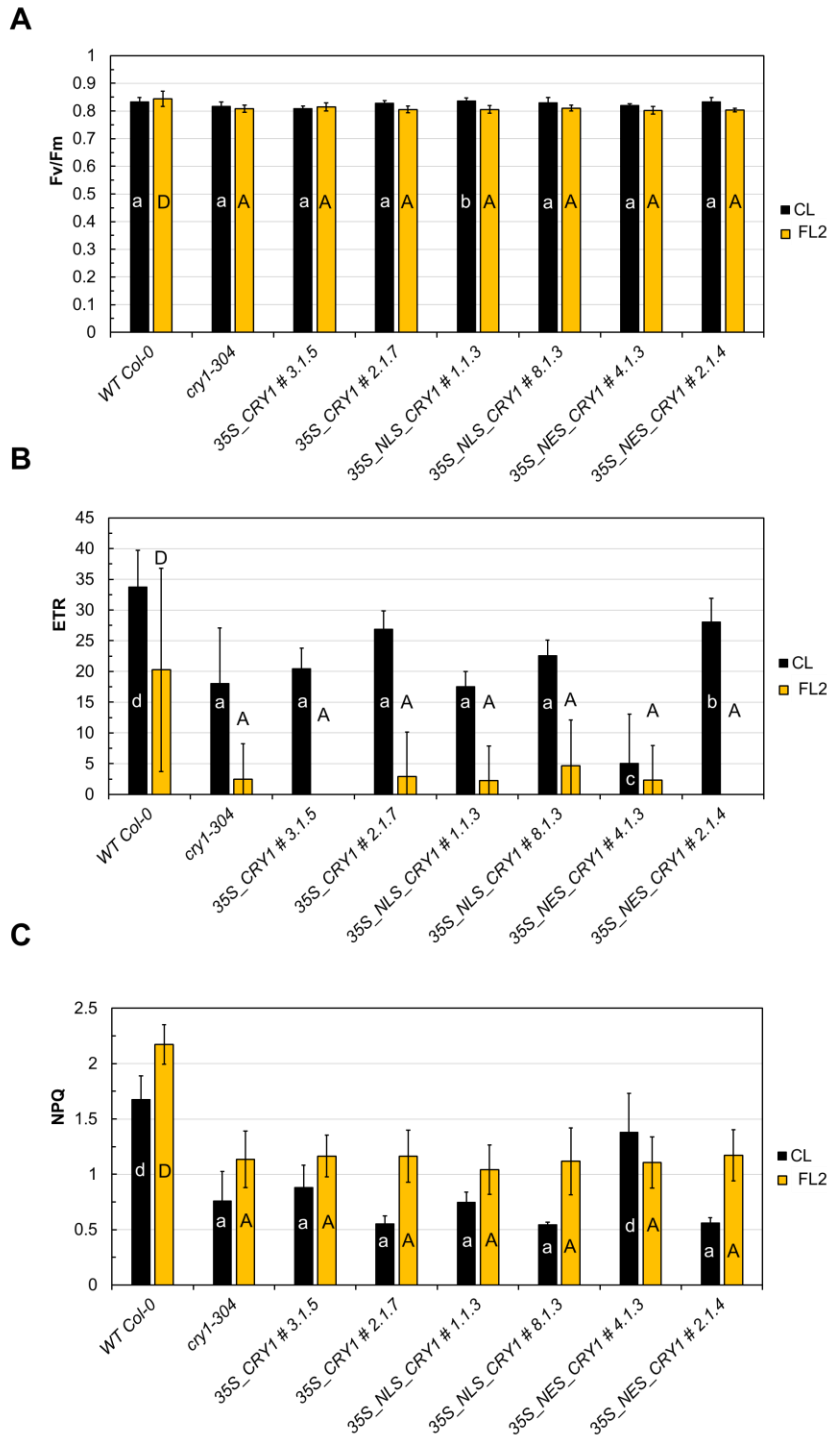


Figure 3.24. Characterization of key photosynthetic parameters under FL2 in WT Col-0, *cry1-304*, *35S_CRY1*, *35S-NLS_CRY1* and *35S_NES_CRY1* extracted from the experiment shown in Figures 3.22, 3.23 and S.3 **A**) Maximum quantum yield of PSII in the overnight dark-adapted state (F_v/F_m). **B**) ETR values at $461 \mu\text{mol photons m}^{-2} \text{s}^{-1}$ **C**) NPQ values at $461 \mu\text{mol photons m}^{-2} \text{s}^{-1}$. Mean values \pm SD ($n = 3-6$) are shown. Significant differences between the genotypes as well as between the light conditions (CL and FL), and the interaction (genotype X light condition) were assessed by two-way ANOVA followed by Tukey's multiple comparison test. Different letters in the panel indicate significant differences compared to *cry1-304* (b, $P \leq 0.05$; c, $P \leq 0.01$; D and d, $P \leq 0.001$). Lowercase and uppercase letters are for the comparison between the genotypes under CL and FL2, respectively. The measurements were conducted by Nina Boots for her bachelor thesis (HHU, 2019).

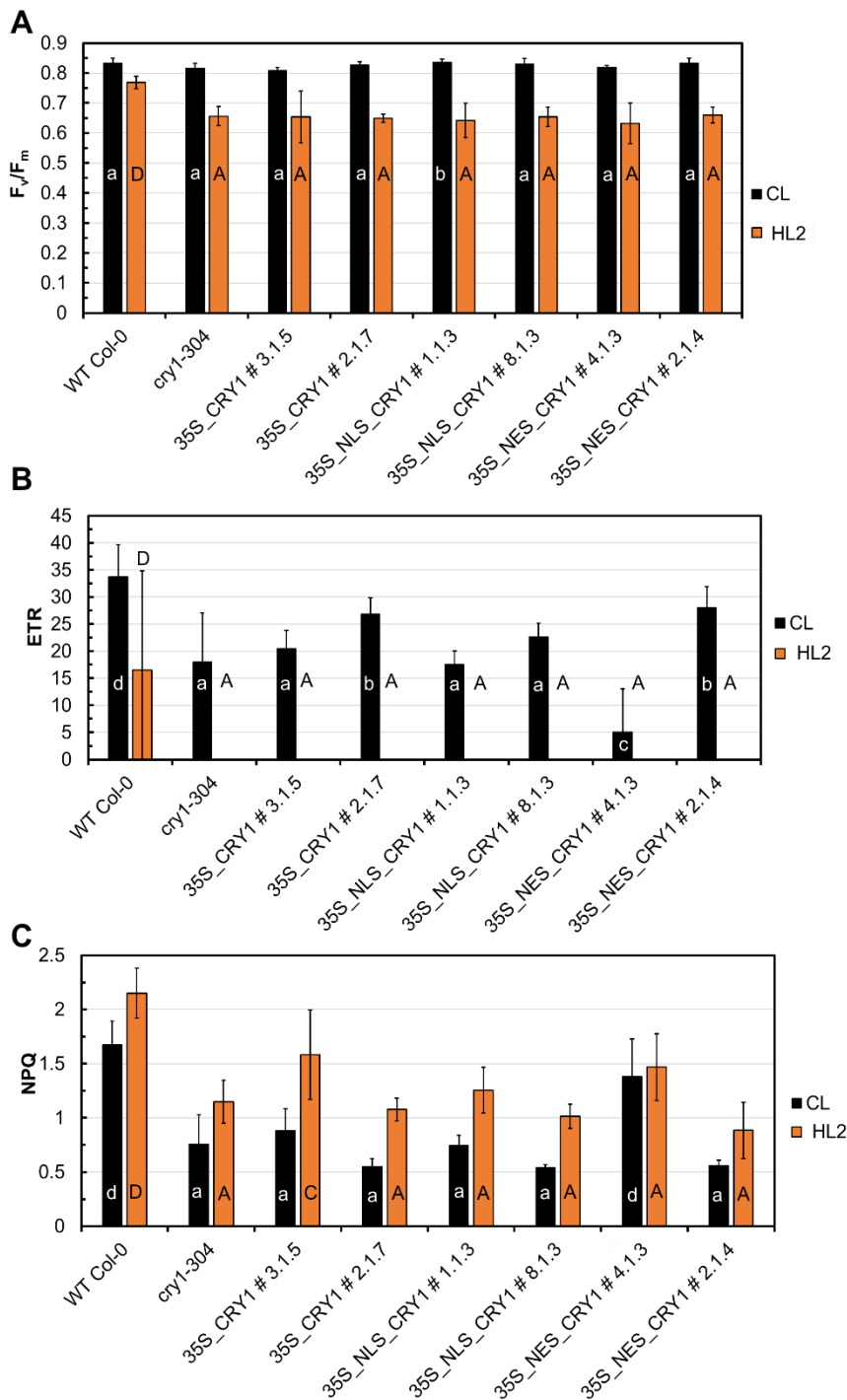


Figure 3.25. Characterization of key photosynthetic parameter under HL2 in WT Col-0, *cry1-304*, *35S_CRY1*, *35S_NLS_CRY1* and *35S_NES_CRY1* extracted from the experiment shown in Figures S.4 – S.6 **A**) Maximum quantum yield of PSII in the overnight dark-adapted state (F_v/F_m). **B**) ETR values at $461 \mu\text{mol photons m}^{-2} \text{s}^{-1}$. **C**) NPQ values at $461 \mu\text{mol photons m}^{-2} \text{s}^{-1}$. Mean values \pm SD ($n = 3-6$) are shown. Significant differences between the genotypes as well as between the light conditions (CL and FL), and the interaction (genotype \times light condition) were assessed by two-way ANOVA followed by Tukey's multiple comparison test. Different letters in the panel indicate significant differences compared to *cry1-304* (b, $P \leq 0.05$, C and c, $P \leq 0.01$, D and d, $P \leq 0.001$). Lowercase and uppercase letters are for the comparison between the genotypes under CL and HL2, respectively. The measurements were conducted by Nina Boots for her bachelor thesis (HHU, 2019).

3.3 Functional characterization of an unknown gene which was upregulated under FL (*AT3G56290*)

A previous transcriptomic study has shown that the gene expression of *AT3G56290* was upregulated in leaves of *A. thaliana* WT Col-0 under FL compared to CL (Schneider et al., 2019). This gene encodes a putative protein with unknown function predicted to be localized in the chloroplast or mitochondria and it was chosen as a candidate for a further study. To identify the potential functions of the gene product of *AT3G56290* in long-term acclimation to FL, phylogenetic distribution of homologous genes and *in silico* protein association network were analyzed first. Targeted KO plants of *AT3G56290* were generated by CRISPR/Cas9 and phenotypes of selected KO plants were characterized under EL conditions.

3.3.1 Phylogenetic analysis

Based on the amino acid sequence analysis, *AT3G56290* seems to be conserved in the most lineages of land plants with high percentages of sequence identity, indicating an important function (**Figure 3.26, Table 3.5**). Indeed, *AT3G56290* is present in both monocotyledons (*Zea mays*, *Oryza sativa*, *Sorghum bicolor* and others) and dicotyledons (*Arabidopsis thaliana*, *Brassica napus*, *Solanum tuberosum*, *Vitis vinifera*, *Beta vulgaris* and others). Interestingly, a protein with high sequence identity has been found also in mosses (*Physcomitrella patens*, *Marchantia polymorpha*) and club mosses (*Selaginella moellendorffii*). Sequences with higher distance were also found in green algae (*Chlorella variabilis* and *Chlamydomonas reinhardtii*) and cyanobacteria (*Thermosynechococcus*), indicating this protein has an ancient origin and it might have acquired more importance upon evolution of land plants. The phylogenetic analysis showed a good separation of sequences in the different taxonomic groups (**Figure 3.26**). Sequences belonging to the same taxonomic group clustered together, meaning that the evolution of this protein reflects the evolution of different systematic groups.

3.3.2 Functional protein association network of AT3G56290

The functional protein association network of AT3G56290 was analyzed by using the online tool STRING Version 11.0 (<https://string-db.org>). Ten genes, which were co-expressed together with *AT3G56290* with high scores (ranging from 0.983 to 0.844), are represented in a triangle-matrix (**Figure 3.27 A**) and in a functional protein association network (**Figure 3.27 B**). Annotation and localization of these proteins are reported in **Table 3.6**. Gene ontology (GO) terms associated with the proteins in the network are reported in **Table 3.7**. *SIGMA FACTOR E (SIGE)*, *SOLANESYL DIPHOSPHATE SYNTHASE 1 (SPS1)* and *SPS2*, *AT1G64500*, *FATTY ACID DESATURASE 4 (FADA)*, *B-BOX ZINC FINGER PROTEIN 25 (STH)* and *AT5G19850* are co-expressed at very high significance levels with the most of the other genes in this matrix. In comparison, the co-expression of *AT5G50100* and *ATP-BINDING CASSETTE F5 (ABCF5)* with the other genes in the matrix is supported at a medium level and *AT4G36530* at low level.

The same genes are also shown in the functional protein association network (**Figure 3.27 B**) which supposedly reflects the functional connection with AT3G56290 and between the network components. These associations are not necessarily physical associations (e.g. physical interactions) but can also be functional associations (e.g. proteins that contribute to a shared function). Network nodes represent proteins produced by a single, protein-coding gene locus and edges indicate experimentally determined (pink lines) or putative protein-protein associations based on gene co-expression database (black lines). The experimentally supported associations are found between ABCF5 and SIGE and between AT5G19850 and SPS1 or SPS2.

The GO terms, which were significantly enriched among the ten proteins in the network, are listed in **Table 3.7** in terms of biological process, molecular function and cellular component. The cellular processes and molecular functions of these proteins are linked mostly to chloroplast lipid and isoprenoid metabolism (such as plastoquinone and phosphatidylglycerol biosynthesis or chlorophyll dephytylation) and photosynthesis (transcriptional regulation of PSII D2 gene) (**Table 3.6**), all of which are essential for proper functioning of thylakoid. Half of these proteins are indeed found or predicted to be localized in chloroplast (**Table 3.6**).

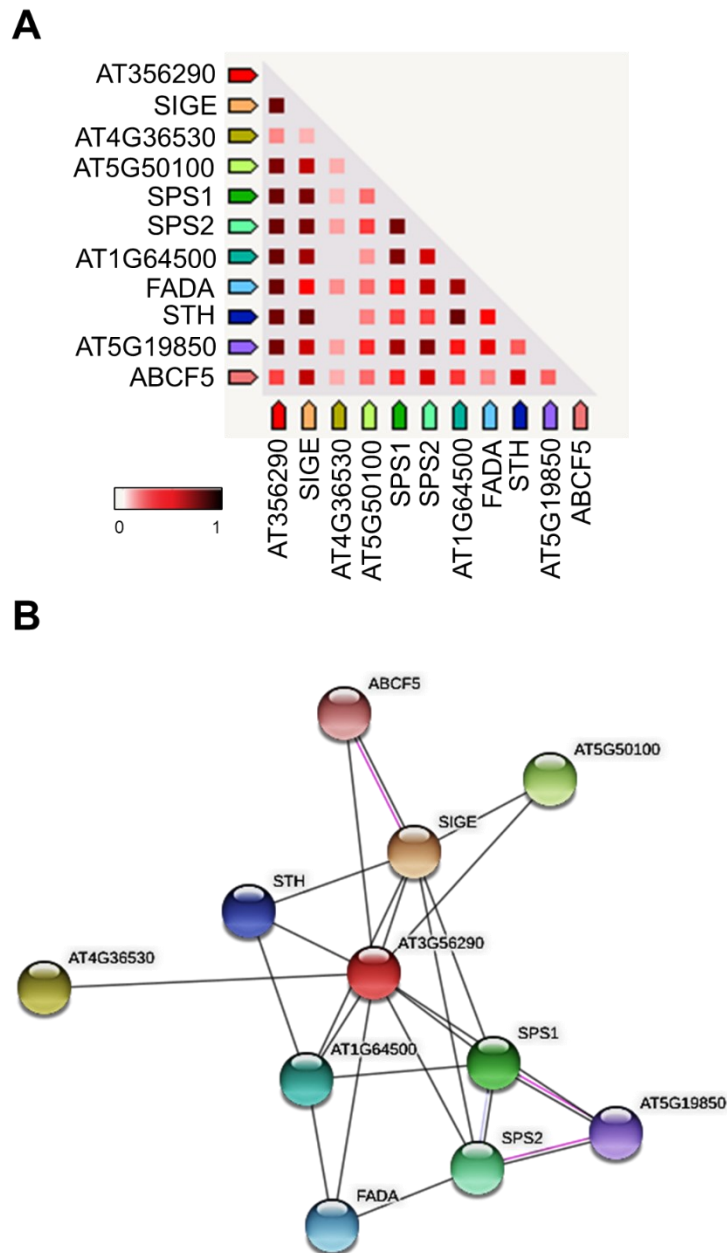


Figure 3.27. Functional protein association network of AT3G56290 obtained by STRING Version 11.0 (<https://string-db.org>). **A)** Prediction of functional association by gene co-expression. In the triangle-matrix the intensity of color indicates the level of confidence that two proteins (genes) are coexpressed. **B)** Prediction of functional interaction network. Pink and black lines indicate the associations with and without experimental support, respectively. Light blue line indicates protein homology. The minimum score of interaction was set as 0.700 for high confidence. ABCF5, ATP-binding cassette F6; SPS2, solanesyl diphosphate synthase 2; SPS1, solanesyl diphosphate synthase 1; STH, B-box zinc finger protein 25; FADA, fatty acid desaturase 4; SIGE, RNA polymerase sigma factor E.

<i>Predicted functional partner</i>	<i>Gene ID</i>	<i>Predicted Localization</i>	<i>Annotation</i>
SPS2	AT1G17050	Chloroplast	Solanesyl diphosphate synthase 2; involved in plastoquinone biosynthesis
AT1G64500	AT1G64500	Unknown	Putative peptide transporter protein; glutaredoxin family protein; cell redox homeostasis;
SPS1	AT1G78510	Endoplasmic reticulum	Solanesyl diphosphate synthase 1; involved in ubiquinone and plastoquinone biosynthesis
STH	AT2G31380	nucleus	B-box zinc finger protein 25 (BBX25); co-regulator of HY5 activity
AT3G56290 (query)	AT3G56290	Unknown	Unknown protein
FADA	AT4G27030	Chloroplast	Fatty acid desaturase 4; involved in phosphatidylglycerol biosynthesis
AT4G36530	AT4G36530	Chloroplast	alpha/beta-Hydrolases superfamily protein; chlorophyll dephytylase 1 (CLD1) homolog
AT5G19850	AT5G19850	Unknown	alpha/beta-Hydrolases superfamily protein; chlorophyll dephytylase 1 (CLD1) homolog
SIGE	AT5G24120	Chloroplast	RNA polymerase sigma factor E; involved in BL-dependent transcription of PSII D2 gene (<i>psbD</i>)
AT5G50100	AT5G50100	Chloroplast/Mitochondria	Uncharacterized protein; putative thiol-disulphide oxidoreductase DCC
ABCF5	AT5G64840	Unknown	ABC transporter superfamily; ATP-binding cassette F5

Table 3.6 Predicted functional partners of AT3G56290 in Figure 3.27 based on gene co-expression analysis by STRING (<https://string-db.org>). AGI code are reported for each entry, together with known or predicted localization and annotation.

Biological process (GO)		
Term description	Matching proteins in the network	False discovery rate
Plastoquinone biosynthetic process	SPS1,SPS2	0.00061
Photosynthesis	SIGE,SPS1,SPS2	0.0047
Quinone metabolic process	SPS1,SPS2	0.0047
Lipid biosynthetic process	FADA,SPS1,SPS2	0.0195
Isoprenoid biosynthetic process	SPS1,SPS2	0.0378
Cellular lipid metabolic process	FADA,SPS1,SPS2	0.0378
Small molecule biosynthetic process	FADA,SPS1,SPS2	0.0378
Isoprenoid metabolic process	SPS1,SPS2	0.0384
Molecular function (GO)		
Term description	Matching proteins in the network	False discovery rate
trans-octaprenyltranstransferase activity	SPS1,SPS2	0.0076
all-trans-nonaprenyl-diphosphate synthase (geranylgeranyl-diphosphate specific) activity	SPS1,SPS2	0.0076
Cellular component (GO)		
Term description	Matching proteins in the network	False discovery rate
plastid	AT5G50100,FADA,SIGE,SPS1,SPS2	0.0252

Table 3.7 Significantly enriched GO terms of the proteins in the association network shown in Figure 3.27. GO terms are listed according to biological process, molecular function and cellular component. Proteins classified in the category of each GO term are reported, as well as the false discovery rate of each prediction.

3.3.3 Generation of *AT3G56290* KO mutants by Crispr/Cas9

Three T-DNA insertion lines are publicly available for *AT3G56290*, of which two are also affected in the neighboring gene *AT3G56300* (cysteinyI-tRNA synthase). In the third line, T-DNA is inserted in the promoter region of *AT3G56290*, which may or may not result in KO. Thus, targeted KO plants of *AT3G56290* were generated by using the CRISPR/Cas9 system in collaboration with Florian Hahn (HHU). WT Col-0 plants were transformed by Agrobacterium-mediated floral dip method with the help of Anh Banh (FZJ, IBG-2). Selection and genotypic characterization of T2 and T3 plants (see section 3.3.3.2) were performed by Vaideki Thayumanavan for her Master thesis (University of Bonn, 2019) under my supervision.

3.3.3.1 CRISPR/Cas9 construct design

The construct designing for CRISPR/Cas9 was the first fundamental step to generate *AT3G56300* KO plants while enabling straightforward selection and simple screening of transformants (**Figure 3.28**). Two good candidates of single guide RNA (SgRNA), having GN followed by 19 nucleotides and the PAM motif NGG (GN19NGG), were identified in the first and largest exon sequence of *AT3G56300* (**Figure 3.28 A**). The design of SgRNA sites was checked for off-targets by using an online tool (www.rgenome.net/cas-offinder) to ensure that these SgRNAs could specifically recognize the gene of interest *AT3G56300* to guide Cas9. The SgRNA1 and SgRNA2 were considered very good sites because they contained restriction sites (for FspBI and PvuI, respectively) near the PAM motif, which could serve as genetic markers for effective and rapid screening of positive KO plants.

Three constructs were prepared using the backbone intermediates and final destination vectors provided by Florian Hahn (Hahn et al., 2017b): PMP7 containing only SgRNA1, PMP8 containing only SgRNA2, and PMP5 in which both SgRNA1 and SgRNA2 were cloned together for double targeting (**Figure 3.28 B**).

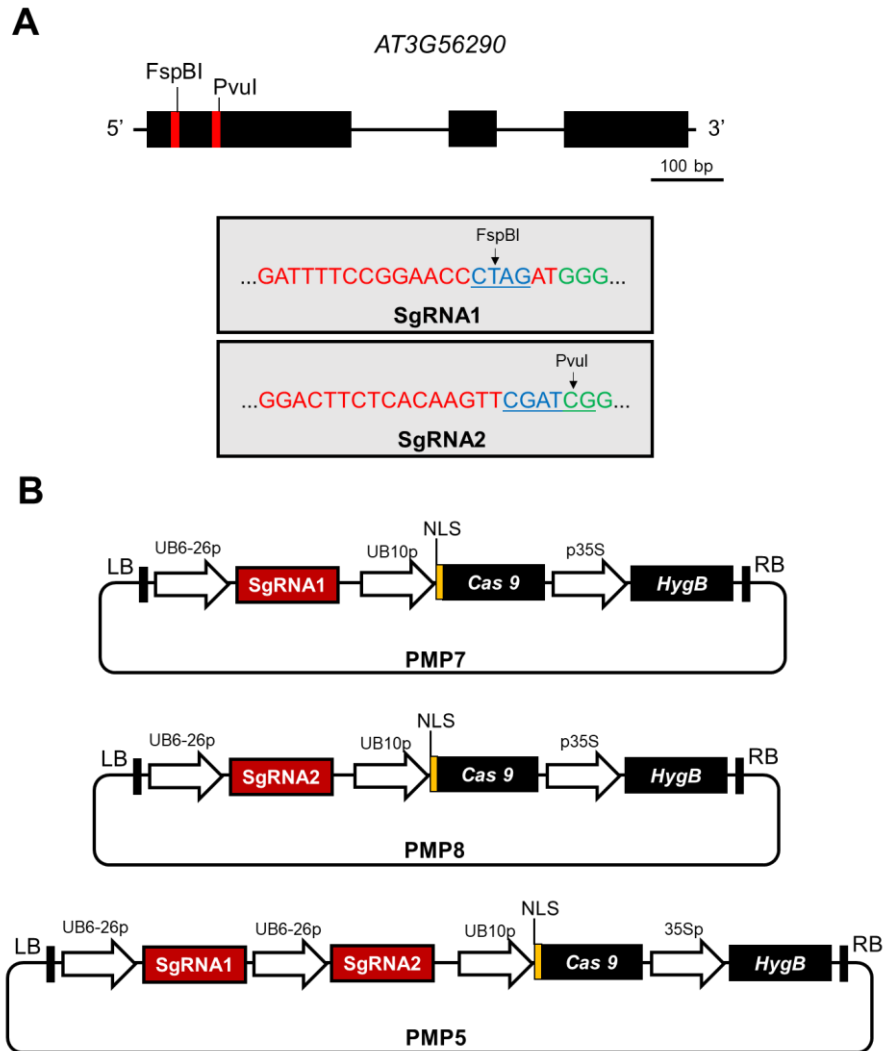


Figure 3.28 CRISPR/Cas9 construct designs for KO of *AT3G56290* gene. **A)** Identification of SgRNA sites in the gene of interest *AT3G56290*. *AT3G56290* gene map shows exons (black blocks) and introns (black line) in scale. The two SgRNA sites (GN19NGG) are indicated as red bars containing the restriction sites of FspBI and PvuI. The DNA sequences of the two SgRNA sites (red) and the restriction sites (light blue, underlined) followed by PAM sequence (NGG, green) are also shown beneath the gene map. SgRNAs were validated to exclude off-target by using the tool available at www.rgenome.net/cas-offinder. **B)** Construct maps of PMP7 (SgRNA1), PMP8 (SgRNA2) and PMP5 (SgRNA1 + SgRNA2). SgRNA sequences (red boxes) were fused with the *UB6-26* promoter (UB6-26p). The *Cas9* gene (black box) is controlled by the *UBIQUITIN10* promoter (UB10p) and addressed to the nucleus by NLS (yellow). The hygromycin B gene (*HygB*), used as selection marker, is under the control of 35S promoter (35Sp). LB, left T-DNA border; RB, right T-DNA border. Gene sizes are not to scale in the panel B. Cloning was performed together with Florian Hanh (HHU).

3.3.3.2 Genotypic characterization and isolation of positive *AT3G56290* KO lines

T1 plants from independently transformed T0 lines were selected based on hygromycin resistance. The resistant T2 and T3 plants were further cultivated in soil and genotypic characterization was performed using leaf samples harvested from these plants. Genetic screening consisted of PCR analysis to check the presence of *CAS9* gene in the genomic DNA and restriction analysis on *AT3G56290* PCR products according to the cleaved amplified polymorphic sequence (CAPS) method (Hahn et al., 2017b; Hahn et al., 2017a; Hahn et al., 2018b). The *CAS9* gene was successfully amplified from genomic DNA of several T3 plants of PMP7 (**Figure 3.29 A**), PMP8 (**Figure 3.29 B**) and PMP5 (**Figure 3.29 C**). The amplified *AT3G56290* PCR products of the *CAS9*-positive PMP7, PMP8 and PMP5 plants were used for CAPS with *Fsp*BI (**Figure 3.30**), *Pvu*I (**Figure 3.31**) and both *Fsp*BI and *Pvu*I (**Figure 3.32**), respectively.

The *AT3G56290* PCR products of PMP7 lines and WT Col-0 were digested with *Fsp*BI, as a restriction site for this enzyme is associated with the sequence of the SgRNA1 used to guide the endonuclease activity of *CAS9* (**Figure 3.30**). The different restriction patterns expected for WT Col-0 and PMP7 are visualized by *in silico* digestion (**Figure 3.30 A**). The *AT3G56290* locus in WT Col-0 has three *Fsp*BI restriction sites which would generate three bands of 430, 264 and 98 bp. The activity of *CAS9* guided by SgRNA1 should interrupt the first *Fsp*BI restriction site, producing two bands of 527 and 264 bp. The expected restriction pattern of *AT3G56290* was confirmed for WT Col-0 but none of the *CAS9*-positive PMP7 plants showed the restriction pattern predicted for positive *AT3G56290* KO (**Figure 3.30 B**). Most of the PMP7 lines showed three bands, which were similar to the ones in WT Col-0. In addition, an extra band appeared in the region of around 500 bp, which may be the 527-bp fragment resulting from partial activity of Cas9.

Analogously, Cas9 activity was also examined in the Cas9-positive plants of PMP8 lines. The *AT3G56290* PCR products of PMP8 lines and WT Col-0 were digested with *Pvu*I, as the restriction site of this enzyme is associated with the sequence of the SgRNA2 (**Figure 3.31**). The restriction patterns expected for WT Col-0 and PMP8 are shown in **Figure 3.31 A**. Digestion of the *AT3G56290* PCR products would generate two bands of 588 and 211 bp for WT-Col-0, but an undigested 799 bp fragment should remain in PMP8.

The restriction pattern of WT Col-0 confirmed the prediction by *in silico* digestion (**Figure 3.31 B**), although an additional band was observed at ca. 800 bp, probably because of incomplete digestion. The WT-like restriction pattern was found in all CAS9-positive PMP8 lines analyzed. Since Cas9 activity will produce a single band of undigested template in PMP8, it is not possible to distinguish partial Cas9 activity (giving rise to 799, 588 and 211 bp bands) from no Cas9 activity with incomplete digestion (the situation in WT Col-0).

In the case of PMP5 lines, the *AT3G56290* PCR products were digested with FspBI and PvuI, as the PMP5 construct contains both SgRNA1 and SgRNA2 (**Figure 3.32**). The three FspBI and one PvuI restriction sites in *AT3G56290* would generate four bands (317 and 264, 113 and 98 bp) in WT Col-0 (**Figure 3.32 A**), although the two smallest fragments would appear as a single band in a gel to result in three bands. Indeed, this was the case in WT Col-0 (**Figure 3.32 B**). The combination of the two SgRNAs creates three possible scenarios of restriction patterns for PMP5: (I) If the mutation occurred in both target sites, a restriction pattern with two bands (526 and 264 bp) will be found; (II) If only the FspBI restriction site was disrupted by the CAS9 activity, three bands (317, 264 and 210 bp) will appear; (III) In the case of single disruption removing the PvuI restriction site, three bands (429, 264 and 98 bp) are expected. While some of the PMP5 lines had WT-like restriction pattern, the plants from the parental T2 line #1.1.10 (3, 5, 6 and 7) and #1.4.1 (1, 2, 3 and 4) displayed the pattern predicted by the second scenario (disruption of the FspBI restriction site). Apparently, targeting of Cas9 activity was successful only by SgRNA1, but not by SgRNA2 in the PMP5 lines.

In order to confirm the mutation, the *AT3G56290* PCR products of the PMP5 lines #1.1.10.3 and #1.4.1.1 were purified and sequenced (**Figure 3.33**). Sequence details of the first ~500 nucleotides of *AT3G56290* are shown in **Figure 3.33 A**, together with the chromatograms of the SgRNA1 target site (**Figure 3.33 B**). The clean peaks of the chromatogram indicate high quality of the sequencing and universal occurrence of the same mutation in the DNAs extracted from the leaf samples of these plants. The Cas9 activity caused a single nucleotide insertion (adenine A in #1.1.10.3 and cytosine C in #1.4.1.1) exactly at the expected position, which is three bp in front of the PAM motif (**Figure 3.33 A**). Single nucleotide insertion would cause frame shift, thus altering the amino acid sequence of the protein. The coding region of native *AT3G56290* in WT Col-0 produces a protein of about 250 amino acids (**Figure 3.34 A**).

With the insertion of A/C in PMP5 #1.1.10.3 (**Figure 3.34 B**) and PMP5 #1.4.1.1 (**Figure 3.34 C**) the reading frame was shifted to generate nine premature STOP codons. Consequently, the mutation carried by these PMP5 lines would lead to premature termination of protein translation and hence a truncated protein which most likely fails to accumulate or fulfill its function.

As the last step of genotypic characterization, the *AT3G56290* gene expression was checked in T4 plants obtained from PMP5 #1.1.10.3 and #1.4.1.1 (**Figure 3.35**). In comparison with two replicate samples of WT Col-0, gene expression of *AT3G56290* was neither substantially decreased nor abolished in the PMP5 plants, for which the quality and concentration of cDNA were confirmed by the positive control (*ACTIN-2*). These results were not surprising since single nucleotide insertion does not necessarily affect gene transcription. However, premature termination of translation would make these plants functional KO lines of *AT3G56290*. Protein accumulation of *AT3G56290* could not be checked due to non-availability of antibody.

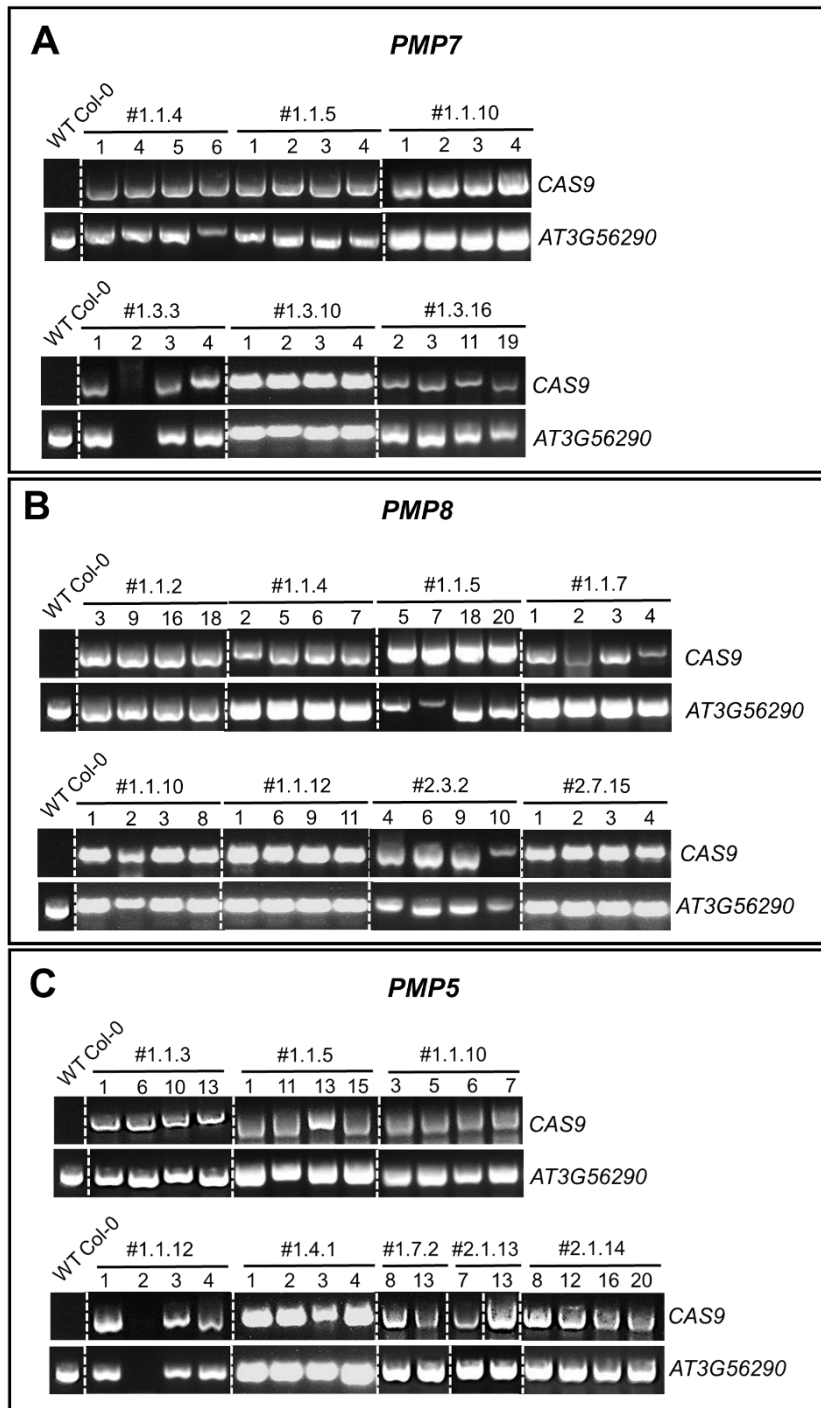


Figure 3.29 Amplification of *CAS9* and *AT3G56290* genes on genomic DNA of WT Col-0 and the selected positive lines of **A**) PMP7, **B**) PMP8 and **C**) PMP5 (all T3 generation). WT Col-0 was used as negative control for *CAS9*. This figure was modified from the master thesis of Vaideki Thayumanavan (University of Bonn, 2019).

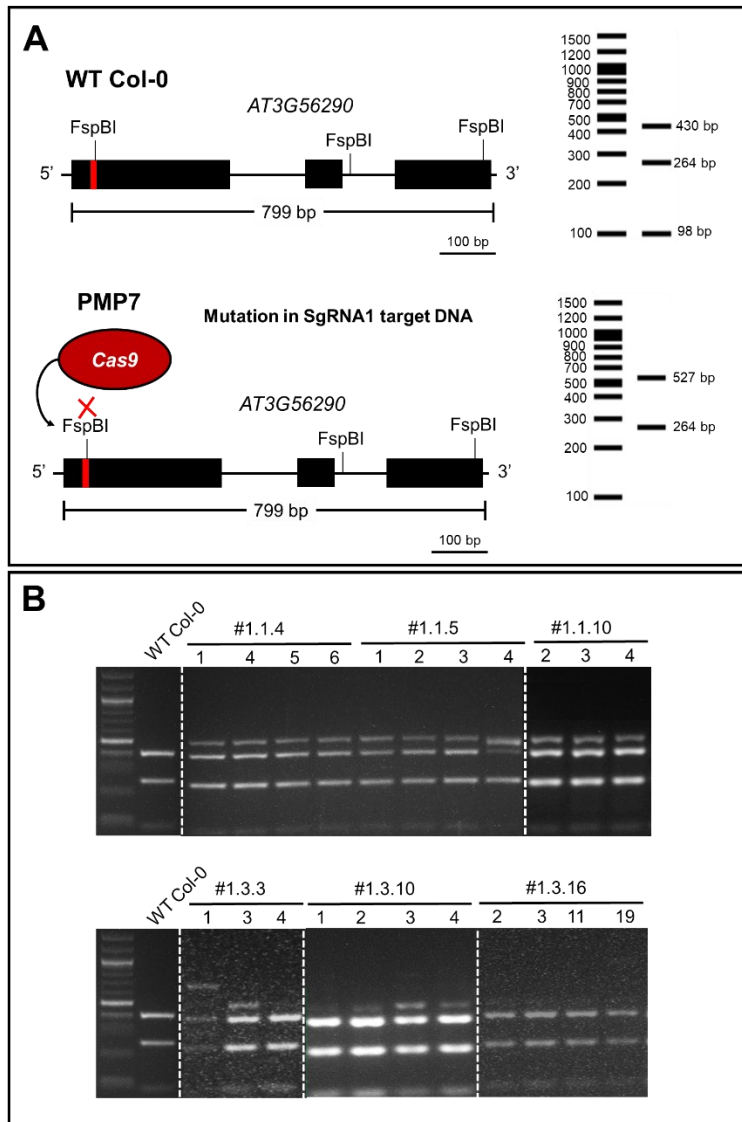


Figure 3.30 Screening by restriction analysis of WT Col-0 and the selected positive PMP7 lines of T3 generation. **A)** Design of the screening strategy by cleaved amplified polymorphic sequence (CAPS) method. Restriction sites and expected restriction patterns (obtained by *in silico* analysis using the Serial Cloner software) are shown for WT Col-0 and PMP7. *AT3G56290* gene map in scale shows the SgRNA1 site (in red) associated with the FspBI restriction site. The other two FspBI restriction sites in the second intron and in the third exon are also indicated. The elimination of the first FspBI restriction site by Cas9 activity should alter the restriction pattern of the PCR products amplified from *AT3G56290* of PMP7 compared to WT Col-0. **B)** Digestion of the *AT3G56290* PCR products of WT Col-0 and the selected positive PMP7 lines with FspBI. The panel B was modified from the master thesis of Vaideki Thayumanavan (University of Bonn, 2019).

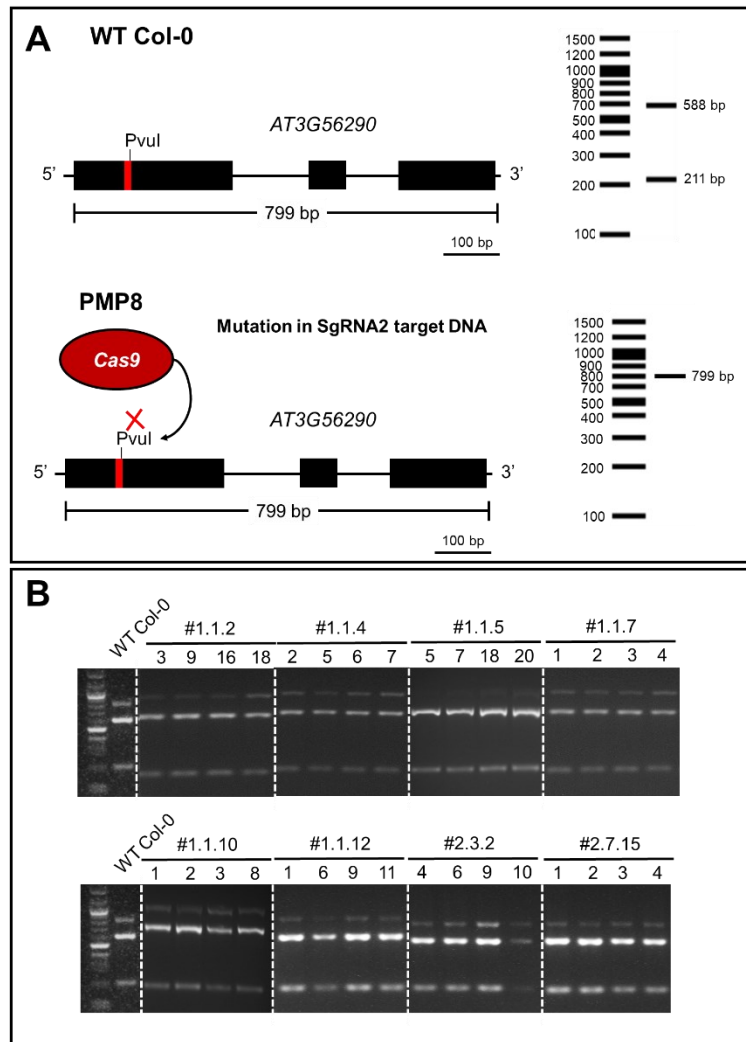


Figure 3.31. Screening by restriction analysis of WT Col-0 and the selected positive PMP8 lines of T3 generation. **A)** Design of the screening strategy by the CAPS method. Restriction sites and expected restriction patterns (obtained by *in silico* analysis using the Serial Cloner software) are shown for WT Col-0 and PMP8. *AT3G56290* gene map in scale shows the SgRNA2 site (in red) associated with the PvuI restriction site in the first exon. The elimination of the PvuI restriction site by Cas9 activity should alter the restriction pattern of the PCR products amplified from *AT3G56290* of PMP8 compared to WT Col-0. **B)** Digestion of the *AT3G56290* PCR products of WT Col-0 and the selected positive PMP8 lines with PvuI. The panel B was modified from the master thesis of Vaideki Thayumanavan (University of Bonn, 2019).

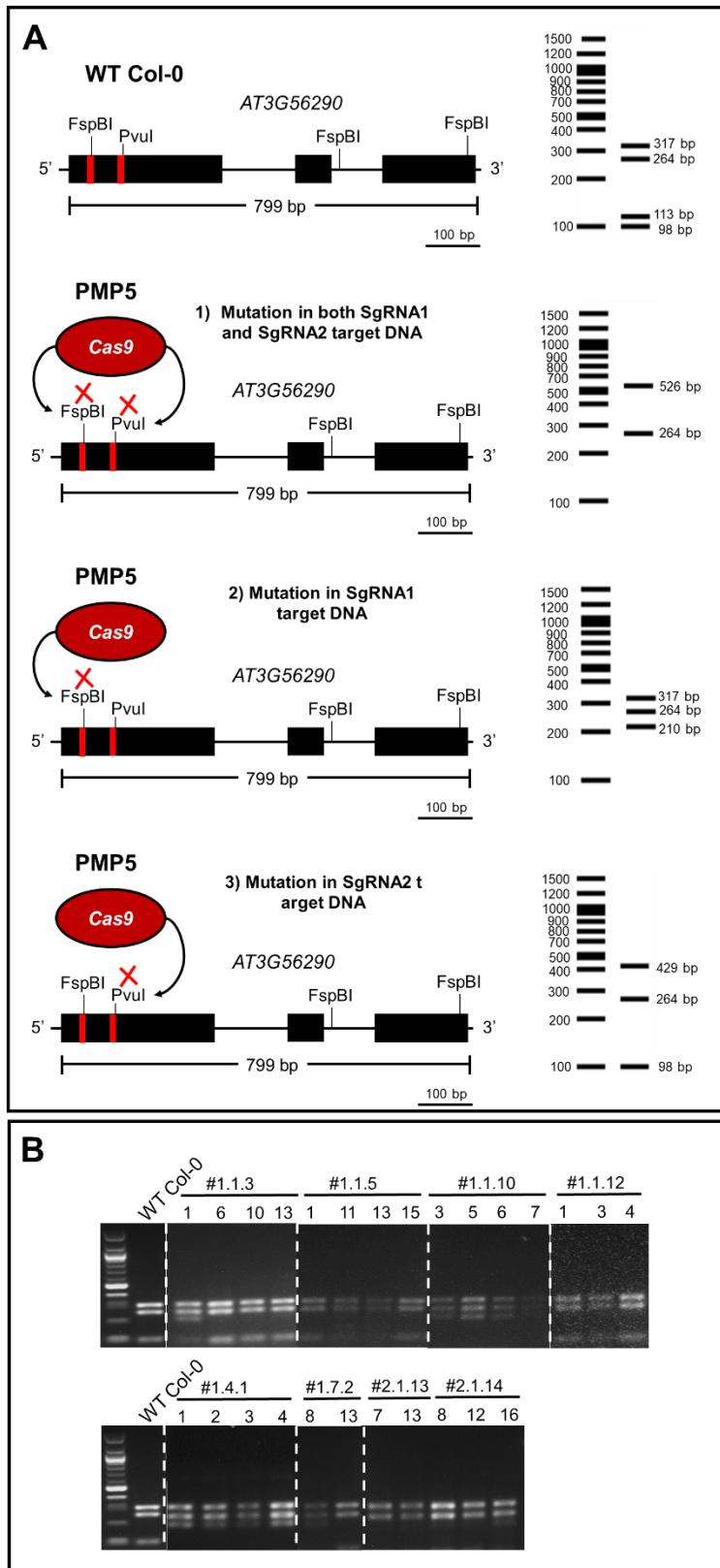


Figure 3.32. Screening by restriction analysis of WT Col-0 and the selected positive PMP5 lines of T3 generation. **A)** Design of the screening strategy by the CAPS method. Restriction sites and expected restriction patterns (obtained by *in silico* analysis using the Serial Cloner software) are shown for WT Col-0 and PMP5. *AT3G56290* gene map in scale shows the SgRNA1 and SgRNA2 sites (in red) associated with the FspBI and PvuI restriction sites, respectively. The other two FspBI restriction sites in the second intron and in the third exon are also indicated. Three restriction scenarios are presented: the activity of Cas9 eliminates **1)** both FspBI and PvuI restriction sites targeted by SgRNA1 and SgRNA2, **2)** only the FspBI restriction site targeted by SgRNA1, and **3)** only the PvuI restriction site targeted by SgRNA2. Each of these scenarios produces distinct restriction patterns in PCR products amplified from *AT3G56290*. **B)** Digestion of the *AT3G56290* PCR products of WT Col-0 and the selected positive PMP5 lines with both FspBI and PvuI. The panel B was modified from the master thesis of Vaideki Thayumanavan (University of Bonn, 2019).

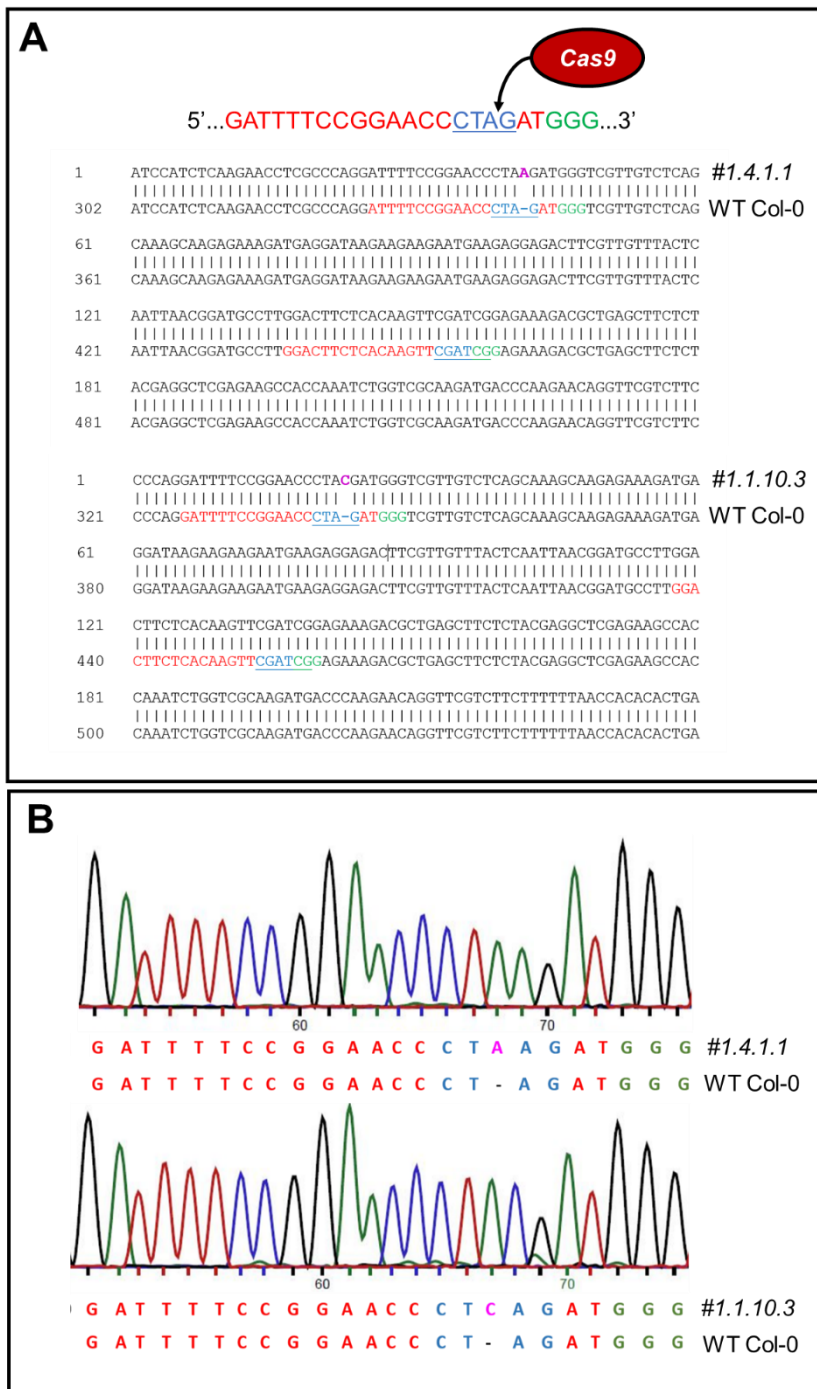


Figure 3.33. Sequencing analysis of PMP5 #1.1.10.3 and #1.4.1.1 lines. **A)** Sequence alignment of *AT3G56290* PCR products of PMP5 #1.1.10.3 and #1.4.1.1 against WT Col-0. The sequences of SgRNA1 and SgRNA2 (red), restriction sites of FspBI and PvuI (underlined and light blue) and NGG sites (green) are indicated in the WT Col-0 sequence. The mutation sites of PMP5 #1.1.10.3 and #1.4.1.1 are indicated in pink. **B)** Chromatograms of the sequencing results of *AT3G56290* PCR products of PMP5 #1.1.10.3 and #1.4.1.1. The color coding of nucleotide sequence is the same as in the panel A. This figure was modified from the master thesis of Vaideki Thayumanavan (University of Bonn, 2019).

A WT Col-0

```

241 AGATGGTTTTAGAGCACTGCCTCTTCAACACAGCAGTGGGTTTCATCTCCACGACCAAAAG
80 K M G F R A L P L Q H S S G F I S T T K

301 TATCCATCTCAAGAACCCTCGCCAGGATTTCCGGAACCTAGATGGGTCGTTGTCTCAG
100 V S I S R T S P R I F R N P R W V V V S

361 CAAAGCAAGAGAAAGATGAGGATAAGAAGAAGATGAAGAGGAGACTTCGTTGTTACTC
120 A K Q E K D E D K K K N E E E T S L F T

421 AATTAACGGATGCCTTGGACTTCTCACAGTTCGATCGGAGAAAGACGCTGAGCTTCTCT
140 Q L T D A L D F S Q V R S E K D A E L L

481 ACCGAGCTCGAGAAGCCACCAATCTGGTCGCAAGATGACCCANGAACAGTATGGGGCAT
160 Y E A R E A T K S G R K M T Q E Q Y G A

541 TGAGGAGAAAAATCGGAGAACATACAAGGACTTTTTAAATCCTACGTGAAGTGGATG
180 L R R K I G G T Y K D F F K S Y V E V D

601 GGCAATATGTGGAGGGGATGGGTGGACAAAACATGTAAGATATGCAAAAAGGACACAA
200 G Q Y V E E G W V D K T C K I C K K D T

661 AGGGTGGGCAAGACAAGTGGACAAGTTAGGGAGATATGCTCATGTCCTTGTCTTCAAA
220 K G E A R Q V D K L G R Y A H V S C L Q

721 ATCCTCCCTCTGAAAATTTCTTACCAGACTCTTCTCTAGAATGATGATGATCAATTCCC
240 N P P S G N F F T R L F S R A T T S I S

```

B PMP5 #1.4.1.1

```

1 ATGGGTTTTAGAGCACTGCCTCTTCAACACAGCAGTGGGTTTCATCTCCACGACCAAAAGTA
1 M G F R A L P L Q H S S G F I S T T K V

61 TCCATCTCAAGAACCCTCGCCAGGATTTCCGGAACCTAGATGGGTCGTTGTCTCAGC
21 S I S R T S P R I F R N P K M G R C L S

121 AAAGCAAGAGAAAGATGGATGAAGAAGAAGATGAGAGGAGACTTCGTTGTTACTCA
41 K A R E R G T E E E R G D F V V Y S

181 AATTAACGGATGCCTTGGACTTCTCACAGTTCGATCGGAGAAAGACGCTGCTTCTCTA
61 I N G C L G L L T S S I G E R R A S L

241 CGAGGCTCGAGAAGCCACCAATCTGGTCGCAAGATGACCCANGAACAGTATGGGGCATT
81 R G S R S H Q I W S Q D D P R T V W G I

301 GAGGAGAAAAATCGGAGAACATACAAGGACTTTTTAAATCCTACGTGAGTGGATGG
101 E E K N R R N I Q G L F I L R S G W

361 GCAATATGTGGAGGGGATGGGTGGACAAAACATGATGATATGCAAAAAGGACACAAA
121 A I C G G G M G G Q N M D M Q K G H K

421 GGCTGGGCAAGACAAGTGGACAAGTTAGGGAGATATGCTCATGTCCTTGTCTTCAAAA
141 G T G K T S G Q V R E I C S C L L S S K

481 TCCTCCCTCTGAAAATTTCTTACCAGACTCTTCTCTAGA
161 S S L W K F L H Q T L L M

```

C PMP5 #1.1.10.3

```

1 ATGGGTTTTAGAGCACTGCCTCTTCAACACAGCAGTGGGTTTCATCTCCACGACCAAAAGTA
1 M G F R A L P L Q H S S G F I S T T K V

61 TCCATCTCAAGAACCCTCGCCAGGATTTCCGGAACCTAGATGGGTCGTTGTCTCAGC
21 S I S R T S P R I F R N P T M G R C L S

121 AAAGCAAGAGAAAGATGGATGAAGAAGAAGATGAGAGGAGACTTCGTTGTTACTCA
41 K A R E R G T E E E R G D F V V Y S

181 AATTAACGGATGCCTTGGACTTCTCACAGTTCGATCGGAGAAAGACGCTGCTTCTCTA
61 I N G C L G L L T S S I G E R R A S L

241 CGAGGCTCGAGAAGCCACCAATCTGGTCGCAAGATGACCCANGAACAGTATGGGGCATT
81 R G S R S H Q I W S Q D D P R T V W G I

301 GAGGAGAAAAATCGGAGAACATACAAGGACTTTTTAAATCCTACGTGAGTGGATGG
101 E E K N R R N I Q G L F I L R S G W

361 GCAATATGTGGAGGGGATGGGTGGACAAAACATGATGATATGCAAAAAGGACACAAA
121 A I C G G G M G G Q N M D M Q K G H K

421 GGCTGGGCAAGACAAGTGGACAAGTTAGGGAGATATGCTCATGTCCTTGTCTTCAAAA
141 G T G K T S G Q V R E I C S C L L S S K

481 TCCTCCCTCTGAAAATTTCTTACCAGACTCTTCTCTAGAATGA
161 S S L W K F L H Q T L L M

```

Figure 3.34. Translation of *AT3G56290* coding region in frame 3 for **A)** WT Col-0, **B)** PMP5 #1.4.1.1 and **C)** PMP5 #1.1.10.3. The start codon ATG and the STOP condons (TAA, TAG, TGA) are highlighted in yellow and green, respectively. The shaded regions indicate the expected protein product. This figure was modified from the master thesis of Vaideki Thayumanavan (University of Bonn, 2019).

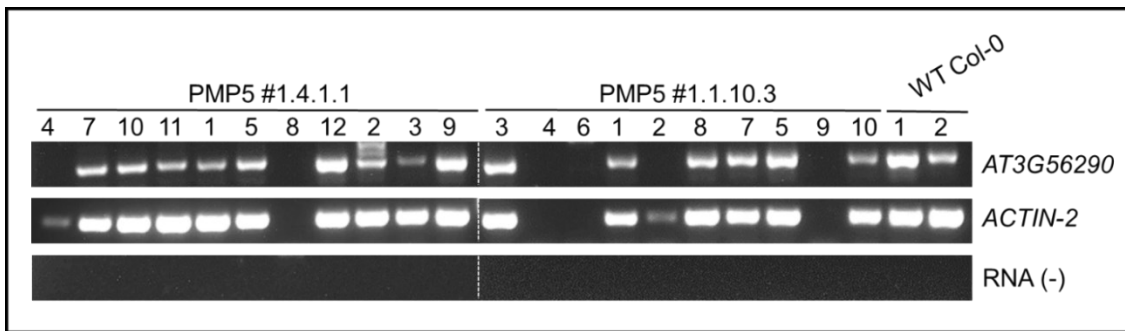


Figure 3.35. *AT3G56290* gene expression analyzed by reverse transcription-PCR (RT-PCR) in leaves of PMP5 #1.1.10.3 and #1.4.1.1 plants screened in T4 generation compared to WT Col-0. For all the plants *ACTIN-2* PCR product was also amplified as positive control and RNA was used as negative control.

3.3.4 Phenotypic characterization of *AT3G56290* KO lines

Preliminary phenotyping was performed on T4 plants of the two PMP5 lines (#1.4.1.1 and #1.1.10.3) in which genotypic characterization confirmed the mutation in the *AT3G56290* gene. Since this gene was upregulated in leaves after three days of exposure to FL-like conditions (Schneider et al., 2019) and it is co-expressed with other genes that are associated with thylakoid lipid metabolism and PSII functioning (**Table 3.6**), plants of transgenic lines and WT Col-0 were exposed to moderate EL (FL2 and HL2, as described in 3.2) for three days to compare their phenotypic responses.

Morphological differences were not observed between the rosettes of the transgenic lines and WT Col-0 under CL, FL2 and HL2 (**Figure 3.36**). Photosynthetic induction curves were measured on mature leaves of the three genotypes after one and three days of FL2, HL2 or CL exposure. After one day of exposure to FL2 and HL2, no clear difference in PSII activity was found between the two PMP5 lines and WT Col-0 (**Figures 3.37** and **3.38**). The induction curves of Y(II) and ETR(II) did not significantly change in WT Col-0 exposed to FL2 and HL2 compared to CL (**Figure 3.37**). Only F_v/F_m and NPQ values significantly changed in WT Col-0 exposed to HL2 (**Figure 3.38 A, C**). In particular, NPQ increased faster in the HL2 plants than in the others upon AL illumination (**Figure 3.37**) even though the NPQ values measured in WT-Col-0 after 160 s of AL were not significantly different between the treatments (**Figure 3.38 C**). Generally, upregulation of NPQ in the EL-treated plants was more evident in young leaves than in mature leaves (**Figure 3.38 D**). The two PMP5 lines exhibited induction curves which were basically similar to those of WT Col-0 (**Figure 3.37**).

The EL-treated plants of PMP5 tended to have slightly lower Y(II) and ETR(II) than WT Col-0 during the induction, but the values varied strongly in individual plants. As Y(II) and ETR(II) were reduced, NPQ increased more strongly in the EL-treated PMP5 plants (**Figure 3.37**). The NPQ levels after 160-s AL exposure were significantly higher in the HL2 plants compared to the corresponding CL plants of these lines (**Figure 3.38 C**). However, when the effects of genotypes and light treatments were tested by two-way ANOVA, no significant difference was found between the NPQ levels in the genotypes, underlining the predominant effect of light conditions on this trait.

The same measurements were repeated after three days of exposure to FL2, HL2 or CL (**Figures 3.39** and **3.40**). Similar to day 1, little difference was detected between the PMP5 lines and WT Col-0. Also, on day 3 the largest differences in induction patterns were found for NPQ, with the highest values in the HL2 plants and the lowest in the CL plants (**Figure 3.39**). The induction curves of Y(II) and ETR(II) were not significantly different between the treatments in all three genotypes. The F_v/F_m values were significantly lower in the HL2-treated plants than in the CL-treated plants decreasing from ca. 0.79 in both CL and FL2 to 0.74-0.72 in HL2 treated plants (**Figure 3.40 A**) and the NPQ values after 160 s of AL significantly increased in both FL2 and HL2 plants compared to the CL plants (**Figure 3.40 C**). However, there was no significant difference between the genotypes. Again, upregulation of NPQ in FL2 and HL2 was more pronounced in younger leaves (**Figure 3.40 D**).

Overall PMP5 lines (#1.4.1.1 and #1.1.10.3) exposed to CL, FL2 and HL2 did not show major changes in morphology and development, or in photosynthetic induction of electron transport and NPQ compared to WT Col-0 under the same conditions.

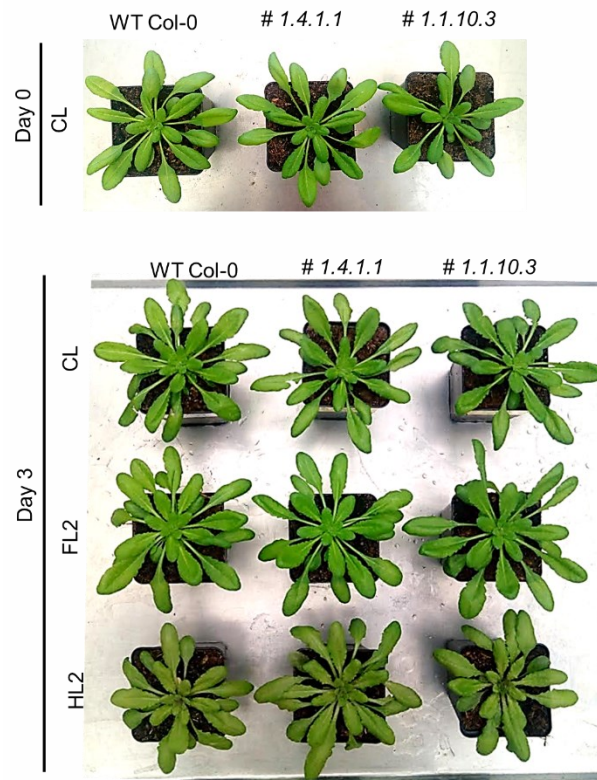


Figure 3.36. Visual phenotypes of WT Col-0, *PMP5* #1.4.1.1 and *PMP5* #1.1.10.3 plants in T4 generation. Representative plants before (day 0) and at the end of the CL, FL2 and HL2 treatments (day 7) are shown.

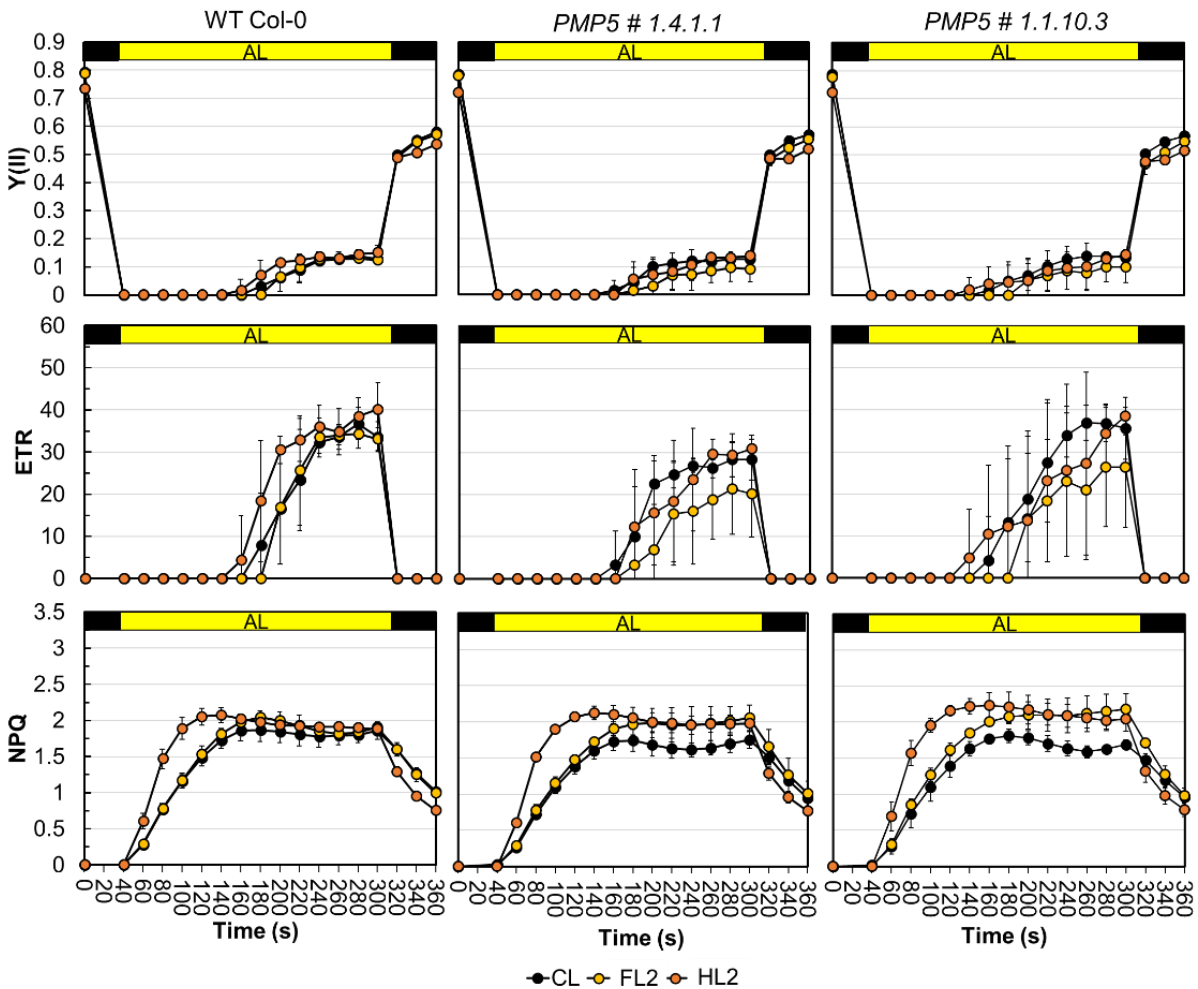


Figure 3.37. Characterization of PSII activity after one day under CL (black symbols), FL2 (yellow symbols) and HL2 (orange symbols) in WT Col-0, *PMP5 #1.4.1.1* and *PMP5 #1.1.10.3*. Measurements were performed in leaves of overnight dark-adapted plants. Photosynthetic induction was evaluated for 260 s under actinic light (AL) illumination of ca. $550 \mu\text{mol photons m}^{-2} \text{s}^{-1}$, during which SPs were triggered every 20 s. The AL period was followed by 60 s of dark relaxation. Y(II), quantum yield of PSII; ETR (II), relative electron transport rate of PSII; NPQ, non-photochemical quenching. Mean values \pm SD are shown ($n = 3-4$ plants).

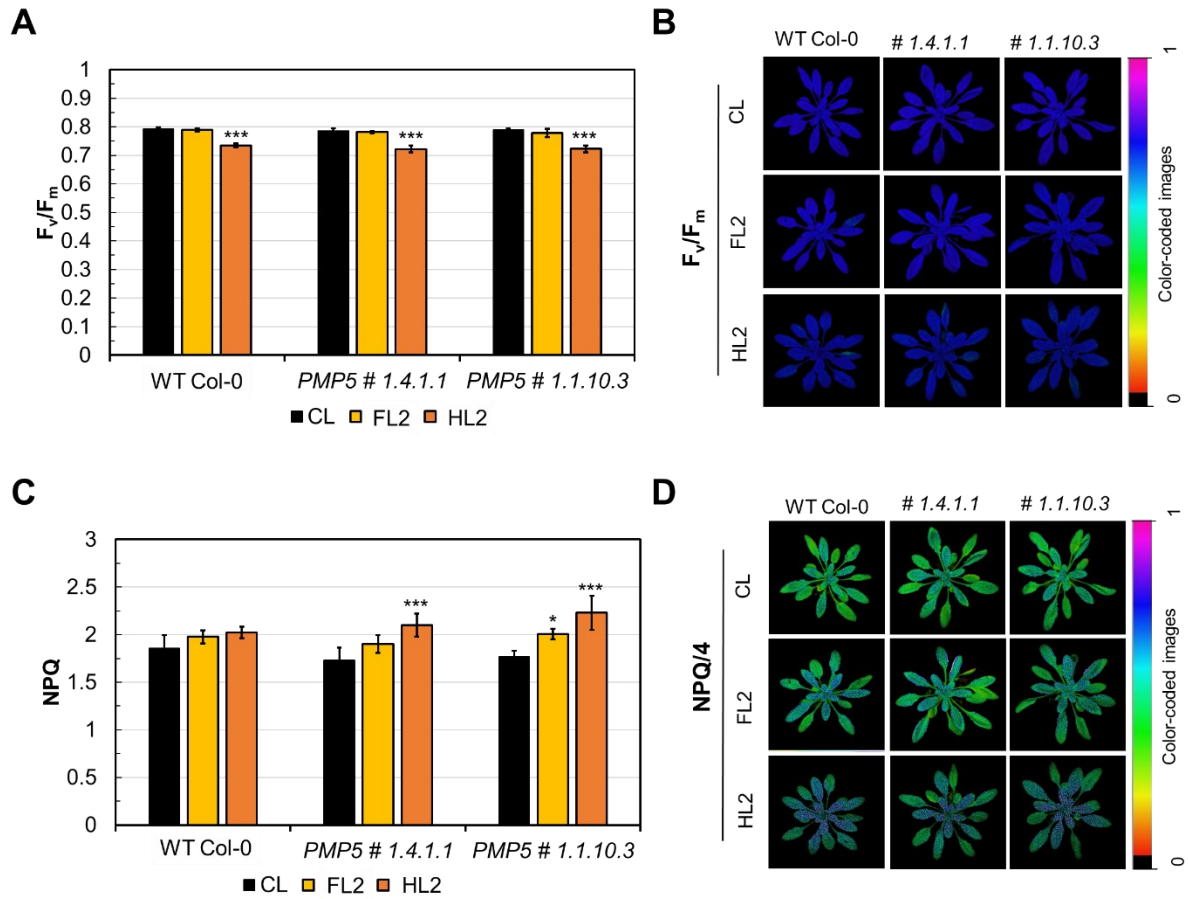


Figure 3.38. Maximum quantum yield of PSII in the overnight dark-adapted state (F_v/F_m) and NPQ after one day under CL, FL2 and HL2 in WT Col-0, *PMP5* #1.4.1.1 and *PMP5* #1.1.10.3. **A)** F_v/F_m values of the mature leaves used for the induction measurements shown in Figure 3.37. **B)** Spatial heterogeneity of F_v/F_m in whole rosettes. The color bars on the right show the scale of the color code. **C)** NPQ values of the mature leaves used for the induction measurements shown in Figure 3.37. The values were taken after 160 s of AL illumination. **D)** Spatial heterogeneity of NPQ after 160 s of AL in whole rosettes. The color bars on the right show the scale of the color code. NPQ values in the images are divided by four (NPQ/4) to use the scale between 0 and 1. No significant difference was found between the genotypes under CL, FL2 or HL2. Significant differences between the different light conditions within the same genotype were assessed by Tukey multiple comparison and are indicated by asterisks (* ≤ 0.05 , *** ≤ 0.001). Mean values \pm SD are shown ($n = 3-4$).

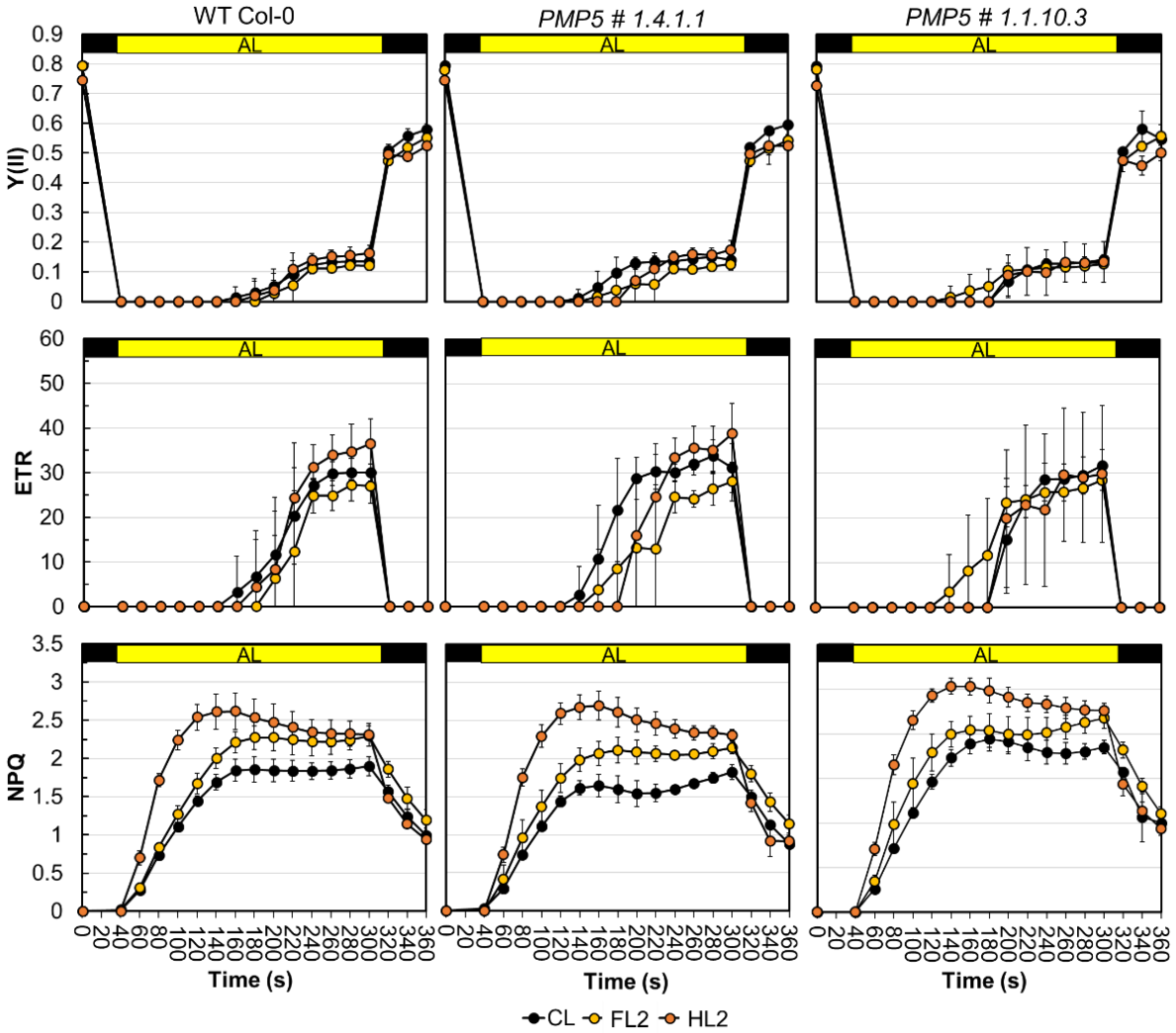


Figure 3.39. Characterization of PSII activity after three days under CL (black symbols), FL2 (yellow symbols) and HL2 (orange symbols) in WT Col-0, *PMP5 #1.4.1.1* and *PMP5 #1.1.10.3*. Measurements were performed in leaves of overnight dark-adapted plants. Photosynthetic induction was evaluated for 260 s under actinic light (AL) illumination of ca. 550 $\mu\text{mol photons m}^{-2} \text{s}^{-1}$, during which SPs were triggered every 20 s. The AL period was followed by 60 s of dark relaxation. Y(II), quantum yield of PSII; ETR (II), relative electron transport rate of PSII; NPQ, non-photochemical quenching. Mean values \pm SD are shown ($n = 3-4$ plants).

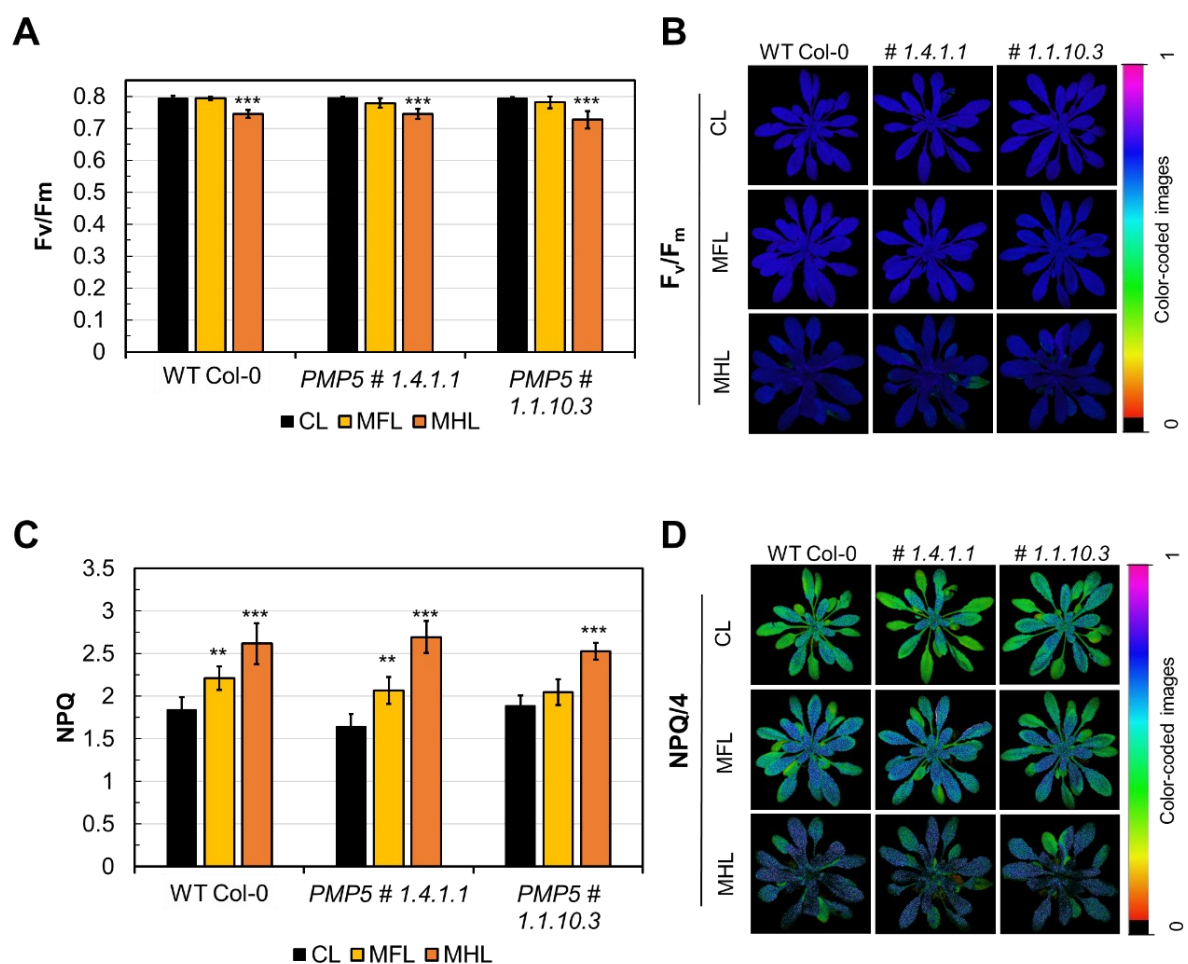
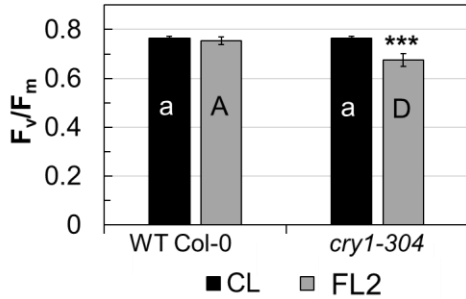


Figure 3.40. Maximum quantum yield of PSII in the overnight dark-adapted state (F_v/F_m) and NPQ after three days under CL, FL and HL in WT Col-0, *PMP5 #1.4.1.1* and *PMP5 #1.1.10.3*. **A)** F_v/F_m values of the mature leaves used for the induction measurements shown in Figure 3.39. **B)** Spatial heterogeneity of F_v/F_m in whole rosettes. The color bars on the right show the scale of the color code. **C)** NPQ values of the mature leaves used for the induction measurements shown in Figure 3.39 after 160 s of AL illumination. **D)** Spatial heterogeneity of NPQ after 160 s of AL in whole rosettes. The color bars on the right show the scale of the color code. NPQ values in the images are divided by four (NPQ/4) to use the scale between 0 and 1. No significant difference was found between the genotypes under CL, FL2 or HL2. Significant differences between the different light conditions within the same genotype were assessed by Tukey multiple comparison and are indicated by asterisks (** $P \leq 0.01$, *** ≤ 0.001). Mean values \pm SD are shown ($n = 3-4$).

3.4 Supplementary figures

A



B

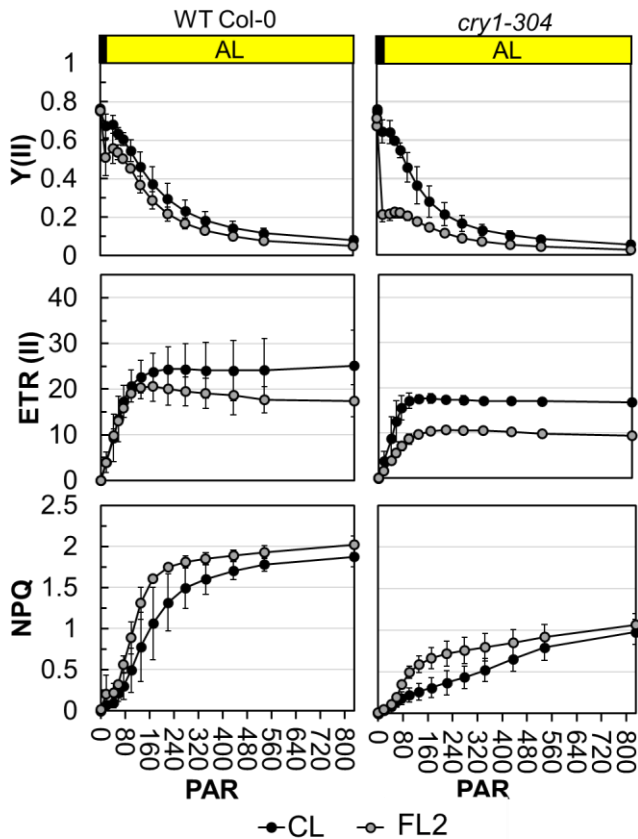


Figure S1. Characterization of PSII after three days under CL and FL2 in WT Col-0 and *cry1-304*. A) F_v/F_m . Significant differences between the genotypes as well as between the light conditions (CL and FL), and the interaction (genotype X light condition) were assessed by two-way ANOVA followed by Tukey's multiple comparison test. Different letters in the panel indicate significant differences in comparison to WT Col-0. Letter shared in common between the genotypes indicate not significant difference between their mean ($D P \leq 0.001$). Lowercase and uppercase letters are for the comparison between the genotypes under CL and FL, respectively. The differences between the light treatments within the same genotype (FL2 vs CL) were assessed by Tukey multiple comparison and is indicated by asterisks ($*** P \leq 0.001$). Mean values \pm SD ($n = 3-6$). B) Rapid light response curves measured in leaves of overnight dark-adapted plants of WT Col-0 and *cry1-304*. The intensity of AL was gradually increased in 14 steps from 0 to $830 \mu\text{mol photons m}^{-2} \text{s}^{-1}$ with 90 s of dwell time at each step. Y(II), quantum yield of PSII; ETR (II), relative electron transport rate of PSII; NPQ, non-photochemical quenching.

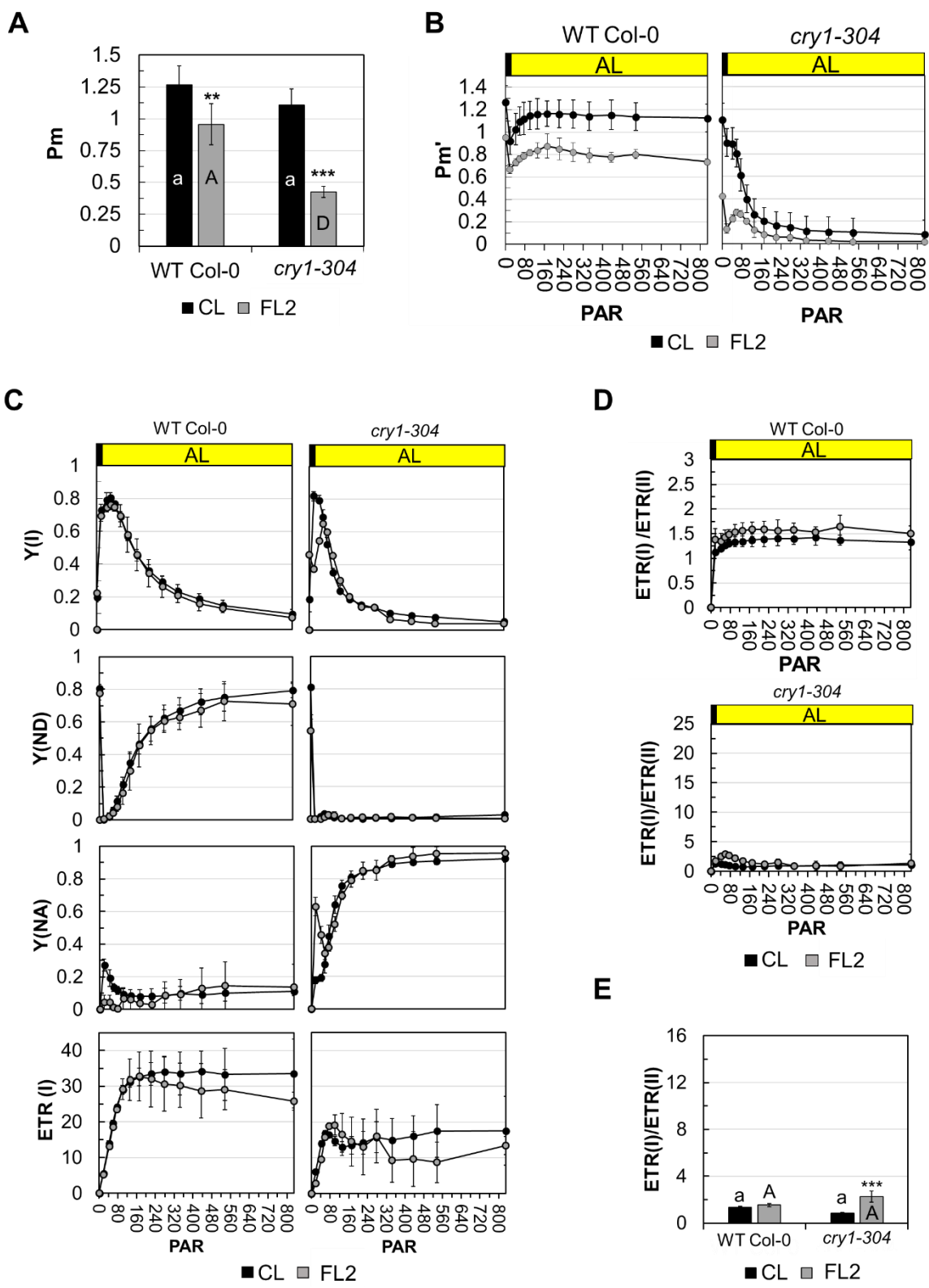


Figure S2. Characterization of PSI after three days under CL and FL2 in WT Col-0 and *cry1-304*. Rapid light response curves were measured in leaves of overnight dark-adapted plants of WT Col-0 and *cry1-304*. The intensity of AL was gradually increased in 14 steps from 0 to 830 $\mu\text{mol photons m}^{-2} \text{s}^{-1}$ with 90 s of dwell time at each step. **A)** P_m , maximal change of the P700 signal upon quantitative transformation of P700 from the fully reduced to the fully oxidized state, determined by Far-Red preillumination and application of a Saturation Pulse. **B)** P_m' , maximal change of the P700 signal in a given light state upon application of a saturation pulse without far red illumination. **C)** $Y(I)$, quantum yield of PSI; $Y(ND)$, quantum yield of PSI donor-side limitation; $Y(NA)$, quantum yield of PSI acceptor-side limitation; $ETR(I)$, relative electron transport rate of PSI. **D)** Ratio between $ETR(II)$ and $ETR(I)$, $ETR(I) / ETR(II)$ **E)** $ETR(I) / ETR(II)$ at the light intensity ($100 \mu\text{mol photons m}^{-2} \text{s}^{-1}$) corresponding to the growth light in CL and the intensity of low-light periods in FL. Significant differences between the genotypes as well as between the light conditions (CL and FL), and the interaction (genotype X light condition) were assessed by two-way ANOVA followed by Tukey's multiple comparison test. Lowercase and uppercase letters indicate the comparison between the genotypes under CL and FL2, respectively. The differences between the light treatments within the same genotype (FL2 vs CL) were assessed by unpaired independent Student t-test and significant differences are indicated by asterisks (***) $P \leq 0.001$. Mean values \pm SD ($n = 3-6$) are shown

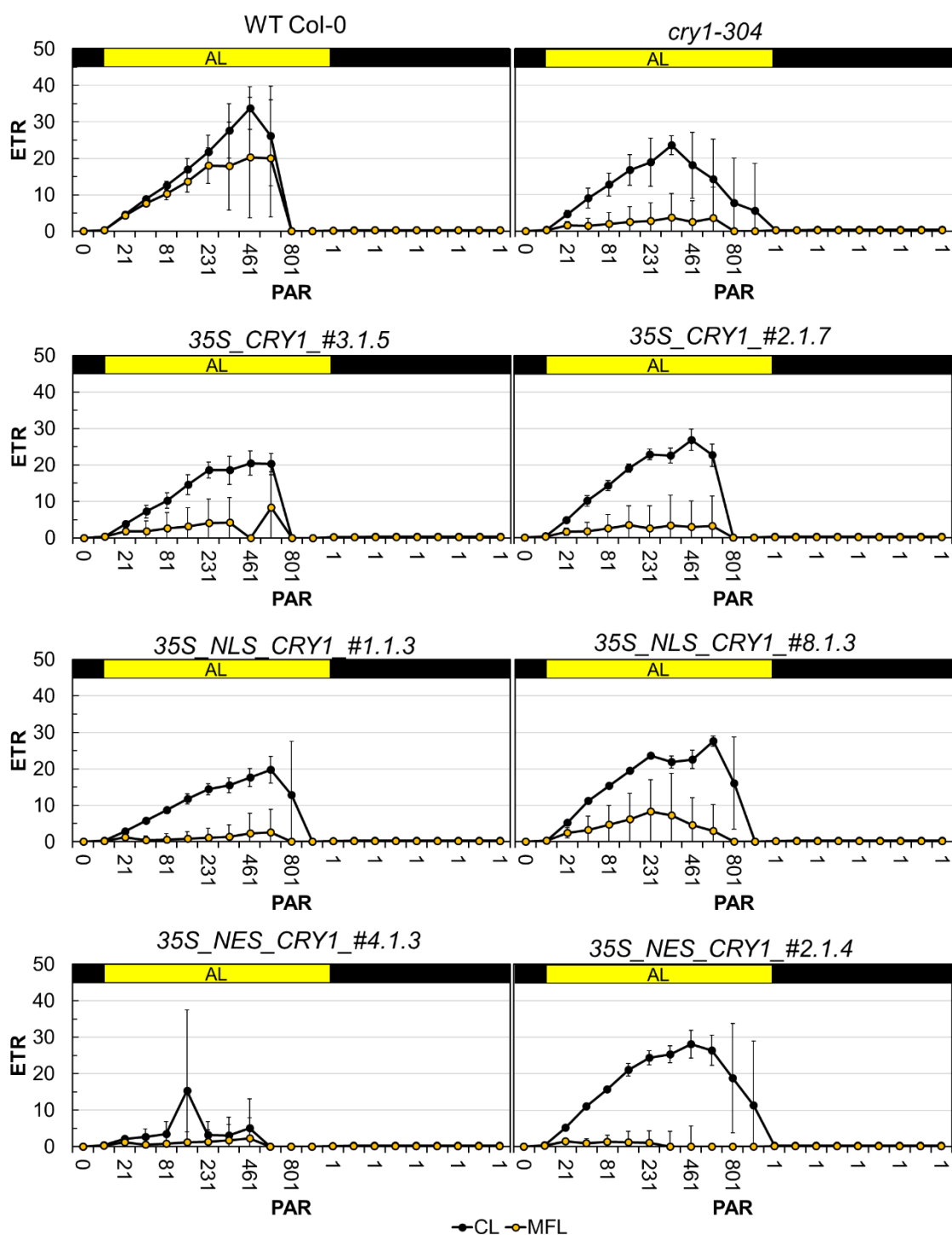


Figure S3. Characterization of relative electron transport rate of PSII (ETR(II)) before the onset of the experiment under CL (black symbols) and after three-day exposure to FL2 (yellow symbols) in selected *CRY1* OE lines. Data are from the same measurements as shown in the rapid light response curves of Fig. 3.22. Mean values \pm SD ($n = 3-6$) are shown. The measurements were conducted by Nina Boots for her bachelor thesis (HHU, 2019).

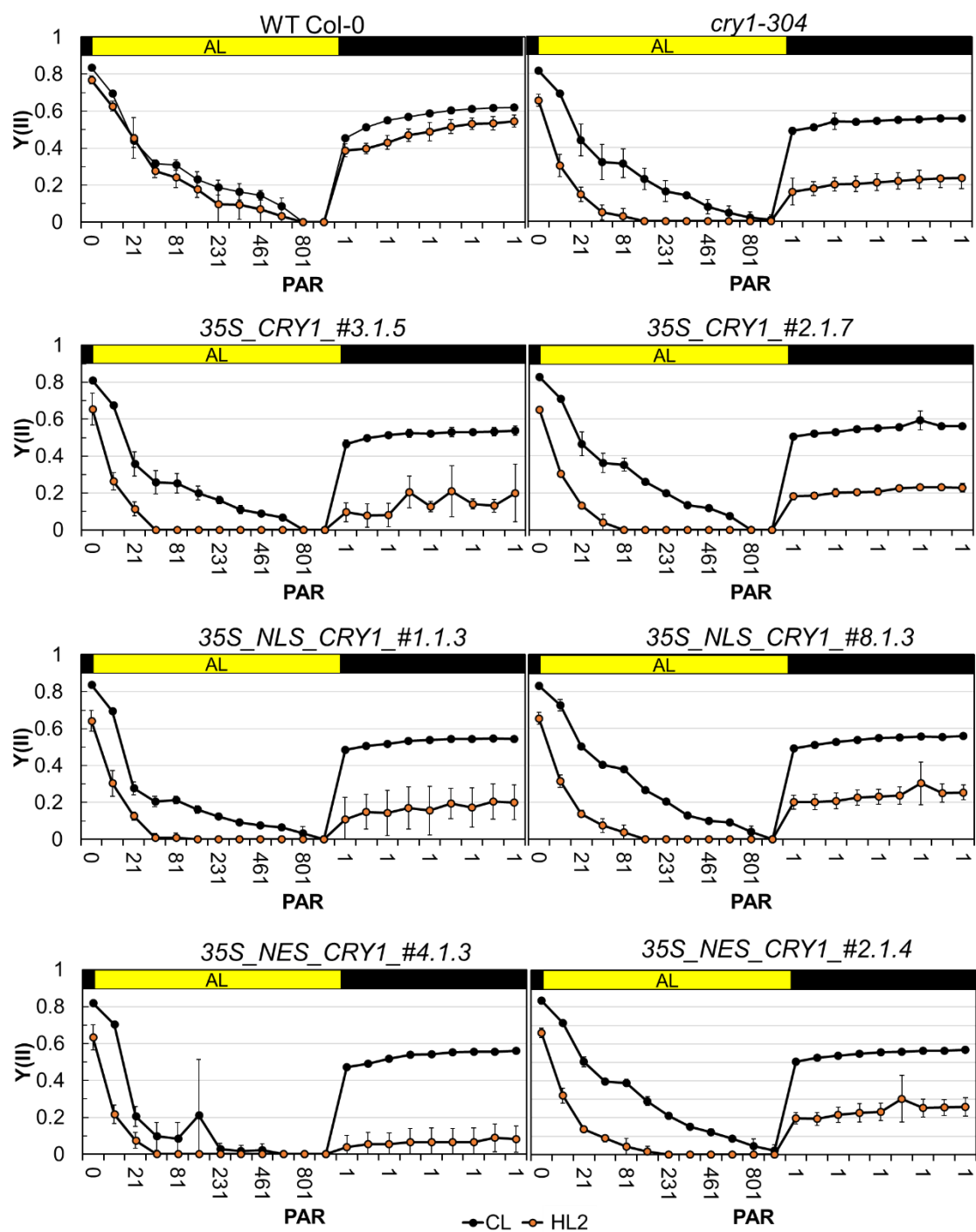


Figure S4. Characterization of PSII quantum yield, $Y(II)$, before the onset of the experiment under CL (black symbols) and after one-day exposure to HL2 (orange symbols) in selected *CRY1* OE lines. Rapid light response curves were measured in leaves of overnight dark-adapted plants of WT Col-0, *cry1-304*, *35S_CRY1*, *35S-NLS_CRY1* and *35S_NES_CRY1*. The intensity of AL was gradually increased in 12 steps from 0 to $1076 \mu\text{mol photons m}^{-2} \text{s}^{-1}$ with 30 s of dwell time at each step. The light response curves were followed by a dark recovery of 90 s with SP every 10 s. Mean values \pm SD ($n = 3-6$) are shown. The measurements were conducted by Nina Boots for her bachelor thesis (HHU, 2019).

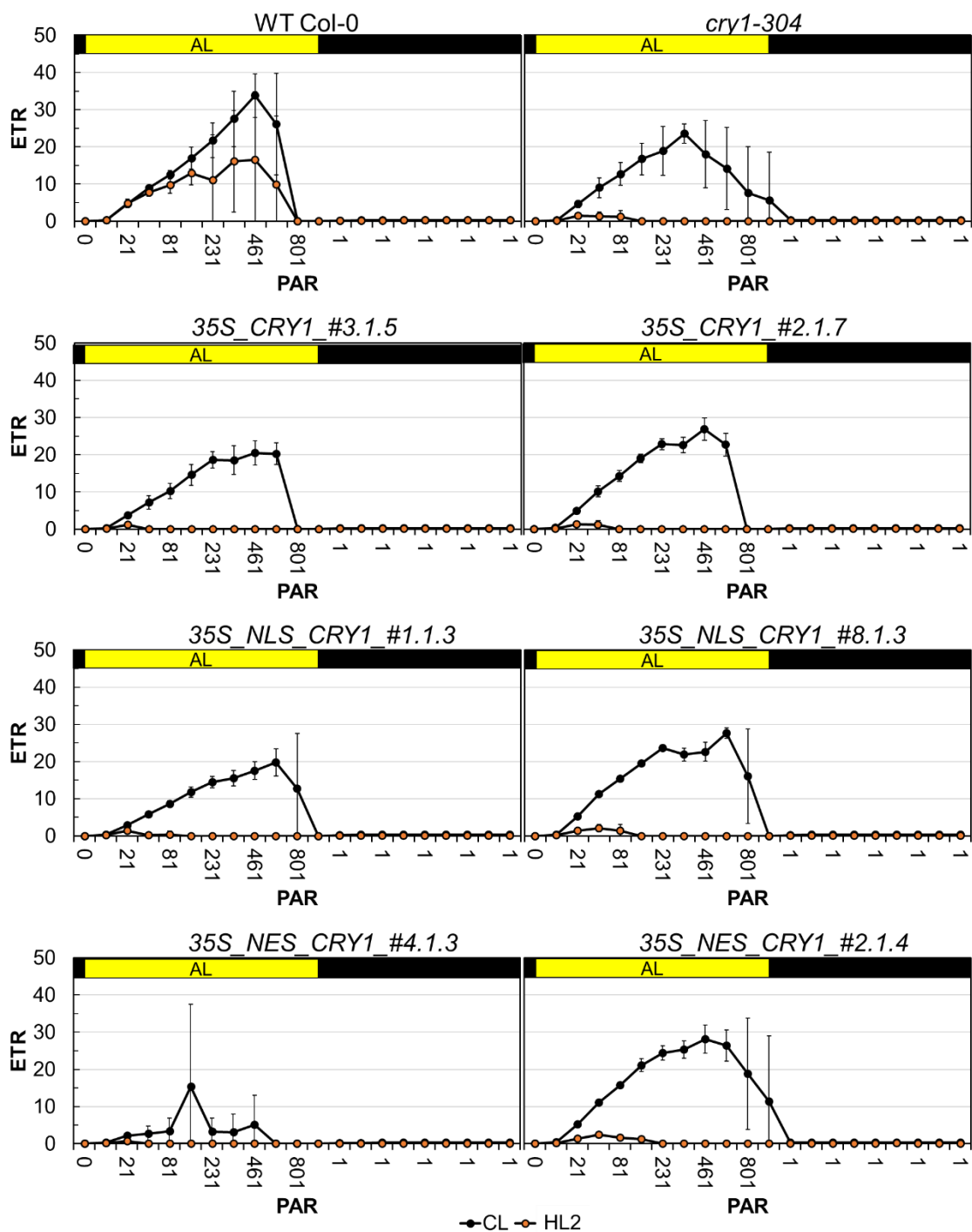


Figure S5. Characterization of relative electron transport rate of PSII (ETR(II)) before the onset of the experiment under CL (black symbols) and after one-day exposure to HL2 (orange symbols) in selected *CRY1* OE lines. Data are from the same measurements as shown in the rapid light response curves of Fig. 3.22. Mean values \pm SD ($n = 3-6$) are shown. The measurements were conducted by Nina Boots for her bachelor thesis (HHU, 2019).

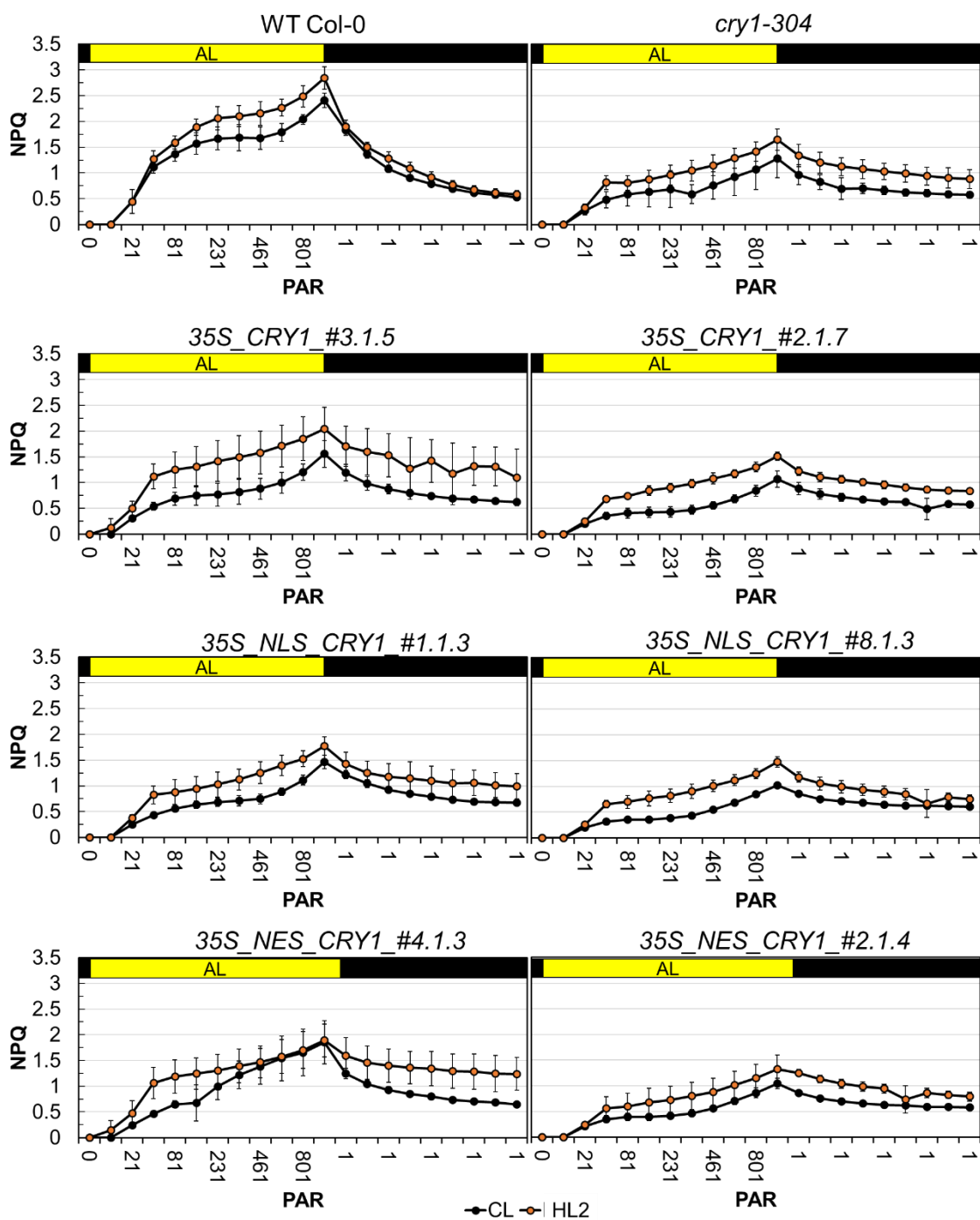


Figure S6. Characterization of non-photochemical quenching (NPQ) before the onset of the experiment under CL (black symbols) and after one-day exposure to HL2 (orange symbols) in selected *CRY1* OE lines. Data are from the same measurements as shown in the rapid light response curves of Fig. 3.22. Mean values \pm SD ($n = 3-6$) are shown. The measurements were conducted by Nina Boots for her bachelor thesis (HHU, 2019).

4. DISCUSSION

The frequent environmental dynamic changes that photosynthetic organisms experience in natural environments, require a series of short- and long-term mechanisms to ensure a good compromise between protection of the photosynthetic machinery and efficient photosynthetic performance in order to prosper in dynamic environments. In this work I studied the dynamic regulation of photosynthesis and the long-term strategies of plants to acclimate their photosynthetic apparatus to photo-oxidative stress induced by EL. *A. thaliana* leaf transcriptome and proteome revealed a dynamic regulation of many genes and proteins under FL compared to CL (Schneider et al., 2019; Niedermaier et al., 2020). Besides individual genes and proteins, the functional relationships between some of these components such as light perception, light signaling and molecular mechanisms underlying the regulation of photosynthetic acclimation, have been studied in this work through the characterization of the UV-A and BL photoreceptor CRY1. Also, by studying the CRY1 localization-dependent function I aimed to better understand the mechanisms by which these cellular network components, that involves multiple organelles and subcellular compartments, are coordinated and mediate global light signaling responses to changing environments. Lastly the role in photosynthetic acclimation to EL of a specific candidate with unknown function, which was found upregulated in FL leaf transcriptome (Schneider et al., 2019) and described as potentially involved in the integration of light and plastid signaling (Ruckle et al.2012), was characterized in this study.

4.1 Physiological role of the photoreceptor CRY1 in sustaining photosynthesis

With the aim to investigate the connection between light perception, light signaling and regulation of photosynthesis, the role of the UV-A and BL photoreceptor CRY1 in photosynthetic responses has been investigated in *A. thaliana*. The role of CRY1 in HL stress responses has been partially investigated previously, pointing out the contribution of CRY1 in regulation of light responsive genes important for photosynthetic responses to photo-oxidative stress (Kleine et al., 2007). The study by Kleine et al. also showed a strong HL-sensitive phenotype of the *cry1-304* plants with significant photoinactivation of PSII. Furthermore, CRY1 has also been identified in a “*gun*-mutant screening” as an important factor in the interaction between plastid and light signaling (Ruckle et al., 2007).

Indeed plastid signals modify light signaling and are important both in chloroplast biogenesis and operational control of chloroplast retrograde signaling (Ruckle et al., 2007). In this thesis *cry1-304* has been characterized in details under CL and EL, and in particular under FL, which was not investigated so far. Growth analyses, photosynthetic responses, protein and pigment accumulation as well as gene expression were evaluated in order to specifically address the following questions: (i) Does CRY1 contribute to proper functioning of photosynthesis under constant low light conditions? (ii) Is CRY1 involved in stress responses and acclimation to photo-oxidative stress induced by EL? (iii) Is the role of CRY1 in photosynthesis and stress responses exclusive or does it involve the concomitant action of multiple photoreceptors (e.g CRY1, CRY2 and PHYB) via the activation of the TFs HY5 and/or HYH?

4.1.1 CRY1 contributes to proper functioning photosynthesis under non-photoinhibitory condition

The analysis of photosynthetic parameters both during induction of photosynthesis (**Figures 3.2-3.4**) and in response to increasing light intensities (**Figure 3.5**) revealed that in a non-photoinhibitory condition, CL plants of *cry1-304* have a reduced Y(II) accompanied by a decrement of ETR(II) (**Figures 3.3** and **3.5**) and lower ability to induce and upregulate NPQ upon increased light intensity, as shown by NPQ values that were ca. 40% lower compared to WT Col-0 (**Figures 3.3-3.5**). The transition of dark-adapted plants to light generates the trans-thylakoid ΔpH responsible for the induction of qE component of NPQ, which is strictly dependent on the presence of the PSBS protein and it is modulated by the amount of Z accumulated upon illumination via de-epoxidation of V by VDE in the xanthophyll cycle (Niyogi et al., 2000; Li et al., 2002; Holt et al., 2004; Li et al., 2004; Jahns and Holzwarth, 2012). Thus, we first hypothesized that the lower NPQ capacity observed in *cry1-304* might be related to a malfunctioning in regulation, activation or accumulation of these components. Indeed, the qE component of NPQ is strongly reduced and decreased in NPQ mutants lacking the main component of qE such as PSBS (*npq4*) and VDE (*npq1*), respectively, while it increases in mutants lacking ZEP, that accumulate high level of Z in all conditions (*npq2*) (Kalituho et al., 2007; Dall'Osto et al., 2014). Also mutants lacking PGRL1 (*pgr1*), and PGR5 (*pgr5*), which are deficient in proton gradient regulation and thus in ΔpH formation, display a impaired qE induction (Kalituho et al., 2007).

However, the lower NPQ ability observed in *cry1-304* was ascribable neither to altered accumulation of PSBS nor malfunctioning of the xanthophyll cycle (**Figure 3.9 B**, and **Table 3.1**) comparable with WT Col-0. Also PGR5 protein levels were in a normal range and did not significantly differ from WT Col-0, even though *PGR5* gene expression was found to be downregulated under 100 and 1000 $\mu\text{mol photons m}^{-2} \text{s}^{-1}$ (similar to CL and HL conditions of this study) in *cry1-304* seedlings (Kleine et al., 2007).

In addition to general downregulation of PSII and NPQ capacity, also PSI was affected in *cry1-304* under CL conditions compared to WT Col-0 (**Figures 3.6** and **3.7**). While the functional fraction of PSI, evaluated by the maximum photo-oxidizable P700 (Pm, **Figure 3.6 A**), was not significantly lower compared to WT Col-0, Pm' values determined after each SP, which show the fraction of PSI that is temporarily oxidizable under a given intensity of AL, progressively decreased from ca 1.0 to 0.1 at light intensity higher than growth light intensity (**Figure 3.6 B**), indicating a decreased ability of PSI to release electrons to the downstream acceptors and thus to maintain a photo-oxidized state. The increased temporarily non-oxidizable PSI (closed RC) fraction observed in *cry1-304* does not necessarily indicate that these fractions are non-functional, but might suggest that they are temporarily overloaded and thus unavailable. Accordingly, the changes in P700 redox state at light intensity higher than the growth light intensity (**Figure 3.7**) displayed a slower oxidation of P700 during the application of SPs, possibly indicating a slower P700 charge separation process. This was not observed in WT Col-0 under the same conditions, in which Pm' values remained stable to ca 1.2 during the exposure to different light intensities from 0 to 830 $\mu\text{mol photons m}^{-2} \text{s}^{-1}$ and P700 was oxidized and reduced at the beginning and at the end of each saturation pulse, respectively, during the entire duration of the measurements (**Figures 3.6 B** and **3.7**). Consistently with the drop of Pm' values upon increasing light intensity, almost the entire PSI capacity (90-95%) was largely limited by saturation of acceptors downstream of PSI, as indicated by the strong increase in Y(NA) (**Figure 3.6 C**). The alleviation of Y(NA) by CET represents an efficient strategy in the photoprotective mechanisms of PSI, allowing the relaxation of the PSI acceptor side (Kono and Terashima, 2016). The rate of CET has been shown to increase during photosynthetic induction (Fan et al., 2007; Suorsa, 2015), preventing PSI acceptor side limitation when the CBB cycle is not yet properly working. Interestingly WT treated with antimycin A, which inhibits CET pathway mediated by PGR5-PGRL1, and PGR5 KO mutant (*pgr5*) have been reported to show high Y(NA) (Kono et al., 2014; Kou et al., 2015) with values very similar to the ones observed in *cry1-304* (**Figure 3.6 C**).

Similarly to *cry1-304*, under CL the PGR5 mutation affected neither the growth nor the accumulation of the major photosynthetic protein complexes, but it lowered ETR (II) and NPQ (qE) induction (Yamamoto and Shikanai, 2019).

Although in our experimental conditions *cry1-304* had normal levels of PGR5 protein (**Figure 3.8**), it might defect in re-directing the electrons through CET during photosynthetic induction, causing over-reduction of the PSI acceptors.

As chloroplast is one of the major sites of ROS production during photosynthetic reaction, a specific scavenging system in the chloroplast is required to avoid photo-oxidative stress. GPX7 is a chloroplast glutathione peroxidase which has been shown to be involved in regulation of photo-oxidative tolerance (Chang et al., 2009). Under CL *GPX7* gene expression was downregulated to 24% compared to WT Col-0 (**Figure 3.10**), suggesting a defective ability of *cry1-304* plants to cope with oxidative stress in the chloroplast, as previously reported in *cry1-304* seedlings exposed to HL (Kleine et al., 2007).

The lower activities of both PSII and PSI observed in *cry1-304* plants might represent signs of photosensitivity even at low light intensity, pointing for the first time to an important role of CRY1 in contributing to homeostasis and proper functioning of photosynthesis under non-stressful constant light conditions. The lower ETR(II) observed in *cry1-304* plants might be a consequence of downregulation of PSII electron transport to prevent PSI photoinhibition. Indeed, regulatory mechanisms such as photosynthetic control at the level of $\text{cyt}_{b_6/f}$ prevent an excess of electron from PSII and protect PSI from photodamage in conditions of excessive pressure at the PSI acceptor side (Gollan et al., 2017; Tikkanen and Grebe, 2018; Lima-Melo et al., 2019b). Our results also highlight a lower NPQ capacity in *cry1-304* plants, not accompanied by defective accumulation of PSBS, PGR5 and Z. While the reasons of this phenotype are not clear, the reduced NPQ might cause excess of electron to PSI, which can partially explain the sensitivity of PSI observed in *cry1-304* plants exposed to increasing light intensity. Indeed, the photo-oxidizable P700, which represents the functional PSI fraction, was found to strongly decrease upon illumination with light intensities higher than growth light, likely as a consequence of the strong acceptor side limitation. Overall, these defects observed in *cry1-304* plants do not affect the composition of the photosynthetic apparatus, as the accumulation of the major photosynthetic proteins did not differ from WT Col-0 (**Figure 3.8**). Under CL condition the reduced photosynthetic capacity at the level of both PSII and PSI did not have negative consequences on plant development and growth (**Figure 3.1**).

4.1.2 CRY1 is important in long-term acclimation to photo-oxidative stress induced by EL

The role of CRY1 in HL stress responses has been partially investigated previously (Kleine et al., 2007), more from a transcriptional point of view. Leaf photobleaching in both seedlings and mature plants of *cry1-304* was previously reported after a 24 h of continuous exposure to HL (Kleine et al., 2007). Here we showed that *cry1-304* quickly displayed bleaching of the leaves after a few days of HL during the 12 hours of light period (**Figure 3.1 A**), suggesting that CRY1 plays a key role in response to HL and/or ROS scavenging. Indeed, photobleaching is known to result from release of chlorophyll and subsequent uncontrolled accumulation of ROS (Tiwari et al., 2016) or a consequence of programmed cell death as results of ROS and retrograde signaling. We confirmed the highly HL-sensitive phenotype of *cry1-304* and we show for the first time a severe growth phenotype both in HL and in FL (**Figure 3.1 B**), which reflects the photo-oxidative stress experienced under these conditions and indicate that CRY1 is required for EL tolerance.

In addition, contrarily to WT Col-0, *cry1-304* did not show anthocyanin accumulation in response to HL (**Figures 3.1 and 3.21 B**), as has been previously reported (Kleine et al., 2007). Accordingly, CRY1 has been shown to be important in inducing the expression of genes involved in anthocyanin biosynthesis via HY5 light signaling (Lin et al., 1996; Shin et al., 2007; Wu and Spalding, 2007; Shin et al., 2013; Gangappa and Botto, 2016). Interestingly, a strong downregulation of *PAP1*, *PAP2* and other structural genes in the anthocyanin biosynthesis pathway, that are normally induced under HL, has been reported in seedlings of *cry1-304* (Kleine et al., 2007). It is known that anthocyanin biosynthesis increases in response to environmental stresses including EL (Gould, 2004) and they are involved in important processes such as protection of the photosynthetic apparatus against damaging levels of light (Gould, 2004; Hatier and Gould, 2008; Maier and Hoecker, 2015). Interestingly, a GUN-dependent retrograde communication for the induction of flavonoid biosynthetic gene expression and accumulation of protective anthocyanin pigments during plastid biogenesis has been recently proposed (Richter et al., 2020).

Repression of photosynthesis associated nuclear genes and induction of flavonoid biosynthetic gene expression through the same signaling pathway during operational control allows proper acclimation to dynamic and/or stressful environmental conditions (Richter et al., 2020).

Under FL conditions (both FL and FL2) anthocyanin accumulation was observed nor in WT Col-0 neither in *cry1-304* (**Figures 3.1** and **3.21 B**). Accordingly, in similar FL conditions genes involved in this route were not differentially expressed compared to CL (Schneider et al., 2019). Together with lower anthocyanin accumulation and photobleaching under HL, Chl content was also found lower in *cry1-304* under HL conditions (Kleine et al, 2007), but not under our FL conditions (**Figure 3.9 A**).

The role of CRY1 was already investigated under constant HL (Kleine et al., 2007), which is quite different from dynamic growth light environments that occur in natural environments. Thus, FL conditions were chosen as the main treatment for most of the analysis in this work, as it allows to study the photosynthetic response in a dynamic environment, still far away but more similar to conditions that plants experience in nature. Furthermore, FL affects the growth in *cry1-304* as much as HL (**Figure 3.1 B**), but it does not damage the leaves allowing us to perform a series of molecular and biochemical analysis in mature plants treated with long-term EL and thus evaluate acclimation processes.

Reorganization and downregulation of light harvesting chlorophyll a/b-protein complex of PSII (LHCII) are essential during acclimation to EL to avoid excessive energy pression to the light harvesting apparatus (Timperio et al., 2012). Following three days of FL exposure the expression of *LHCB1.2* was strongly downregulated in both WT Col-0 and *cry1-304* under FL at similar levels (**Figure 3.10**), indicating the capacity to downregulate the light harvesting as protection mechanism against EL. However, *cry1-304* plants displayed a much more severe PSII photoinhibition compared to WT Col-0 (**Figure 3.2 A** and **B**).

Correlation between photoinhibition and malfunctioning of D1 repair mechanisms, including inactivation, degradation, repair and replacement, have been extensively studied. ROS generated at the level of PSII irreversibly damage D1 protein, and its turnover has been shown to be an essential requisite to recover PSII from photoinhibition (Allahverdiyeva and Aro, 2012; Li et al., 2018). Although the D1 protein levels did not differ in FL-treated plants of WT Col-0 and *cry1-304*, the accumulation of D1 increased in FL-treated plants of WT Col-0 compared to CL plants, but it remained unchanged in *cry1-304* plants (**Figure 3.8 A** and **B**), possibly indicating a not optimal rate of D1 repair mechanisms.

Interestingly, while *ELIP2* was found downregulated in *cry1-304* seedlings under HL (Kleine et al., 2007), we found it strongly upregulated in both WT Col-0 and *cry1-304* under FL compared to CL. *ELIP2*, together with and *ELIP1*, are thylakoidal proteins belonging to the Chl *a/b*-binding protein family involved in protective mechanisms, typically expressed under environmental conditions inhibiting photosynthesis (Hayami et al., 2015, Adamska et al., 1999). It has been reported that while the expression of *ELIP1* gradually increases as with increasing PSII photodamage, accumulation of *ELIP2* shows a stepwise response, remaining low until 40% of PSII reaction centers are photodamaged and increasing strongly after severe photodamage (Heddad et al., 2006). The upregulation of *ELIP2* in *cry1-304* under FL is in line with the PSII photoinhibition observed after three days of FL exposure (**Figure 3.2 A**) and it highlights that other factors are involved in the regulation of its expression under non-standard conditions. In fact, while the *ELIP-1* and *2* induction is mainly controlled by *CRY1*, a minor contribution of *PHYB* has been proposed, as *phyB* and *phyAphyB* mutants displayed a lower induction of *ELIP1* and *2* than WT, but higher than *cry1-304* (Kleine et al., 2007). At the contrary both *CRY2* and *PHYA* do not contribute to the induction of *ELIP1* and *2*, as similarly to WT, *cry2* and *phyA* mutants have been shown to have a strong induction of *ELIP1* and *ELIP2* expression (Kleine et al., 2007), consistently with light inactivation of *CRY2* and *PHYA* under light exposure (Somers and Quail, 1995; Clough and Vierstra, 1997; Clough et al., 1999; Wang and Wang Deng, 2004; Rattanapisit et al., 2016) and high fluencies (Ahmad et al., 1998a; Lin et al., 1998; Lin, 2002; Shalitin et al., 2002; Kleine et al., 2007).

During the first part of photosynthetic induction, the exposure of dark-adapted plants to a fully saturating light intensity, such as 550 $\mu\text{mol photons m}^{-2} \text{s}^{-1}$, caused saturation of PSII both in WT Col-0 and *cry1-304* under both CL and FL (**Figure 3.3**). However, in FL plants of *cry1-304* the PSII remains fully reduced during the entire duration of the measurement. It might indicate both a delayed activation of photosynthesis or a permanent damage of PSII under these conditions. Since in the dark photosynthesis is not yet induced, many light- and redox-regulated enzymes in the CBB cycle are inactivated and some of the intermediates are depleted (Buchanan, 2016; Sharkey, 2019). Thus, further analysis, such as longer induction or measurement on pre-illuminated plants might explain the observed phenotype. However, during the light response curves (**Figure 3.5**), FL plants of *cry1-304* had low but positive *Y(II)* and *ETR*. It is therefore likely that 550 $\mu\text{mol photons m}^{-2} \text{s}^{-1}$ immediately caused full reduction of PSII and these plants were less tolerant to EL.

Pre-illumination at low light intensity might therefore cause a smoother activation of photosynthesis, even though at lower levels compared to WT Col-0. Furthermore, the abrupt dark to light transition might have caused a full saturation not only of PSII but of the entire photosynthetic electron transport chain, consequently increasing PSI acceptor side limitation, when the light dependent redox-activation of the downstream reactions by the chloroplast TRXs were not yet completely operating. The TRX system might be an other target to take into account and further investigate in relation with the *cry1-304* phenotype upon dark to light transition and LL to HL. The Chloroplast TRX redox system protect chloroplast against oxidative damage in FL environments, as it balances photosynthetic reactions at level of both electron transport and carbon fixation and it regulates photoprotective mechanisms as well as the metabolism of ROS produced within the chloroplast during photosynthetic reactions (Pérez-Ruiz et al., 2006; Schürmann and Buchanan, 2008; Nikkanen et al., 2016; Nikkanen et al., 2018; Nikkanen and Rintamäki, 2019). NTRC is particularly important in the dark to light transition as the NTRC pool present in the dark can transiently activate CET that helps to balance electron transport around PSI, alleviating the pressure at the PSI acceptor side before the full activation of the CBB cycle, ATP synthase and redox-regulated enzymes of the CBB cycle, increasing the electron sink capacity of the stroma and alleviating the PSI acceptor side limitation (Carrillo et al., 2016; Thormählen et al., 2017; Nikkanen et al., 2018; Nikkanen and Rintamäki, 2019). In conjunction with NTRC activity (Nikkanen et al., 2016; Nikkanen and Rintamäki, 2019), FTR types TRXs are activated under growth light and higher irradiance, by the photosynthetically reduced fd and further activate CET (Nikkanen et al., 2018; Nikkanen and Rintamäki, 2019).

The diminished capacity to rapidly induce photosynthesis and develop NPQ (specifically qE) upon illumination was already detected under CL in *cry1-304* but it was strongly exacerbated following a few days of FL exposure (**Figure 3.3**). Indeed, under these conditions NPQ values induced by light exposure were surprisingly lower not only compared to WT Col-0 under the same conditions but also compared CL-*cry1-304* plants. After 160s of AL exposure, when the WT reached the steady state part of NPQ induction the NPQ level in *cry1-304* were ca. 81% lower than WT and ca 40% lower compared to CL *cry1-304* plants (**Figure 3.4**). Notably, qI component of NPQ was already present in those plants, accordingly with the lower F_v/F_m values (**Figure 3.2**), suggesting that the inability to further induce NPQ upon illumination might be related to the presence of a dark sustained qI component, which is likely to be caused by the extensive FL treatment.

During the measurement of light response curves FL- and CL-treated *cry1-304* plants displayed similar abilities to increase NPQ with increasing light intensity up to 480 $\mu\text{mol photons m}^{-2} \text{ s}^{-1}$, but at higher light intensities FL-treated plants had lower NPQ levels (**Figure 3.5**) as observed also during the induction measurements (**Figure 3.3**). However, when a milder FL treatment was applied (**Figure S.1**), FL2 plants of *cry1-304* displayed a milder response at the level of PSII photoinhibition, Y(II) and ETR(II), and they were able to increase NPQ upon increase in light intensity even at higher light intensities. It is thus likely that the severe NPQ inhibition observed in *cry1-304* under the FL condition is dependent on the light intensity applied and also is partially a consequence of the decreased electron transport capacity and formation of proton motif force across the thylakoid membrane. While the mutants lacking PSBS, VDE and PGR5 have been shown to have similarly low levels of qE induction as FL plants of *cry1-304*, (Kalituho et al., 2007; Dall'Osto et al., 2014), the levels of both PSBS and PGR5 did not significantly differ from WT Col-0 under the same conditions (**Figure 3.8**), indicating that this phenotype cannot be attributed to a defect in their accumulation. Also, the NPQ deficient phenotype observed in FL-treated *cry1-304* (**Figures 3.3 – 3.5**) does not seem to be related to limited Z (or A) accumulation in the xanthophyll cycle, as *cry1-304* mutants were able to operate the xanthophyll cycle normally, having enough amounts of Z and a large VAZ pool size to activate and sustain NPQ (**Figure 3.9 B**). These pieces of evidence suggest that the photoprotection deficiency observed in *cry1-304* is neither due to an insufficient accumulation of PSBS and/or PGR5, nor to a malfunctioning of the xanthophyll cycle. It might be related to their functional regulation or to other more indirect factors which interact with these components.

It is interesting to note that the growth of *cry1-304* did not differ from WT Col-0 in CL, but it was affected both in HL and FL (**Figure 3.1**). Interestingly, while *npq1* and *npq4* mutants did not show defects in growth and any visible phenotype under dynamic conditions such as rapid fluctuation of light (Tikkanen et al., 2010), *PGR5* mutation is lethal under FL (Tikkanen et al., 2010; Suorsa et al., 2016) but not under HL (Yamamoto and Shikanai, 2019).

Notably, FL *cry1-304* plants displayed higher levels of A and Z (especially A) already in the dark, as shown also by a DES of 0.4 against the 0.2 in WT Col-0 (**Table 3.1**), and they were not able to significantly increase their A and Z levels and reduce the V content upon AL exposure, resulting in no increase in DES after 260s of AL followed by 1-min dark adaptation (**Tables 3.1 and 3.3**). The dark retention of Z and A found in *cry1-304* under FL (**Figure 3.9**) is consistent with the observed photoinhibition (low F_v/F_m) (**Figure 3.2 A**).

Indeed, dark retention of high levels of A and Z accompanied with sustained Δ pH-independent energy dissipation and down-regulation of PSII activity have been observed in plants under severe stress, especially in over-wintering evergreen plants (Verhoeven et al., 1998; Adams III et al., 2002; Öquist and Huner, 2003; Adams et al., 2004; Yamazaki et al., 2011), and this has been associated with PSII photoinhibition and the qI component of NPQ. qI has been found to include mechanisms for sustained quenching, as demonstrated by retention of high level of Z, which is very slowly reconverted to V due to the gradual downregulation and degradation of ZEP upon exposure to photoinhibitory conditions (Reinhold et al., 2008; Nilkens et al., 2010; Jahns and Holzwarth, 2012; Townsend et al., 2018; Bethmann et al., 2019). Relaxation of qI component can take several hours and requires PSII repair processes and D1 turnover. The dark sustained high DES observed in FL-*cry1-304* plants can be related to a slow D1 turnover and therefore PSII photoinhibition. Further experiments are needed to take into account the D1 turnover and PSII efficiency at different time points together with ZEP accumulation and degradation in order to clarify whether the photoinhibition observed in FL-*cry1-304* plants is reversible or irreversible and the connection with the dark retention of A and Z.

Not only PSII, but also PSI displayed strong photoinhibition in FL-treated *cry1-304* plants compared to both WT Col-0 and CL-treated plants (**Figure 3.6 A**). The functional PSI, measured as the maximum photo-oxidizable PSI (Pm), decreased to ca 25% of the CL levels in the FL plants of *cry1-304* (**Figure 3.6 A**). Imbalance between the donor and acceptor sides of PSI can lead to its inactivation and thus PSI photoinhibition (Lima-Melo et al., 2019a). Even though PSI photoinhibition seems stronger than PSII photoinhibition (**Figure 3.2**), the relative electron transport through PSI [ETR(I)] was higher than the one through PSII [ETR(II)] (**Figures 3.3 and 3.6 D and E**). Therefore, the lower rate of PSII electron transport, observed in both induction and light response curve measurements (**Figures 3.3 and 3.5 B**), was associated with a higher Y(ND) in FL plants of *cry1-304*, compared to the CL conditions, reaching almost the levels observed in WT Col-0. Contrarily to CL plants, Y(NA) decreased in FL *cry1-304*, but still remained higher than in WT Col-0 (**Figure 3.6 C**). The reduced LET coming from PSII might be a consequence of PSII photoinhibition, indicating that the PSII photodamage is affecting the ability to transfer electron to PSI. However, the PSII photoinhibition observed in FL-treated *cry1-304* (**Figure 3.3**) together with the decreased electron transport in PSII (**Figures 3.3 and 3.5 B**) might indicate a mechanism to protect PSI from excess of electrons that might cause further damage to PSI by ROS production.

While PSII is extremely sensitive to EL and its damage is linearly dependent on light intensity (Tikkanen et al., 2014b), PSI is more tolerant to EL but it is extremely sensitive to excess of electron coming from PSI electron donors on the lumenal side or/and insufficient capacity of electron acceptors at the stromal side (Tiwari et al., 2016) and it gets damaged only when electron flow from PSII exceeds the capacity of PSI electron acceptors to cope with the electrons (Tikkanen et al., 2014b). Once excess of electrons accumulate at the acceptor side, electrons can reduce O_2 and produce superoxide anion radical ($O_2^{\cdot-}$), which is known to permanently inactivate PSI iron-sulfur (FeS) clusters and cause PSI inhibition (Kono and Terashima, 2016; Takagi et al., 2016; Tiwari et al., 2016; Tikkanen and Grebe, 2018; Lima-Melo et al., 2019a; Yamamoto and Shikanai, 2019). Once produced, $O_2^{\cdot-}$ can immediately damage PSI and/or trigger the production of $\cdot OH$ (Shimakawa and Miyake, 2018). Downregulation at the PSI donor side includes pH-dependent mechanisms, such as photoprotective mechanisms acting at level of PSII (NPQ), as well as photosynthetic control at level of $cytb_6f$ (Barbato et al., 2020).

Photoinhibition of both photosystems has been reported in *A. thaliana* mutants defective in the ΔpH -dependent photosynthetic control, such as *pgr5* mutants, irrespectively of whether NPQ or state transitions defects were present or not in the same mutant (Barbato et al., 2020). Ultimately, downregulation and/or inactivation of PSII by PSII photoinhibition is photoprotective for PSI, as it prevent further pressure on PSI by limiting excess of electrons coming from the PSI donor side (Tikkanen et al., 2014b; Lima-Melo et al., 2019b; Lima-Melo et al., 2019a; Barbato et al., 2020). This is reasonable, as PSII recovery from photoinhibition is faster than PSI: while PSII repair only requires the degradation and replacement of the damaged D1, which can happen in several hours (Zhang and Scheller, 2004; Shimakawa and Miyake, 2018), PSI photoinhibition cause permanent loss of PSI activity and photoinhibited PSI RCs complexes are not repaired and/or replaced during the photoinhibitory conditions (Kudoh and Sonoike, Sonoike, 2011).

PSI repair has been shown to be a very slow process that starts only when plants are back to recovery conditions and it can take several days or weeks (Zhang and Scheller, 2004; Allahverdiyeva and Aro, 2012; Li et al., 2018; Shimakawa and Miyake, 2018; Tikkanen and Grebe, 2018; Barbato et al., 2020). Further experiments including a recovery period from FL are required to investigate the repair and the recovery of *cry1-304* mutants from photoinhibition of both photosystems.

Interactions between PSII and PSI photoinhibition has been recently addressed by studying the responses to HL of *Arabidopsis* WT and *pgr5* mutant plants (Lima-Melo et al., 2019b). The characterization of *pgr5* under EL has been proposed as model to study photoinhibition of PSI (Lima-Melo et al., 2019b; Lima-Melo et al., 2019a). Comparison of *cry1-304* with *pgr5* as model of PSI photoinhibition under FL conditions might provide insights about the functioning of these processes and the photosynthetic phenotype observed in this study.

Even though the PSI photoinhibition was severe in FL-treated plants of *cry1-304* plants protein level of PSAA was comparable in *cry1-304* and WT Col-0 and there was no detectable decrease in the abundance of PSAA in FL-treated plants compared to CL conditions (**Figure 3.8**). This is in line with the observations that the proteolytic removal and turnover of photoinhibited PSI begin only after photoinhibitory conditions are removed as part of the repair processes during the recovery period (Kudoh and Sonoike; Zhang and Scheller, 2004; Sonoike, 2011). Only the accumulation of PsaB proteins was found decreased proportionally with the rate of PSI photoinhibition in HL-treated *pgr5* mutants (Lima-Melo et al., 2019b). It would be interesting to evaluate the protein levels of PsaB in *cry1-304* under FL condition used in this work.

Remarkably, under FL *cry1-304* had very low values of Pm' (**Figure 3.6 B**) which in contrast to CL-plants were stable and did not decrease further. Consistently it was not able to fully oxidize the P700 during the application of saturation pulse even at low light intensity (**Figure 3.7**). The effects of P700 oxidation on the alleviation of PSI photoinhibition has been directly linked to the quenching of excess light energy in PSI (Tiwari et al., 2016; Shimakawa and Miyake, 2018). Indeed, PSI is known to be stable under saturating light conditions, as when P700 is oxidized it is a good quencher of excess energy (Tiwari et al., 2016; Shimakawa and Miyake, 2018). Since the fraction of photo-oxidizable PSI in FL-treated *cry1-304* plants is not enough and it decreases inversely with the increase of light intensity, it might have contributed to photodamage and photoinhibition of both PSII and PSI upon exposure to FL.

In addition, PSI photoinhibition has been shown to correlate linearly with decrease in Y(II) and NPQ (Kadota et al., 2019; Shimakawa and Miyake, 2019). Thus, the phenotype observed in *cry1-304* at the level of both photosystems and the deficiency in photoprotective mechanisms are interconnected with the phenotype observed at the level of PSI.

The extreme imbalance between PSI and PSII electron transport is reflected in the higher ETR(I)/ETR(II) observed in *cry1-304* under FL (**Figure 3.6 D and E**). ETR(I)/ETR(II) is often used as a measure of CET (Yamori et al., 2011; Kono et al., 2014), which is known to be activated more under EL to avoid an excessive PSI reduction and prevent acceptor side limitation (Munekage et al., 2002; DalCorso et al., 2008; Munekage et al., 2008; Suorsa et al., 2012; Suorsa et al., 2013; Suorsa, 2015; Colombo et al., 2016; Suorsa et al., 2016). This is visible in FL-treated plants of WT, in which Y(NA) slightly decreased compared to CL plants (**Figure 3.6 C**) and ETR(I)/ETR(II) increased, as CET is activated, releasing the pressure at the acceptor side of PSI (**Figure 3.6 D and E**). However, the observations made in this study suggest that this might not be the case for *cry1-304* plants:

(I) Under CL, where the Y(NA) was hugely higher than in FL conditions (**Figure 3.6 A**), the ETR(I)/ETR(II) was much higher in *cry1-304* than in WT Col-0, but much lower than the one observed in the FL-treated plants of *cry1-304*, in which also the Y(NA) levels decreased, concomitantly with an increment of Y(ND).

(II) There were not significant differences in PGR5 protein levels (**Figure 3.8**) between FL-treated plants of *cry1-304* compared to WT and to CL-treated plants. The contribution of NDH-mediated CET was not investigated in this work. As PGR5, PGRL1 and several subunit of NDH-1 complex were found upregulated under FL (Schneider et al., 2019), It would be worth to compare *cry1-304* with PGR5 and NDH loss of function mutants, with or without antimycin, which is known to inhibit PGR5-dependent CET (Kono et al., 2014; Kou et al., 2015).

The higher ETR(I)/ETR(II) in FL-treated plants is likely caused by the photodamage at the level of PSII, which is highlighted by both photoinhibition (**Figures 3.2 and 3.5 A**) and decreased photosynthetic capacity of electron transport Y(II) and ETR(II) (**Figures 3.3 and 3.5 B**). Thus, downregulation of PSII electron transport caused a drop in ETR (II) and therefore an increment in ETR(I)/ETR(II), which in this case is not the most suitable parameter to quantify CET.

Interestingly, FL2-treated plants of *cry1-304* displayed an intermediate phenotype between CL and FL: PSII and PSI photoinhibition as well as ETR(II) and NPQ phenotypes were milder than the ones observed in CL, but notably the plants still kept high Y(NA) at the level of PSI with intermediate values of ETR(I)/ETR(II) (**Figure S.2**), indicating that these phenotypes are partially dependent on the severity of the EL experienced in the growth conditions.

Increased photo-oxidative stress in the chloroplast of FL-treated *cry1-304* plants was further confirmed by the fact that *GPX7* was strongly upregulated compared to CL-treated plants and WT Col-0 under FL (**Figure 3.10**). It is not clear whether the higher oxidative stress and the imbalance in redox control observed in *cry1-304* are consequences of photodamage of PSII and PSI and photoprotection deficiency, or the other way around, if the observed photosynthetic phenotype is a consequence of an increased oxidative stress and/or insufficient capacity of anti-oxidant system which is unable to protect the photosynthetic apparatus against ROS produced in EL.

The characterization of *cry1-304* in this thesis highlights for the first time the contribution of CRY1 in sustaining photosynthesis also in non-stressful steady-state conditions. The photosynthetic imbalance in *cry1-304* was evident at the level of both PSII and PSI, revealing a lower NPQ capacity (**Figure 3.4** and **3.5**) and a strong limitation in the reactions downstream of PSI (**Figure 3.6**), which leads to slower oxidation of PSI at increasing light intensities (**Figure 3.7**). The observed phenotype was intensified under FL conditions, where both PSII and PSI displayed intense photoinhibition together with strongly decreased PSII electron transport capacity (**Figure 3.2** and **3.6**). Downregulation of PSI electron donors resulting in very limited electron transport at level of PSII to build up ΔpH it is likely the cause of the decreased qE component of NPQ in this mutant (**Figure 3.4**), as a similar phenotype was not observed under milder FL conditions (FL2) in which the treatment neither caused strong PSII photoinhibition nor downregulated the PSII electron transport (**Figure S1** and **S2**). A decreased capacity of build up ΔpH might also lead to a decreased ΔpH -dependent photosynthetic control, which might explain the more severe PSI photoinhibition in FL compared to FL2 (**Figure 3.6** and **S.2**). In line with PSI photoinhibition, a strong imbalance between donor and acceptor side of PSI was observed in FL-treated plants of *cry1-304* (**Figure 3.6**), together with a very low oxidizable fraction of P700 (**Figure 3.7**).

4.1.3 The role of CRY1 in regulation of photosynthesis in mature leaves does not involve crosstalk between CRY1 and PHYB via HY5/HYH light signaling pathway

Signals from multiple photoreceptors converge in the transcriptional regulation of light responsive genes via interaction and inhibition of the COP1/SPA1 complex in the nucleus and the activation of the TF HY5 (Holtkotte et al., 2017; Podolec and Ulm, 2018). Thus, the PSII photosynthetic responses of KO plants *phyB*, *cry1cry2* and *hy5hyh* exposed to FL and CL were measured and compared with the corresponding WT and *cry1-304* plants in order to clarify whether the EL tolerance mediated by CRY1 is CRY1-specific or it involves the concomitant action of multiple photoreceptors via the activation of the TFs HY5 and/or HYH (**Figures 3.2-3.4**).

After three days of FL exposure photosynthetic parameters of *phyB* and *hy5hyh* did not differ much from the corresponding WT under the same conditions. *cry1cry2* was only slightly impaired (**Figures 3.2-3.4**). Indeed, while *cry1cry2* was not photoinhibited (**Figure 3.2**), it showed slightly lower ETR (II) under CL compared to WT Col-0 (ca. 16.2 %). Still, it was able to perform ETR comparably to WT under FL. Also, FL plants of *cry1cry2* displayed significantly lower NPQ levels compared to WT under the same conditions and FL did not increase the NPQ capacity of *cry1cry2*. However, the NPQ phenotype was not as severe as the one observed in *cry1-304*. The lack of severe photosynthetic phenotype in *cry1cry2* might be due to mutation in a different allele of *CRY1* in *cry1cry2* plants, which might lead to slight phenotypic differences. Further investigations are needed to support allelic effects of *CRY1*.

Another hypothesis is that the absence of both CRY1 and CRY2 can somehow compensate in part for the negative effects of CRY1 deficiency on photosynthetic phenotype. Similar to the observations made in this study, *cry1cry2* was shown to be only slightly impaired under HL compared to WT, with lower levels of F_v/F_m but hardly any differences in NPQ and ETR (Brelsford et al., 2019). Together, these data suggest that the response observed in *cry1-304* is specific to CRY1 mutation.

4.2 Role of differential subcellular localization of CRY1 in photosynthetic acclimation to EL

The characterization of the KO mutant *cry1-304* described in the previous section (4.1) supports the hypothesis that CRY1 has a physiological role in sustaining photosynthesis under EL and its activity seems to play a role in proper functioning of photosynthesis under both non-stressful and stressful light conditions. The activity and therefore the physiological function of many plant photoreceptors is dependent on their subcellular localization, as it is well documented for PHYs and PHOTs (Kong et al., 2006; Fankhauser and Chen, 2008; Kong et al., 2013; Liscum, 2016). Native *A. thaliana* CRY1 lacks a localization signal and has been detected both in the nucleus and cytoplasm (Cashmore et al., 1999). Since regulation of gene expression is generally associated with nuclear localization and CRY1 is known to affect gene expression of a large number of light-regulated genes via its interaction with the E3 ubiquitin ligase system COP1/SPA1 in the nucleus (Wang et al., 2001; Yang et al., 2001; Liu et al., 2016; Podolec and Ulm, 2018), it is reasonable to assume that CRY1 exerts its function when it is in the nucleus. Thus, a mechanism of shuttling between these two compartments upon transition from dark to BL has been proposed (Ahmad et al., 1998; Yang et al., 2000; Lin and Shalitin, 2003). However, such relocation of CRY1 was observed in wheat (Xu et al., 2009) but not in rice (Matsumoto et al., 2003). The functions of two differentially localized pools of CRY1 are still unclear.

A study carried out by Wu and Spalding (2007) has demonstrated separate functions for nuclear and cytoplasmic CRY1 in controlling distinct processes related to photomorphogenesis in *Arabidopsis* seedlings. In this study they generated complementation lines by using the KO mutant *cry1-304* as background and overexpressing *GFP-CRY1* (*cry1_{control}*) under the control of strong 35S promoter. Also, they generated lines overexpressing *GFP-CRY1* with nuclear localization signal (NLS) or nuclear export signal (NES) to target CRY1 protein to the nucleus (*cry1_{NLS}*) or the cytoplasm (*cry1_{NES}*), respectively (Wu and Spalding, 2007). The *cry1_{control}* line offered us the opportunity to address the question as to whether the photosynthetic phenotype observed in *cry1-304* is due to the *CRY1* mutation (thus can be rescued by re-introduction of CRY1 in *cry1_{control}*) or due to unknown secondary effects presents in this line. Further, *cry1_{NLS}* and *cry1_{NES}* lines together with *cry1_{control}* will allow us to clarify whether the photosynthetic effects of CRY1 are brought by the nuclear CRY1 pool through gene expression regulation or by the cytoplasmic pool through unknown mechanisms, or by a combination of both.

However, the confocal microscopy experiment in seedling roots did not confirm the expected GFP localization and thus the likely presence of CRY1 in *cry1_{control}*: the GFP signal was detected mostly in the nucleus, while the signal of the cytoplasmic fraction was very weak (**Figure 3.11 A**). Since the cytoplasmic GFP-CRY1 pool is poorly represented in these lines, it is likely that these lines are not suitable to answer the first question. Similarly, the exclusive nuclear GFP signal, as reported by Wu and Spalding (2007), was not detected in *cry1_{NLS}*. Solely *cry1_{NES}* showed the exclusive localization of the GFP signal in the cytoplasm (**Figure 3.11 A**). Thus, the lines *cry1_{control}* (GFP mostly in the nucleus, weakly in the cytoplasm) and *cry1_{NES}* (GFP only in the cytoplasm) were used to investigate the nuclear and cytoplasmic functions of CRY1 in photosynthetic acclimation (**Figure 3.13**). The RT-qPCR analysis indicated a very low recovery of *CRY1* gene expression in *cry1_{control}* compared to *cry1-304* and WT Col-0, while it was overexpressed in *cry1_{NES}* (**Figure 3.11 B**).

Morphologically, *cry1_{control}* displayed a constitutive inhibition of growth (**Figure 3.13 A**) probably due to the stronger accumulation of CRY1 in the nucleus compared to the cytoplasm (Wu and Spalding, 2007). A similar dwarf phenotype with shorter cotyledon and leaf petioles, smaller rosettes, reduced leaf size, shorter inflorescence and reduced size in every organ was previously observed in other *A. thaliana* *CRY1* OE lines (Lin et al., 1996) which were also hypersensitive to BL, UV/A and green light for the inhibition of hypocotyl response. Also Tomato *CRY1a* OE lines displayed a dwarf phenotype (Liu et al., 2018). Interestingly, also the mutant lines lacking COP or SPA have been reported to show a similar constitutive photomorphogenic phenotypes with reduced cotyledon expansion, as observed in *cry1_{control}* (Ranjan et al., 2014; Sreeramaiah Gangappa and Vinod Kumar Correspondence, 2018). This is in line with the CRY1-dependent inactivation of the COP/SPA complex in the nucleus, which presumably happens at a higher rate in *cry1_{control}*, in which the GFP signal attached to CRY1 was detected mostly in the nucleus. Interestingly *A. thaliana* overexpression lines of PHYA and/or PHYB lead to a peculiar short hypocotyl phenotype compared to WT (Boylan and Quail, 1991; Wagner et al., 1991). Plants overexpressing UVR8 showed several growth defects likely due to inhibition of cell expansion, displaying a dwarf phenotype together with a reduced root development and a stronger accumulation of flavonoids compared to control plants (Fasano et al., 2014).

The growth of *cry1_{control}* seemed to be impaired during the EL treatments. In contrast to *cry1-304*, HL plants of *cry1_{control}* recovered the ability to accumulate anthocyanin, confirming the role of CRY1 in regulating the gene expression of anthocyanin biosynthesis (Lin et al., 1996; Shin et al., 2007; Wu and Spalding, 2007; Shin et al., 2013; Gangappa and Botto, 2016). On the other hand, *cry1_{NES}* had a WT-like morphology in CL and under both HL and FL it showed a complete rescue of the growth phenotype observed in *cry1-304* together with the recovery of anthocyanin accumulation under HL (**Figure 3.13 A**). Also, FL plants of *cry1_{NES}* were rescued from PSII photoinhibition and displayed a normal ability to induce NPQ similarly to WT Col-0 (**Figure 3.13 B**). These results suggest that the cytoplasmic CRY1 pool might be involved in photosynthetic acclimation to EL. In contrast, FL plants of *cry1_{control}* displayed a photosynthetic phenotype very similar to *cry1-304*, presenting PSII photoinhibition and low NPQ capacity, which might indicate that the mostly nuclear pool of CRY1 in this line is not enough to rescue the photosynthetic impairment observed in *cry1-304*. However, it is also possible that the photosynthetic phenotype of *cry1_{control}* (**Figure 3.13 B**) is a consequence of the constitutive inhibition in growth (**Figure 3.13 A**) and/or the overall lower expression of *CRY1* (**Figure 3.11 B**) compared to WT Col-0 and *cry1_{NES}*. It is difficult to connect altered photosynthetic phenotypes in mutants displaying defective growth, as the reasons for the diminished photosynthetic performances can be due to genetic differences in addition to the growth alterations. Similarly to *A. thaliana*, tomato *cry1a* KO mutants are relatively tall and in addition they accumulate low biomass, and bear more fruits, whereas *OE-CRY1a* plants displayed a dwarf phenotype and bear less fruits (Liu et al., 2018). In addition, due to the short stature of *OE-CRY1a* an enhancement in photosynthetic rate lead to an improved leaf biomass (Liu et al., 2018). Similar dwarf phenotypes were also observed when *CRY1* was overexpressed in other species, such as *Oryza sativa* (Zhang et al., 2006), *Brassica napus* (Chatterjee et al., 2006; Sharma et al., 2014) and *Artemisia annua* (Hong et al., 2009).

While Wu and Spalding (2007) attributed the BL-dependent inhibition of hypocotyl elongation to the nuclear fraction of CRY1, which presumably is absent in *cry1_{NES}*, the BL inhibition of hypocotyl elongation in *cry1_{NES}* plants was not completely suppressed as observed in *cry1-304*, but it was somehow between WT Col-0 and *cry1-304* (**Figure 3.12**).

To sum up, *cry1_{NES}* displayed complete rescue of growth, photosynthesis and anthocyanin accumulation and partial rescue of hypocotyl elongation compared to *cry1-304*, whereas *cry1_{control}* exhibited strong growth inhibition (both in rosette and hypocotyl) and recovery of anthocyanin accumulation but no rescue of photosynthetic phenotype. These results may imply a primary function of the nuclear and cytoplasmic CRY1 pool in regulating leaf expansion and photosynthetic phenotype, respectively. It should be noted, however, that these experiments were lacking important control plants to make an unequivocal conclusion about the localization-dependent functions of CRY1. In order to answer these questions, we need to compare the phenotypes of *cry1_{NES}* with those plants in which CRY1 is localized in both cell compartments or exclusively in the nucleus. Further, it is critical that CRY1 is expressed at similar levels in all lines to evaluate the localization-dependent effects, not the dosis-dependent effects. Also, while the GFP fusion allowed us to infer CRY1 protein localization (**Figure 3.11 A**), it may affect the CRY1 activity.

Thus, by using an approach similar to the one described by Wu and Spalding (2007), additional *CRY1* OE lines were generated by overexpressing *CRY1* gene but without GFP (**Figures 3.14-3.16, Table 3.4**) in order to study the localization-dependent effects of CRY1 on photosynthesis. With the aim to investigate the interaction partners of the differentially localized pools of CRY1, attempts were also made to generate similar lines carrying a Gs-TAP instead GFP. However, positive transformants were isolated only for 35S_GsTAP_NES_CRY1 (**Figure 3.17, Table 3.4**). All the positive lines, which were selected for phenotypic characterization, had higher levels of *CRY1* gene expression than WT Col-0 (**Figure 3.18**).

Contrarily to what was described by Wu and Spalding (2007), the photomorphogenic phenotype of *cry1-304* could not be rescued in any of the transgenic plants studied (**Figure 3.19**); all lines displayed elongated hypocotyls under LL, as observed in *cry1-304*. As CRY1 is known to modulate BL-dependent anthocyanin accumulation (Lin et al., 1996; Shin et al., 2007; Wu and Spalding, 2007; Shin et al., 2013; Gangappa and Botto, 2016) and *cry1-304* does not accumulate anthocyanin after exposure to prolonged HL treatments (**Figure 3.1**), morphological differences and anthocyanin accumulation were assessed during exposure to EL (FL2 and HL2) treatments. The same morphological phenotype as *cry1-304* was observed in the different transgenic lines, which displayed bleaching under HL2 together with little anthocyanin accumulation in the interveinal regions of leaf lamina (**Figure 3.20 A and B**).

In the experiments performed by Wu and Spalding (2007), not only the *cry1_{control}*, but also *cry1_{NLS}* were shown to accumulate leaf anthocyanin to the levels which were even higher than in WT Col-0, while the levels in *cry1_{NES}* were comparable with WT Col-0 (Wu and Spalding, 2007).

Similarly to *cry1-304*, growth of the HL2-treated transgenic lines was impaired compared to WT Col-0, especially during the first four days of treatment, while it partially recovered between day 5 and 7 (**Figure 3.21**). When photosynthetic phenotype was evaluated in the *CRY1* OE lines, the maximum PSII efficiency showed no rescue of the *cry1-304* phenotype in *CRY1* OE lines both under FL2 and HL2, as indicated by the lower values of F_v/F_m (**Figures 3.24 A** and **3.25 A**), $Y(II)$ (**Figures 3.22** and **S4**) and $ETR(II)$ (**Figures 3.24 B**, **3.25 B**, **S3** and **S5**) compared to WT. These parameters suggest increased PSII photoinhibition and a poor electron transport capacity, as reported in the previous section for *cry1-304* under similar but slightly different EL conditions. Also, NPQ was not recovered in the *CRY1* gene OE lines. The NPQ values of the transgenic lines were significantly lower than that of WT Col-0 in all the treatments applied, being mostly similar to the *cry1-304* phenotype (**Figures 3.23**, **3.24 C**, **S6** and **3.25 C**). Together, these fluorescence data indicate a failure in rescuing the photosynthetic phenotype of *cry1-304* in the *CRY1* OE lines.

Notably, unlike FL and HL conditions used in the previous section (**Figures 3.3**, **3.4** and **3.5**), both FL2 and HL2 did not cause downregulation of NPQ in *cry1-304*. All the *CRY1* OE plants as well as *cry1-304* were able to upregulate NPQ compared to CL conditions, even though their NPQ levels were still lower than in WT (**Figures 3.23**, **3.24 C**, **S6** and **3.25 C**). It is likely that the NPQ deficiency of *cry1-304* is a consequence of the electron transport impairment and not the direct effect of *CRY1* on the expression or accumulation of NPQ components. WT plants did not seem to show this doses effect of EL, suggesting that the severity of the phenotype observed in *cry1-304* is proportional to the EL experienced by the plants. Accordingly, subtle changes in light conditions can affect the expression of photosynthetic phenotypes in *cry1-304*.

Overall, the severe phenotype observed in *cry1-304* was not rescued in any of the *CRY1* gene overexpression lines newly generated, regardless of the localization signal, the light treatment applied and the parameters evaluated in this study. A possible explanation is the failure of *CRY1* protein expression in these lines. At least the expression of *CRY1* gene was higher in all the lines used for the phenotypic characterization compared to WT Col-0 (**Figure 3.18**).

Unfortunately, the only commercially available anti-CRY1 antibody did not have the sensitivity and specificity that are high enough to specifically detect and discriminate between CRY1 and CRY2. Hence, it was not possible to verify CRY1 protein accumulation in the *CRY1* gene overexpression lines. However, in the case of *35S_GsTAP_NES_CRY1*, accumulation of protein G fused to CRY1 could be confirmed in several lines, in which also *CRY1* gene was highly expressed (**Figure 3.17 C**). A band of molecular weight corresponding to the size of protein G plus the expected CRY1 protein size was detected in the selected *35S_GsTAP_NES_CRY1* lines and it was absent in the negative control *cry1-304* (**Figure 3.17 C**), suggesting that CRY1 proteins linked to protein G were expressed and accumulating in these transgenic lines. As the vector construct of *35S_GsTAP_NES_CRY1* was designed in the same way as those of *35S_NES_CRY1*, *35S_CRY1* and *35S-NLS_CRY1* except for the absence of the GsTAP and the presence or absence of the localization signal (NLS or NES), the overexpression of *CRY1* gene most likely led to CRY1 protein accumulation also in the lines without GsTAP.

Another possibility could be that the *cry1-304* phenotype is not entirely caused by the absence of the photoreceptor CRY1, but it might be a consequence of combination of unknown additional mutations. However, previous studies have reported the rescue of photomorphogenic and anthocyanin phenotypes of *cry1KO* mutants by *CRY1 OE* in *A. thaliana* (Wu and Spalding, 2007), as well as an increased accumulation of anthocyanin in WT overexpressing *CRY1* (Lin et al., 1996). Similar phenotypes were also observed when *CRY1* was overexpressed in other species, such as *Oryza sativa* (Zhang et al., 2006), *Brassica napus* (Chatterjee et al., 2006; Sharma et al., 2014) and *Artemisia annua* (Hong et al., 2009). Thus, at least these phenotypes must be rescued in some of the *CRY1* gene overexpression lines, regardless of the presence or absence of additional unknown mutations, if the expressed CRY1 protein was functional and active. None of the overexpression lines of this study exhibited rescue of these phenotypes.

A third explanation, which could possibly explain the lack of phenotypic changes in the *CRY1* gene over expression lines, is point mutation in the *CRY1* gene sequence. If point mutation was introduced during generation of the transgenic lines, this might have caused misfolding or inactivation of the CRY1 protein. Depending on the position of mutation, it might interfere, for example, with the key function of CRY1, such as the light-triggered phosphorylation, dimerization, and interaction with other proteins or protein complexes like COP/SPA, all of which are necessary for proper functioning of this photoreceptor.

For example, mutations which inactivate the N-terminal PHR domain would lead to inability of light perception and dimerization, while mutations that inactivate the C-terminal CCE domain would interfere with BL-dependent phosphorylation events which take place at multiple sites along the CCE domain (Shalitin et al., 2002; Shalitin et al., 2003; Tan et al., 2013; Liu et al., 2016). It is therefore important to check the genomic sequence of the transgenic lines to verify the absence of point mutation. Also, CRY1 protein levels need to be evaluated in the overexpression lines. Furthermore, sequencing of the entire genome of *cry1-304* mutant seems necessary to exclude possible effects of any secondary unknown mutations and ensure that the observed phenotype of this mutant is caused only by the absence of CRY1. Characterization of additional CRY1 loss-of-function mutants, such as *cry1-1* (CS9854) in the background of Landsberg *erecta* (WT *Ler-0*), could also validate the *cry1-304* phenotype and provide more robust collective evidence of CRY1 function in photosynthetic acclimation to EL.

4.3 Functional characterization of an unknown gene which was upregulated under FL (*AT3G56290*)

The unknown gene *AT3G56290* was selected as promising candidate to study acclimation to photooxidative stress induced by EL as it was found upregulated in the nuclear transcriptome of FL-treated young and mature leaves of *A. thaliana* in the morning and at the end of day compared to the corresponding leaves and time points in CL (Schneider et al., 2019). Also, it was identified in a screening study of genes that contribute to the integration of light and plastid signaling in Arabidopsis; the gene *AT3G56290* had the second highest light-induced upregulation in seedlings treated with lincomycin, a light-independent suppressor of chloroplast biogenesis that inhibits plastid translation (Ruckle et al., 2012). Indeed, genes, which were upregulated by light in lincomycin-treated seedlings compared to untreated seedlings, are good candidates which might contribute to chloroplast-to-nucleus retrograde signaling. In addition, *AT3G56290* is conserved in the most lineages of land plants, including moss and club mosses, but also in algae and cyanobacteria even though the sequences are more divergent (**Figure 3.26, Table 3.5**).

AT3G56290 has also been shown to be regulated in WT Col-0 under UV-B light, suggesting that its expression might be modulated by the photoreceptor UVR8, which also regulates gene expression of the transcription factor HY5 together with cryptochromes and phytochromes (Brown et al., 2005).

According to databases, such as TAIR, ARAPORT and ensembled, AT3G56290 has been recently annotated as potassium antiporter, albeit without any reference and substantial information supporting this function. The size of the coding sequence of genes belonging to known potassium transporter families in *A. thaliana* (e.g. KT, TRH, HAK, KAT, KUP, KEA, GORK and SPIK) is much larger than the size of AT3G56290, suggesting that the gene AT3G56290 is unlikely to act as a potassium transporter.

In line with the prediction of the localization of AT3G56290 in chloroplast and/or mitochondria, *in silico* protein association network revealed that AT3G56290 is co-expressed with genes related to these compartments necessary for maintaining the chloroplast structure and function, as well as involved in light and chloroplast-to-nucleus retrograde signaling (**Figure 3.27, Tables 3.6 and 3.7**).

Among them, AT1G64500, named THRUMIN1 has been described as an important link between PHOTs activity at the plasma membrane involved in the light- and PHOT-dependent chloroplast movements along actin filament (Whippo et al., 2011), which are known to be an important mechanism of photoprotection to prevent EL absorption. In *A. thaliana* SPS1 (AT1G78510) and SPS2 (AT1G17050) are two solanesyl diphosphate synthases involved in the synthesis of the isoprenoid side chain of either plastoquinone, which are essential constituents of photosynthetic and respiratory electron transport chains in chloroplasts and mitochondria, respectively (Lange and Ghassemian, 2003; Jun et al., 2004). While SPS1 is localized in the chloroplast, SPS2 has been reported to be localized in the endoplasmic reticulum (ER) (Jun et al., 2004), but a localization in the chloroplast has been postulated (Block et al., 2013). It has been reported that both *sps1* and *sps2* single KO display lower levels of plastoquinone-9 compared to WT. *sps1sps2* double KO has almost abolished accumulation of plastoquinone-9 and is unable to grow photoautotrophically (Block et al., 2013). Interestingly, the *sps2* KO displays a severe growth phenotype when grown under 500 $\mu\text{mol photons m}^{-2} \text{s}^{-1}$ together with severe photoinhibition and decreased NPQ after 2, 24 and 48 hours of exposure to 800 $\mu\text{mol photons m}^{-2} \text{s}^{-1}$ (Block et al., 2013).

STH (AT2G31380) is a BBX protein which is known to interact with HY5 and regulate plant growth and development (Gangappa et al., 2013a; Job et al., 2018). FADA (AT4G27030) is a membrane-bound fatty acid desaturases targeted to the plastid and involved in the synthesis of a chloroplasts-specific type of phosphatidylglycerol (Gao et al., 2009). AT4G36530 and AT5G19850 are homologous to chlorophyll dephytylase 1 (CLD1), a chlorophyllase which has been shown to be involved in Chl turnover in *A. thaliana* (Lin et al., 2016). SIGE (AT5G24120), also known as SIG5, is a nuclear-encoded SIG necessary for the transcription of plastid-encoded genes by PEP RNA polymerase. In particular, SIG5 is involved in the transcription of the PSII RC protein D2 encoded by the gene *PSBD* (Onda et al., 2008). It has been proposed that SIG5 integrates the plastid light-responsive transcription through photoreceptors PHYs and CRYs (Onda et al., 2008; Belbin et al., 2017). DCC1 (AT5G50100) is a mitochondrial thioredoxin which interacts directly with γ CARBONIC ANHYDRASE-2 (γ CA2), which is part of a plant-specific complex essential for the stability of the respiratory chain NADH dehydrogenase complex (Complex I). DCC1 has been shown to regulate the Complex I activity via redox modification of γ CA2 protein and mutation of DCC1 or γ CA2 led to reduced Complex I activity and triggered mitochondrial ROS production, resulting in altered shoot regeneration (Zhang et al., 2018).

Interestingly, in young plants of *A. thaliana* it has been shown that the absence of the respiratory Complex I causes profound changes at the level of both mitochondria and chloroplast, leading to a reorganization of the respiratory chain and photosynthetic machinery together with ROS and stress-related responses. In particular, it has been reported that the lack of Complex I due to the absence of mitochondrial CAs leads to defects in accumulation of the major photosynthetic proteins involved in light reactions (including component of PSII, PSI, ATPase) as well as CBB cycle enzymes, photorespiration, and tetrapyrrole biosynthesis. At the same time the respiratory metabolism increases together with stress- and ROS-related proteins (Fromm et al., 2016). These studies suggest a strong interaction and crosstalk between chloroplasts and mitochondria. Interestingly, the functional association between DCC1 and SPS1 and SPS2 has been experimentally proven (**Figure 3.27B**), indicating further a strict interconnection between ER, chloroplast and mitochondria. AT5G64840, also known as, ABCF5 or GCN5, is a histone acetyl transferase which has been reported to directly associate with the promoters of important light-responsive genes such as RBCS, CAB2 and CHS, promoting their gene expression (Benhamed et al., 2006).

In the predicted functional association network GCN5 is shown to be functionally associated with SIGE (**Figure 3.27B**), in line with the transcriptional regulation of light responsive genes. Although co-expression networks do not necessarily describe physical associations, they offer a general overview of the context in which they are co-regulated, and might suggest functional associations (e.g. proteins that contribute to a shared function). In general, it appears that the genes co-expressed with AT3G56290 are mostly involved in chloroplast lipid and isoprenoid metabolism (SPS1, SPS2 and FADA) and transcriptional regulation of photosynthetic genes (STH, SIGE, ABCF5) (**Table 3.7**). The analysis also points to a possible functional role of AT3G56290 in organelle crosstalk (ER, mitochondria and chloroplast) and chloroplast-to-nucleus retrograde signaling.

Targeted KO plants of AT3G56290 were successfully generated by using the CRISPR/Cas9 (**Figures 3.28-3.34**). Both the positive lines *PMP5* #1.1.4.1 and #1.1.10.3 displayed single nucleotide insertion (adenine A in #1.1.10.3 and cytosine C in #1.1.4.1) 3 bp in front of the PAM motif (**Figure 3.33 A**). While the mutation did not change the expression of the gene AT3G56290 (**Figure 3.35**), point mutation involving 1-bp insertion or deletion has been reported as one of the common mutations caused by CRISPR/Cas9-mediated NHEJ, which can potentially cause frame shift of the reading frame (Feng et al., 2014; Hahn et al., 2017b; Yamaguchi et al., 2017; Hahn et al., 2018b). Indeed, this single nucleotide insertion results in a frame shift generating nine premature STOP codons, leading to truncated proteins which most likely fail to accumulate or to fulfill its function (**Figure 3.34**). Because of non-availability of a commercial antibody against AT3G56290 protein, the lack of AT3G56290 protein accumulation could not be confirmed in these lines. The analysis of AT3G56290 protein levels should be performed in the future.

Since *AT3G56290* was found upregulated in leaves after three days of exposure to FL conditions (Schneider et al., 2019) and it is co-expressed with other genes that are associated with thylakoid lipid metabolism and PSII functioning (**Table 3.6**), the photosynthetic phenotype of *PMP5* #1.1.4.1 and #1.1.10.3 was analyzed in plants exposed to FL2 and HL2 and compared with CL and WT Col-0 under the same conditions. However, the *PMP5* lines showed evident changes neither in morphology and development (**Figure 3.36**) nor in photosynthetic induction of electron transport and NPQ compared to WT Col-0 under the experimental conditions used in this study (**Figures 3.37-3.40**).

Both *PMP5* lines were able to induce normal levels of electron transport and upregulate NPQ after one day of HL2 exposure and after three days of FL2 and HL2 exposure (**Figures 3.37-3.40**).

In the future, the absence of an active protein of AT3G56290 should be confirmed by protein levels to ensure that AT3G56290 protein does not accumulate in the KO produced. Also, as AT3G56290 has also been shown to be upregulated under UV-B light and it has been suggested to be regulated by UVR8 (Brown et al., 2005), exposure to UV-B light and other environmental conditions might reveal its function. Also, it would be interesting to evaluate the expression levels and/or the protein levels of the genes which appeared to be co-expressed with AT3G56290 (**Figure 3.27, Tables 3.6 and 3.7**) in *PMP5* plants exposed to different environmental conditions. Such experiments could also validate the co-expression network predicted by the database analysis. In case some of them show concomitant downregulation in *PMP5* plants, generation of mutants lacking and or overexpressing those genes that present an altered gene expression together with *AT3G56290* might provide further insight about the role of this gene together with other candidate targets and their functional connection. Depending on the preliminary results on the phenotype observed in these mutants, other experiments will be useful to provide further insights. For example, since the functional connection with SPS1, SPS2 and FADA, chloroplast lipid and isoprenoid metabolism should be evaluated in these mutants, together with the expression levels of photosynthetic genes, whose transcription is regulated through STH, SIGE, ABCF5 accordingly with the co-expression network. Also, since the functional connection with DCC1 the mitochondrial respiratory chain integrity might be compromised in these mutants, together with photosynthetic function as results of impaired chloroplast-mitochondria cross-talk.

5. CONCLUDING REMARKS AND FUTURE PERSPECTIVES

The analysis of *cry1-304* performed in this thesis provide original findings supporting a specific contribution of CRY1 in sustaining photosynthesis in terms of electron transport and photoprotection. In addition, the data provide evidence that CRY1 plays an essential role not only under HL, as previously shown (Kleine et al., 2007), but also under LL conditions in which plants are not exposed to photoinhibitory environmental stress, and under dynamic FL. This role is specific to CRY1 and cannot be substituted by other photoreceptors such as PHYB through HY5- or HYH-dependent light signaling pathways. The photosynthetic imbalance in *cry1-304* plants affects both photosystems, as reflected by lower electron transport capacity and NPQ at level of PSII and a strong limitation in the reactions at the PSI acceptor side, which leads to slower oxidation of PSI at increasing light intensities. FL condition induces strong photoinhibition of both PSII and PSI in *cry1-304* plants, together with huge reduction of the PSII electron transport capacity and consequent limitation at the PSI electron donor side. The limited electron transport at level of PSII was likely not enough to build up ΔpH , which can explain the decreased qE component of NPQ in *cry1-304* plants. In line with PSI photoinhibition, a strong imbalance between donor and acceptor side of PSI was observed in FL-treated plants of *cry1-304*, together with a very low oxidizable fraction of P700.

One of the most novel finding of this work was related to the PSI imbalance observed in both CL and FL-treated plants of *cry1-304* and the PSI photoinhibition observed under FL. Further studies are needed to clarify whether the observed photosynthetic phenotype in *cry1-304* it is due to defective pmf formation, which can be the cause of the reduced NPQ and PSI photoinhibition. Comparison of *cry1-304* with *pgr5* as model of PSI photoinhibition under FL conditions might provide insights about the functioning of these processes. Also, comparison of *cry1-304* with PGR5 and NDH loss of function mutants, with or without antimycin, which is known to inhibit PGR5-dependent CET (Kono et al., 2014; Kou et al., 2015) will be useful in order to evaluate CET in these plants. Further experiments including a recovery period from FL are required to investigate the repair and the recovery of *cry1-304* mutants from photoinhibition of both photosystems.

Complementation of *cry1-304* is necessary to prove that the observed phenotype is related solely to the *CRY1* mutation and not to secondary unknown mutations. The use of the *CRY1* endogenous promoter it would be a better alternative compared to strong promoter such as 35S. Also, sequencing the entire genome of *cry1-304* would help identify exactly the position(s) of the mutation(s), including the presence of additional unknown genetic defects that have not been reported so far. Furthermore, despite the detailed phenotype described in this work, we are not able yet to pinpoint specific targets or factors responsible for the observed phenotype. As *CRY1* is a very upstream factor in the light signaling pathways, its photosynthetic phenotype most likely involves a combination of multiple components that are mis-regulated in *cry1-304* mutant. In the future, a forward genetic approach, such as EMS mutagenesis, would represent an excellent tool to identify the suppressor(s) of the severe phenotype observed in *cry1-304* and provide more detailed insights about the mechanisms by which it sustains photosynthesis. To identify and characterize these *CRY1*-controlled photosynthetic components (*sensu lato*) represent a next goal to understand light and plastid signaling networks, as well as the role of this UV-A and BL photoreceptor in photosynthetic and photoprotective acclimation. More investigations are needed to understand how the light-dependent signaling networks, controlled by *CRY1*, and redox signals coming from the chloroplast, are integrated during the process of long-term photosynthetic acclimation.

Another goal of this study was also to clarify whether the photosynthetic effects of *CRY1* are exerted by the nuclear *CRY1* pool through transcriptional regulation, by the cytoplasmic pool through unknown mechanisms, or by a combination of both. Unfortunately, neither the already existing lines (Wu and Spalding, 2007) nor the new lines generated in this thesis provided clear proofs of *CRY1* localization-dependent functions. Further efforts are needed to clarify these points as well as the interaction partners of *CRY1* in these two different cell compartments.

The *in silico* characterization of the gene *AT3G56290* performed in this work represents an important first step in discovering new factors involved in acclimation to photo-oxidative stress induced by EL. In line with the prediction of the localization of *AT3G56290* in chloroplast and/or mitochondria, *in silico* association network revealed that *AT3G56290* is co-expressed with genes coding for proteins involved in chloroplast lipid and isoprenoid metabolism and transcriptional regulation of photosynthetic genes. From this analysis a possible role of *AT3G56290* in organelle crosstalk (ER, mitochondria and chloroplasts) and chloroplast-to-nucleus retrograde signaling can also be speculated. Targeted KO plants of *AT3G56290* were successfully generated in this work to study the function of this gene *in vivo*.

The preliminary phenotyping of these lines under EL conditions did not provide any indication of an essential role of *AT3G56290* in photosynthetic acclimation. Further investigations with measurements of additional parameters under different environmental conditions may uncover hidden phenotypes of the KO plants.

6. EXPERIMENTAL PROCEDURES

6.1 Plant material

Arabidopsis thaliana mutants *cry1-304* (Bruggemann et al., 1996), *cry1_{control}*, *cry1_{NLS}*, *cry1_{NES}*, (Wu and Spalding, 2007), *cry1cry2* (Mockler, 1999), and *phyB* (Reed et al., 1993) were all in wild type Columbia-0 (WT Col-0, CS76778) background and *hy5hyh* (Holm et al., 2002b) was in wild type Wassilewskija (WT Ws, CS28823). The transgenic CRY1 lines generated in this work (35S_CRY, 35S_NLS-CRY, and 35S_NES-CRY1) were all in *cry1-304* background. The PMP5 lines were all in WT Col-0 background. The transgenic lines *cry1-304*, *cry1_{control}*, *cry1_{NLS}* and *cry1_{NES}* were provided by Edgar Spalding (University of Wisconsin-Madison), *cry1cry2* was provided by Alfred Batschauer (University of Marburg), *phyB* was provided by Ute Höcker (University of Cologne) and *hy5hyh* and WT Ws by Eva Farrè (Michigan state university).

6.2 Growth conditions

Seeds were sown on moist soil (type Pikier; Balster Einheitserdewerk; Fröndenberg, Germany) in germination trays and stratified at 4°C in the dark for three days before transferring to the climate chamber. The growth conditions in the climate chamber were 12 h/12 h light/dark with ca. 75 $\mu\text{mol photons m}^{-2} \text{s}^{-1}$ (Fluora L36 W/77; Osram, Munich, Germany), 23°C/18°C and 60% relative humidity. After two weeks, seedlings were transferred to pots (7 x 7 x 8 cm) filled with soil (type *Dachstaudensubstrat*, HAWITA GRUPPE GmbH) and grown in these conditions. For some experiments and selection of transgenic lines, plants were also grown in Murashige and Skoog (MS) agar plant medium (Murashige and Skoog, 1962) with or without the indicated antibiotic.

6.2.1 Light conditions and treatments

Plants were grown until they reached a leaf area of 2 or 8-10 cm^2 (i.e., ca. 3- or 5-week-old) and then divided into homogeneous groups and exposed to the following light conditions: one group was kept in Constant Light (CL = the growth light condition as described above) while the second group was transferred to Fluctuating Light (FL) condition in which the intensity of LED lamps (HelioSpectra A4, LED grows light) was switching between ca. 75 (570 s) and 1000 $\mu\text{mol photons m}^{-2} \text{s}^{-1}$ (30 s) during the light period.

FL2-treated plants were exposed to 15-s pulses of ca. 1000 $\mu\text{mol photons m}^{-2} \text{s}^{-1}$ applied by LED lamps (IP65, as-Schwabe, Eutingen, Germany) moving over the plants every 5 min under the CL condition during the light period as described previously (Schneider et al., 2019). The HL conditions were and 1000 $\mu\text{mol photons m}^{-2} \text{s}^{-1}$ during the light period, provided by LED lamps (HelioSpectra A4, LED grows light). In HL2 light was provided by white LED lamps (SL 3500-W-G, Photon Systems Instruments, Drasov, Czech Republic). The light intensity was 1000 $\mu\text{mol photons m}^{-2} \text{s}^{-1}$ in the central space of the HL conditions, while it was ca. 600-800 $\mu\text{mol photons m}^{-2} \text{s}^{-1}$ for the plants located in the margins. To avoid positional effects, the positions of plants belonging to different genotypes were randomized and rotated daily.

6.3 Growth analysis

Growth analysis was started in ca. 3-week-old plants while all the other analyses reported in this work (Chl fluorescence, P700, pigments, proteins and gene expression measurements) were performed in 5-week-old plants after three days of exposure to the different light conditions described above. Leaf growth was monitored by measuring the projected area of whole rosette by using the GROWSCREEN-FLUORO method (Jansen et al. 2009). Measurements were performed when leaves were in almost horizontal positions, i.e. 4 h after the light was switched on in the climate chamber.

6.4 Chlorophyll fluorescence and P700 measurements

Induction curves were analyzed by measuring Chl fluorescence with an Imaging-PAM MAXI (Heinz Walz, Effeltrich, Germany) while rapid light response curves were analyzed with a Dual PAM-100 (Walz) to probe Chl fluorescence and P700⁺ absorption in parallel. Both induction and light response curves were measured in the 3rd and 4th true leaves of overnight dark-adapted plants. For the induction curves, area of interest was selected and the first saturation pulse was applied in the dark to measure the maximal PSII efficiency (F_v/F_m). After 40 s, blue actinic light (AL) of ca. 550 $\mu\text{mol photons m}^{-2} \text{s}^{-1}$ was applied for 260 s followed by 60 s of dark relaxation. During the entire duration of the measurements, SPs were applied every 20 s. For the rapid light response curves, leaves were pre-illuminated with far red light prior to determination of F_v/F_m and P_m . Then, red AL was applied and the intensity was gradually increased from 0 to 830 $\mu\text{mol photons m}^{-2} \text{s}^{-1}$ with a dwell time of 90 s.

SPs were applied at the end of each light intensity to obtain the following PSII and PSI parameters: $F_v/F_m = (F_m - F_0)/F_m$, $Y(II) = (F_m' - F)/F_m'$; $ETR(II) = PAR \times 0.84 \times 0.5 \times (F_m' - F)/F_m'$; NPQ, $(F_m - F_m')/F_m'$; $Y(I) = 1 - Y(ND) - Y(NA)$; $Y(NA) = (P_m - P_m')/P_m$; $Y(ND) = (1 - P700 \text{ red})$. PAR, photosynthetically active radiation (in $\mu\text{mol photons m}^{-2} \text{s}^{-1}$).

6.5 Pigment Analysis

Pigment composition was analyzed in the 3rd and 4th leaves taken at the end of overnight dark adaptation (dark-adapted) and after exposure to 260-s AL (ca. 550 $\mu\text{mol photons m}^{-2} \text{s}^{-1}$) followed by 60 s of dark as described for the MAXI-PAM measurements. Samples were immediately frozen in liquid nitrogen and stored at -80°C until extraction. Pigment extraction and separation by HPLC was performed by Anh Binh (IBG-2, FZJ).

6.6 qRT-PCR analysis

For qRT-PCR analysis the 3rd and 4th leaves were taken after 2-h exposure to the light conditions and immediately frozen in liquid nitrogen. Total RNA was extracted by using QIAGEN RNeasy Plant Mini Kit (ID: 74904) together with DNaseI treatment (QIAGEN RNase-Free DNase Set, ID: 79254) to eliminate genomic DNA. 1 μg of total RNA was retrotranscribed to cDNA using iScript cDNA synthesis kit (BIORAD # 1708890) and diluted 1:10 with RNase free H₂O. When possible, primers were designed to span between two exons near 3'-UTR. Sequences of the primers are shown in Table S1. The qRT-PCR reactions were performed in iCycler (BIO-RAD) with iQ SYBR Green Supermix (BIORAD #1708880) following manufacturer's instructions. *RCE1* (*RUB1 CONJUGATING ENZYME 1*) (AT4G36800) was used as reference gene to normalize the transcript abundance of target genes.

6.7 SDS-PAGE and western blotting

After 4-h exposure to the light conditions the 3rd and 4th leaves were collected and immediately frozen in liquid nitrogen. Total leaf proteins were extracted by grinding the frozen leaf material in an extraction buffer containing 50 mM Tris-HCl (pH 7,6), 7 M Urea and 5% SDS. The extracts were centrifuged for 15 min at 4°C and 16000 rcf and the supernatant was used for the subsequent analysis. Pigments were extracted by adding 10 μL of the total protein extract to 900 μL of 80% aqueous acetone buffered with decahydrate Na₂CO₃. Following centrifugation at 4°C and 16000 rcf for 15 min, the total Chl content was quantified as follows: $\text{Chl } a + \text{Chl } b (\mu\text{g mL}^{-1}) = 17.76 \times A_{646,6} + 7.34 A_{663,6}$ (Porra, 2002).

Protein samples containing equal amounts of Chl were prepared by mixing 9 part of 4X Laemmli sample buffer (BIORAD #1610747) and 1 part of beta-mercaptoethanol (ROTH, #4227.1). Samples were then incubated at 70 °C for 10 minutes and separated at room temperature by SDS-PAGE at 60-110 V in 12% Tris-glycine gels in inner chamber running buffer (0.25mM Tris Base, 2 mM Glycine, 0.1% SDS pH 8.3) and outer chamber running buffer (0.25mM Tris Base, 2 mM Glycine, pH 8.3). Proteins were transferred onto nitrocellulose membrane (0.45 µm pore-size; BIORAD #1620145) and stained with ponceau red staining solution (3% acetic acid, 0.2 % Ponceau red) for ca. 3 min, followed by washing with ddH₂O. Blots were incubated for 1 h at room temperature in blocking solution containing 5% low fat milk powder in TBS-T buffer (0.2 mM Tris Base, 1.5 mM NaCl, 0.05% Tween-20, pH 7.2-7.4). Overnight incubation with specific primary antibodies (anti-D1, anti-LHCB1, anti-PSBS, anti-PSAA, anti-ATPC, anti-RBCL; all from Agrisera, catalog numbers #AS05084, #AS09522, #AS09533, # AS06172, # AS08312, # AS03037) was performed in the blocking solution at room temperature under constant agitation following manufacturer's recommendation. Blots were then incubated one hour at room temperature with the secondary antibody (anti-Rabbit IgG; Sigma-Aldrich # A3687) in the blocking solution and the target proteins were detected by alkaline phosphatase reaction using the developing solution [15 mL Alkaline Phosphatase Buffer (100mM Tris Base, 100mM NaCl, 5mM MgCl₂, pH 9.5), 100 µL NBT stock solution (5% NBT in 70% dimethylformamide, DMF), 50µL BCIP stock solution (5% BCIP in 70% DMF)]. The reaction was stopped by adding 15 mL of ddH₂O with 1% HCl. After short air drying, images of the membranes were acquired by using gel doc camera (BIORAD). The protein levels were quantified by using the software Image Studio™ Lite (Li-Cor).

6.8 Statistical tests

Statistical tests were performed by using the software GraphPad prism8 (<https://www.graphpad.com/scientific-software/prism/>). Significant differences between the genotypes as well as between the light conditions and the interaction (e.g genotype X light condition) were assessed by two-way or three-way ANOVA followed by Tukey's multiple comparison test and/or unpaired independent Student t-test.

6.9 Subcellular localization of CRY1-GFP

Subcellular localization of chimeric CRY1-GFP proteins was observed in root tips of 4-day old seedlings of *cry1_{control}*, *cry1_{NES}*, *cry1_{NLS}* and *cry1-304* (as negative control) by confocal microscopy (Leica, TCS SP8) to detect the GFP signal.

6.10 Generation and genotypic characterization of CRY1 complementation overexpression lines

The new CRY1 overexpression lines were generated by using Gateway™ technology (<https://www.thermofisher.com/us/en/home/life-science/cloning/gateway-cloning.html>). All the PCRs for cloning purposes were performed by using a high-fidelity proof-reading DNA polymerase (Phusion High-Fidelity DNA Polymerase, Thermofisher Scientific, #F530). CRY1 gene was amplified from cDNA of WT Col-0 by using the primers CRY1-FWD and CRY1-REV_2 (Table 5.2). The PCR product was purified by gel excision using a commercial kit (GeneJET Gel Extraction Kit, Thermofisher Scientific # K0692). The NLS and NES sequences were added to the CRY1 PCR product as described previously (Wu and Spalding, 2007) by using the primers NLS-CRY1_FWD_Spald and NES-CRY1_FWD_Spald in combination with CRY1_REV_2 (Table 5.2). PCR products were purified from gel. To allow the cloning into a donor vector, AttB1 and AttB2 sites were added at the 5' and 3' CRY1, NLS-CRY1 and NES-CRY1 PCR products by using the primers AttB1_CRY1_FWD, AttB1_NLS-CRY1_FWD and AttB1_NES-CRY1_FWD in combination with CRY1_withSTOP_AttB2_REV (Table 5.2). As we were planning to generate N-terminal fusions, the STOP codon at the end of the 3'-terminal was included. AttB1-CRY1-AttB2, AttB1-NLS-CRY1-AttB2 and AttB1-NES-CRY1-AttB2 PCR products were purified from gel and used in the BP reaction with pDONR221 (Gateway™ pDONR™221 Vector, Thermofisher Scientific, #12536017) to generate a donor vector following the manufacturer's instructions. BP reactions of CRY1, NLS-CRY and NES-CRY1 were used to transform the suitable chemically competent *E. coli* cells (One Shot™ TOP10, Thermofisher Scientific, #C404003) which were selected in LB selective medium containing 50 µg/µL of kanamycin. In order to ensure that the insert was correctly inserted in the vector, positive colonies were screened by PCR using primer designed on CRY1 (CRY1_col_FOR) in combination with primer designed on the backbone of the pDONR221 vector (pDONR_col_REV).

Plasmid DNA from positive clones was extracted by using a commercially available kit following the manufacturer's instructions (GeneJET Plasmid Miniprep Kit, ThermoFisher Scientific, #K0503), and it was sequenced with the primer M13_FWD (Table 5.2). Clones that showed the expected sequence with CRY1, NLS-CRY and NES-CRY1 correctly inserted in the pDONR221 vector were used as entry vector in the LR reaction in the destination vector pK2GW7 (Mansour Karimi, 2002) containing the 35S promoter at the N-Terminal. A multi-site LR reaction was also performed by using CRY1, NLS-CRY and NES-CRY1 entry vectors and the entry vector pEN-L4-2L3 (containing the 35S promoter) together with the destination vector pKN_GsTAP containing the GsTAP at the N-terminal, respectively, as described previously (Van Leene et al., 2008). After *E. coli* transformation and overnight incubation in medium containing 100 µg/µL of spectinomycin, positive clones were checked by PCR using the primers 35S_promoter_FWD and CRY1_REV_mid with DreamTaq™ Hot Start Green PCR Master Mix (ThermoFisher Scientific, #K9021). Clones in pK2GW7 were sequenced only with CRY1_REV_mid, designed in the middle of CRY1 sequence, while clones in pKN_GsTAP were separately sequenced with both 35S_promoter_FWD and CRY1_REV_mid in order to capture the entire insert sequence and make sure that the localization signals, the entire CRY1 sequence and the GsTAP were present in the vectors. The positive clones of 35S_CRY1, 35S_NLS-CRY1, 35S_NES-CRY1 and 35S_GsTAP_NES-CRY1 were then used to transform *Agrobacterium tumefaciens* GV3101 chemical competent cells.

After checking colonies and plasmid DNA, liquid cultures of *A. tumefaciens* were then used to transform *cry1-304* plants by floral dipping method (Clough and Bent, 1998). Seeds of primary transformant (T₀) were harvested and selected in MS medium containing a broad spectrum antibiotic for pathogen (Cefotaxime 200 µg/mL) and a specific selection for resistant plants (kanamycin 50 µg/mL). Resistant T1 plants were then transferred in soil and grown for seed harvesting. T1 seeds were again grown in selective medium and T2 resistant plants were used for genotyping characterization.

gDNA was extracted from T2 plants with the commercial kit innuPREP Plant DNA Kit (analytik-jena, #845-KS-1060250) and positive lines were detected by amplification of a region mapping on both the vector and CRY1 sequence by using the primers 35S_promoter_FWD and CRY1_REV_mid.

RNA was extracted from positive T2 plants. 1 mL of TRI-reagent (Sigma, #T9424) was added to 100-250 µL of grounded tissue and samples were vortexed for 15 seconds.

To ensure complete dissociation of nucleoprotein complexes, samples were incubated 5 min at room temperature. 200 μ L of chloroform was added and the samples were vortexed for 15 s and incubated for 15 min at room temperature. The resulting mixture was centrifuged at 12000 rcf for 15 min at 4 °C. The colorless upper aqueous phase (containing RNA) was transferred to a fresh tube containing 500 μ L of isopropanol and the samples were incubated for 10 min at room temperature. The samples were centrifuged at 12000 rcf for 10 min at 4 °C. The supernatant was discarded and the RNA pellet was washed by adding 1 mL of cold 75% ethanol. After vortexing, they were centrifuged at 12000 rcf for 5 min at 4 °C. The RNA pellet was air-dried for 5-10 min and resuspended in 50 μ L of RNase free water. To facilitate dissolution, samples were incubated at 60 °C for 15 min and vortexed every 2 min. DNaseI treatment was performed to eliminate gDNA contamination by using a commercial kit (DNase I RNase-free, thermo scientific, #EN0521) and following the manufacturer's instructions. cDNA synthesis was performed by using the M-MLV Reverse Transcriptase (SIGMA, #M1302) following the instruction provided with the enzyme. cDNA was used as template to amplify the CRY1 gene and confirm its expression.

Four or five-weeks-old plants of 35S_CRY1, 35S_NLS-CRY1, and 35S_NES-CRY1 lines, showing the expression of CRY1 similar to or higher than WT Col-0, were used for the phenotypic characterization. CRY1 protein accumulation in the lines of 35S_GsTAP_NES-CRY1 was tested by using an anti-protein G antibody (NOVUSBIO, #NB120-7248) by Western blot analysis. Protein extraction and western blot analysis were performed as described in the section 5.7. The primary antibody anti-protein G was used at a concentration of 1 μ g/mL.

Gene	Primer name	Sequence (5'→3')	use
CRY1 (AT4G08920)	CRY1-FWD	TCTGGTTCTGTATCTGGTTGTGGTTC	RT PCR
	CRY1_REV2	TTACCCGGTTTGTGAAAGCCGTCT	
LHCB 1.2 (AT1G29910)	LHCB2.1-F	CCCATTGGGTCTTGCTACC	qRT PCR
	LHCB2.1-R	CCGTTCTTGAGCTCCTTCAC	
ELIP2 (AT4G14690)	qRT_ELIP2_FWD	CACCACAAATGCCACAGTCT	qRT PCR
	qRT_ELIP2_REV	TGCTAGTCTCCCGTTGATCC	
GPX7 (AT4G31870)	qRT_GPX7_FWD	CAATGCTGGTGGTTTCCTTGG	qRT PCR
	qRT_GPX7_REV	GCCGCAAGCAACTTCTGGAT	
HY5 (AT5G11260)	qRT_HY5for	TTTCAGCTCAGCAAGCAAGA	qRT PCR
	qRT_HY5rev	CAGCATTAGAACCACCACCA	
HYH (AT3G17609)	qRT_HYHfor	TGGTTCCTGACATGGAAGCA	qRT PCR
	qRT_HYHrev	TGCTTGTTGCGCTGATACTC	
RCE1 (AT4G36800)	qRT_UBI-like_FWD	CTGTTACGGAACCCAATTC	qRT PCR
	qRT_UBI-like_REV	GGAAAAAGGTCTGACCGACA	

Table 5.1 Primers used for RT and quantitative RT PCRs.

Primer name	Sequence (5'→3')	use
CRY1-FWD	TCTGGTTCTGTATCTGGTTGTGGTTC	RT PCR and cloning
CRY1_REV2	TTACCCGGTTTGTGAAAGCCGTCT	
AttB1_CRY1_FWD	GGGGACAAGTTTGTACAAAAA AGCAGGCTTCACCTCTGGTTC TGTATCTGGTTGTGGT	AttB-PCR product preparation
CRY1_withSTOP_AttB2_R	GGGGACAAGTTTGTACAAAAA GCAGGCTTCACCTCTGGTTCTG TATCTGGTTGTGGT	
NLS-CRY1_FWD_Spald	GGCTCGAGcctaagaagaagagaaaggtt TCTGGTTCTGTATCTGGTTGTGGTTC	NLS-CRY1 PCR product preparation
NES-CRY1_FWD_Spald	GGCTCGAGcttgctctaagttggctggacttg atattTCTGGTTCTGTATCTGGTTGTGGTTC	AttB-PCR product preparation
AttB1_CRY1_FWD	GGGGACAAGTTTGTACAAAAA AGCAGGCTTCACCTCTGGTTC TGTATCTGGTTGTGGT	
AttB1_NLS_CRY1_FWD	GGGGACAAGTTTGTACAAAAA GCAGGCTTCACCGGCTCGAG cctaagaagaaga	
attB1_NES_CRY1_FWD	GGGGACAAGTTTGTACAAAAA GCAGGCTTCACCGGCTCGAG cttgctctaagttggctggacttg	
CRY1_withSTOP_AttB2_R	GGGGACAAGTTTGTACAAAAA GCAGGCTTCACCTCTGGTTCTG TATCTGGTTGTGGT	
CRY1_col_FOR	CTTGGGCTGTGGATGAGAAC	
pDONR_col_REV	GTAACATCAGAGATTTTGAGACAC	
M13_FWD	TGTA AACGACGGCCAGT	Sequencing clones in pDONR221
35S_promoter_FWD	AGGAAGGTGGCACCTACAAAT	Colony PCR and sequencing of CRY1, NLS-CRY1 and NES-CRY1 in dest vectors
CRY1_REV mid	CACCAATGGATCCGCAACACA	

Table 5.2 Primers used for cloning and generation of vector for CRY1, NLS-CRY1 and NES-CRY1 overexpressor lines

6.11 Generation and genotypic characterization of *AT3G56290* KO mutants by CRISPR/Cas9

The constructs designing to generate *AT3G56300* KO plants by CRISPR/Cas9 was performed together with Florian Hahn (HHU) as described in (Hahn et al., 2017a; Hahn et al., 2017b). SgRNA sites were searched in gDNA of *AT3G56300* having GN followed by 19 nucleotides and the PAM motif NGG (GN19NGG). The design of the two SgRNA sites was validated for off-targets by using an online tool (www.rgenome.net/cas-offinder) to ensure that these SgRNAs could specifically recognize the gene of interest *AT3G56300* to guide Cas9. SgRNA1 and SgRNA2 were also selected as they contained restriction sites (for FspBI and PvuI, respectively) 3 bp in front of NGG near the PAM motif, which could serve as genetic markers for later effective and rapid screening of positive KO plants. The primers MP3 and MP5, corresponding to SgRNA1 and SgRNA2 were designed on the 3'→5' genomic DNA sequence of *AT3G56300* (**Table 5.3**). The overlaps TTCG and AAAC sequences were added in front of MP3 and MP5 to allow the recombination in PFH6 vector (Hahn, Eisenhut, et al. 2017). Complementary sequences of MP3 and MP5 primers (MP4 and MP6) were also designed. 10 µm primers dilutions of MP3-MP4 and MP5-MP6 were combined in a ratio of 1:1 and annealed by incubating at 98°C for 10 min followed by an incubation at 55°C for 10 min. pFH6 vector, which contains U6-26p::SgRNA scaffold and ampicillin resistance (Hahn, Eisenhut, et al. 2017), was digested with BpsI (NEB, #R3539S) and the backbone of ca. 3612 bp was excised from the agarose gel and purified. The annealed primers MP3-MP4 and MP5-MP6 were then ligated in pFH6, generating the vectors PMP3 and PMP4, respectively, by using T4 DNA ligase (NEB, #M0202S). Colony PCR was performed with MP3 and MP5 primers for PMP3 and PMP4, respectively, in combination with M13_REV which maps in the backbone of pFH6 (**Table 5.3**) and positive clones were sequenced with M13_REV. The final destination vector pFH1 (Hahn et al., 2017a) containing UB10 promoter, Cas9, bacteria kanamycin resistance and plant hygromycin B resistance was digested with KpnI-HF, HindIII-HF (NEB, #R3142S and #R3104S), gel excised and purified before the cloning reactions. Plasmid DNA from positive clones was used as template to amplify SgRNA1 from PMP3 and SgRNA2 from PMP4 with the primers FH41-FH254 and FH255-FH42. PCR products were excised from gel, purified and cloned in pFH1 by using the Gibson Assembly Cloning Kit (NEB, #E5510S). Three different constructs have been generated: PMP5, carrying both SgRNA1 and SgRNA2 from PMP3 and PMP4, PMP7 and PMP8 which contained only SgRNA1 or SgRNA2 from PMP3 and PMP4, respectively.

Colony PCR was performed with M13_FWD and FH179 (**Table 5.3**) and sequenced with both primers. Plasmid DNA from positive clones was used to transform *A. thumefaciens* and plant transformation in *A. thaliana* WT Col-0 by the floral dip method (Clough and Bent, 1998).

Primer name	Sequence (5'→3')	use
MP3	TTCGGATTTTCCGGAACCCTAGAT	SgRNA1 amplification and annealing
MP4	AAACATCTAGGGTTCCGGAATAATC	
MP5	TTCGGGACTTCTCACAAGTTCGAT	SgRNA2 amplification and annealing
MP6	AAACATCGAACTTGTGAGAAGTCC	
M13_REV	CAGGAAACAGCTATGAC	Colony PCR PMP3 and PMP4 and sequencing
FH41	AAACGACGGCCAGTGCCAGAATTGGGCCCGACGTCG	Amplification of SgRNA1 from PMP3
FH254	GCCCAATTCCAAGCTATGCATCCAACGCG	
FH255	CATAGCTTGAATTGGGCCCGACGTCG	Amplification of SgRNA2 from PMP4
FH42	TACTGACTCGTCGGGTACCAAGCTATGCATCCAACGCG	
M13_FWD	GTAAAACGACGGCCAG	Colony PCR PMP5, PMP7 and PMP8 and sequencing
FH179	TATTACTGACTCGTCGGGTA	

Table 5.3 Primers used for cloning and generation of vector for AT3G56290 CrisprCas9 KO.

Seeds of primary transformant (T₀) and WT Col-0 were sown on selective MS medium containing cefotaxime (200 µg/mL) and hygromycin (50 µg/mL). T1 plants that were resistant to the first selection were transferred in soil and grown for seed harvesting. T2 and T3 plants were grown in selective medium and used for genotyping characterization. Template gDNA was prepared from leaves of the transgenic plants and WT Col-0 by using Phireplant direct PCR kit (ThermoFisher scientific, #F160L) following the instructions provided. The presence of the CAS9 gene was confirmed by using the primers FH_61 and FH_201 (**Table 5.4**). WT Col-0 was used as negative control. Also, AT3G56290 gene was amplified from PMP5, PMP7 and PMP8 plants with the primers MP7 and MP8 (**Table 5.4**) and the PCR products were used to perform restriction analysis according to the cleaved amplified polymorphic sequence (CAPS) method (Hahn et al., 2017a; Hahn et al., 2017b).

AT3G56290 PCR products from PMP7 and PMP8 were digested with FspBI (NEB, #R0568S), PvuI (NEB, #R3150S), respectively, as these enzymes have their restriction sites in SgRNA1 and SgRNA2. AT3G56290 PCR products from PMP5 were digested with both FspBI and PvuI, as PMP5 contain both SgRNA1 and SgRNA2. The software Serial cloner 2.6.1 (<http://serialbasics.free.fr>) was used to generate *in silico* digestion patterns expected for WT Col-0 and transgenic lines.

A stringent gDNA extraction was performed with leaf samples of the lines showing the expected digestion patterns for AT3G56290 mutation by using a commercial kit (analytik-jena, #845-KS-1060250) and the AT3G56290 PCR products were gel-excised, purified and sequenced with both MP7 and MP8 primers. T3 Plants showing mutation at the target sites were propagated for T4 generation. Leaves of T4 plants were harvested and the RNA was extracted with the same procedure as described in 5.9. The expression of AT3G56290 was checked in these plants by using MP7 and MP8 primers (**Table 5.4**). 4-5 weeks old T4 plants were used for phenotypic characterization.

Gene	Primer name	Sequence (5'→3')	use
CAS9	FH_61	ATGGGTTTTAGAGCACTGCC	Confirm CAS9
	FH_201	TTCACCAGACTCTTCTCTAGATGA	
AT3G56300	MP7	CTGCCCAACGAGAAGGTGC	Amplify AT3G56300
	MP8	CATCAACCGCCTGTCCGACT	

Table 5.4. Primers used for Cas9 and AT3G56290 gene amplification.

LIST OF FIGURES

Figure 1.1 Transmission electron microscopy image of a tobacco chloroplast.

Figure 1.2 Overviews of the dimeric PSII core associated with LHCII.

Figure 1.3. Structure and organization of the *Pisum Sativum* PSI-LHCI supercomplex.

Figure 1.4. Xanthophyll binding sites in spinach LHCII structure.

Figure 1.5 Schematic representation of LET in the thylakoid membrane of chloroplasts.

Figure 1.6. Schematic diagram of photoprotective processes occurring within chloroplasts.

Figure 1.7. Possible destiny of excited Chl.

Figure 1.8 Violaxanthin cycle.

Figure 1.9. Model of PSBS activation and conformational change upon protonation of glutamate residues exposed to the luminal side of thylakoid membrane.

Figure 1.10. Physiological functions of PSI CET.

Figure 1.11. EL perception and gene expression regulation through plastid and photoreceptor signaling.

Figure 1.12. Photoreceptors and their roles in photomorphogenesis.

Figure 1.13. Domain structure of CRYs and associated chromophores.

Figure 3.1. Visual and growth phenotypes of WT Col-0 and *cry1-304* growing under different light regimes (constant low light, CL, fluctuating light, FL and constant high light, HL).

Figure 3.2: Maximum quantum yield of PSII in the overnight dark-adapted state (F_v/F_m) after three days under CL and FL.

Figure 3.3: Characterization of PSII activity after three days under CL and FL in leaves of overnight dark-adapted plants of WT Col-0, *cry1-304*, *cry1cry2*, *phyB*, WT Ws and *hy5hyh*.

Figure 3.4. NPQ measured after 160-s of AL illumination in WT Col-0, *cry1-304*, *cry1cry2*, *phyB*, WT Ws and *hy5hyh* after three days under CL and FL.

Figure 3.5. Characterization of PSII after three days under CL and FL in plants of WT Col-0 and *cry1-304*.

Figure 3.6. Characterization of PSI after three days under CL and FL. Rapid light response curves were measured in leaves of overnight dark-adapted plants of WT Col-0 and *cry1-304*.

Figure 3.7: Changes in P700 redox state during light response measurements in WT Col-0 and *cry1-304* after three days under CL and FL.

Figure 3.8. Levels of key proteins of photosynthesis and its regulation (D1, LHCB1, PSBS, PSA-A, ATPC, RBCL and PGR5) in leaves of WT Col-0 and *cry1-304* after three days under CL and FL.

Figure 3.9. Leaf pigment composition in dark- and light-adapted leaves of WT Col-0 and *cry1-304* after three days under CL and FL.

Figure 3.10. Expression of *LHCB1.2*, *ELIP2*, *GPX7*, *HY5* and *HYH* genes in WT Col-0 and *cry1-304* after three days of exposure to CL and FL.

Figure 3.11. Subcellular localization of chimeric CRY1-GFP proteins in root and CRY1 gene expression in leaves of *cry1_{control}* and *cry1_{NES}* compared to WT Col-0 and *cry1-304*.

Figure 3.12 Visual phenotype of seedlings of WT Col-0, *cry1-304* and *cry1_{NES}* grown in the dark or under low-fluence blue light.

Figure 3.13. Visual phenotypes and photosynthetic characterization of WT Col-0, *cry1_{control}*, *cry1_{NES}* and *cry1-304* growing under CL, FL and HL

Figure 3.14. Construct and genotypic characterization of CRY1 overexpressor lines under the control of 35S promoter (35S_CRY1).

Figure 3.15 Construct and genotypic characterization of CRY1 OE lines with nuclear localization signal under the control of the 35S promoter (35S_NLS_CRY1).

Figure 3.16. Construct and genotypic characterization of CRY1 OE lines with nuclear export signal under the control of the 35S promoter (35S_NES_CRY1).

Figure 3.17. Construct and genotypic characterization of CRY1 OE lines with the nuclear export signal and GsTAP under the control of the 35S promoter (35S_GsTAP_NES_CRY1).

Figure 3.18 *CRY1* gene expression analyzed by reverse transcription-PCR (RT-PCR) in leaves of plants positively screened in T3 generation.

Figure 3.19 Visual phenotype of seedlings of CRY1 OE lines grown for 4 days.

Figure 3.20. Visual phenotypes of WT Col-0, *cry1-304*, *35S_CRY1*, *35S_NLS_CRY1* and *35S_NES_CRY1* before the onset of the CL, FL2 and HL2 treatments (day 0) and at the end of the treatments (day 7).

Figure 3.21. Leaf expansion growth of WT Col-0, *cry1-304*, *35S_CRY1*, *35S_NLS_CRY1* and *35S_NES_CRY1* monitored as changes in the total projected leaf area (cm²) for seven days of exposure to CL, FL2 and HL2.

Figure 3.22. Characterization of PSII quantum yield, Y(II), before the onset of the experiment under CL (black symbols) and after three-day exposure to FL2 (yellow symbols) in WT Col-0, *cry1-304*, *35S_CRY1*, *35S_NLS_CRY1* and *35S_NES_CRY1*.

Figure 3.23. Characterization of non-photochemical quenching (NPQ) before the onset of the experiment under CL (black symbols) and after three-day exposure to FL2 (yellow symbols) in WT Col-0, *cry1-304*, *35S_CRY1*, *35S_NLS_CRY1* and *35S_NES_CRY1*.

Figure 3.24. Characterization of key photosynthetic parameters under FL2 in WT Col-0, *cry1-304*, *35S_CRY1*, *35S_NLS_CRY1* and *35S_NES_CRY1* extracted from the experiment shown in Figures 3.22, 3.23 and S.3

Figure 3.25. Characterization of key photosynthetic parameter under HL2 in WT Col-0, *cry1-304*, *35S_CRY1*, *35S_NLS_CRY1* and *35S_NES_CRY1* extracted from the experiment shown in Figures S.4 – S.6

Figure 3.26. Phylogenetic analysis of the unknown protein AT3G56290

Figure 3.27. Functional protein association network of AT3G56290 obtained by STRING Version 11.0 (<https://string-db.org>).

Figure 3.28 CRISPR/Cas9 construct designs for KO of *AT3G56290* gene.

Figure 3.29 Amplification of *CAS9* and *AT3G56290* genes on genomic DNA of WT Col-0 and the selected positive lines.

Figure 3.30 Screening by restriction analysis of WT Col-0 and the selected positive PMP7 lines of T3 generation.

Figure 3.31. Screening by restriction analysis of WT Col-0 and the selected positive PMP8 lines of T3 generation.

Figure 3.32. Screening by restriction analysis of WT Col-0 and the selected positive PMP5 lines of T3 generation.

Figure 3.33. Sequencing analysis of PMP5 #1.1.10.3 and #1.4.1.1 lines.

Figure 3.34. Translation of *AT3G56290* coding region in frame 3 for WT Col-0, PMP5 #1.4.1.1 and PMP5 #1.1.10.3.

Figure 3.35. *AT3G56290* gene expression analyzed by reverse transcription-PCR (RT-PCR) in leaves of PMP5 #1.1.10.3 and #1.4.1.1 plants screened in T4 generation compared to WT Col-0.

Figure 3.36. Visual phenotypes of WT Col-0, *PMP5 #1.4.1.1* and *PMP5 #1.1.10.3* plants in T4 generation.

Figure 3.37. Characterization of PSII activity after one day under CL, FL2 and HL2 in WT Col-0, *PMP5 #1.4.1.1* and *PMP5 #1.1.10.3*.

Figure 3.38. Maximum quantum yield of PSII in the overnight dark-adapted state (F_v/F_m) and NPQ after one day under CL, FL2 and HL2 in WT Col-0, *PMP5 #1.4.1.1* and *PMP5 #1.1.10.3*.

Figure 3.39. Characterization of PSII activity after three days under CL (black symbols), FL2 and HL2 in WT Col-0, *PMP5 #1.4.1.1* and *PMP5 #1.1.10.3*.

Figure 3.40. Maximum quantum yield of PSII in the overnight dark-adapted state (F_v/F_m) and NPQ after three days under CL, FL and HL in WT Col-0, *PMP5 #1.4.1.1* and *PMP5 #1.1.10.3*.

Figure S1. Characterization of PSII after three days under CL and FL2 in WT Col-0 and *cry1-304*.

Figure S2. Characterization of PSI after three days under CL and FL2 in WT Col-0 and *cry1-304*.

Figure S3. Characterization of relative electron transport rate of PSII (ETR(II)) before the onset of the experiment under CL (black symbols) and after three-day exposure to FL2 (yellow symbols) in selected *CRY1* gene OE lines.

Figure S4. Characterization of PSII quantum yield, $Y(II)$, before the onset of the experiment under CL and after one-day exposure to HL2 in selected *CRY1* gene OE lines.

Figure S5. Characterization of relative electron transport rate of PSII (ETR(II)) before the onset of the experiment under CL and after one-day exposure to HL2 in selected *CRY1* gene OE lines.

Figure S6. Characterization of non-photochemical quenching (NPQ) before the onset of the experiment under CL and after one-day exposure to HL2) in selected *CRY1* gene OE lines.

LIST OF TABLES

Table 1.1 Key genes that are regulated by HY5

Table 3.1. De-epoxidation state (DES) of VAZ calculated as $(A + Z) / (V + A + Z)$.

Table 3.2. Differences between the genotypes (WT Col-0 and *cry1-304*), the light conditions (CL and FL) and the pigments levels in the dark or after 260 s of exposure to AL as well as the interactions between these factors were tested by three-way ANOVA

Table 3.3. Significant differences in pigment levels reported in **Figure 3.8** and **Table 3.1** were tested by multiple comparison tests (Tukey).

Table 3.4. Summary of genotypic characterization of transgenic lines 35S_CRY1, 35S_NLS_CRY1, 35S_NES_CRY1 and 35S_GsTAP_NES_CRY1 in T2 generation.

Table 3.5 Distribution of protein homologous to AT3G56290 in dicots, monocots, club-mosses, mosses, green algae and cyanobacteria.

Table 3.6 Predicted functional partners of AT3G56290 in Figure 3.27 based on gene co-expression analysis by STRING (<https://string-db.org>).

Table 3.7 Significantly enriched GO terms of the proteins in the association network shown in Figure 3.27.

Table 5.1 Primers used for RT and quantitative RT PCRs.

Table 5.2 Primers used for cloning and generation of vector for CRY1, NLS-CRY1 and NES-CRY1 overexpressor lines

Table 5.3 Primers used for cloning and generation of vector for *AT3G56290* CrisprCas9 KO.

Table 5.4. Primers used for Cas9 and *AT3G56290* gene amplification.

LIST OF ABBREVIATIONS

$^1\text{O}_2$	Singlet oxygen
35S	Cauliflower mosaic virus promoter
$^3\text{Chl}^*$	Chl triplets
ABCF5	ATP-BINDING CASSETTE F5
AL	Actinic light
ATP	Adenosine triphosphate ATP
ATPase	ATP-synthase complex
BBX	B-box
BIC1	BLUE-LIGHT INHIBITOR OF CRYPTOCHROMES-1
BL	Blue light
bZIP	Basic domain/leucine zipper
CAPS	Cleaved amplified polymorphic sequence
Car	Carotenoids
CBB cycle	Calvin-Benson-Bassham cycle
CCE	CRY C-terminal extension domain
CET	Cyclic electron transport
Chl	Chlorophylls
CL	Constant low light
CO	CONSTANS
CO_2	Carbon dioxide
COP1	CONSTITUTIVELY PHOTOMORPHOGENIC-1
<i>CRY1</i> OE	<i>CRY1</i> gene Overexpressor lines
CRY1	CRYPTOCHROME 1
CRY1	CRYPTOCHROME-1
CRYs	Cryptochromes
Cyt b_6/f	Cytochrome b_6/f complex
DES	De-epoxidation state
EL	Excess of light
ELIP1	EARLY LIGHT INDUCED PROTEIN-1
ELIP2	EARLY LIGHT INDUCED PROTEIN-1
EM	Chloroplast envelope EM
ETR (I)	Relative electron transport rate of PSI
ETR(II)	Relative electron transport rate of PSII
FAD	Flavin adenine dinucleotide
FADA	FATTY ACID DESATURASE 4
FBPase	Fructose-1,6-bisphosphatase
Fd	Ferredoxin
FL	Fluctuating light
FNR	Fd-NADP-oxidoreductase
FTR	Ferredoxin-thioredoxin reductases
F_v/F_m	Maximum quantum yield of PSII in the overnight dark-adapted state
G3P	Glyceraldehyde 3-phosphate
GAPDH	Glyceraldehyde-3-phosphate dehydrogenase
γCA2	γ CARBONIC ANHYDRASE-2
GPXs	Glutathione peroxidases
GsTAP	Gs tandem affinity purification tag
GUN	Genomes uncoupled
H_2O_2	Hydrogen peroxide
HFR	LONG HYPOCOTYL IN FAR-RED-1
HL	Constant High Light
HY5	LONG HYPOCOTYL-5
HYH	ELONGATED HYPOCOTYL 5-HOMOLOG

KO	knock-out
LAF1	LONG HYPOCOTYL AFTER FAR-RED-1
LCNP	Plastid lipocalin
LET	Linear electron transport
LHC	Light Harvesting Complexes
LL	Low light
Lut	Lutein
MTHF	5, 10-methenyl tetrahydrofolate
N	Neoxanthin
NADP ⁺ , NADPH	Adenine dinucleotide phosphate
NDH-1 complex	Chloroplast NADH dehydrogenase-1 like complex
NEP	Nuclear-encoded proteins
NES	Nuclear export signal
NF	Norflurazon
NGE	Nuclear gene expression
NLS	Nuclear localization signal
NPQ	Non Photochemical Quenching
NTRC	NADPH-dependent thioredoxin reductase
O ₂ ^{·-}	Superoxide anion radical
OEC	Oxygen-evolving complex
OH [·]	Hydroxyl radical
PAP1	PRODUCTION OF ANTHOCYANIN PIGMENT1; MYB75
PAP2	PRODUCTION OF ANTHOCYANIN PIGMENT2, MYB90
PAR	Photosynthetically active radiation
Pc	Plastocyanin
PEG	Plastid-encoded genes
PEP	Plastid-encoded-plastid RNA polymerase
PET	Photosynthetic electron transport
Pfr	PHY active form
PGR5	Proton Gradient Regulator 5
PGRL1	PGR5-Like 1 (PGRL1)
PHR	CRY1 N-terminal photolyase homology-related domain
PHYs	Phytochromes
PIFs	PHYTOCHROME INTERACTING FACTORS
Pm	Maximum photo-oxidizable P700 (Pm)
Pmf	Proton motive force
PORC	PROTOCHLOROPHYLLIDE REDUCTASE C
PQ ^{·-}	Plastosemiquinone
Pr	PHY inactive form
PRK	Phosphoribulokinase
PSBS	PSII subunit S
PSI	Photosystem I
PSII	Photosystem II
PSY	PHYTOENE SYNTHASE
qE	NPQ Energy-dependent quenching component
ql	Photoinhibitory quenching
qZ	NPQ Z-dependent quenching
RC	Reaction center
RCE1	RUB1 CONJUGATING ENZYME 1
RES	Reactive electrophile species
RFL	Far-red light
RL	Red light
ROS	Reactive oxygen species
SAR	Shade avoidance response
SBPase	Seduheptulose-1,7-bisphosphatase

SgRNA	Single guide RNA
SIG	Nuclear-encoded sigma factor
SIGE	SIGMA FACTOR E
SOQ1	SUPPRESSOR OF QUENCHING-1
SP	saturation pulse
SPA	SUPPRESSOR OF PHYA-105
SPS1	SOLANESYL DIPHOSPHATE SYNTHASE 1
SPS2	SOLANESYL DIPHOSPHATE SYNTHASE 2
STH	B-BOX ZINC FINGER PROTEIN 25
TF	Transcription factor
Trx	Thioredoxins
UVR8	ULTRAVIOLET-B RECEPTOR-8
V	Violaxanthin
VAZ	Total xanthophyll-cycle pool
VDE	Violaxanthin de-epoxidase
WT	Wild type
Y(I)	Quantum yield of PSI
Y(II)	Quantum yield of PSII in the light
Y(NA)	PSI acceptor side limitation
Y(ND)	PSI donor side limitation
Z	Zeaxanthin
ZEP	Zeaxanthin epoxidase
ZTL	Zeitlupe family receptors

REFERENCES

- Abbas N, Maurya JP, Senapati D, Gangappa SN, Chattopadhyaya S** (2014) Arabidopsis CAM7 and HY5 physically interact and directly bind to the HY5 promoter to regulate its expression and thereby promote photomorphogenesis. *Plant Cell* **26**: 1036–1052
- Adams III WW, Demmig-Adams B, Rosenstiel TN, Brightwell AK, Ebbert V** (2002) Photosynthesis and Photoprotection in Overwintering Plants. *Plant Biol* **4**: 545–557
- Adams W, Demmig-Adams B** (1992) Operation of the xanthophyll cycle in higher plants in response to diurnal changes in incident sunlight. *Planta* **186**: 390–398
- Adams WW, Zarter CR, Ebbert V, Demmig-Adams B** (2004) Photoprotective Strategies of Overwintering Evergreens. *Bioscience* **54**: 41–49
- Adamska I, Roobol-Bóza M, Lindahl M, Andersson B** (1999) Isolation of pigment-binding early light-inducible proteins from pea. *Eur J Biochem* **260**: 453–60
- Adir N, Zer H, Shochat S, Ohad I** (2003) Photoinhibition - A historical perspective. *Photosynth Res* **76**: 343–370
- Ahmad M, Cashmore AR** (1997) The blue-light receptor cryptochrome 1 shows functional dependence on phytochrome A or phytochrome B in *Arabidopsis thaliana*. *Plant J* **11**: 421–7
- Ahmad M, Cashmore AR** (1996) Seeing blue: the discovery of cryptochrome. *Plant Mol Biol* **30**: 851–861
- Ahmad M, Grancher N, Heil M, Black RC, Giovani B, Galland P, Lardemer D** (2002) Action Spectrum for Cryptochrome-Dependent Hypocotyl Growth Inhibition in *Arabidopsis* 1. doi: 10.1104/pp.010969
- Ahmad M, Jarillo JA, Cashmore AR** (1998a) Chimeric proteins between cry1 and cry2 *Arabidopsis* blue light photoreceptors indicate overlapping functions and varying protein stability. *Plant Cell* **10**: 197–207
- Ahmad M, Jarillo JA, Smirnova O, Cashmore AR** (1998b) Cryptochrome blue-light photoreceptors of *Arabidopsis* implicated in phototropism. *Nature* **392**: 720–723
- Ahmad M, Lin C, Cashmore AR** (1995) Mutations throughout an *Arabidopsis* blue-light photoreceptor impair blue-light-responsive anthocyanin accumulation and inhibition of hypocotyl elongation. *Plant J* **8**: 653–8
- Al-Sady B, Ni W, Kircher S, Schäfer E, Quail PH** (2006) Photoactivated Phytochrome Induces Rapid PIF3 Phosphorylation Prior to Proteasome-Mediated Degradation. *Mol Cell* **23**: 439–446
- Alboresi A, Dall'osto L, Aprile A, Carillo P, Roncaglia E, Cattivelli L, Bassi R** (2011) Reactive oxygen species and transcript analysis upon excess light treatment in wild-type *Arabidopsis thaliana* vs a photosensitive mutant lacking zeaxanthin and lutein. *BMC Plant Biol* **11**: 62
- Alboresi A, Storti M, Morosinotto T** (2019) Balancing protection and efficiency in the regulation of photosynthetic electron transport across plant evolution. *New Phytol* **221**: 105–109
- Allahverdiyeva Y, Aro E-M** (2012) Photosynthetic Responses of Plants to Excess Light: Mechanisms and Conditions for Photoinhibition, Excess Energy Dissipation and Repair. pp 275–297
- Allahverdiyeva Y, Suorsa M, Tikkanen M, Aro EM** (2015) Photoprotection of photosystems in fluctuating light intensities. *J Exp Bot* **66**: 2427–2436
- Amstutz CL, Fristedt R, Schultink A, Merchant SS, Niyogi KK, Malnoë A** (2020) An atypical short-chain dehydrogenase–reductase functions in the relaxation of photoprotective qH in *Arabidopsis*. *Nat Plants* **6**: 154–166
- Amunts A, Toporik H, Borovikova A, Nelson N** (2010) Structure Determination and Improved Model of Plant Photosystem I * □ S. *J Biol Chem* **285**: 3478–3486
- Antelmann H, Hellmann JD** (2011) Thiol-based redox switches and gene regulation. *Antioxidants Redox Signal* **14**: 1049–1063
- Arnon DI, Chain RK** (1975) Regulation of ferredoxin-catalyzed photosynthetic phosphorylations. *Proc Natl Acad Sci U S A* **72**: 4961–5

- Aro EM, McCaffery S, Anderson JM** (1993) Photoinhibition and D1 protein degradation in peas acclimated to different growth irradiances. *Plant Physiol* **103**: 835–843
- Avendaño-Vázquez A-O, Cordoba E, Llamas E, San Román C, Nisar N, De la Torre S, Ramos-Vega M, Gutiérrez-Nava M de la L, Cazzonelli CI, Pogson BJ, et al** (2014) An Uncharacterized Apocarotenoid-Derived Signal Generated in ζ -Carotene Desaturase Mutants Regulates Leaf Development and the Expression of Chloroplast and Nuclear Genes in Arabidopsis. *Plant Cell* **26**: 2524–2537
- Baena-González E, Aro E-M** (2002) Biogenesis, assembly and turnover of photosystem II units. *Philos Trans R Soc Lond B Biol Sci* **357**: 1451–9; discussion 1459–60
- Ballottari M, Alcocer MJP, D'Andrea C, Viola D, Ahn TK, Petrozza A, Polli D, Fleming GR, Cerullo G, Bassi R** (2014) Regulation of photosystem I light harvesting by zeaxanthin. *Proc Natl Acad Sci U S A* **111**: E2431–8
- Ballottari M, Dall'Osto L, Morosinotto T, Bassi R** (2007) Contrasting behavior of higher plant photosystem I and II antenna systems during acclimation. *J Biol Chem* **282**: 8947–8958
- Ballottari M, Govoni C, Caffarri S, Morosinotto T** (2004) Stoichiometry of LHCl antenna polypeptides and characterization of gap and linker pigments in higher plants Photosystem I. *Eur J Biochem* **271**: 4659–4665
- Barbato R, Tadini L, Cannata R, Peracchio C, Jeran N, Alboresi A, Morosinotto T, Bajwa AA, Paakkarinen V, Suorsa M, et al** (2020) Higher order photoprotection mutants reveal the importance of Δ pH-dependent photosynthesis-control in preventing light induced damage to both photosystem II and photosystem I. *Sci Rep*. doi: 10.1038/s41598-020-62717-1
- Bassham JA, Benson AA, Kay LD, Harris AZ, Wilson AT, Calvin M** (1954) The Path of Carbon in Photosynthesis. XXI. The Cyclic Regeneration of Carbon Dioxide Acceptor ¹. *J Am Chem Soc* **76**: 1760–1770
- Bassi R, Caffarri S** (2000) Lhc proteins and the regulation of photosynthetic light harvesting function by xanthophylls. *Photosynth Res* **64**: 243–256
- Bela K, Horváth E, Gallé Á, Szabados L, Tari I, Csiszár J** (2015) Plant glutathione peroxidases: emerging role of the antioxidant enzymes in plant development and stress responses. *J Plant Physiol* **176**: 192–201
- Belbin FE, Noordally ZB, Wetherill SJ, Atkins KA, Franklin KA, Dodd AN** (2017) Integration of light and circadian signals that regulate chloroplast transcription by a nuclear-encoded sigma factor. *New Phytol* **213**: 727–738
- Bellafiore S, Barneche F, Peltier G, Rochaix J-D** (2005) State transitions and light adaptation require chloroplast thylakoid protein kinase STN7. *Nature* **433**: 892–895
- Benhamed M, Bertrand C, Servet C, Zhou DX** (2006) Arabidopsis GCN5, HD1, and TAF1/HAF2 interact to regulate histone acetylation required for light-responsive gene expression. *Plant Cell* **18**: 2893–2903
- Bethmann S, Melzer M, Schwarz N, Jahns P** (2019) The zeaxanthin epoxidase is degraded along with the D1 protein during photoinhibition of photosystem II. *Plant Direct* **3**: e00185
- van Bezouwen LS, Caffarri S, Kale RS, Kouřil R, H Thunnissen A-MW, Oostergetel GT, Boekema EJ** (2017) Subunit and chlorophyll organization of the plant photosystem II supercomplex. **3**: 17080
- Binkert M, Kozma-Bognár L, Terecskei K, De Veylder L, Nagy F, Ulm R** (2014) UV-B-Responsive association of the Arabidopsis bZIP transcription factor ELONGATED HYPOCOTYL5 with target genes, including its own promoter. *Plant Cell* **26**: 4200–4213
- Block A, Fristedt R, Rogers S, Kumar J, Barnes B, Barnes J, Elowsky CG, Wamboldt Y, Mackenzie SA, Redding K, et al** (2013) Functional modeling identifies paralogous solanesyl-diphosphate synthases that assemble the side chain of plastoquinone-9 in plastids. *J Biol Chem* **288**: 27594–27606
- Bobik K, Burch-Smith TM, Burgess SJ, Pasternak TP, Pfannschmidt T, Burch-Smith TM, Bobik K, Burch-Smith TM** (2015) Chloroplast signaling within, between and beyond cells. *Front Plant Sci* **6**: 781
- Boccalandro HE, Rugnone ML, Moreno JE, Ploschuk EL, Serna L, Yanovsky MJ, Casal JJ** (2009) Phytochrome B enhances photosynthesis at the expense of water-use efficiency in arabidopsis 1[W][OA]. *Plant Physiol* **150**: 1083–1092
- Boyer PD, Chance B, Ernster L, Mitchell P, Racker E, Slater EC** (1977) Oxidative Phosphorylation and Photophosphorylation. *Annu Rev Biochem* **46**: 955–966

- Boylan MT, Quail PH** (1991) Phytochrome A overexpression inhibits hypocotyl elongation in transgenic Arabidopsis. *Proc Natl Acad Sci U S A* **88**: 10806–10810
- Brelsford CC, Morales LO, Nezval J, Kotilainen TK, Hartikainen SM, Aphalo PJ, Robson TM** (2019) Do UV-A radiation and blue light during growth prime leaves to cope with acute high light in photoreceptor mutants of Arabidopsis thaliana? *Physiol Plant* **165**: 537–554
- Brooks MD, Sylak-Glassman EJ, Fleming GR, Niyogi KK** (2013) A thioredoxin-like/ β -propeller protein maintains the efficiency of light harvesting in Arabidopsis. *Proc Natl Acad Sci U S A* **110**: E2733
- Brown BA, Cloix C, Jiang GH, Kaiserli E, Herzyk P, Kliebenstein DJ, Jenkins GI** (2005) A UV-B-specific signaling component orchestrates plant UV protection. *Proc Natl Acad Sci U S A* **102**: 18225–18230
- Bruggemann E, Handwerger K, Essex C, Storz G** (1996) Analysis of fast neutron-generated mutants at the Arabidopsis thaliana HY4 locus. *Plant J* **10**: 755–760
- Buchanan BB** (2016) The carbon (formerly dark) reactions of photosynthesis. *Photosynth Res* **128**: 215–217
- Buchanan BB, Grussem W, Jones RL** Biochemistry & molecular biology of plants.
- Caffarri S, Croce R, Cattivelli L, Bassi R** (2004) A look within LHCI: Differential analysis of the Lhcb1-3 complexes building the major trimeric antenna complex of higher-plant photosynthesis. *Biochemistry* **43**: 9467–9476
- Carrillo LR, Froehlich JE, Cruz JA, Savage LJ, Kramer DM** (2016) Multi-level regulation of the chloroplast ATP synthase: the chloroplast NADPH thioredoxin reductase C (NTRC) is required for redox modulation specifically under low irradiance. *87*: 654–663
- Cashmore AR, Jarillo JA, Wu YJ, Liu D** (1999) Cryptochromes: blue light receptors for plants and animals. *Science* **284**: 760–5
- Castillon A, Shen H, Huq E** (2007) Phytochrome Interacting Factors: central players in phytochrome-mediated light signaling networks. *Trends Plant Sci* **12**: 514–521
- Chalker-Scott L** (1999) Invited Review Environmental Significance of Anthocyanins in Plant Stress Responses.
- Chang CCC, Slesak I, Jordá L, Sotnikov A, Melzer M, Miszalski Z, Mullineaux PM, Parker JE, Karpinska B, Karpinski S** (2009) Arabidopsis chloroplastic glutathione peroxidases play a role in cross talk between photooxidative stress and immune responses. *Plant Physiol* **150**: 670–83
- Chatterjee M, Sharma P, Khurana JP** (2006) Cryptochrome 1 from *Brassica napus* Is Up-Regulated by Blue Light and Controls Hypocotyl/Stem Growth and Anthocyanin Accumulation. *Plant Physiol* **141**: 61–74
- Chaux F, Peltier G, Johnson X** (2015) A security network in PSI photoprotection: Regulation of photosynthetic control, NPQ and O₂ photoreduction by cyclic electron flow. *Front Plant Sci* **6**: 875
- Chaves I, Pokorny R, Byrdin M, Hoang N, Ritz T, Brettel K, Essen L-O, van der Horst GTJ, Batschauer A, Ahmad M** (2011) The Cryptochromes: Blue Light Photoreceptors in Plants and Animals. *Annu Rev Plant Biol* **62**: 335–364
- Chen M, Chory J** (2011) Phytochrome signaling mechanisms and the control of plant development. *Trends Cell Biol* **21**: 664–671
- Chotewutmontri P, Barkan A** (2016) Dynamics of Chloroplast Translation during Chloroplast Differentiation in Maize. *PLoS Genet*. doi: 10.1371/journal.pgen.1006106
- Cloix C, Kaiserli E, Heilmann M, Baxter KJ, Brown BA, O'Hara A, Smith BO, Christie JM, Jenkins GI** (2012) C-terminal region of the UV-B photoreceptor UVR8 initiates signaling through interaction with the COP1 protein. *Proc Natl Acad Sci U S A* **109**: 16366–70
- Clough RC, Jordan-Beebe ET, Lohman KN, Marita JM, Walker JM, Gatz C, Vierstra RD** (1999) Sequences within both the N- and C-terminal domains of phytochrome A are required for PFR ubiquitination and degradation. *Plant J* **17**: 155–167
- Clough RC, Vierstra RD** (1997) Phytochrome degradation. *Plant, Cell Environ* **20**: 713–721
- Clough SJ, Bent AF** (1998) Floral dip: A simplified method for Agrobacterium-mediated transformation of Arabidopsis thaliana. *Plant J* **16**: 735–743
- Colombo M, Suorsa M, Rossi F, Ferrari R, Tadini L, Barbato R, Pesaresi P** (2016) Photosynthesis control: An underrated short-term regulatory mechanism essential for plant viability. *Plant Signal Behav* **11**: e1165382

- Consentino L, Lambert S, Martino C, Jourdan N, Bouchet PE, Witczak J, Castello P, El-Esawi M, Corbineau F, d'Harlingue A, et al** (2015) Blue-light dependent reactive oxygen species formation by Arabidopsis cryptochrome may define a novel evolutionarily conserved signaling mechanism. *New Phytol* **206**: 1450–1462
- Correa-Galvis V, Poschmann G, Melzer M, Stühler K, Jahns P** (2016) PsbS interactions involved in the activation of energy dissipation in Arabidopsis. doi: 10.1038/NPLANTS.2015.225
- Croce R** (2015) PsbS is the plants' pick for sun protection. *Nat Struct Mol Biol* **22**: 650–652
- Croce R, Morosinotto T, Castelletti S, Breton J, Bassi R** (2002) The Lhca antenna complexes of higher plants photosystem I. *Biochim Biophys Acta* **1556**: 29–40
- Cukier RI, Nocera DG** (1998) PROTON-COUPLED ELECTRON TRANSFER. *Annu Rev Phys Chem* **49**: 337–369
- Czarnocka W, Karpiński S** (2018) Friend or foe? Reactive oxygen species production, scavenging and signaling in plant response to environmental stresses. *Free Radic Biol Med* **122**: 4–20
- D'Amico-Damião V, Carvalho RF** (2018) Cryptochrome-related abiotic stress responses in plants. *Front Plant Sci*. doi: 10.3389/fpls.2018.01897
- DalCorso G, Pesaresi P, Masiero S, Aseeva E, Schünemann D, Finazzi G, Joliet P, Barbato R, Leister D** (2008) A Complex Containing PGRL1 and PGR5 Is Involved in the Switch between Linear and Cyclic Electron Flow in Arabidopsis. *Cell* **132**: 273–285
- Dall'Osto L, Cazzaniga S, Wada M, Bassi R** (2014) On the origin of a slowly reversible fluorescence decay component in the Arabidopsis npq4 mutant. *Philos Trans R Soc B Biol Sci*. doi: 10.1098/rstb.2013.0221
- Dall'Osto L, Holt NE, Kaligotla S, Fuciman M, Cazzaniga S, Carbonera D, Frank HA, Alric J, Bassi R** (2012) Zeaxanthin protects plant photosynthesis by modulating chlorophyll triplet yield in specific light-harvesting antenna subunits. *J Biol Chem* **287**: 41820–41834
- Davis MC, Fiehn O, Durnford DG** (2013) Metabolic acclimation to excess light intensity in *Chlamydomonas reinhardtii*. *Plant, Cell Environ* **36**: 1391–1405
- Dekker JP, Van Grondelle R** (2000) Primary charge separation in Photosystem II. *Photosynth Res* **63**: 195–208
- Demarsy E, Goldschmidt-Clermont M, Ulm R** (2018) Coping with 'Dark Sides of the Sun' through Photoreceptor Signaling. *Trends Plant Sci* **23**: 260–271
- Demmig-Adams B** (1990) Carotenoids and photoprotection in plants: A role for the xanthophyll zeaxanthin. *Biochim Biophys Acta - Bioenerg* **1020**: 1–24
- Demmig-Adams B, Adams WW** (1993) The xanthophyll cycle. *Carotenoids Photosynth*. Springer Netherlands, Dordrecht, pp 206–251
- Dietz K-J** (2015) Efficient high light acclimation involves rapid processes at multiple mechanistic levels. doi: 10.1093/jxb/eru505
- Dietz K-J, Pfannschmidt T** (2011) Novel regulators in photosynthetic redox control of plant metabolism and gene expression. *Plant Physiol* **155**: 1477–85
- El-Esawi M, Arthaut LD, Jourdan N, d'Harlingue A, Link J, Martino CF, Ahmad M** (2017) Blue-light induced biosynthesis of ROS contributes to the signaling mechanism of Arabidopsis cryptochrome. *Sci Rep*. doi: 10.1038/s41598-017-13832-z
- Endo T, Shikanai T, Takabayashi A, Asada K, Sato F** (1999) The role of chloroplastic NAD(P)H dehydrogenase in photoprotection. *FEBS Lett* **457**: 5–8
- Engelhard C, Wang X, Robles D, Moldt J, Essen L-O, Batschauer A, Bittl R, Ahmad M** (2014) Cellular metabolites enhance the light sensitivity of Arabidopsis cryptochrome through alternate electron transfer pathways. *Plant Cell* **26**: 4519–31
- Estavillo GM, Crisp PA, Pornsiriwong W, Wirtz M, Collinge D, Carrie C, Giraud E, Whelan J, David P, Javot H, et al** (2011) Evidence for a SAL1-PAP chloroplast retrograde pathway that functions in drought and high light signaling in Arabidopsis. *Plant Cell* **23**: 3992–4012
- Fan DY, Nie Q, Hope AB, Hillier W, Pogson BJ, Chow WS** (2007) Quantification of cyclic electron flow around Photosystem I in spinach leaves during photosynthetic induction. *Photosynth Res* **94**: 347–357

- Fan M, Li M, Liu Z, Cao P, Pan X, Zhang H, Zhao X, Zhang J, Chang W** (2015) Crystal structures of the PsbS protein essential for photoprotection in plants. *Nat Publ Gr.* doi: 10.1038/nsmb.3068
- Fankhauser C, Chen M** (2008) Transposing phytochrome into the nucleus. *Trends Plant Sci* **13**: 596–601
- Fankhauser C, Staiger D** (2002) Photoreceptors in *Arabidopsis thaliana*: light perception, signal transduction and entrainment of the endogenous clock. *Planta* **216**: 1–16
- Fankhauser C, Ulm R** (2011) Light-regulated interactions with SPA proteins underlie cryptochrome-mediated gene expression. *Genes Dev* **25**: 1004–9
- Farmer EE, Mueller MJ** (2013) ROS-Mediated Lipid Peroxidation and RES-Activated Signaling. *Annu Rev Plant Biol* **64**: 429–450
- Fasano R, Gonzalez N, Tosco A, Dal Piaz F, Docimo T, Serrano R, Grillo S, Leone A, Inzé D** (2014) Role of *Arabidopsis* UV RESISTANCE LOCUS 8 in Plant Growth Reduction under Osmotic Stress and Low Levels of UV-B. *Mol Plant* • **7**: 773–791
- Favory J-J, Stec A, Gruber H, Rizzini L, Oravec A, Funk M, Albert A, Cloix C, Jenkins GI, Oakeley EJ, et al** (2009) Interaction of COP1 and UVR8 regulates UV-B-induced photomorphogenesis and stress acclimation in *Arabidopsis*. *EMBO J* **28**: 591–601
- Feng Z, Mao Y, Xu N, Zhang B, Wei P, Yang DL, Wang Z, Zhang Z, Zheng R, Yang L, et al** (2014) Multigeneration analysis reveals the inheritance, specificity, and patterns of CRISPR/Cas-induced gene modifications in *Arabidopsis*. *Proc Natl Acad Sci U S A* **111**: 4632–4637
- Fittinghoff K, Laubinger S, Nixdorf M, Fackendahl P, Baumgardt R-L, Batschauer A, Hoecker U** (2006) Functional and expression analysis of *Arabidopsis* SPA genes during seedling photomorphogenesis and adult growth. *Plant J* **47**: 577–590
- Fortunato AE, Annunziata R, Jaubert M, Bouly J-P, Falciatore A** (2015) Dealing with light: The widespread and multitasking cryptochrome/photolyase family in photosynthetic organisms. *J Plant Physiol* **172**: 42–54
- Fox KF, Balevičius V, Chmeliov J, Valkunas L, Ruban A V, Duffy CDP** (2017) The carotenoid pathway: what is important for excitation quenching in plant antenna complexes? *Phys Chem Chem Phys* **19**: 22957–22968
- Foyer CH** (2018) Reactive oxygen species, oxidative signaling and the regulation of photosynthesis. *Environ Exp Bot* **154**: 134–142
- Franklin KA, Quail PH** (2010) Phytochrome functions in *Arabidopsis* development. *J Exp Bot* **61**: 11–24
- Fromm S, Senkler J, Eubel H, Peterhänsel C, Braun HP** (2016) Life without complex I: Proteome analyses of an *Arabidopsis* mutant lacking the mitochondrial NADH dehydrogenase complex. *J Exp Bot* **67**: 3079–3093
- Fufezan C, Simionato D, Morosinotto T** (2012) Identification of key residues for pH dependent activation of violaxanthin de-epoxidase from *Arabidopsis thaliana*. *PLoS One.* doi: 10.1371/journal.pone.0035669
- Fujiwara M, Nagashima A, Kanamaru K, Tanaka K, Takahashi H** (2000) Three new nuclear genes, sigD, sigE and sigF, encoding putative plastid RNA polymerase sigma factors in *Arabidopsis thaliana*. *FEBS Lett* **481**: 47–52
- Gangappa SN, Babu Rajendra Prasad V, Chattopadhyay S** (2010) Functional interconnection of MYC2 and SPA1 in the photomorphogenic seedling development of *Arabidopsis*. *Plant Physiol* **154**: 1210–1219
- Gangappa SN, Botto JF** (2016) The Multifaceted Roles of HY5 in Plant Growth and Development. *Mol Plant* **9**: 1353–1365
- Gangappa SN, Crocco CD, Johansson H, Datta S, Hettiarachchi C, Holm M, Botto JF** (2013a) The *Arabidopsis* B-BOX protein BBX25 interacts with HY5, negatively regulating BBX22 expression to suppress seedling photomorphogenesis. *Plant Cell* **25**: 1243–1257
- Gangappa SN, Holm M, Botto JF** (2013b) Molecular interactions of BBX24 and BBX25 with HYH, HY5 HOMOLOG, to modulate *Arabidopsis* seedling development. *Plant Signal Behav.* doi: 10.4161/psb.25208
- Gangappa SN, Maurya JP, Yadav V, Chattopadhyay S** (2013c) The Regulation of the Z- and G-Box Containing Promoters by Light Signaling Components, SPA1 and MYC2, in *Arabidopsis*. *PLoS One.* doi: 10.1371/journal.pone.0062194

- Gangappa SN, Srivastava AK, Maurya JP, Ram H, Chattopadhyay S** (2013d) Z-Box binding transcription factors (ZBFs): A new class of transcription factors in arabidopsis seedling development. *Mol Plant* **6**: 1758–1768
- Gao J, Ajjawi I, Manoli A, Sawin A, Xu C, Froehlich JE, Last RL, Benning C** (2009) FATTY ACID DESATURASE4 of Arabidopsis encodes a protein distinct from characterized fatty acid desaturases. *Plant J* **60**: 832–839
- Gärtner W** (2017) In-Planta Expression: Searching for the Genuine Chromophores of Cryptochrome-3 from Arabidopsis thaliana. *Photochem Photobiol* **93**: 382–384
- Ghassemian M, Lutes J, Tepperman JM, Chang HS, Zhu T, Wang X, Quail PH, Markus Lange B** (2006) Integrative analysis of transcript and metabolite profiling data sets to evaluate the regulation of biochemical pathways during photomorphogenesis. *Arch Biochem Biophys* **448**: 45–59
- Gollan PJ, Lima-Melo Y, Tiwari A, Tikkanen M, Aro E-MM** (2017) Interaction between photosynthetic electron transport and chloroplast sinks triggers protection and signalling important for plant productivity. *Philos Trans R Soc B Biol Sci*. doi: 10.1098/rstb.2016.0390
- Gollan PJ, Tikkanen M, Aro EM** (2015) Photosynthetic light reactions: Integral to chloroplast retrograde signalling. *Curr Opin Plant Biol* **27**: 180–191
- Gould KS** (2004) Nature's Swiss Army Knife: The Diverse Protective Roles of Anthocyanins in Leaves. *J Biomed Biotechnol*. doi: 10.1155/S1110724304406147
- Gray JC, Sullivan JA, Wang J-H, Jerome CA, MacLean D** (2003) Coordination of plastid and nuclear gene expression. *Philos Trans R Soc London Ser B Biol Sci* **358**: 135–145
- Gururani MA, Venkatesh J, Tran LSP** (2015) Regulation of photosynthesis during abiotic stress-induced photoinhibition. *Mol Plant* **8**: 1304–1320
- Hahn A, Vonck J, Mills DJ, Meier T, Kühlbrandt W** (2018a) Structure, mechanism, and regulation of the chloroplast ATP synthase. *Science* (80-). doi: 10.1126/science.aat4318
- Hahn F, Eisenhut M, Mantegazza O, Weber A** (2017a) Generation of Targeted Knockout Mutants in Arabidopsis thaliana Using CRISPR/Cas9. *BIO-PROTOCOL*. doi: 10.21769/bioprotoc.2384
- Hahn F, Eisenhut M, Mantegazza O, Weber APM** (2018b) Homology-directed repair of a defective glabrous gene in arabidopsis with cas9-based gene targeting. *Front Plant Sci* **9**: 424
- Hahn F, Mantegazza O, Greiner A, Hegemann P, Eisenhut M, Weber APM** (2017b) An efficient visual screen for CRISPR/CAS9 activity in arabidopsis thaliana. *Front Plant Sci* **8**: 39
- Hasanuzzaman M, Nahar K, Anee TI, Fujita M** (2017) Glutathione in plants: biosynthesis and physiological role in environmental stress tolerance. *Physiol Mol Biol Plants* **23**: 249–268
- Hatier J-HB, Gould KS** (2008) Anthocyanin Function in Vegetative Organs. *Anthocyanins*. Springer New York, New York, NY, pp 1–19
- Havaux M** (2014) Carotenoid oxidation products as stress signals in plants. *Plant J* **79**: 597–606
- Havaux M, Eymery F, Porfirova S, Rey P, Dörmann P** (2005) Vitamin E Protects against Photoinhibition and Photooxidative Stress in *Arabidopsis thaliana*. *Plant Cell* **17**: 3451–3469
- Havaux M, Kloppstech K** (2001) The protective functions of carotenoid and flavonoid pigments against excess visible radiation at chilling temperature investigated in Arabidopsis npq and tt mutants. *Planta* **213**: 953–966
- Hayami N, Sakai Y, Kimura M, Saito T, Tokizawa M, Iuchi S, Kurihara Y, Matsui M, Nomoto M, Tada Y, et al** (2015) The Responses of Arabidopsis Early Light-Induced Protein2 to Ultraviolet B, High Light, and Cold Stress Are Regulated by a Transcriptional Regulatory Unit Composed of Two Elements. *Plant Physiol* **169**: 840–855
- He H, Van Breusegem F, Mhamdi A** (2018) Redox-dependent control of nuclear transcription in plants. *J Exp Bot* **69**: 3359–3372
- Heddad M, Norén H, Reiser V, Dunaeva M, Andersson B, Adamska I** (2006) Differential expression and localization of early light-induced proteins in Arabidopsis. *Plant Physiol* **142**: 75–87
- Heijde M, Binkert M, Yin R, Ares-Orpel F, Rizzini L, Van De Slijke E, Persiau G, Nolf J, Gevaert K, De Jaeger G, et al** (2013) Constitutively active UVR8 photoreceptor variant in Arabidopsis. *Proc Natl Acad Sci U S A* **110**: 20326–20331

- Hirschfeld M, Tepperman JM, Clack T, Quail PH, Sharrock RA** (1998) Coordination of phytochrome levels in phyB mutants of *Arabidopsis* as revealed by apoprotein-specific monoclonal antibodies. *Genetics* **149**: 523–35
- Hisabori T, Sunamura EI, Kim Y, Konno H** (2013) The chloroplast ATP synthase features the characteristic redox regulation machinery. *Antioxidants Redox Signal* **19**: 1846–1854
- Hoang N, Bouly JP, Ahmad M** (2008) Evidence of a light-sensing role for folate in *Arabidopsis* cryptochrome blue-light receptors. *Mol Plant* **1**: 68–74
- Hoecker U** (2005) Regulated proteolysis in light signaling. *Curr Opin Plant Biol* **8**: 469–476
- Holm M, Ma LG, Qu LJ, Deng XW** (2002a) Two interacting bZIP proteins are direct targets of COP1-mediated control of light-dependent gene expression in *Arabidopsis*. *Genes Dev* **16**: 1247–1259
- Holm M, Ma LG, Qu LJ, Deng XW** (2002b) Two interacting bZIP proteins are direct targets of COP1-mediated control of light-dependent gene expression in *Arabidopsis*. *Genes Dev* **16**: 1247–1259
- Holt NE, Fleming GR, Niyogi KK** (2004) Toward an Understanding of the Mechanism of Nonphotochemical Quenching in Green Plants ? *Biochemistry* **43**: 8281–8289
- Holtkotte X, Ponnu J, Ahmad M, Hoecker U** (2017) The blue light-induced interaction of cryptochrome 1 with COP1 requires SPA proteins during *Arabidopsis* light signaling. *PLOS Genet* **13**: e1007044
- Hong GJ, Hu WL, Li JX, Chen XY, Wang LJ** (2009) Increased accumulation of artemisinin and anthocyanins in *Artemisia annua* expressing the *Arabidopsis* blue light receptor CRY1. *Plant Mol Biol Report* **27**: 334–341
- Hu W, Franklin KA, Sharrock RA, Jones MA, Harmer SL, Lagarias JC** (2013) Unanticipated regulatory roles for *Arabidopsis* phytochromes revealed by null mutant analysis. *Proc Natl Acad Sci U S A* **110**: 1542–1547
- Huang X, Ouyang X, Yang P, Lau OS, Chen L, Wei N, Deng XW** (2013) Conversion from CUL4-based COP1-SPA E3 apparatus to UVR8-COP1-SPA complexes underlies a distinct biochemical function of COP1 under UV-B. *Proc Natl Acad Sci U S A* **110**: 16669–16674
- Ishikawa N, Endo T, Sato F** (2008) Electron transport activities of *Arabidopsis thaliana* mutants with impaired chloroplastic NAD(P)H dehydrogenase. *J Plant Res* **121**: 521–526
- Jackowski G, Olkiewicz P, Zelisko A** (2003) The acclimative response of the main light-harvesting chlorophyll a/b-protein complex of photosystem II (LHCII) to elevated irradiances at the level of trimeric subunits. *J Photochem Photobiol B Biol* **70**: 163–170
- Jahns P, Holzwarth AR** (2012) The role of the xanthophyll cycle and of lutein in photoprotection of photosystem II. *Biochim Biophys Acta - Bioenerg* **1817**: 182–193
- Jahns P, Latowski D, Strzalka K** (2009) Mechanism and regulation of the violaxanthin cycle: The role of antenna proteins and membrane lipids. *Biochim Biophys Acta - Bioenerg* **1787**: 3–14
- Jahns P, Wehner A, Paulsen H, Hobe S** (2001) De-epoxidation of violaxanthin after reconstitution into different carotenoid binding sites of light-harvesting complex II. *J Biol Chem* **276**: 22154–9
- Jansen M, Gilmer F, Biskup B, Nagel KA, Rascher U, Fischbach A, Briem S, Dreissen G, Tittmann S, Braun S, et al** (2009) Simultaneous phenotyping of leaf growth and chlorophyll fluorescence via GROWSCREEN FLUORO allows detection of stress tolerance in *Arabidopsis thaliana* and other rosette plants. *Funct Plant Biol* **36**: 902
- Jansson S, Andersson J, Kim SJ, Jackowski G** (2000) An *Arabidopsis thaliana* protein homologous to cyanobacterial high-light-inducible proteins. *Plant Mol Biol* **42**: 345–51
- Jiang M, Ren L, Lian H, Liu Y, Chen H** (2016) Novel insight into the mechanism underlying light-controlled anthocyanin accumulation in eggplant (*Solanum melongena* L.). *Plant Sci* **249**: 46–58
- Jiao Y, Lau OS, Deng XW** (2007) Light-regulated transcriptional networks in higher plants. *Nat Rev Genet* **8**: 217–230
- Jing Y, Zhang D, Wang X, Tang W, Wang W, Huai J, Xu G, Chen D, Li Y, Lin R** (2013) *Arabidopsis* chromatin remodeling factor PICKLE interacts with transcription factor HY5 to regulate hypocotyl cell elongation. *Plant Cell* **25**: 242–256
- Job N, Yadukrishnan P, Bursch K, Datta S, Johansson H** (2018) Two B-box proteins regulate photomorphogenesis by oppositely modulating HY5 through their diverse C-terminal domains. *Plant Physiol* **176**: 2963–2976

- Joliot P, Johnson GN** (2011) Regulation of cyclic and linear electron flow in higher plants. *Proc Natl Acad Sci U S A* **108**: 13317–22
- Jun L, Saiki R, Tatsumi K, Nakagawa T, Kawamukai M** (2004) Identification and Subcellular Localization of Two Solanelyl Diphosphate Synthases from *Arabidopsis thaliana*. *Plant Cell Physiol* **45**: 1882–1888
- Junge W, Nelson N** (2015) ATP Synthase. *Annu Rev Biochem* **84**: 631–657
- Kadota K, Furutani R, Makino A, Suzuki Y, Wada S, Miyake C** (2019) Oxidation of P700 induces alternative electron flow in photosystem I in wheat leaves. *Plants*. doi: 10.3390/plants8060152
- Kalituho L, Beran KC, Jahns P** (2007) The Transiently Generated Nonphotochemical Quenching of Excitation Energy in *Arabidopsis* Leaves Is Modulated by Zeaxanthin. *Plant Physiol* **143**: 1861–1870
- Kami C, Lorrain SS, Hornitschek P, Fankhauser C** (2010) Light-regulated plant growth and development. *Curr. Top. Dev. Biol.* Academic Press Inc., pp 29–66
- Kanazawa A, Ostendorf E, Kohzuma K, Hoh D, Strand DD, Sato-Cruz M, Savage L, Cruz JA, Fisher N, Froehlich JE, et al** (2017) Chloroplast ATP synthase modulation of the thylakoid proton motive force: implications for photosystem I and photosystem II photoprotection. *Front Plant Sci*. doi: 10.3389/fpls.2017.00719
- Karpinski S, Escobar C, Karpinska B, Creissen G, Mullineaux PM** (1997) Photosynthetic electron transport regulates the expression of cytosolic ascorbate peroxidase genes in *Arabidopsis* during excess light stress. *Plant Cell* **9**: 627–640
- Kawashima R, Sato R, Harada K, Masuda S** (2017) Relative contributions of PGR5- and NDH-dependent photosystem I cyclic electron flow in the generation of a proton gradient in *Arabidopsis* chloroplasts. *Planta* **246**: 1045–1050
- Keller MM, Jaillais Y, Pedmale U V, Moreno JE, Chory J, Ballaré CL** (2011) Cryptochrome 1 and phytochrome B control shade-avoidance responses in *Arabidopsis* via partially independent hormonal cascades. *Plant J* **67**: 195–207
- Kendrick RE, Kronenberg GHM, eds** (1994) Photomorphogenesis in Plants. doi: 10.1007/978-94-011-1884-2
- Kleine T, Kindgren P, Benedict C, Hendrickson L, Strand A** (2007) Genome-wide gene expression analysis reveals a critical role for CRYPTOCHROME1 in the response of *Arabidopsis* to high irradiance. *Plant Physiol* **144**: 1391–1406
- Kleine T, Leister D** (2016) Retrograde signaling: Organelles go networking. *Biochim Biophys Acta - Bioenerg* **1857**: 1313–1325
- Kleine T, Lockhart P, Batschauer A** (2003) An *Arabidopsis* protein closely related to *Synechocystis* cryptochrome is targeted to organelles. *Plant J* **35**: 93–103
- Kleiner O, Kircher S, Harter K, Batschauer A** (1999) Nuclear localization of the *Arabidopsis* blue light receptor cryptochrome 2. *Plant J* **19**: 289–96
- Kliebenstein DJ, Lim JE, Landry LG, Last RL** (2002) *Arabidopsis* UVR8 regulates ultraviolet-B signal transduction and tolerance and contains sequence similarity to human regulator of chromatin condensation 1. *Plant Physiol* **130**: 234–43
- Kong S-G, Suetsugu N, Kikuchi S, Nakai M, Nagatani A, Wada M** (2013) Both Phototropin 1 and 2 Localize on the Chloroplast Outer Membrane with Distinct Localization Activity. *Plant Cell Physiol* **54**: 80–92
- Kong S-G, Suzuki T, Tamura K, Mochizuki N, Hara-Nishimura I, Nagatani A** (2006) Blue light-induced association of phototropin 2 with the Golgi apparatus. *Plant J* **45**: 994–1005
- Kono M, Noguchi K, Terashima I** (2014) Roles of the cyclic electron flow around PSI (CEF-PSI) and O₂-dependent alternative pathways in regulation of the photosynthetic electron flow in short-term fluctuating light in *Arabidopsis thaliana*. *Plant Cell Physiol* **55**: 990–1004
- Kono M, Terashima I** (2014) Long-term and short-term responses of the photosynthetic electron transport to fluctuating light. *J Photochem Photobiol B* **137**: 89–99
- Kono M, Terashima I** (2016) Elucidation of photoprotective mechanisms of PSI against fluctuating light photoinhibition. *Plant Cell Physiol* **57**: 1405–1414

- Kono M, Yamori W, Suzuki Y, Terashima I** (2017) Photoprotection of PSI by Far-Red Light Against the Fluctuating Light-Induced Photoinhibition in *Arabidopsis thaliana* and Field-Grown Plants *Masaru*. **58**: 35–45
- Kornas A, Kuźniak E, Slesak I, Miszalski Z** (2010) The key role of the redox status in regulation of metabolism in photosynthesizing organisms. *Acta Biochim Pol* **57**: 143–51
- Kou J, Takahashi S, Fan DY, Badger MR, Chow WS** (2015) Partially dissecting the steady-state electron fluxes in photosystem I in wild-type and *pgr5* and *ndh* mutants of *Arabidopsis*. *Front Plant Sci*. doi: 10.3389/fpls.2015.00758
- Krahmer J, Ganpudi A, Abbas A, Romanowski A, Halliday KJ** (2018) Phytochrome, carbon sensing, metabolism, and plant growth plasticity. *Plant Physiol* **176**: 1039–1048
- Kreslavski VD, Los DA, Schmitt FJ, Zharmukhamedov SK, Kuznetsov V V., Allakhverdiev SI** (2018) The impact of the phytochromes on photosynthetic processes. *Biochim Biophys Acta - Bioenerg* **1859**: 400–408
- Kress E, Jahns P** (2017) The Dynamics of Energy Dissipation and Xanthophyll Conversion in *Arabidopsis* Indicate an Indirect Photoprotective Role of Zeaxanthin in Slowly Inducible and Relaxing Components of Non-photochemical Quenching of Excitation Energy. *Front Plant Sci*. doi: 10.3389/fpls.2017.02094
- Krieger-Liszkay A** (2005) Singlet oxygen production in photosynthesis. *J. Exp. Bot.* pp 337–346
- Kudoh H, Sonoike AK** Irreversible damage to photosystem I by chilling in the light: cause of the degradation of chlorophyll after returning to normal growth temperature. doi: 10.1007/s00425-002-0790-9
- Lange BM, Ghassemian M** (2003) Genome organization in *Arabidopsis thaliana*: A survey for genes involved in isoprenoid and chlorophyll metabolism. *Plant Mol Biol* **51**: 925–948
- Larkin RM, Alonso JM, Ecker JR, Chory J** (2003) GUN4, a Regulator of Chlorophyll Synthesis and Intracellular Signaling. *Science* (80-) **299**: 902–906
- Larkin RM, Ruckle ME** (2008) Integration of light and plastid signals. *Curr Opin Plant Biol* **11**: 593–599
- Latowski D, Burda K, Strzałka K** (2000) A mathematical model describing kinetics of conversion of violaxanthin to zeaxanthin via intermediate antheraxanthin by the xanthophyll cycle enzyme violaxanthin de-epoxidase. *J Theor Biol* **206**: 507–514
- Latowski D, Kruk J, Burda K, Skrzynecka-Jaskier M, Kostecka-Gugała A, Strzałka K** (2002) Kinetics of violaxanthin de-epoxidation by violaxanthin de-epoxidase, a xanthophyll cycle enzyme, is regulated by membrane fluidity in model lipid bilayers. *Eur J Biochem* **269**: 4656–4665
- Lau K, Podolec R, Chappuis R, Ulm R, Hothorn M** (2019a) Plant photoreceptors and their signaling components compete for COP 1 binding via VP peptide motifs. *EMBO J*. doi: 10.15252/embj.2019102140
- Lau K, Podolec R, Chappuis R, Ulm R, Hothorn M** (2019b) Plant photoreceptors and their signaling components compete for binding to the ubiquitin ligase COP1 using their VP-peptide motifs. *bioRxiv* 568618
- Lee J, He K, Stolz V, Lee H, Figueroa P, Gao Y, Tongprasit W, Zhao H, Lee I, Xing WD** (2007) Analysis of transcription factor HY5 genomic binding sites revealed its hierarchical role in light regulation of development. *Plant Cell* **19**: 731–749
- Van Leene J, Witters E, Inzé D, De Jaeger G, Inzé D, De Jaeger G** (2008) Boosting tandem affinity purification of plant protein complexes. *Trends Plant Sci* **13**: 517–520
- Leister D** (2017) Piecing the Puzzle Together: The Central Role of Reactive Oxygen Species and Redox Hubs in Chloroplast Retrograde Signaling. *Antioxid Redox Signal* **30**: 1206–1219
- Leister D, Wang L, Kleine T** (2017) Organellar Gene Expression and Acclimation of Plants to Environmental Stress. *Front Plant Sci* **8**: 387
- Leivar P, Monte E** (2014) PIFs: Systems integrators in plant development. *Plant Cell* **26**: 56–78
- Leivar P, Quail PH** (2011) PIFs: Pivotal components in a cellular signaling hub. *Trends Plant Sci* **16**: 19–28
- Leivar P, Tepperman JM, Monte E, Calderon RH, Liu TL, Quail PH** (2009) Definition of early transcriptional circuitry involved in light-induced reversal of PIF-imposed repression of photomorphogenesis in young *Arabidopsis* seedlings. *Plant Cell* **21**: 3535–3553
- Li L, Aro EM, Millar AH** (2018) Mechanisms of Photodamage and Protein Turnover in Photoinhibition. *Trends Plant Sci* **23**: 667–676

- Li L, Nelson CJ, Trösch J, Castleden I, Huang S, Millar AH** (2017) Protein degradation rate in *Arabidopsis thaliana* leaf growth and development. *Plant Cell* **29**: 207–228
- Li X-P, Gilmore AM, Caffarri S, Bassi R, Golan T, Kramer D, Niyogi KK** (2004) Regulation of Photosynthetic Light Harvesting Involves Intrathylakoid Lumen pH Sensing by the PsbS Protein. *J Biol Chem* **279**: 22866–22874
- Li X-P, Muller-Moule P, Gilmore AM, Niyogi KK** (2002) PsbS-dependent enhancement of feedback de-excitation protects photosystem II from photoinhibition. *Proc Natl Acad Sci U S A* **99**: 15222–7
- Liguori N, Campos SRR, António A, Baptista M, Croce R** (2019) Molecular Anatomy of Plant Photoprotective Switches: The Sensitivity of PsbS to the Environment, Residue by Residue. doi: 10.1021/acs.jpcclett.9b00437
- Lima-Melo Y, Alencar VTCB, Lobo AKM, Sousa RHV, Tikkanen M, Aro EM, Silveira JAG, Gollan PJ** (2019a) Photoinhibition of photosystem I provides oxidative protection during imbalanced photosynthetic electron transport in *Arabidopsis thaliana*. *Front Plant Sci* **10**: 1–13
- Lima-Melo Y, Gollan PJ, Tikkanen M, Silveira JAG, Aro EM** (2019b) Consequences of photosystem-I damage and repair on photosynthesis and carbon use in *Arabidopsis thaliana*. *Plant J* **97**: 1061–1072
- Lin C** (2002) Blue light receptors and signal transduction. *Plant Cell* **14 Suppl**: S207-25
- Lin C, Ahmad M, Cashmore AR** (1996) *Arabidopsis* cryptochrome 1 is a soluble protein mediating blue light-dependent regulation of plant growth and development. *Plant J* **10**: 893–902
- Lin C, Shalitin D** (2003) CRYPTOCHROME STRUCTURE AND SIGNAL TRANSDUCTION. *Annu Rev Plant Biol* **54**: 469–496
- Lin C, Todo T** (2005) The cryptochromes. *Genome Biol* **6**: 220
- Lin C, Yang H, Guo H, Mockler T, Chen J, Cashmore AR** (1998) Enhancement of blue-light sensitivity of *Arabidopsis* seedlings by a blue light receptor cryptochrome 2. *Plant Biol* **95**: 2686–2690
- Lin YP, Wu MC, Chang YY** (2016) Identification of a chlorophyll dephytylase involved in chlorophyll turnover in *Arabidopsis*. *Plant Cell* **28**: 2974–2990
- Liscum E** (2016) Blue Light-Induced Intracellular Movement of Phototropins: Functional Relevance or Red Herring? *Front Plant Sci* **7**: 827
- Liu B, Yang Z, Gomez A, Liu B, Lin C, Oka Y** (2016) Signaling mechanisms of plant cryptochromes in *Arabidopsis thaliana*. *J Plant Res*. doi: 10.1007/s10265-015-0782-z
- Liu CC, Ahammed GJ, Wang GT, Xu CJ, Chen KS, Zhou YH, Yu JQ** (2018) Tomato CRY1a plays a critical role in the regulation of phytohormone homeostasis, plant development, and carotenoid metabolism in fruits. *Plant Cell Environ* **41**: 354–366
- Liu Q, Wang Q, Deng W, Wang X, Piao M, Cai D, Li Y, Barshop WD, Yu X, Zhou T, et al** (2017) Molecular basis for blue light-dependent phosphorylation of *Arabidopsis* cryptochrome 2. *Nat Commun* **8**: 15234
- Liu Z, Yan H, Wang K, Kuang T, Zhang J, Gui L, An X, Chang W** (2004a) Crystal structure of spinach major light-harvesting complex at 2.72 Å resolution.
- Liu Z, Yan H, Wang K, Kuang T, Zhang J, Gui L, An X, Chang W** (2004b) Crystal structure of spinach major light-harvesting complex at 2.72 Å resolution. *Nature* **428**: 287–292
- Llamas E, Pulido P, Rodriguez-Concepcion M** (2017) Interference with plastome gene expression and Clp protease activity in *Arabidopsis* triggers a chloroplast unfolded protein response to restore protein homeostasis. *PLOS Genet* **13**: e1007022
- Lu X-D, Zhou C-M, Xu P-B, Luo Q, Lian H-L, Yang H-Q** (2015a) Red-light-dependent interaction of phyB with SPA1 promotes COP1-SPA1 dissociation and photomorphogenic development in *Arabidopsis*. *Mol Plant* **8**: 467–78
- Lu XD, Zhou CM, Xu PB, Luo Q, Lian HL, Yang HQ** (2015b) Red-light-dependent interaction of phyB with SPA1 promotes COP1-SPA1 dissociation and photomorphogenic development in *Arabidopsis*. *Mol Plant* **8**: 467–478
- Maier A, Hoecker U** (2015) COP1/SPA ubiquitin ligase complexes repress anthocyanin accumulation under low light and high light conditions. *Plant Signal Behav* **10**: e970440-1-e970440-3
- Malnoë A** (2018) Photoinhibition or photoprotection of photosynthesis? Update on the (newly termed) sustained quenching component qH. *Environ Exp Bot* **154**: 123–133

- Malnoë A, Schultink A, Shahrasbi S, Rumeau D, Havaux M, Niyogi KK** (2018) The plastid lipocalin LCNP is required for sustained photoprotective energy dissipation in arabidopsis. *Plant Cell* **30**: 196–208
- Mansour Karimi DI and AD** (2002) GATEWAY™vectors for Agrobacterium -mediated plant transformation. *Tech Appl GATEWAY™vectors* **7**: 193–195
- Mao J, Zhang Y-C, Sang Y, Li Q-H, Yang H-Q** (2005) From The Cover: A role for Arabidopsis cryptochromes and COP1 in the regulation of stomatal opening. *Proc Natl Acad Sci U S A* **102**: 12270–5
- Martín M, Noarbe DM, Serrot PH, Sabater B** (2015) The rise of the photosynthetic rate when light intensity increases is delayed in *ndh* gene-defective tobacco at high but not at low CO₂ concentrations. *Front Plant Sci* **6**: 34
- Matsumoto N, Hirano T, Iwasaki T, Yamamoto N** (2003) Functional Analysis and Intracellular Localization of Rice Cryptochromes. *PLANT Physiol* **133**: 1494–1503
- Mazor Y, Borovikova A, Caspy I, Nelson N** (2017) Structure of the plant photosystem I supercomplex at 2.6 Å resolution. *Nat Plants* **3**: 17014
- Mazor Y, Borovikova A, Nelson N** (2015) The structure of plant photosystem I super-complex at 2.8 Å resolution. *Elife* **4**: e07433
- Mekala NR, Suorsa M, Rantala M, Aro E-M, Tikkanen M** (2015) Plants Actively Avoid State Transitions upon Changes in Light Intensity: Role of Light-Harvesting Complex II Protein Dephosphorylation in High Light 1[OPEN]. *Plant Physiol* **168**: 721–734
- Mellenthin M, Ellersiek U, Börger A, Baier M** (2014) Expression of the Arabidopsis Sigma Factor SIG5 Is Photoreceptor and Photosynthesis Controlled. *Plants (Basel, Switzerland)* **3**: 359–91
- Millenaar FF, Van Zanten M, Cox MCH, Pierik R, Voeselek LACJ, Peeters AJM** (2009) Differential petiole growth in Arabidopsis thaliana: photocontrol and hormonal regulation. *New Phytol* **184**: 141–152
- Miret JA, Munné-Bosch S** (2015) Redox signaling and stress tolerance in plants: a focus on vitamin E. *Ann N Y Acad Sci* **1340**: 29–38
- Mishra S, Khurana JP** (2017) Emerging Roles and New Paradigms in Signaling Mechanisms of Plant Cryptochromes. *CRC Crit Rev Plant Sci* **36**: 89–115
- Mishra Y, Jänkänpää HJ, Kiss AZ, Funk C, Schröder WP, Jansson S** (2012) Arabidopsis plants grown in the field and climate chambers significantly differ in leaf morphology and photosystem components. *BMC Plant Biol* **12**: 6
- Mitchell P** (2011) Chemiosmotic coupling in oxidative and photosynthetic phosphorylation. *Biochim Biophys Acta - Bioenerg* **1807**: 1507–1538
- Mitchell P** (1975) The protonmotive Q cycle: A general formulation. *FEBS Lett* **59**: 137–139
- Mochizuki N, Brusslan JA, Larkin R, Nagatani A, Chory J** (2001) Arabidopsis genomes uncoupled 5 (GUN5) mutant reveals the involvement of Mg-chelatase H subunit in plastid-to-nucleus signal transduction. *Proc Natl Acad Sci U S A* **98**: 2053–8
- Mockler TC** (1999) Photoreceptors and Arabidopsis flowering time.
- Morosinotto T, Caffarri S, Dall’Osto L, Bassi R** (2003) Mechanistic aspects of the xanthophyll dynamics in higher plant thylakoids. *Physiol Plant* **119**: 347–354
- Müller P, Li X-P, Niyogi KK** (2001) Update on Photosynthesis Non-Photochemical Quenching. A Response to Excess Light Energy 1.
- Mullineaux PM, Exposito-Rodriguez M, Laissue PP, Smirnov N, Park E** (2020) Spatial chloroplast-to-nucleus signalling involving plastid–nuclear complexes and stromules. *Philos Trans R Soc B Biol Sci* **375**: 20190405
- Munekage Y, Hashimoto M, Miyake C, Tomizawa K-I, Endo T, Tasaka M, Shikanai T** (2004) Cyclic electron flow around photosystem I is essential for photosynthesis.
- Munekage Y, Hojo M, Meurer J, Endo T, Tasaka M, Shikanai T** (2002) PGR5 is involved in cyclic electron flow around photosystem I and is essential for photoprotection in Arabidopsis. *Cell* **110**: 361–71
- Munekage YN, Genty B, Peltier G** (2008) Effect of PGR5 impairment on photosynthesis and growth in Arabidopsis thaliana. *Plant Cell Physiol* **49**: 1688–1698

- Murashige T, Skoog F** (1962) A Revised Medium for Rapid Growth and Bio Assays with Tobacco Tissue Cultures. *Physiol Plant* **15**: 473–497
- Nagashima A, Hanaoka M, Shikanai T, Fujiwara M, Kanamaru K, Takahashi H, Tanaka K** (2004) The Multiple-Stress Responsive Plastid Sigma Factor, SIG5, Directs Activation of the psbD Blue Light-Responsive Promoter (BLRP) in *Arabidopsis thaliana*. *Plant Cell Physiol* **45**: 357–368
- Nelson N, Yocum CF** (2006) STRUCTURE AND FUNCTION OF PHOTOSYSTEMS I AND II. *Annu Rev Plant Biol* **57**: 521–565
- Ngoc Pham V, Kumar Kathare P, Huq E** (2018) Update on Phytochromes and Phytochrome Interacting Factors
Phytochromes and Phytochrome Interacting Factors 1[OPEN] The basic helix-loop-helix domain-containing transcription factors that interact physically with the. doi: 10.1104/pp.17.01384
- Niedermaier S, Schneider T, Bahl M-O, Matsubara S, Pitter F, Faculty M, Huesgen PF** (2020) Photoprotective acclimation of the *Arabidopsis thaliana* leaf proteome to fluctuating light. *Front Genet* **11**: 154
- Nikkanen L, Rintamäki E** (2019) Chloroplast thioredoxin systems dynamically regulate photosynthesis in plants. *Biochem J* **476**: 1159–1172
- Nikkanen L, Rintamäki E** (2014) Thioredoxin-dependent regulatory networks in chloroplasts under fluctuating light conditions. *Philos Trans R Soc Lond B Biol Sci* **369**: 20130224
- Nikkanen L, Toivola J, Rintamäki E** (2016) Crosstalk between chloroplast thioredoxin systems in regulation of photosynthesis. *Plant Cell Environ* **39**: 1691–1705
- Nikkanen L, Toivola J, Trotta A, Diaz MG, Tikkanen M, Aro EM, Rintamäki E** (2018) Regulation of cyclic electron flow by chloroplast NADPH-dependent thioredoxin system. *Plant Direct*. doi: 10.1002/pld3.93
- Nilkens M, Kress E, Lambrev P, Miloslavina Y, Müller M, Holzwarth AR, Jahns P** (2010) Identification of a slowly inducible zeaxanthin-dependent component of non-photochemical quenching of chlorophyll fluorescence generated under steady-state conditions in *Arabidopsis*. *Biochim Biophys Acta - Bioenerg* **1797**: 466–475
- Ninu L, Ahmad M, Miarelli C, Cashmore AR, Giuliano G** (1999) Cryptochrome 1 controls tomato development in response to blue light. *Plant J* **18**: 551–556
- Nisar N, Li L, Lu S, Khin NC, Pogson BJ** (2015) Carotenoid Metabolism in Plants. *Mol Plant* **8**: 68–82
- Nishio JN, Whitmarsh J** (1993) Dissipation of the Proton Electrochemical Potential in Intact Chloroplasts (II. The pH Gradient Monitored by Cytochrome f Reduction Kinetics). *Plant Physiol* **101**: 89–96
- Niyogi KK** (1999a) PHOTOPROTECTION REVISITED: *Genetic and Molecular Approaches*. *Annu Rev Plant Physiol Plant Mol Biol* **50**: 333–359
- Niyogi KK** (1999b) PHOTOPROTECTION REVISITED: Genetic and Molecular Approaches.
- Niyogi KK, Bjorkman O, Grossman AR** (1997a) *Chlamydomonas* Xanthophyll Cycle Mutants Identified by Video Imaging of Chlorophyll Fluorescence Quenching. *Plant Cell* **9**: 1369–1380
- Niyogi KK, Björkman O, Grossman AR** (1997b) The roles of specific xanthophylls in photoprotection. *Proc Natl Acad Sci U S A* **94**: 14162–7
- Niyogi KK, Grossman AR, Björkman O** (1998) *Arabidopsis* mutants define a central role for the xanthophyll cycle in the regulation of photosynthetic energy conversion. *Plant Cell* **10**: 1121–34
- Niyogi KK, Li X-P, Björkman O, Shih C, Grossman AR, Rosenquist M, Jansson S** (2000) A pigment-binding protein essential for regulation of photosynthetic light harvesting. *Nature* **403**: 391–395
- Noctor G, Reichheld J-P, Foyer CH** (2018) ROS-related redox regulation and signaling in plants. *Semin Cell Dev Biol* **80**: 3–12
- Noctor G, Veljovic-Jovanovic S, Foyer CH** (2000) Peroxide processing in photosynthesis: antioxidant coupling and redox signalling. *Philos Trans R Soc Lond B Biol Sci* **355**: 1465–75
- Ongishi M, Saji K, Okada K, Sakai T** (2004) Functional analysis of each blue light receptor, cry1, cry2, phot1, and phot2, by using combinatorial multiple mutants in *Arabidopsis*. *Proc Natl Acad Sci U S A* **101**: 2223–2228

- Onda Y, Yagi Y, Saito Y, Takenaka N, Toyoshima Y** (2008) Light induction of Arabidopsis SIG1 and SIG5 transcripts in mature leaves: Differential roles of cryptochrome 1 and cryptochrome 2 and dual function of SIG5 in the recognition of plastid promoters. *Plant J* **55**: 968–978
- Öquist G, Huner NPA** (2003) P HOTOSYNTHESIS OF O VERWINTERING E VERGREEN P LANTS. *Annu Rev Plant Biol* **54**: 329–355
- Osterlund MT, Wei N, Deng XW** (2000) The roles of photoreceptor systems and the COP1-targeted destabilization of HY5 in light control of Arabidopsis seedling development. *Plant Physiol* **124**: 1520–4
- Otani T, Kato Y, Shikanai T** (2018) Specific substitutions of light-harvesting complex I proteins associated with photosystem I are required for supercomplex formation with chloroplast NADH dehydrogenase-like complex. *Plant J* **94**: 122–130
- PAGE M, SULTANA N, PASZKIEWICZ K, FLORANCE H, SMIRNOFF N** (2012) The influence of ascorbate on anthocyanin accumulation during high light acclimation in Arabidopsis thaliana: further evidence for redox control of anthocyanin synthesis. *Plant Cell Environ* **35**: 388–404
- Pan X, Li M, Wan T, Wang L, Jia C, Hou Z, Zhao X, Zhang J, Chang W** (2011) Structural insights into energy regulation of light-harvesting complex CP29 from spinach. *Nat Struct Mol Biol* **18**: 309–315
- Park' Y-L, Chow WS, Anderson JM** (1997) Antenna Size Dependency of Photoinactivation of Photosystem II in Light-Acclimated Pea Leaves.
- Pearce S, Kippes N, Chen A, Debernardi JM, Dubcovsky J** (2016) RNA-seq studies using wheat PHYTOCHROME B and PHYTOCHROME C mutants reveal shared and specific functions in the regulation of flowering and shade-avoidance pathways. *BMC Plant Biol* **16**: 141
- Peltier G, Aro E-M, Shikanai T** NDH-1 and NDH-2 Plastoquinone Reductases in Oxygenic Photosynthesis. *Annu Rev Plant Biol* **67**: 55–80
- Pérez-Ruiz JM, Spínola MC, Kirchsteiger K, Moreno J, Sahrawy M, Cejudo FJ** (2006) Rice NTRC is a high-efficiency redox system for chloroplast protection against oxidative damage. *Plant Cell* **18**: 2356–2368
- Pesaresi P, Hertle A, Pribil M, Kleine T, Wagner R, Strissel H, Ihnatowicz A, Bonardi V, Scharfenberg M, Schneider A, et al** (2009) Arabidopsis STN7 kinase provides a link between short- and long-term photosynthetic acclimation. *Plant Cell* **21**: 2402–23
- Pesaresi P, Hertle A, Pribil M, Schneider A, Kleine T, Leister D** (2010) Optimizing photosynthesis under fluctuating light: the role of the Arabidopsis STN7 kinase. *Plant Signal Behav* **5**: 21–5
- Pesaresi P, Kim C, Kim · Chanhong, Kim C** (2019) Current understanding of GUN1: a key mediator involved in biogenic retrograde signaling. *Plant Cell Rep* **38**: 819–823
- Petersen J, Förster K, Turina P, Gräber P** (2012) Comparison of the H⁺/ATP ratios of the H⁺-ATP synthases from yeast and from chloroplast. *Proc Natl Acad Sci U S A* **109**: 11150–11155
- Petroutsos D, Tokutsu R, Maruyama S, Flori S, Greiner A, Magneschi L, Cusant L, Kottke T, Mittag M, Hegemann P, et al** (2016) A blue-light photoreceptor mediates the feedback regulation of photosynthesis. *Nature* **537**: 563–566
- Pfalz J, Liebers M, Hirth M, Grübler B, Holtzegel U, Schröter Y, Dietzel L, Pfannschmidt T** (2012) Environmental control of plant nuclear gene expression by chloroplast redox signals. *Front Plant Sci* **3**: 257
- Phua SY, Yan D, Chan KX, Estavillo GM, Nambara E, Pogson BJ** (2018) The Arabidopsis SAL1-PAP Pathway: A Case Study for Integrating Chloroplast Retrograde, Light and Hormonal Signaling in Modulating Plant Growth and Development? *Front Plant Sci*. doi: 10.3389/fpls.2018.01171
- Pinnola A, Bassi R** (2018) Molecular mechanisms involved in plant photoprotection. *Biochem Soc Trans* **46**: 467–482
- Podolec R, Ulm R** (2018) Photoreceptor-mediated regulation of the COP1/SPA E3 ubiquitin ligase. *Curr Opin Plant Biol* **45**: 18–25
- Pogson BJ, Woo NS, Förster B, Small ID** (2008) Plastid signalling to the nucleus and beyond. *Trends Plant Sci* **13**: 602–609

- Pokorny R, Klar T, Hennecke U, Carell T, Batschauer A, Essen L-O** (2008) Recognition and repair of UV lesions in loop structures of duplex DNA by DASH-type cryptochrome. *Proc Natl Acad Sci U S A* **105**: 21023–7
- Porra RJ** (2002) The chequered history of the development and use of simultaneous equations for the accurate determination of chlorophylls a and b. *Photosynth Res* **73**: 149–156
- Pospišil P** (2016) Production of Reactive Oxygen Species by Photosystem II as a Response to Light and Temperature Stress. *Front Plant Sci* **7**: 1950
- Pribil M, Pesaresi P, Hertle A, Barbato R, Leister D** (2010) Role of plastid protein phosphatase TAP38 in LHCII dephosphorylation and thylakoid electron flow. *PLoS Biol* **8**: e1000288
- Quail PH** (1994) Phytochrome genes and their expression. *Photomorphogenesis. Plants*. Springer Netherlands, Dordrecht, pp 71–104
- Ramel F, Birtic S, Ginies C, Soubigou-Taconnat L, Triantaphylidès C, Havaux M** (2012) Carotenoid oxidation products are stress signals that mediate gene responses to singlet oxygen in plants. *Proc Natl Acad Sci U S A* **109**: 5535–40
- Ranjan A, Dickopf S, Ullrich KK, Rensing SA, Hoecker U** (2014) Functional analysis of COP1 and SPA orthologs from *Physcomitrella* and rice during photomorphogenesis of transgenic *Arabidopsis* reveals distinct evolutionary conservation. *BMC Plant Biol* **14**: 178
- Rantala S, Lempiäinen T, Gerotto C, Tiwari A, Aro EM, Tikkanen M** (2020) PGR5 and NDH-1 systems do not function as protective electron acceptors but mitigate the consequences of PSI inhibition. *Biochim Biophys Acta - Bioenerg*. doi: 10.1016/j.bbabi.2020.148154
- Rattanapisit K, Cho M-H, Bhoo SH** (2016) Lysine 206 in *Arabidopsis* phytochrome A is the major site for ubiquitin-dependent protein degradation. *J Biochem* **159**: 161–9
- Reed JW, Nagpal P, Poole DS, Furuya M, Chory J** (1993) Mutations in the gene for the red/far-red light receptor phytochrome B alter cell elongation and physiological responses throughout *arabidopsis* development. *Plant Cell* **5**: 147–157
- Reinhold C, Niczyporuk S, Beran KC, Jahns P** (2008) Short-term down-regulation of zeaxanthin epoxidation in *Arabidopsis thaliana* in response to photo-oxidative stress conditions. *Biochim Biophys Acta - Bioenerg* **1777**: 462–469
- Richter AS, Tohge T, Fernie AR, Grimm B** (2020) The genomes uncoupled-dependent signalling pathway coordinates plastid biogenesis with the synthesis of anthocyanins. *Philos Trans R Soc B Biol Sci*. doi: 10.1098/rstb.2019.0403
- Rizzini L, Favory J-J, Cloix C, Faggionato D, O'Hara A, Kaiserli E, Baumeister R, Schafer E, Nagy F, Jenkins GI, et al** (2011a) Perception of UV-B by the *Arabidopsis* UVR8 Protein. *Science* (80-) **332**: 103–106
- Rizzini L, Favory JJ, Cloix C, Faggionato D, O'Hara A, Kaiserli E, Baumeister R, Schäfer E, Nagy F, Jenkins GI, et al** (2011b) Perception of UV-B by the *arabidopsis* UVR8 protein. *Science* (80-) **332**: 103–106
- Rockwell NC, Lagarias JC** (2010) A brief history of phytochromes. *Chemphyschem* **11**: 1172–80
- Rockwell NC, Su Y-S, Lagarias JC** (2006) Phytochrome structure and signaling mechanisms. *Annu Rev Plant Biol* **57**: 837–58
- Rolland N, Kosmala A, Santabarbara S, Johnson GN, E Miller MA, Karim MF, Mae M, Selley J, Knight D, Hubbard SJ** (2017) Dynamic Acclimation to High Light in *Arabidopsis thaliana* Involves Widespread Reengineering of the Leaf Proteome. doi: 10.3389/fpls.2017.01239
- Roman Kouřil, Agnieszka Zygadlo, Ana A. Arteni ‡, Chantal D. de Wit II, Jan P. Dekker II, Poul Erik Jensen §, Henrik Vibe Scheller § and, Egbert J. Boekema** (2005) Structural Characterization of a Complex of Photosystem I and Light-Harvesting Complex II of *Arabidopsis thaliana*†. doi: 10.1021/BI051097A
- Roose JL, Frankel LK, Mummadisetti MP, Bricker TM** (2016) The extrinsic proteins of photosystem II: update. *Planta* **243**: 889–908
- Ruckle ME, Burgoon LD, Lawrence LA, Sinkler CA, Larkin RM** (2012) Plastids Are Major Regulators of Light Signaling in *Arabidopsis* 1[W][OA]. doi: 10.1104/pp.112.193599
- Ruckle ME, DeMarco SM, Larkin RM** (2007) Plastid Signals Remodel Light Signaling Networks and Are Essential for Efficient Chloroplast Biogenesis in *Arabidopsis*. *Plant Cell* **19**: 3944–3960

- Ruckle ME, Larkin RM** (2009) Plastid signals that affect photomorphogenesis in. *New Phytol* **367**–379
- Rusaczonok A, Czarnocka W, Kacprzak S, Wito? D, ?lesak I, Szechy?ska-Hebda M, Gawro?ski P, Karpi?ski S** (2015) Role of phytochromes A and B in the regulation of cell death and acclimatory responses to UV stress in *Arabidopsis thaliana*. *J Exp Bot* **66**: 6679–6695
- Sacharz J, Giovagnetti V, Ungerer P, Mastroianni G, Ruban A V** (2017) The xanthophyll cycle affects reversible interactions between PsbS and light-harvesting complex II to control non-photochemical quenching. *Plant Physiol* **162**: 225
- Saijo Y, Sullivan JA, Wang H, Yang J, Shen Y, Rubio V, Ma L, Hoecker U, Deng XW** (2003) The COP1-SPA1 interaction defines a critical step in phytochrome A-mediated regulation of HY5 activity. *Genes Dev* **17**: 2642–7
- Saxena C, Wang H, Kavakli IH, Sancar A, Zhong D** (2005) Ultrafast dynamics of resonance energy transfer in cryptochrome. *J Am Chem Soc* **127**: 7984–7985
- Scarpeci TE, Zanon MI, Carrillo N, Mueller-Roeber B, Valle EM** (2008) Generation of superoxide anion in chloroplasts of *Arabidopsis thaliana* during active photosynthesis: a focus on rapidly induced genes. *Plant Mol Biol* **66**: 361–78
- Schneider T, Bolger A, Zeier J, Preiskowski S, Benes V, Trenkamp S, Usadel B, Farré EM, Matsubara S** (2019) Fluctuating light interacts with time of day and leaf development stage to reprogram gene expression. *Plant Physiol* **179**: 1632–1657
- Schumann T, Paul S, Melzer M, Dörmann P, Jahns P** (2017) Plant Growth under Natural Light Conditions Provides Highly Flexible Short-Term Acclimation Properties toward High Light Stress. *Front Plant Sci* **8**: 681
- Schürmann P, Buchanan BB** (2008) The ferredoxin/thioredoxin system of oxygenic photosynthesis. *Antioxidants Redox Signal* **10**: 1235–1273
- Shalitin D, Yang H, Mockler TC, Maymon M, Guo H, Whitelam GC, Lin C** (2002) Regulation of *Arabidopsis* cryptochrome 2 by blue-light-dependent phosphorylation. *Nature* **417**: 763–767
- Shalitin D, Yu X, Maymon M, Mockler T, Lin C** (2003) Blue light-dependent in vivo and in vitro phosphorylation of *Arabidopsis* cryptochrome 1. *Plant Cell* **15**: 2421–9
- Sharkey TD** (2019) Discovery of the canonical Calvin–Benson cycle. *Photosynth Res* **140**: 235–252
- Sharma P, Chatterjee M, Burman N, Khurana JP** (2014) Cryptochrome 1 regulates growth and development in *Brassica* through alteration in the expression of genes involved in light, phytohormone and stress signalling. *Plant, Cell Environ* **37**: 961–977
- Sheerin DJ, Menon C, Oven-Krockhaus S Zur, Enderle B, Zhu L, Johnen P, Schleifenbaum F, Stierhof YD, Huq E, Hiltbrunner A** (2015) Light-activated phytochrome A and B interact with members of the SPA family to promote photomorphogenesis in *Arabidopsis* by reorganizing the COP1/SPA complex. *Plant Cell* **27**: 189–201
- Shikanai T** (2015) Chloroplast NDH: A different enzyme with a structure similar to that of respiratory NADH dehydrogenase. *Biochim Biophys Acta - Bioenerg*. doi: 10.1016/j.bbabi.2015.10.013
- Shikanai T, Yamamoto H** (2017) Contribution of Cyclic and Pseudo-cyclic Electron Transport to the Formation of Proton Motive Force in Chloroplasts. doi: 10.1016/j.molp.2016.08.004
- Shimakawa G, Miyake C** (2018) Oxidation of P700 ensures robust photosynthesis. *Front Plant Sci*. doi: 10.3389/fpls.2018.01617
- Shimakawa G, Miyake C** (2019) What quantity of photosystem i is optimum for safe photosynthesis? *Plant Physiol* **179**: 1479–1485
- Shin DH, Choi M, Kim K, Bang G, Cho M, Choi S-B, Choi G, Park Y-I** (2013) HY5 regulates anthocyanin biosynthesis by inducing the transcriptional activation of the MYB75/PAP1 transcription factor in *Arabidopsis*. *FEBS Lett* **587**: 1543–1547
- Shin J, Park E, Choi G** (2007) PIF3 regulates anthocyanin biosynthesis in an HY5-dependent manner with both factors directly binding anthocyanin biosynthetic gene promoters in *Arabidopsis*. *Plant J* **49**: 981–994
- Somers DE, Quail PH** (1995) Temporal and spatial expression patterns of PHYA and PHYB genes in *Arabidopsis*. *Plant J* **7**: 413–427
- Sonoike K** (2011) Photoinhibition of photosystem I. *Physiol Plant* **142**: 56–64

- Sreeramaiah Gangappa AN, Vinod Kumar Correspondence S** (2018) DET1 and COP1 Modulate the Coordination of Growth and Immunity in Response to Key Seasonal Signals in Arabidopsis. *Cell Rep* **25**: 29–37
- Standfuss J, Terwisscha van Scheltinga AC, Lamborghini M, Kühlbrandt W** (2005) Mechanisms of photoprotection and nonphotochemical quenching in pea light-harvesting complex at 2.5 Å resolution. *EMBO J* **24**: 919–28
- Storti M, Puggioni MP, Segalla A, Morosinotto T, Alboresi A** (2020a) The chloroplast NADH dehydrogenase-like complex influences the photosynthetic activity of the moss *Physcomitrella patens*. *J Exp Bot*. doi: 10.1093/jxb/eraa274
- Storti M, Segalla A, Mellon M, Alboresi A, Morosinotto T** (2020b) Regulation of electron transport is essential for photosystem I stability and plant growth. *New Phytol* nph.16643
- Strand DD, Fisher N, Kramer DM** (2017) The higher plant plastid NAD(P)H dehydrogenase-like complex (NDH) is a high efficiency proton pump that increases ATP production by cyclic electron flow. *J Biol Chem* **292**: 11850–11860
- Suorsa M** (2015) Cyclic electron flow provides acclimatory plasticity for the photosynthetic machinery under various environmental conditions and developmental stages. *Front Plant Sci*. doi: 10.3389/fpls.2015.00800
- Suorsa M, Grieco M, Järvi S, Gollan PJ, Kangasjärvi S, Tikkanen M, Aro EM** (2013) PGR5 ensures photosynthetic control to safeguard photosystem I under fluctuating light conditions. *Plant Signal Behav* **8**: 167–172
- Suorsa M, Järvi S, Grieco M, Nurmi M, Pietrzykowska M, Rantala M, Kangasjärvi S, Paakkarinen V, Tikkanen M, Jansson S, et al** (2012) PROTON GRADIENT REGULATION5 is essential for proper acclimation of Arabidopsis photosystem I to naturally and artificially fluctuating light conditions. *Plant Cell* **24**: 2934–48
- Suorsa M, Rossi F, Tadini L, Labs M, Colombo M, Jahns P, Kater MMMM, Leister D, Finazzi G, Aro E-MM, et al** (2016) PGR5-PGRL1-Dependent Cyclic Electron Transport Modulates Linear Electron Transport Rate in Arabidopsis thaliana. *Mol Plant* **9**: 271–88
- Susek RE, Ausubel FM, Chory J** (1993) Signal transduction mutants of Arabidopsis uncouple nuclear CAB and RBCS gene expression from chloroplast development. *Cell* **74**: 787–99
- Suzuki N, Koussevitzky S, Mittler R, Miller G** (2012) ROS and redox signalling in the response of plants to abiotic stress. *Plant, Cell Environ* **35**: 259–270
- Tadini L, Pesaresi P, Kleine T, Rossi F, Guljamow A, Sommer F, Mühlhaus T, Schroda M, Masiero S, Pribil M, et al** (2016) GUN1 Controls Accumulation of the Plastid Ribosomal Protein S1 at the Protein Level and Interacts with Proteins Involved in Plastid Protein Homeostasis. *Plant Physiol* **170**: 1817–30
- Takagi D, Takumi S, Hashiguchi M, Sejima T, Miyake C** (2016) Superoxide and singlet oxygen produced within the thylakoid membranes both cause photosystem I photoinhibition. *Plant Physiol* **171**: 1626–1634
- Tan S-T, Dai C, Liu H-T, Xue H-W** (2013) Arabidopsis casein kinase1 proteins CK1.3 and CK1.4 phosphorylate cryptochrome2 to regulate blue light signaling. *Plant Cell* **25**: 2618–32
- Tepperman JM, Hudson ME, Khanna R, Zhu T, Chang SH, Wang X, Quail PH** (2004) Expression profiling of *phyB* mutant demonstrates substantial contribution of other phytochromes to red-light-regulated gene expression during seedling de-etiolation. *Plant J* **38**: 725–739
- Thompson WF, White MJ** (1991) PHYSIOLOGICAL AND MOLECULAR STUDIES OF LIGHT-REGULATED NUCLEAR GENES IN HIGHER PLANTS.
- Thormählen I, Zupok A, Rescher J, Leger J, Weissenberger S, Groysman J, Orwat A, Chatel-Innocenti G, Issakidis-Bourguet E, Armbruster U, et al** (2017) Thioredoxins Play a Crucial Role in Dynamic Acclimation of Photosynthesis in Fluctuating Light. *Mol Plant* **10**: 168–182
- Tian L, Xu P, Chukhutsina VU, Holzwarth AR, Croce R** (2017) Zeaxanthin-dependent nonphotochemical quenching does not occur in photosystem I in the higher plant *Arabidopsis thaliana*. *Proc Natl Acad Sci* **114**: 4828–4832
- Tikhonov AN** (2018) The cytochrome b6f Complex: Biophysical aspects of its functioning in chloroplasts. *Subcell. Biochem.* pp 287–328
- Tikhonov AN** (2017) Photosynthetic Electron and Proton Transport in Chloroplasts: EPR Study of $\hat{\text{I}}^{\text{m}}$ pH Generation, an Overview. *Cell Biochem Biophys* **75**: 421–432

- Tikkanen M, Gollan PJ, Mekala NR, Isojärvi J, Aro EM** (2014a) Light-harvesting mutants show differential gene expression upon shift to high light as a consequence of photosynthetic redox and reactive oxygen species metabolism. *Philos Trans R Soc B Biol Sci* **369**: 20130229
- Tikkanen M, Grebe S** (2018) Switching off photoprotection of photosystem I – a novel tool for gradual PSI photoinhibition. *Physiol Plant* **162**: 156–161
- Tikkanen M, Grieco M, Kangasjärvi S, Aro E-MM** (2010) Thylakoid protein phosphorylation in higher plant chloroplasts optimizes electron transfer under fluctuating light. *Plant Physiol* **152**: 723–735
- Tikkanen M, Grieco M, Nurmi M, Rantala M, Suorsa M, Aro EM** (2012) Regulation of the photosynthetic apparatus under fluctuating growth light. *Philos Trans R Soc B Biol Sci* **367**: 3486–3493
- Tikkanen M, Mekala NR, Aro EM** (2014b) Photosystem II photoinhibition-repair cycle protects Photosystem I from irreversible damage. *Biochim Biophys Acta - Bioenerg* **1837**: 210–215
- Timmis JN, Ayliff MA, Huang CY, Martin W** (2004) Endosymbiotic gene transfer: Organelle genomes forge eukaryotic chromosomes. *Nat Rev Genet* **5**: 123–135
- Timperio AM, Gevi F, Ceci LR, Zolla L** (2012) Acclimation to intense light implies changes at the level of trimeric subunits involved in the structural organization of the main light-harvesting complex of photosystem II (LHCII) and their isoforms. *Plant Physiol Biochem* **50**: 8–14
- Tiwari A, Mamedov F, Grieco M, Suorsa M, Jajoo A, Styring S, Tikkanen M, Aro EM** (2016) Photodamage of iron-sulphur clusters in photosystem I induces non-photochemical energy dissipation. *Nat Plants* **2**: 1–9
- Toledo-Ortiz G, Johansson H, Lee KP, Bou-Torrent J, Stewart K, Steel G, Rodríguez-Concepción M, Halliday KJ** (2014) The HY5-PIF Regulatory Module Coordinates Light and Temperature Control of Photosynthetic Gene Transcription. *PLoS Genet* **10**: e1004416
- Townsend AJ, Ware MA, Ruban A V.** (2018) Dynamic interplay between photodamage and photoprotection in photosystem II. *Plant Cell Environ* **41**: 1098–1112
- Traber MG, Stevens JF** (2011) Vitamins C and E: beneficial effects from a mechanistic perspective. *Free Radic Biol Med* **51**: 1000–13
- Tsunoyama Y, Morikawa K, Shiina T, Toyoshima Y** (2002) Blue light specific and differential expression of a plastid sigma factor, Sig5 in *Arabidopsis thaliana*. *FEBS Lett* **516**: 225–8
- Ueda M, Kuniyoshi T, Yamamoto H, Sugimoto K, Ishizaki K, Kohchi T, Nishimura Y, Shikanai T** (2012) Composition and physiological function of the chloroplast NADH dehydrogenase-like complex in *Marchantia polymorpha*. *Plant J* **72**: 683–693
- Di Valentin M, Biasibetti F, Ceola S, Carbonera D** (2009) Identification of the Sites of Chlorophyll Triplet Quenching in Relation to the Structure of LHC-II from Higher Plants. Evidence from EPR Spectroscopy. *J Phys Chem B* **113**: 13071–13078
- Verhoeven AS, Adams WW, Demmig-Adams B** (1998) Two forms of sustained xanthophyll cycle-dependent energy dissipation in overwintering *Euonymus kiautschovicus*. *Plant Cell Environ* **21**: 893–903
- Wagner D, Tepperman JM, Quail PH** (1991) Overexpression of phytochrome B induces a short hypocotyl phenotype in transgenic *Arabidopsis*. *Plant Cell* **3**: 1275–1288
- Walters RG, Rogers JJM, Shephard F, Horton P** (1999) Acclimation of *Arabidopsis thaliana* to the light environment: The role of photoreceptors. *Planta* **209**: 517–527
- Wang H, Ma LG, Li JM, Zhao HY, Xing Wang Deng** (2001) Direct interaction of *Arabidopsis* cryptochromes with COP1 in light control development. *Science* (80-) **294**: 154–158
- Wang H, Wang Deng X** (2004) Phytochrome Signaling Mechanisms. *Arab B* **9**: e0148
- Wang L, Kim C, Xu X, Piskurewicz U, Dogra V, Singh S, Mahler H, Apel K** (2016) Singlet oxygen- and EXECUTER1-mediated signaling is initiated in grana margins and depends on the protease FtsH2. *Proc Natl Acad Sci* **113**: E3792–E3800
- Wehner A, Grasses T, Jahns P** (2006) De-epoxidation of Violaxanthin in the Minor Antenna Proteins of Photosystem II, LHCb4, LHCb5, and LHCb6 *. doi: 10.1074/jbc.M602915200

- Wehner A, Storf S, Jahns P, Schmid VHR** (2004) De-epoxidation of Violaxanthin in Light-harvesting Complex I Proteins*. doi: 10.1074/jbc.M402399200
- Wei X, Su X, Cao P, Liu X, Chang W, Li M, Zhang X, Liu Z** (2016) Structure of spinach photosystem II-LHCII supercomplex at 3.2 Å resolution. *Nature* **534**: 69–74
- Weston E, Thorogood K, Vinti G, López-Juez E** (2000) Light quantity controls leaf-cell and chloroplast development in *Arabidopsis thaliana* wild type and blue-light-perception mutants. *Planta* **211**: 807–815
- Whippo CW, Khurana P, Davis PA, Deblasio SL, Desloover D, Staiger CJ, Hangarter RP** (2011) THRUMIN1 is a light-regulated actin-bundling protein involved in chloroplast motility. *Curr Biol* **21**: 59–64
- Wientjes E, Van Amerongen H, Croce R** (2013) LHCII is an antenna of both photosystems after long-term acclimation. *Biochim Biophys Acta - Bioenerg* **1827**: 420–426
- Woodson JD, Chory J** (2008) Coordination of gene expression between organellar and nuclear genomes. *Nat Rev Genet* **9**: 383–95
- Woodson JD, Perez-Ruiz JM, Chory J** (2011) Heme synthesis by plastid ferrochelatase I regulates nuclear gene expression in plants. *Curr Biol* **21**: 897–903
- Wu G-Z, Meyer EH, Wu S, Bock R** (2019) Title: Extensive Post-Transcriptional Regulation of Nuclear Gene Expression by Plastid Retrograde Signals. doi: 10.1104/pp.19.00421
- Wu G, Spalding EP** (2007) Separate functions for nuclear and cytoplasmic cryptochrome 1 during photomorphogenesis of *Arabidopsis* seedlings. *Proc Natl Acad Sci U S A* **104**: 18813–18818
- Xiao Y, Savchenko T, Baidoo EEK, Chehab WE, Hayden DM, Tolstikov V, Corwin JA, Kliebenstein DJ, Keasling JD, Dehesh K** (2012) Retrograde signaling by the plastidial metabolite MECPP regulates expression of nuclear stress-response genes. *Cell* **149**: 1525–35
- Xu P, Xiang Y, Zhu H, Xu H, Zhang Z, Zhang C, Zhang L, Ma Z** (2009) Wheat cryptochromes: subcellular localization and involvement in photomorphogenesis and osmotic stress responses. *Plant Physiol* **149**: 760–74
- Xu X, Paik I, Zhu L, Bu Q, Huang X, Deng XW, Huq E** (2014) PHYTOCHROME INTERACTING FACTOR1 enhances the E3 ligase activity of CONSTITUTIVE PHOTOMORPHOGENIC1 to synergistically repress photomorphogenesis in *Arabidopsis*. *Plant Cell* **26**: 1992–2006
- Xu Z, Mahmood K, Rothstein SJ** (2017) ROS Induces Anthocyanin Production Via Late Biosynthetic Genes and Anthocyanin Deficiency Confers the Hypersensitivity to ROS-Generating Stresses in *Arabidopsis*. *Plant Cell Physiol* **58**: 1364–1377
- Yamaguchi YL, Ishida T, Yoshimura M, Imamura Y, Shimaoka C, Sawa S** (2017) A Collection of Mutants for CLE-Peptide-Encoding Genes in *Arabidopsis* Generated by CRISPR/Cas9-Mediated Gene Targeting. *Plant Cell Physiol* **58**: 1848–1856
- Yamamoto H, Shikanai T** (2019) PGR5-dependent cyclic electron flow protects photosystem I under fluctuating light at donor and acceptor sides. *Plant Physiol* **179**: 588–600
- Yamamoto Y** (2016) Quality control of photosystem II: The mechanisms for avoidance and tolerance of light and heat stresses are closely linked to membrane fluidity of the thylakoids. *Front Plant Sci*. doi: 10.3389/fpls.2016.01136
- Yamashita E, Zhang H, Cramer WA** (2007) Structure of the Cytochrome b6f Complex: Quinone Analogue Inhibitors as Ligands of Heme cn. *J Mol Biol* **370**: 39–52
- Yamazaki J, Kamata K, Maruta E** (2011) Seasonal changes in the excess energy dissipation from Photosystem II antennae in overwintering evergreen broad-leaved trees *Quercus myrsinaefolia* and *Machilus thunbergii*. *J Photochem Photobiol B Biol* **104**: 348–356
- Yamori W, Makino A, Shikanai T** (2016) A physiological role of cyclic electron transport around photosystem I in sustaining photosynthesis under fluctuating light in rice. *Sci Rep* **6**: 20147
- Yamori W, Sakata N, Suzuki Y, Shikanai T, Makino A** (2011) Cyclic electron flow around photosystem I via chloroplast NAD(P)H dehydrogenase (NDH) complex performs a significant physiological role during photosynthesis and plant growth at low temperature in rice. *Plant J* **68**: 966–976
- Yamori W, Shikanai T** (2016) Physiological Functions of Cyclic Electron Transport Around Photosystem I in Sustaining Photosynthesis and Plant Growth. *Annu Rev Plant Biol* **67**: 81–106

- Yamori W, Shikanai T, Makino A** (2015) Photosystem I cyclic electron flow via chloroplast NADH dehydrogenase-like complex performs a physiological role for photosynthesis at low light. *Sci Rep* **5**: 13908
- Yang D, Seaton DD, Krahme J, Halliday KJ** (2016) Photoreceptor effects on plant biomass, resource allocation, and metabolic state. *Proc Natl Acad Sci U S A* **113**: 7667–7672
- Yang H-Q, Tang R-H, Cashmore AR** (2001) The Signaling Mechanism of Arabidopsis CRY1 Involves Direct Interaction with COP1. *Plant Cell* **13**: 2573–2587
- Yang HQ, Wu YJ, Tang RH, Liu D, Liu Y, Cashmore AR, Wit J de, Verkerk A, Eker A., Leenen D van, et al** (2000) The C termini of Arabidopsis cryptochromes mediate a constitutive light response. *Cell* **103**: 815–27
- Yoshida K, Hara S, Hisabori T** (2015) Thioredoxin Selectivity for Thiol-based Redox Regulation of Target Proteins in Chloroplasts. *J Biol Chem* **290**: 14278–88
- Yu X, Klejnot J, Zhao X, Shalitin D, Maymon M, Yang H, Lee J, Liu X, Lopez J, Lin C** (2007) *Arabidopsis* Cryptochrome 2 Completes Its Posttranslational Life Cycle in the Nucleus. *Plant Cell* **19**: 3146–3156
- Yu X, Liu H, Klejnot J, Lin C** (2010) The Cryptochrome Blue Light Receptors. *Arab B* **8**: e0135
- Zhang H, Zhang TT, Liu H, Shi DY, Wang M, Bie XM, Li XG, Zhang XS** (2018) Thioredoxin-mediated ROS homeostasis explains natural variation in plant regeneration. *Plant Physiol* **176**: 2231–2250
- Zhang S, Scheller HV** (2004) Photoinhibition of Photosystem I at Chilling Temperature and Subsequent Recovery in *Arabidopsis thaliana*. *Plant Cell Physiol*. doi: 10.1093/PCP/PCH180
- Zhang YC, Gong SF, Li QH, Sang Y, Yang HQ** (2006) Functional and signaling mechanism analysis of rice CRYPTOCHROME 1. *Plant J* **46**: 971–983
- Zhu D, Maier A, Lee JH, Laubinger S, Saijo Y, Wang H, Qu LJ, Hoecker U, Deng XW** (2008) Biochemical characterization of Arabidopsis complexes containing constitutively photomorphogenic1 and suppressor of PHYA proteins in light control of plant development. *Plant Cell* **20**: 2307–2323
- Zhu L, Bu Q, Xu X, Paik I, Huang X, Hoecker U, Deng XW, Huq E** (2015) CUL4 forms an E3 ligase with COP1 and SPA to promote light-induced degradation of PIF1. *Nat Commun*. doi: 10.1038/ncomms8245
- Zirak P, Penzkofer A, Moldt J, Pokorny R, Batschauer A, Essen L-O** (2009) Photocycle dynamics of the E149A mutant of cryptochrome 3 from *Arabidopsis thaliana*. *J Photochem Photobiol B* **97**: 94–108

ACKNOWLEDGMENTS

This research was mostly carried out in the laboratory of Shizue Matsubara at the IBG-2, FZJ in the context of the iGRAD PhD program, at the University of Duesseldorf, HHU. I truly appreciate for the opportunity to perform my PhD work in this great graduate program and I acknowledge for financial support. Many people have helped and supported me during the past four years and I am sincerely grateful to each of them.

I would first like to thank my committee members, Shizue Matsubara, Andreas Weber and Peter Jahns for the excellent guide and the precious suggestions that I received from them during our meetings. A special thanks goes to Shizue, who allowed me to perform my research in her group and has been always available for discussing the experiments and exchanging ideas. From her guide I could learn a lot. I am grateful to Andreas Weber for being my mentor and allow me to perform my 2nd lab rotation in his lab, where I could learn from Florian how to use the Crispr Cas method. Thank you, Andreas and Florian. Peter Jahns, thank you so much for welcoming me in your lab during my 3rd lab rotation to perform the photosynthetic light responses curves and PSI analysis. I am also grateful for the opportunity to spend my research stint period at MSU in the laboratory of ShinHan Shiu. Petra Fackendahl, thank you for all your support, before, during and after the end of my PhD you were always helping with bureaucracy, organization and tips.

A very big thank you goes to my workmate, Anh Banh, who not only help me with pigment analysis and plant transformation, but was also a very nice person to work with and a great friend. I would like to acknowledge also all the members of the shoot dynamics group in IBG-2 for the interesting seminars and meetings, our collaborators Stefan Niedermaier and Pitter Huesgen (ZEA-3, FZJ) for the CRY1 proteomic work, my two trainees (Sven and Nadine) who helped me with selection and genotypic characterization of CRY1 OE transgenic plants, and Nina, for the phenotypic characterization experiments on these lines, Vaideki for helping me with the isolation and characterization of CrisprCas9 mutants, Beate, Sabine, Andrea and Katrin for technical assistance in the greenhouse, laboratory and GROWSCREEN.

Thank you to all the TM's lab in Padova: even though I am far away since many years I still enjoy to visit you as much as I can, you are a big source of inspiration, and still I get so much enthusiasm and I remember where I came from and all the insights I had learned there.

This thesis has been written in at least six different cities and three different country (Germany, Italy and United States) and I had the amazing opportunity to meet many people around the world: each of you have a special place in my heart. I could not be happier for the life experiences that I had the opportunity to live. Thank you to all my officemates and colleagues from IBG-2: Dhazjaner, Fang, Kelvin, Vikas, Nicolas, Anh, Martino, Francesco, Giulia and Valerio. Beat, thank you for playing with me and be so excited to measure photosynthesis together, for the pizza, for the biking and for all the funny moments we had together; Francisco, our time together was very short, but we have developed a true friendship and you teached me spanish that is now almost my native language; Thank you Pablo for all the nice moments together, for helping me with german transaltions (including the abstract of this thesis) and teaching me how to cook arepas de huevo. Ivan, you were so damn supporting during all these years, I could not thank you enough. Pepe and Carola, thank you for taking care of me and share your chilean pisco! Winder, my big twin, you are an artist, a scientist a such talented man; you teached me that it does not matter what's going on, laugh is always the answer and there are so many reasons to smile. A big thanks goes also to Alexandra, Ana, Raquel, Otavio, Daniela, Ricardo, Maria, Mauricio, Daniela, Elisa, and all the "corazoncitos". Also, the support of my friends from my hometown was always present and I want to say thank you to Francesca, Federico, Marco, Elisabetta and Antonella for being always at my side besides the distance. I finally would like to thank all the friends that I met at MSU during the first and during the second time in here: Clizia, Francesco, Amy, Mattia, Jessica, Nathan, Leo, Iso, Omar, Tatiana, Juan, Andres, David, Gianni and Luciana. Thank you, Jose, for giving me a little place of peace in your house to focus during the harder writing moment. Aimer, thank you for supporting me in your unique ways, for showing me different perspectives, for being on my side and make my life wonderful and full of happiness, love and colors.

The most profound gratitude goes to my family: my parents, Giovanni and Letizia, my brothers, Carlo and Vincenzo, my sister, Bonaria and my grandparents, Vincenzo, Bonaria, Cenzo e Paola. Your constant support is always the most important thing in my life and it worth a lot for me. I love you so much.

A handwritten signature in black ink that reads "Paola". The script is cursive and fluid, with the 'P' being particularly large and stylized.